Structural and Mechanical Investigations of Polyelectrolyte Films

Hegaard, Frederik

Publication date:
2022

Document Version
Publisher's PDF, also known as Version of record

Structural and Mechanical Investigations of Polyelectrolyte Films

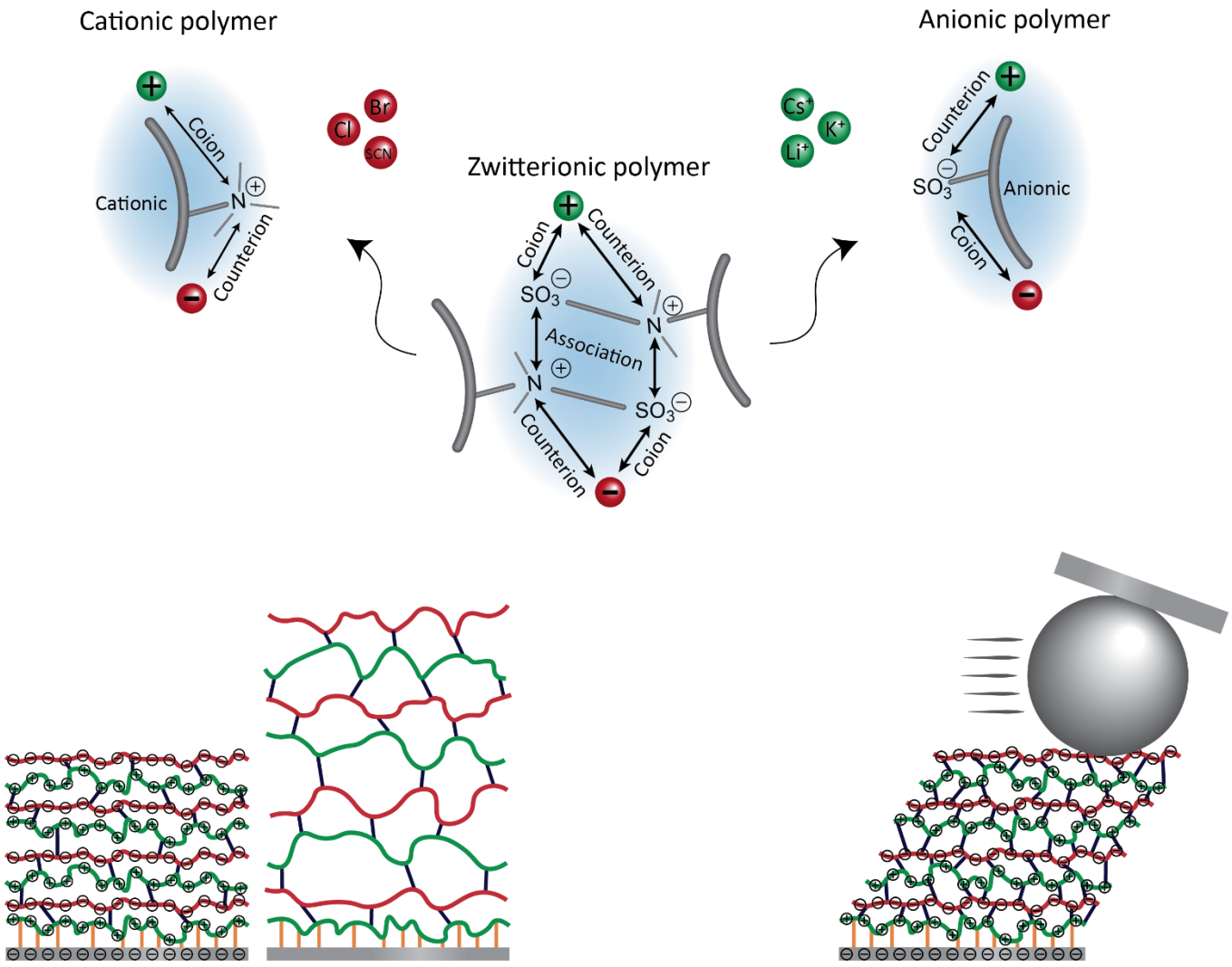

PhD Dissertation

Frederik Hegaard

Supervisor: Esben Thormann

October 2022

DTU Chemistry

Department of Chemistry

Abstract

Polyelectrolyte films have attracted significant research interest due to their wide range of potential applications. The fundamental understanding of these films is a vital foundation to improve upon as it ensures the most favorable terms of success for its applications. This project has aimed to improve the current knowledge of specific types of film's swelling responses and their underlying mechanisms.

In this project, polyzwitterionic film's specific ion-induced swelling has been the focus of an experimental study. The swelling of polycationic and polyanionic films containing the same charge groups as the polyzwitterionic film was studied systematically with different ion types and concentrations using ellipsometry. With the learnings from these films, it was shown that the swelling of polyzwitterionic films is a result of two mechanisms: The physical crosslinks are broken when the salt concentration is increased as it then becomes favorable for the positively charged immobile cations to bind to the mobile anions at a concentration which depends on the specific anion. The cation then counters the positively charged immobile anions resulting in increased osmotic pressure inside the film. The foundation for a theoretical model describing the mechanisms in the film was created, but it is needing further work before it can fully describe the effects that were observed experimentally. The understanding of the mechanisms driving the swelling in the polyzwitterionic film was applied to significantly more complex multilayer films of weak polyelectrolytes. These films' buildup and swelling responses were again systematically studied with various salt types and concentrations under different pH values. From ellipsometry and quartz crystal microbalance with dissipation measurements, it was shown that the multilayer film's responses can be described as a combination of weak polyelectrolyte films and polyzwitterionic films. It was likewise shown how it is necessary to carefully consider the ion concentration and types when designing multilayer films with a specific target pH response. As an extension of the study on the multilayer films, the friction between the films and colloidal probe under different salt and pH conditions was measured with an atomic force microscope. A significant amount of preparation goes into preparing the microscope for friction measurements and analyzing the data obtained to show an actual friction force. In this project, the microscope's cantilever was calibrated with a method that uses the thermal perturbations on the cantilever. As the sensitivity of the cantilever changes depending on the medium, a geometrical approach is suggested as a tool to describe how the sensitivity is changing when the cantilever is used in a liquid instead of air.

Resume

Polyelektrolytte film har modtaget stor videnskabelig interesse grundet deres store potentiale for anvendelser i en bred vifte af områder. Den fundamentale forståelse af disse film er vital da denne danner grundlaget for at kunne sikres filmenes potentielle anvendelser de bedst mulige forudsætninger for at lykkes. I dette projekt har fokusset været på at udvide den nuværende fundamentale forståelse af specifikke typer af polyelektrolytte films respons på ændringer i salt og pH.

Zwitterioniske polymer films reaktioner på øget salt koncentration og specifikke typer af ioner har været fokusset i et eksperimentel studie. Her var det fundet at filmenes tykkelse blev øget med saltkoncentrationen i en grad der afhang af de specifikke anioner i opløsningen. Ved at lave lignende målinger på kationiske og anioniske polymerfilm, blev det muligt at forstå hvordan krydsbindinger i de polyzwitterioniske film blev brudt af anioner mens effekten af kationer var at agere som modioner og derved øge det osmotiske tryk. Begge disse effekter er medvirkende til øgningen af filmens tykkelse.

Den øgede forståelse af mekanismerne for polyzwitterioniske film blev brugt til at forstå responset en mere kompleks filmtype. Multilagfilm af svage polyelektrolytter er film dannet med vekslende lag af positive ladet kationiske og negativt ladet anioniske polymerer. Den svage natur af disse polyelektrolytter betyder at deres ladning er påvirket af både pH og salt koncentration, hvilket i kombination med deres vekslende struktur i multilaget gør denne filmtypes respons vanskelig at forstå. Multilagfilmene var dannet under varierede forudsætninger og efterfølgende var deres respons til pH målt ved forskellige saltkoncentrationer og ved forskellige ion typer. Ud fra disse målinger var det muligt at vise at multilag filmene ved de pH værdier hvor de var bygget havde en næsten neutral overordnet ladning og ved høj pH havde en overvægt af negative ladninger. I de tilfælde hvor ladningen var ens kunne forståelsen af zwitterioniske film bruges til at beskrive multilags filmens tykkelsesændring ved øget salt koncentration. På samme måde kunne filmens tykkelses ændring ved høj pH beskrives som en kombination af en traditionel svag polyanionisk film og den polyzwitterioniske film.

Acknowledgments

Throughout this project, I have received help and support in different ways from a range of people. To these people, I would like to extend my sincerest gratitude.

First of all, I would like to thank my supervisor Esben Thormann who is the main reason that it has been possible for me to work on this project. During this project, we have had numerous academic discussions where he has helped me to find my way back on the right track. Esben's vast scientific knowledge has helped me improve my way of thinking scientifically and his positive attitude and curiosity have often shown to be contagious. During this project, which has had both its scientific challenges and more unforeseen such as the Covid-19 lockdown, I appreciate that he has made himself available for discussions, both about the project and about life in general.

I would also like to thank my colleagues in our group for always being willing to offer their help with any problems that I encountered. Thank you Achebe Nzulumike, Anand Palanisamy, Christina Nielsen, Daniel Hansen, Fatemeh Keshavarzi, Ingrid Sørensen, Johannes Eiler, Junhao Huang, Junjie Kang, Koosha Ehtiati, Marius Kubus, Robert Biro, and Runtian Qie for bringing fun and warmth to the daily life.

During my external stay at the University of Cagliari in Italy, I was working with Drew Parsons, who besides guiding me in the academic work also showed me around in the area and saw that I was settling down well. I am grateful that Drew took his time to ensure I had a very good experience during my entire external stay.

Finally, I would like to thank my family and friends, and in particular my girlfriend Belinda, for the support throughout the project and for bringing me joy. I am thankful that these people have provided me with excuses for pausing this project and clearing my head, at appropriate intervals.

List of abbreviations

^{1}H-NMR	Proton nuclear magnetic resonance
ACVA	4,4'-Azobis(4-cyanovaleric acid)
ADA	Alginate dialdehyde
AFM	Atomic force microscope
AMA	Allyl methacrylate
ASV	Automated selector valve
BMA	Butyl methacrylate
Br^-	Bromide
CDPA	4-cyano-4-[(dodecylsulfanylthiocarbonyl)sulfanyl] pentanoic acid
CHI	Chitosan
Cl^-	Chloride
Cs^-	Cesium
DMF	Dimethylformamide
GPS	3-glycidoxypropyltrimethoxysilane
K^+	Potassium
Li^-	Lithium
METAC	2-(methacryloyloxy)ethyl]trimethylammonium chloride
MPTMS	3-mercaptopropyl trimethoxysilane
MSE	Mean squared error
PETMP	Pentaerythritol tetrakis(3-mercaptopropionate)
PMABS	Poly[N-(2-methacryloyloxyethyl)-N,N-dimethylammonio butanesulfonate]
PMPC	poly(2-(methacryloyloxy)- ethyl phosphorylcholine
QCM-D	Quartz crystal microbalance with dissipation monitoring
SCN^-	Thiocyanate
SPMAK	3-Sulfopropyl methacrylate potassium
TFE	2,2,2-Trifluoroethanol

List of papers

1. Ion-specific antipolyelectrolyte effect on the swelling behavior of polyzwitterionic layers.

   Frederik Hegaard, Robert Biro, Koosha Ehtiati and Esben Thormann

   (Submitted)

2. Influence of ionic strength and specific ion effects on the pH responsiveness of weak polyelectrolyte multilayer films.

   Frederik Hegaard and Esben Thormann

   (To be submitted)

Contents

Introduction

In this PhD project, charged polymer films and their structural and mechanical properties have been studied. The studies performed on these films can be divided into three objectives. 1) Understanding charged polymer films with both negative and positive charges and their specific ion-dependent swelling responses, 2) investigating the mechanisms of swelling responses of charged multilayer polymer film to pH, and 3) studying friction on layered polymer films under varied pH, ion types, and ion concentrations. The common overall goal was to develop the fundamental understanding of systems with charged polymer films, to further improve the possibilities of tuning the properties of the films, and thereby enhance their practical application potential.

The first aim was to improve the fundamental understanding of polymer films with both positive and negative charges and their response to different types of ions. These films are attracting significant research interest because of their diverse applications originating from their tunable properties. They have significant application potential ranging from antifouling of proteins[1–3] and stimuli-responsive emulsification[4,5] to lubrication[6–8]. A fundamental understanding of the films will be beneficial for all these applications. However, to date, these films have not been completely understood due to their complexity. Previously, our group developed a thorough understanding of polymer films with either positive or negative charge and improved the understanding of how these films interact with ions. Herein, this knowledge has been utilized for designing experiments involving a system with higher complexity. Thus, the current understanding of the different responses of the film to salt changes could be further improved. Based on the results of this study, a paper has been submitted, and it is included in Appendix A. A discussion of the findings and their interpretation are presented in section 5.1. In addition to the experimental aspect of this study, the basis for a theoretical model describing the swelling behavior has also been created. The features implemented in this model and the corresponding output is described in section 4.

The second objective focuses on multilayer films of two different and oppositely charged polymers and the effect of changes in pH and salt concentration on the hydration of the films. These studies were performed to understand the mechanisms behind the observed trends on a fundamental level. However, this type of film is significantly more complex than the single component film. The significant interest in this specific type of film is due to the fact that it has shown promising for different biomedical applications, such as tissue engineering and drug delivery[9–16]. Especially, application in drug delivery, where the tunable properties of the film are utilized, seems promising; however, a specific swelling response of the film is

required for this application at the pH value and ionic composition of the target area in the body[17,18]. In this study, the swelling response has been studied using different techniques. In addition, the drastic changes in the swelling behavior have been investigated under different pH environments with varying salt concentration. From these results, it was found that the film can be described from a combination of the description develop for the previously investigated film and a different well-described film type. This aspect seems to be overlooked in some studies when the properties of the film are tuned for a specific purpose. These results have been included in Appendix B, and the results are presented and discussed in section 5.2.

The third objective involves the same multilayer film as that in the second; however, this objective focuses on the friction of the film, which corresponds to energy dissipation. The friction was measured at different pH values and salt concentrations. These measurements could be used together with the findings of the second objective to improve the understanding of the configuration inside the film. However, as the film is quite complex and has not been completely understood, it was difficult to draw convincing conclusions based on these results. These results are presented in section 5.3. Originally, these friction studies were planned to be a significantly larger part of the project than they ended up becoming. Therefore, a significant amount of time was spent preparing an atomic force microscope (AFM) for friction measurements. This required both practical preparations of the components and careful considerations as to how the AFM should be calibrated for these measurements, along with the calculations necessary to perform and validate these calibrations. These aspects are discussed in detail in section 3.

1 Background

In this PhD project, the foundation of the studies included investigations of different types of charged polymer films, both in simple and complex forms. Charged polymer films have been a huge focal point of research, and the studies in this project therefore further develop on the already existing knowledge in an attempt to improve the relevant fundamental understanding of these types of systems. In this section, the fundamental principles of polymers are discussed, along with the common understanding of their behavior when structured as a film. These discussions of the films are used as the foundation to interpret the results obtained in this PhD project.

1.1 Polymers at interfaces

The simplest type of a hydrated polymer system is a single uncharged polymer in a solution. This results in a polymer having a configuration which is an intermediate state between fully stretched and fully collapsed[19,20]. The configuration and hydration of such a polymer can be described by its radius of gyration, R_g, which is the average of the mean square radius of the repeating units with respect to the center of mass, C_m,[21,22] (Illustrated in Figure 1.1A). The radius of gyration increases if the size or the number of repeating units are increased. The interplay between the polymer and the solvent can significantly affect the radius of gyration. This was described independently by Flory and Huggins as an interaction parameter, which today is more commonly referred to as the solvent quality[23,24]. A good solvent quality indicates a good affinity between the polymer and the solvent, resulting in an increased radius of gyration and a higher degree of hydration compared to those of the same polymer in a solution with poor solvent quality.

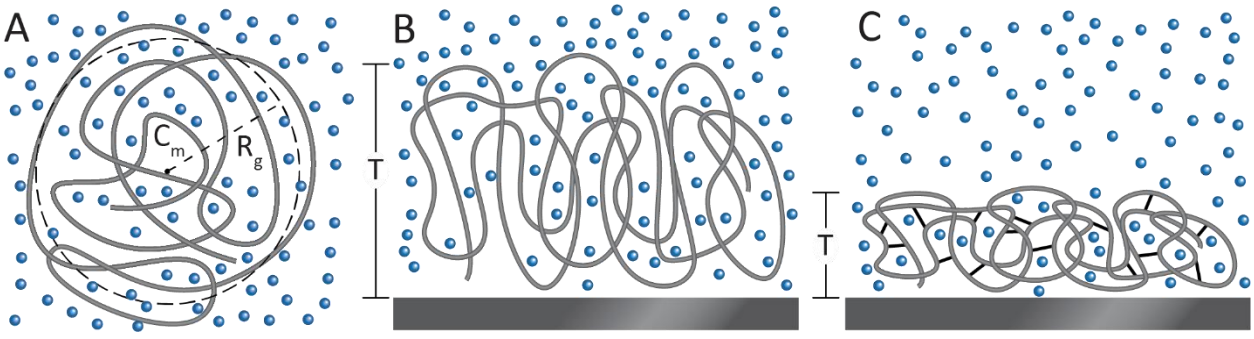

Figure 1.1: Illustration of a free hydrated uncharged polymer in solution and its radius of gyration (A), an uncharged hydrated polymer film on a substrate with a thickness (B), and uncharged hydrated crosslinked polymer film on a substrate with a decreased thickness (C).

When the system consists of multiple polymers bound to a surface, it will be more restricted instead of one free polymer in a solution. Therefore, the polymers would not have the freedom to expand in three

dimensions and would be significantly restricted. If the polymers on the surface attain a sufficiently high density, they will interact with the neighboring polymers during expansion. This leads to the polymers only being able to expand in the dimension away from the surface. Although this system introduces some restrictions and internal interactions that were not present in the single polymer in solution, the overall dynamics are similar if the radius of gyration is reformulated as the thickness, T, of the polymer film, as illustrated in Figure 1.1B[25]. An increase in the density of repeated units or the size of the units increases the thickness of the film, and the solvent quality will either cause swelling or collapse of the film depending on whether it is good or poor, respectively[26].

Crosslinking of the polymers will further increase the complexity. This could result in the formation of physical or chemical bonds between two random repeating units, increasing the rigidity of the film. As the degree of crosslinking of the film is increased, the consequent increase in rigidity will reduce the swelling of the film[27], as illustrated in Figure 1.1C. This structure of polymers bound to a surface and crosslinked together is the foundation for the films that have been studied in this project. However, instead of neutral polymers, the polymers used in this study contain charged groups, which makes them more complicated but also leads to more interesting responses and possible applications.

1.2 Polyelectrolyte Films and charge types

If a polymer has ionizable groups, it can carry a charge caused by dissociation in polar solvents such as water. This type of polymer is called a polyelectrolyte and it can either be a polycation, polyanion, or polyampholyte. Polycations and polyanions are polymers where the charges are either exclusively positive or negative, respectively. A polyampholyte contains both positive and negative charges[28]. In this project, the polyampholytes involved are zwitterionic polymers (betaines) which are polymers containing equal amounts of oppositely charged groups on the same monomer, resulting in overall charge neutrality[29]. The charges in the polycation and polyanion films are always countered by oppositely charged ions that result in overall charge neutrality of these types of films[30]. Because the charges of a hydrated polycation or polyanion film are neutralized by counterions, they do not cause the film to swell due to repulsion[31–33]. However, the charges in a zwitterionic polymer will interact when the polymer film is hydrated in water. In addition, as the film contains both positive and negative charges, they can bind to each other and result in a lower film thickness compared to that of a neutral polymer film[34,35]. The charges in a polyzwitterionic film can interact either by binding with the opposite charges from the same monomer or with opposite charges on different monomers; these interactions are referred to as intrachain and interchain bonding, respectively. Depending on the conditions of hydration, polyzwitterionic films can neutralize their charge

both using counterions and intra-/interchain bonds. The balance between which method is more favorable depends on the type of charged groups of the polyzwitterion and their spacer length, along with the salt concentration and ion types in the solution[36].

1.2.1 Strong and weak polyelectrolytes

Polyelectrolytes are divided into strong or weak, depending on how their charge is affected by pH. Strong polyelectrolytes are completely dissociated when hydrated and their overall charge is independent of the pH value at which they are hydrated. On the contrary, weak polyelectrolytes have a dissociation degree that is dependent on the pH they are hydrated in. Weak polyelectrolytes have a pKa value which corresponds to the pH at which half of the ionizable groups are dissociated. Consequently, while strong polycations will have a constant positive charge, weak polycations will have no charge at pH values much higher than their pKa value and will become completely positively charged at pH values much lower than their pKa value. Similarly, strong polyanions will have a constant negative charge, whereas weak polyanions will be completely negatively charged at pH values much higher than their pKa value, and have no charge at pH values much lower than their pKa value[37–41]. The different charge dependencies of the polyelectrolytes on pH are illustrated in Figure 1.2.

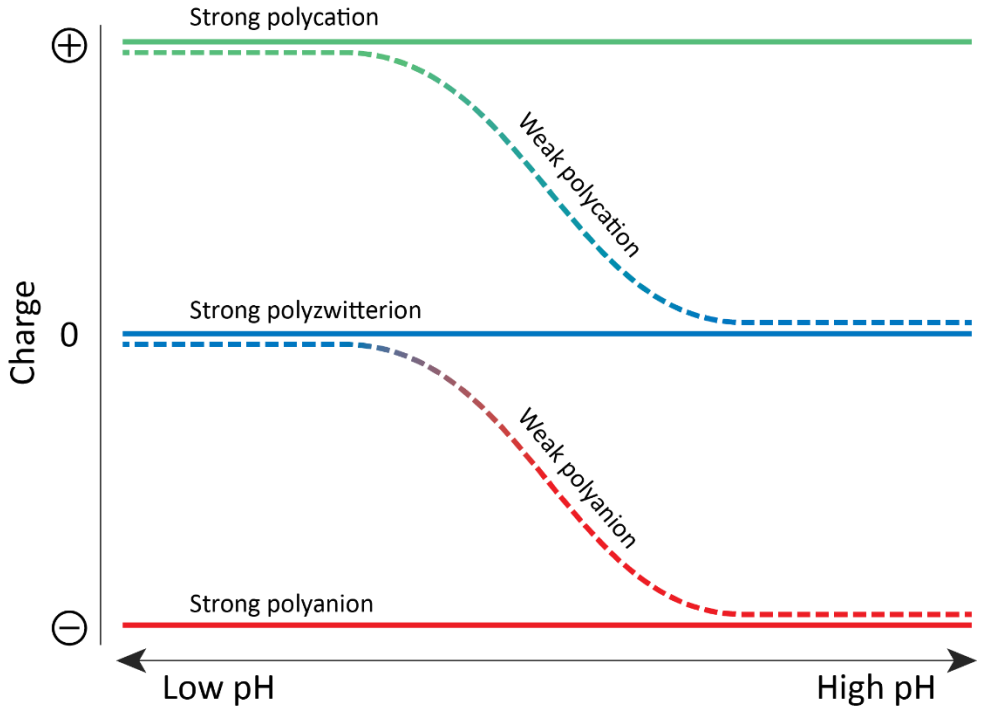

Figure 1.2: Illustration of the number of charges in different types of strong and weak polyelectrolytes and the effect of pH value.

At a given pH value the dissociation degree is an equilibrium between the charged and uncharged ionizable groups for the weak polyelectrolytes. The addition of salt, and the specific type of salt, will affect this equilibrium and shift it toward a more dissociated state as this is favored by the increased screening[42]. Because of their sensitivity to both pH and salt according to their dissociation, the weak polyelectrolytes are significantly more complicated to understand than the strong; thus, it is more difficult to predict their behavior.

1.3 Swelling behavior of strong polyelectrolyte films

A part of the significant research interest in strong polyelectrolyte films is due to their wide range of possible applications. The polycationic and polyanionic films are useful for several applications, such as colloidal stabilization, lubrication, and adhesion[43–47], whereas the applications of polyzwitterionic films include antifouling capabilities[1–3,48–50], stimuli-responsive emulsification[4,5], lubrication[6–8], and biomedical sensors[51,52]. The charged surfaces of polycationic and polyanionic films usually result in poor biocompatibility; therefore, bacteria and proteins can attach to the surface and cause biofouling. However, the inter/intrachain bonds of the polyzwitterionic film have a greatly improved biocompatibility[53–55].

These possible applications are linked with the swelling and charge state of the films, which can be altered by changing the conditions of the solutions they are hydrated in. In this study, the strong polyelectrolytes were investigated by forming cationic, anionic, and zwitterionic polymer films and measuring their swelling under varied salt concentrations and ion types.

While a strong polyelectrolyte film is not affected by pH, the salt concentration it is hydrated in significantly affects the film. For hydrated strong polycationic and polyanionic films, the dependency of thickness on the salt concentration of the medium has three different behavioral regimes: the osmotic regime, salted regime, and quasineutral regime, which are illustrated in Figure 1.3[56–59]. These regimes primarily arise from the difference in osmotic pressure between the counterions inside the film and the free ions outside the film. The osmotic regime is observed at low salt concentrations where the free ion concentration in the medium is much lower than the concentration of counterions inside the film, causing a higher osmotic pressure inside the film and resulting in a swollen regime. In this regime, the swelling is determined by a balance between the force from the osmotic pressure causing swelling and the entropic elasticity of the polymers that favors a more collapsed state. When the salt concentration in the medium is sufficiently increased, such that it is comparable to that of the counterions inside the film, the salted regime starts and a decrease in the swelling is observed, with a decrease in the osmotic pressure

difference between the inside and outside of the film. In this regime, the swelling gradually decreases until the salt concentration of the medium results in the same osmotic pressure as the counterions inside the film. When very high salt concentrations are reached, the film enters the quasineutral regime where screening effects become large, and the film again becomes independent of further increases in the salt concentration. In this regime, the osmotic pressure difference is lowered, allowing the solvent quality to have a greater influence on the thickness of the film. The effects of solvent quality depend on the dynamic between the medium and polymers, and how the properties of the medium are controlled by the salt concentration and its ion types. In the most common combinations of polymers and monovalent salt for swelling studies, the solvent quality effects are so small that the swelling stays constant in the quasineutral regime. However, some ions, e.g., SCN^-, have been shown to increase the thickness at high salt concentration[60,61].

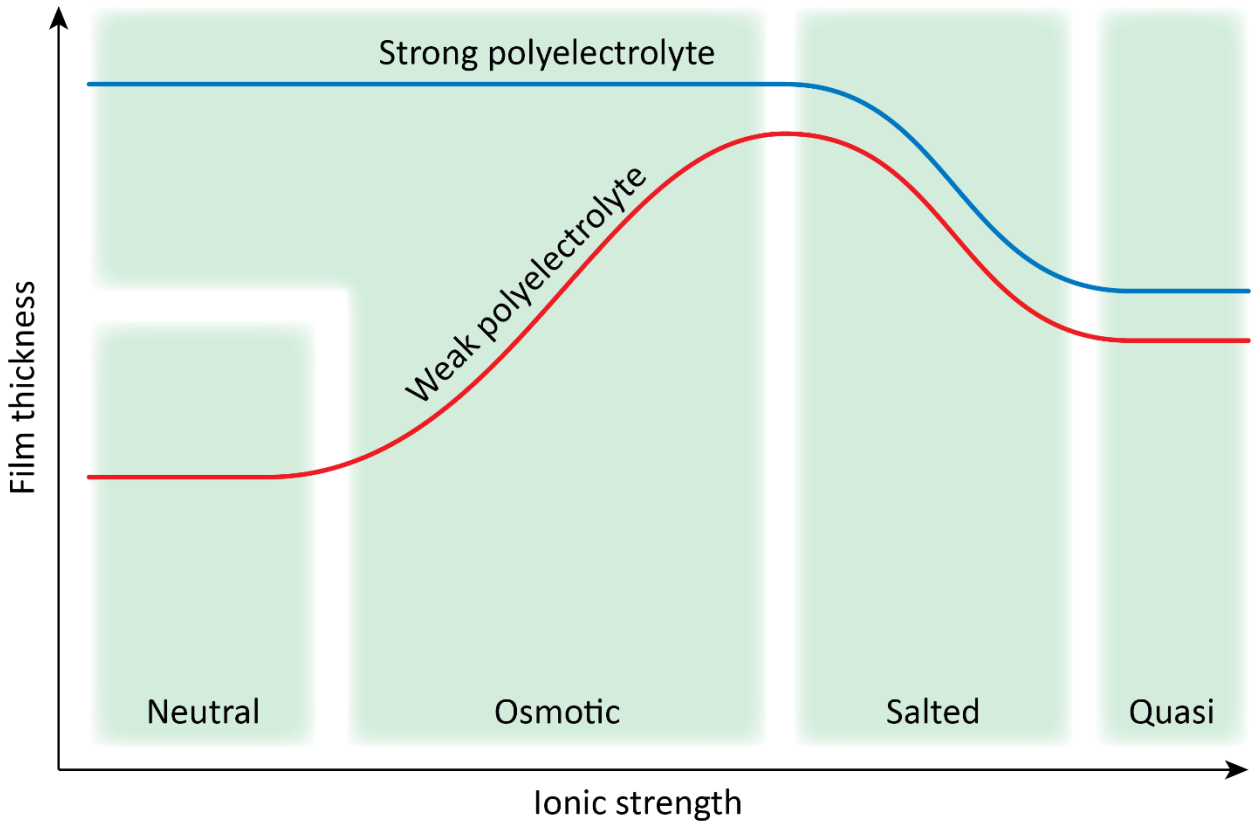

Figure 1.3: Illustration of swelling behavior of strong and weak polyelectrolyte films in salt solutions of varying concentrations. The behavior of the films is described by different regimes dependent on the salt concentration. Adapted with permission from [62].

Originally, the ions in the medium hydrating the polyelectrolyte film have been considered as point charges. Therefore, a range of properties of the ions have been ignored and the choice of the specific type of monovalent ion has been considered indifferent to the swelling[56]. However, experiments have

contradicted this, and it has been established that different ion types affect the swelling of polyelectrolyte films differently[60,63,64]. The trends of swelling with varied types of ions follow the same order as the Hofmeister series, which is an experimentally determined ordering of the ions related to their specific abilities to stabilize or precipitate proteins and macromolecules[65,66]. This series is found to describe the ordering of specific ion effects for a variety of systems; although it is linked to ion hydration and ion paring, its origin is still not fully understood[67–69]. Polyelectrolyte films can be significantly affected by specific ion effects, and several reasons for this have been discussed and hypothesized over time. The currently accepted explanation is that the counterions inside the film form ion pairs with the charged groups, which affect the osmotic pressure[63]. These pairings decrease the osmotic activity inside the film, causing the film to collapse[60]. The formation of these ion pairs depends on their interaction energies, which have been calculated and found to be proportional to the hydrophilicity of the ions[60,70]. The effect of anions on the swelling of a cationic film is illustrated in Figure 1.4 for a particular selection of anions, specifically, the anions that have been used in the present experiments.

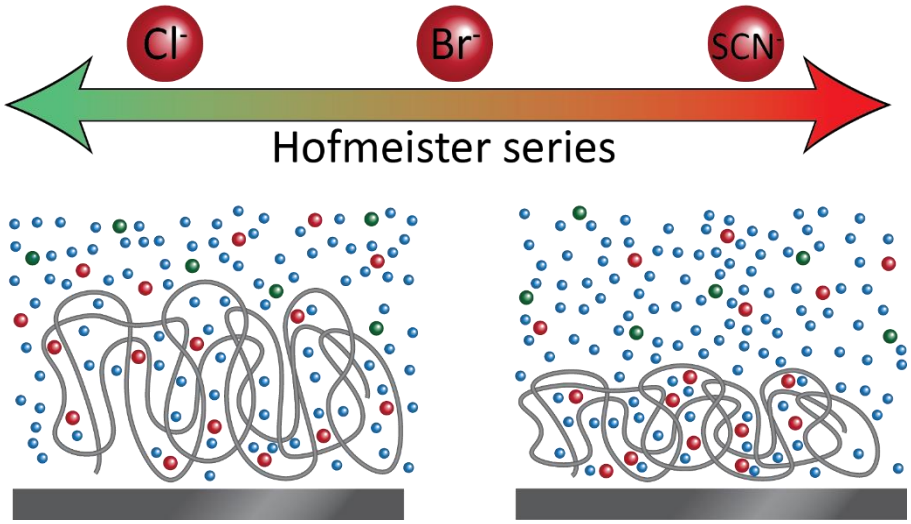

Figure 1.4: The ordering of chosen anions according to the Hofmeister series and illustration of their effect on swelling of a polycationic film.

In this study, the swelling was found to be significantly affected by changes in the anion, while the cation only seems to have very small effects. At low ionic strength, theoretical studies have linked the effects of the ions to their polarizability. The polarizability of the ions influences the swelling because it indicates how favorable it is for the ions to form ion pairs, and thereby change their osmotic activity[71,72].

1.3.1 Swelling behavior of polyzwitterionic films

Instead of being swollen at low salt concentrations because of osmotic pressure difference, similar to that for cationic and anionic films, the behavior of polyzwitterionic films is determined by their intra-/interchain bonds. Similarly, the response of polyzwitterionic film to increases in the salt concentration is completely different from those of the polycationic and polyanionic films. The complexity of polyzwitterionic films has been documented through a range of studies on different types of systems. The dependency of the swelling states of a polyzwitterionic film on the salt concentration is not established for all systems; some types of systems do not depend on the salt concentration and ion types (e.g. for PMPC (poly(2-(methacryloyloxy)- ethyl phosphorylcholine) films)[73–75]. Other polyzwitterionic systems (including sulfobetaine which is the system used in this project) show a clear dependency on both salt concentration and anion type. Experimentally, several studies have reported that with an increase in the salt concentration, sulfobetaine polyzwitterionic films start to swell[76–80]. The trends observed in these studies indicate that at low salt concentrations there is a regime in which the polyzwitterionic film is independent of changes in salt concentration and specific ion types. After this regime, the film starts to swell with an increase in the salt concentration, at a rate that can be affected by the anions present, as illustrated in Figure 1.5. This is called the "anti-polyelectrolyte" effect, as the polyzwitterionic film responds opposite to that of a polycationic or polyanionic film when hydrated in salt solutions[36,81]. In addition to the ion types, the swelling behavior is also affected by the type of charge groups and the charge density of the film. However, the mechanisms causing the changes in swelling behavior are still not properly understood [76,77,80,82,83].

It has been consistently observed that the thickness of sulfobetaine polyzwitterionic films increases when the salt concentration is increased, and the effect of change in ion types follows the same order as that of the Hofmeister series, where, e.g., SCN^- ions cause larger swelling than that with Cl^- ions[76,84–86]. Most experimental studies on polyzwitterionic films have focused on the specific anion effects, mainly because the cation type does not have a significant effect, and therefore, it is difficult to be used for improving the understanding of the behavior[82].

Although the intra-/interchain bonds exist in salt-free solutions, these bonds are broken as the salt concentration increases, and instead, the ions are bound to some of the charges[73,77]. The reason for this has not been convincingly elucidated. Nevertheless, a consensus seems to have been formed that this bond breakage is mostly caused by electrostatic screening[78,80,87–89].

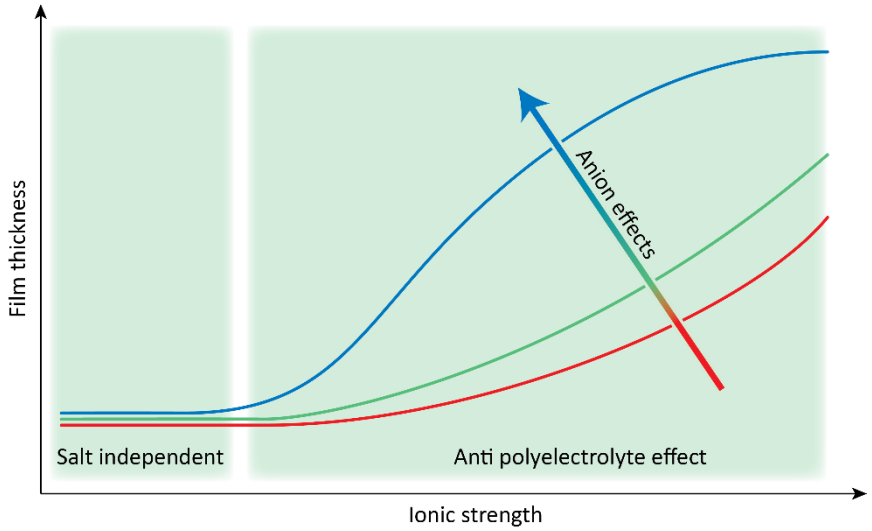

Figure 1.5: Illustration of typical swelling behavior of a polyzwitterionic sulfobetaine film and the possible effects of variation in the anions.

This explains the effect of increasing the salt concentration, but not the effects of specific ions. The most convincing explanation of the specific ion effects can be found in studies using molecular dynamics simulations. The binding affinity of a range of ions has been investigated for different types of polyzwitterionic films with these studies. Different types of anions demonstrate significant variations in the association with sulfobetaine and they are ordered consistently with the Hofmeister series[83,90–93]. The variations in the affinity of different cation types and sulfobetaine were found to be relatively small compared to those of anions[94].

Although these studies on polyzwitterionic systems offer explanations for the mechanisms driving the swelling trends observed, studies that can provide a convincing and full understanding are still lacking. To improve the understanding of polyzwitterionic films, systematic experiments were designed such that they build on the current knowledge of polycationic and polyanionic films. Based on these understandings, the fundamental understanding of polyzwitterionic films can be discussed more convincingly. These results form the basis for the paper in Appendix A, and the main points of the paper are discussed in section 5.1.

1.4 Weak polyelectrolyte multilayer films

In this study, a weak multilayer polyelectrolyte film refers to a coating consisting of two oppositely charged weak polyelectrolytes in alternate layers on a substrate. These film types have shown promising possibilities for a variety of applications, leading to an increase in research interest[95,96]. Such films are typically responsive to the salt concentration, salt type, and pH, and their responsiveness can be tuned

using the preparation method. As they consist of two different weak polymer components in a tunable ratio, the internal dynamics of these film types and their responses to stimuli are, on a fundamental level, significantly more complicated to discuss than that of the monocomponent strong polyelectrolyte film. Despite the huge research interest, they are still not fully understood[97–99]. Their complexity can explain why some of the research attention on multilayers is focused on adjusting the parameters to further improve the multilayers for a specific application, instead of enhancing the understanding of underlying mechanics. In this section, the current understanding of the multilayers will be discussed considering the importance of the parameters of the building process and the responses to different stimuli.

The multilayer films were deposited using a layer-by-layer technique, where the first layer was chemically grafted to a substrate. The next layer was then electrostatically bonded to the charges of the first layer, and this was continued until the desired number of layers was obtained. This electrostatically controlled adsorption is a stable method for depositing layers of similar thickness that grow fairly uniformly; thus, films deposited on smooth substrates stay fairly smooth, at least within the number of layers deposited in this study[100,101].

In this study, the components of the multilayered film include the weak polyelectrolytes chitosan (CHI) and alginate dialdehyde (ADA), which interact through the positively charged ammonium group of CHI and the negatively charged carboxylate group of ADA. A multilayer that is only electrostatically bonded together will disintegrate if the dissociation of one of the polyelectrolytes is changed, which is desired for some applications (e.g., drug delivery), but not for the investigations in this study. The benefit of CHI and ADA is that they not only bind electrostatically but also create covalent bonds through a Schiff base reaction between amine groups of CHI and aldehyde groups of ADA[102–104]. The oxidation degree of ADA determines the degree of crosslinking, which was fixed at 20% in this study. This makes the film stable such that even if the environment is changed, the film will return to a similar state when the environment changes back.

1.4.1 Building a multilayer film

The charge configuration of the polyelectrolytes is an important factor in the formation of the film because it controls the adsorbed mass in each layer.[105,106] The first layer will adsorb to the substrate electrostatically to counter the charges of the substrate. Thus, much more polyelectrolytes will be required to bind if the polyelectrolyte contains a low amount of charge, compared to the one with a high amount of charge.[107,108] The charges on the outside of this layer will not be neutralized by the underlying polymers/substrate, but instead by counterions. The next layer will bind to these charges and release the

counterions with an entropic gain, which drives the adsorption of the next layer[109,110]. This layer-by-layer process of depositing the film is illustrated in Figure 1.6

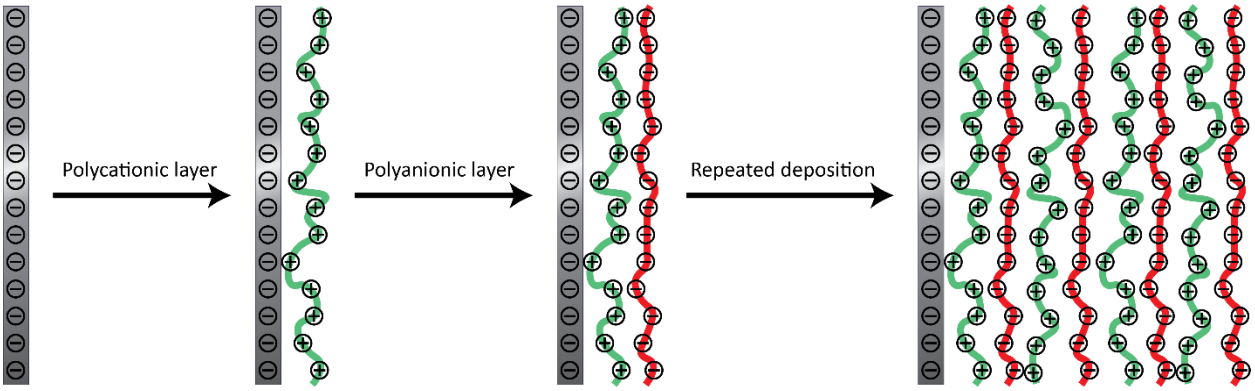

Figure 1.6: Illustration of the layer-by-layer technique used to create multilayer polyelectrolyte films.

While the effects of the charge density of the polyelectrolytes are complicated to predict, it is well documented that factors such as the pH and salt concentration of the solution in which the film is prepared, and the molar weight of the polyelectrolytes, can significantly affect the formation of the film [111–116]. The deposition conditions of the film can be tuned by changing some of these parameters, which then changes the responsiveness of the final film. However, the complicated nature of this type of film makes it difficult to predict the effect of tuning these parameters[117–119]. The effects of changing the pH on the construction of multilayer films have been the subject of several studies. The overall trend observed was that at conditions where both polyelectrolytes had a high charge and similar concentration, the resulting film would be thin compared to the conditions that lead to a large charge density mismatch[120–122].

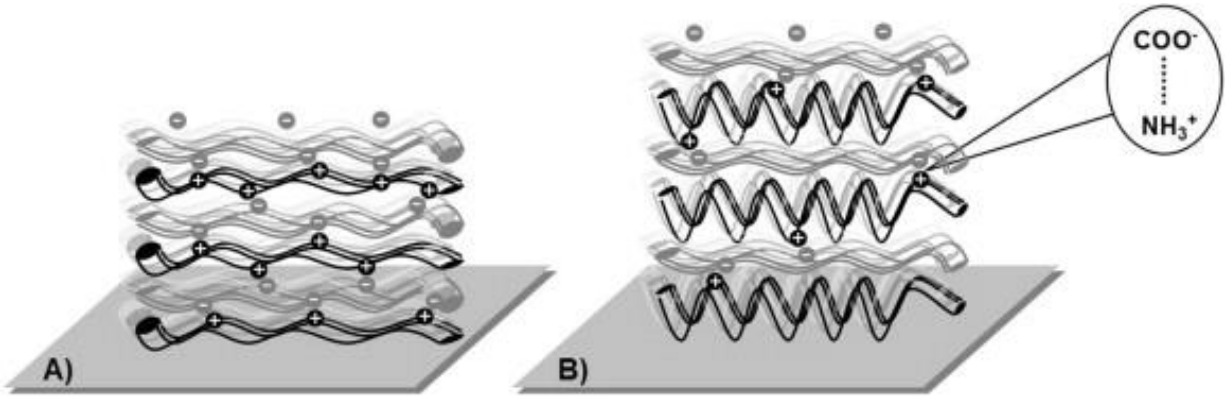

Figure 1.7: Illustration of typical multilayer film created with an equal charge density of the two polyelectrolyte types (A) and uneven charge density (B). Reprinted with permission from G. V. Martins, J. F. Mano, and N. M. Alves, Carbohydrate Polymers, 2010 80, 570-573. Copyright 2009 Elsevier Ltd.[114]

A film obtained at pH conditions with a mismatch of charge density will typically result in one layer being thicker to counter the charges, yielding a thicker film, as illustrated in Figure 1.7. These results also show that by altering the pH, the increase in the thickness of the deposited film thickness can be changed from linear to exponential with the number of layers.

1.4.2 Response of pH on swelling of multilayer films

The swelling of a multilayer film is affected by changes in the pH, as the multilayer is considered to be close to its charge equilibrium under the conditions it was created. By changing the pH, a charge imbalance is introduced due to the change in dissociation degree of the weak polyelectrolytes in the multilayer film. This broken charge equilibrium introduces unmatched charges which require counterions to enter the film, and thus restore the overall charge balance[17,18,123–125]. Effectively, the change in pH from the equilibrium condition will result in film swelling. This is caused by the excess charges in the film which result in counterions entering the film and leading to an increased osmotic pressure[126–130]. When the pH is decreased, the charge on ADA will decrease while that on CHI will increase, leading to an overall more positively charged layer; whereas, increasing the pH will have the opposite effect. Consequently, both decreasing and increasing the pH from the pH at which the film was built will lead to swelling (not necessarily at the same rate), which will increase with further increases/decreases in pH.

In some cases, the effect of pH is studied in buffer solutions where the ionic strength is not considered carefully or where the ionic strength or ion types are not fixed between different pH values.[131,132] In my study, it was observed that the salt concentration, and to some degree the ion type at which the pH is varied, can have a substantial effect on the swelling response between different pH values.

1.4.3 Response of salt on swelling of multilayer films

The salt present with the multilayer film is an important factor affecting the degree of swelling. While changes in pH cause opposite dissociation changes in the two polyelectrolytes comprising the multilayer film, an increased salt concentration results in the dissociation of both polyelectrolytes. When the concentration of salt is increased, the Debye length, which describes the range of the electrostatic potential, also decreases, indicating a more favorable dissociation[133,134]. A charge group of one of the polyelectrolytes competes for either binding to an oppositely charged group of the other polyelectrolyte or with a counterion. With an increase in the salt concentration, and the consequent increase in screening, the interaction of the polyelectrolyte with the counterions becomes more favorable. This increases the

swelling due to the breakage of the interchain bonds of the polyelectrolytes and increased osmotic pressure, as illustrated in Figure 1.8.[127,135]

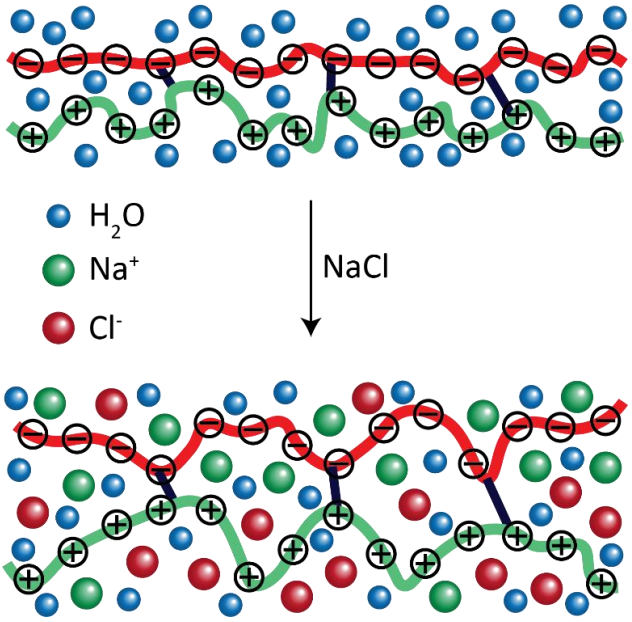

Figure 1.8: Illustration of the effect of salt concentration on the association of multilayer polyelectrolytes.

The typical swelling of a monocomponent weak polyelectrolyte film will be affected by salt, as illustrated in Figure 1.3.[5,37,40,58,136–138] At low salt concentrations (in the neutral regime), the film will have a constant thickness. When salt concentration is increased, the film enters an osmotic regime where it swells because of the increased dissociation on account of the salt concentration. After this regime, the film enters first a salted and then a quasi-neutral regime, where it follows the same swelling trend as that of a strong polyelectrolyte film.

The multilayer film is a more complex system, and film swelling response to changes in salt concentration is similarly difficult to understand completely.[139,140] In this study, to describe the response of the film, it has been considered as a combination of a zwitterionic and a weak monocomponent polyelectrolyte film. When the multilayer film is at charge equilibrium, the internal structure is similar to that of a polyzwitterionic film, where the charges of one polyelectrolyte are paired with the opposite charge of the other polyelectrolyte to form increased crosslinking. If the charge of one of the polyelectrolytes is completely removed, the film becomes similar to a weak cationic/anionic polymer film and has similar swelling behavior under changing salt concentrations as in Figure 1.3. The corresponding results are presented and discussed in section 5.2.

1.5 Friction in weak multilayer films

Originally the plan for this PhD project was to perform friction measurements on the multilayer system as a major part. However, as the project evolved, this system was found to be very complex, and it was more beneficial to spend some more time improving the fundamental understanding with different techniques before considering friction. The results collected from the friction measurements in this study are poorly understood. However, as the preparations for performing these measurements constituted a significant part of this study, these have also been included. The technique chosen to measure the friction requires calibrations which are not straightforward; they can be performed in several different ways, all of which have some drawbacks[141–146]. The method used in this study and how it was implemented is included in section 3 and Appendix C.

Friction is the energy dissipated due to sliding two surfaces against each other and affects everything containing moving parts[147,148]. Therefore, it is interesting to study the fundamental aspects of friction on a molecular scale, which is possible using an AFM. The mechanism and operating procedure of AFM are described in section 2.5. Friction on this scale is important for a range of fields, such as biomedical applications, where obtaining low friction is an important parameter[149–151]. In this study, friction measurements have been used in an effort to improve the understanding of multilayer films.

1.5.1 Amontons' law

The first systematic and significant study on friction was performed by Leonardo da Vinci in the 15th century[152]. He studied the behavior of two macroscopic objects sliding against each other for different types of objects of different sizes. Approximately 200 years later Guillaume Amontons' continued this work and mathematically formulated the discoveries, into an elegant and simple equation, which is known as Amontons law[153]:

$$F_f = \mu F_N \qquad 1.1$$

In this equation, F_f is the friction force opposite to the sliding direction of the moving object, F_N is the normal force exerted from the sliding object, and μ is the friction coefficient that is only dependent on the two types of materials in contact. Based on this, the counterintuitive conclusion was that the friction between two objects was independent of the contact area. This was found to be true for the apparent contact area on a macroscopic scale. However, when looking at smaller scales, defining the contact area becomes more complex and Amontons' law is insufficient to describe friction[154,155].

1.5.2 Contact area

At first glance, the contact area between two objects is quite simple to define. On a macroscopic scale, the apparent contact area of an object is the area hidden by the other object. As most surfaces are not molecularly flat, and instead consist of small asperities, significant apparent contact areas can potentially exist that are not part of the real contact area. It has been shown through resistance measurements that the apparent contact area can be up to 10^4 times larger than the real contact area[156]. This concept is illustrated in Figure 1.9a.

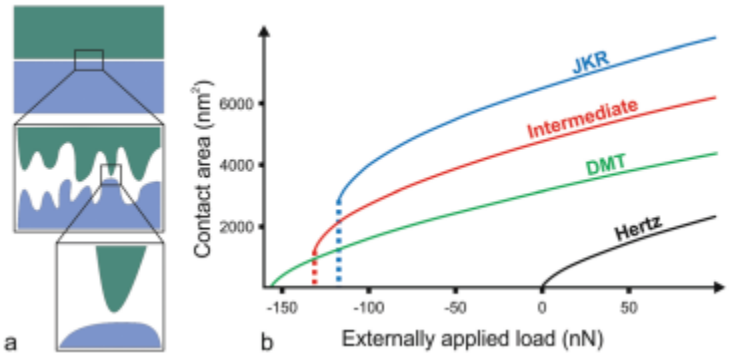

Figure 1.9: a) Apparent contact area on a macroscopic scale and real contact area on a microscopic scale with asperities. b) The dependency of real contact area on applied load according to different models. Reproduced with permission from E. Liamas, S. D. Connell, S. N. Ramakrishna, and A. Sarkar, Nanoscale, 2020, 12, from the Royal Society of Chemistry from which it is adapted with permission from J. Y. Park and M. Salmeron, Chem. Rev., 2014, 114, 677–71141 Copyright 2014 American Chemical Society [157,158]

When the normal force between two surfaces is increased within the range of elastic deformation, the real contact area changes, and this can be described in different ways, including JKR (Johnson– Kendall–Roberts), Hertz, DMT (Derjaguin–Muller–Toporov), and intermediate models. Although these models differ from each other, each of them show that the real contact area increases when the normal force is increased, as shown in Figure 1.9b. From the figure, it can also be observed that the models predict a nonlinear region at the lowest normal forces, and when a sufficiently high force is reached, the contact area almost increases linearly with the normal force. Applying this knowledge to Amontons' law, it follows that friction does depend on the real contact area because the normal force and friction are linearly proportional[159].

1.5.3 Friction mechanisms

There are several mechanisms that influence friction, and they are often not related in a straightforward manner. Therefore, it is challenging, and perhaps even impossible, to describe friction at all length and time scales using a single universal law, as Amontons had attempted. On the nanoscale, parameters such

as surface roughness[160], deformation[161], and sliding speed[157] can give rise to differences in the friction forces between two surfaces. The friction force can roughly be divided into two different types. Mechanical friction which occurs due to surface roughness and asperities interlocking, and friction occurring due to the breakage of physical bonds either at the interface between the two surfaces or inside one of the objects[162]. These two types of friction depend on different parameters. However, to understand to underlying dynamics causing friction, it is preferable to simplify the system such that one of these types becomes significantly dominant.

An additional contributing factor to the friction between two surfaces is their forces perpendicular to the surface. If the surfaces have large repulsive forces, a strong normal force is required before they come into contact with each other. This typically results in low friction, as mechanical friction is not present here and the formation of bonds between the surfaces is not favorable. Contrastingly, if the surfaces show adhesion, a non-zero friction force can be obtained at zero normal force, which is not consistent with Amontons' law. However, by introducing a constant adhesion force together with the normal force, the equation can be adapted to fit situations that include adhesion. This results in an offset where zero normal force does not necessarily result in zero friction[155]. The tweaked version of Amontons law, where F_0 is the adhesion force, can be written as:

$$F_f = \mu(F_0 + F_N) \qquad 1.2$$

In this study, the friction on multilayer films of ADA and CHI under different swelling conditions was measured against a CHI coated probe and compared to the swelling results of the film. These results and their interpretations are presented in section 5.3.

2 Methods of preparation and analysis

In this section, the procedures for preparing the different films studied in this project and the techniques used to investigate them are discussed. The list of chemicals used can be found in the two papers in Appendices A and B.

2.1 Synthesis of monocomponent polymer films

The polymers used in section 5.1 and in the paper in Appendix A were synthesized and applied to the substrate by a fellow PhD student in our group. Three different types of charged polymer films with varied crosslinking abilities and otherwise similar properties were created. They were therefore created using three different monomers, including one charged, one cross-linkable, and one nonionic. The charged monomer contained 25 mol% of either 2-(methacryloyloxy)ethyl]trimethylammonium chloride (METAC), 3-Sulfopropyl methacrylate potassium (SPMAK), or N-(2-methacryloyloxyethyl)-N,N-dimethylammonio butanesulfonate (PMABS) for cationic, anionic, and zwitterionic films, respectively. The cross-linkable monomer was either 5, 10, or 15 mol% allyl methacrylate (AMA) depending on the degree of crosslinking required. Subsequently, the final nonionic polymer was either 70, 65, or 60 mol% butyl methacrylate (BMA). The chemical structures of the polymers are shown in Figure 2.1.

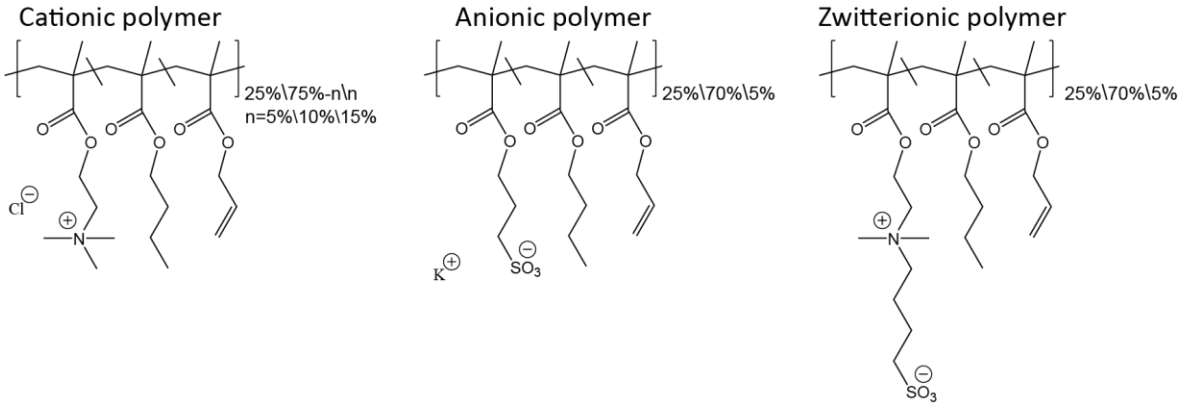

Figure 2.1: Chemical structures of cationic, anionic, and zwitterionic polymers.

Synthesis of polymers: During the synthesis, the charged monomer was polymerized with AMA and BMA in the targeted molar ratio using 4-cyano-4-[(dodecylsulfanylthiocarbonyl)sulfanyl] pentanoic acid (CDPA) and 4,4'-Azobis(4-cyanovaleric acid (ACVA). The cationic and anionic polymers were synthesized in a 4:1 DMF/H_2O solution, whereas the zwitterionic polymers were synthesized in 2,2,2-trifluoroethanol (TFE). The total monomer concentration was maintained at 2 M, and the solution was degassed by sparging with nitrogen for 30 min before the temperature was raised to 70 °C, initiating the polymerization. The

polymerization was performed in a nitrogen atmosphere and monitored using ^{1}H nuclear magnetic resonance spectroscopy (^{1}H-NMR) until nearly complete. Subsequently, the reaction precipitated to yield cold stirred diethyl ether. After collecting using vacuum filtration, the product was dried overnight at 30 °C in a vacuum oven and characterized by ^{1}H-NMR to obtain the approximate composition of the polymer.

Preparing the substrate: The silicon wafers used as the substrate for the films were functionalized with silane before the film could be added. The wafers were rinsed twice with water, ethanol, and acetone, and then with a nitrogen stream. Subsequently, they were plasma cleaned for 180 sec under a 500 mTorr water vapor atmosphere, before being submerged in a 15 vol.% 3-mercaptopropyl trimethoxysilane (MPTMS) in toluene solution and stirred. After 3 h, the functionalized wafers were removed from the solution, dried using a nitrogen gas stream, and placed in a 130 °C vacuum oven to induce silanization.

Coating of the substrate: The polymer solution was spin-coated onto the functionalized wafer and anchored with thermally initiated crosslinking. First, a 1 wt.% polymer in TFE solution was prepared, along with tetra-functional thiol Pentaerythritol tetrakis(3-mercaptopropionate) (PETMP) and radical initiator ACVA. The PETMP, though tetra-functional, is loaded at a 1:1 molar ratio to that of the -ene- functionality of the polymer, and the amount of ACVA added is lower at a 1:4 molar ratio to that of the -ene functionality. After stirring for 30 min the solution was spin-coated onto the previously prepared thiol-functionalized silicon wafer (2000 rpm for 40 sec).

Crosslinking the film: The substrate was placed in a 90 °C oven for 2 h to induce a thermally initiated thiol–ene crosslinking reaction. The wafers were then removed from the oven and cooled to 23 °C (room temperature) before being washed twice with an excess of water, to remove any unattached materials, and then dried with nitrogen gas.

2.2 Creating multilayer films

The multilayer films used in sections 5.2 and 5.3 and in the paper in Appendix B were prepared using CHI and ADA. While CHI was used directly without any modification after purchase, ADA was synthesized from alginate. The films are created using a layer-by-layer technique in either a custom-made flow cell or in the flow cell of a quartz crystal microbalance with dissipation monitoring (QCM-D). In this section, the steps to prepare these films are presented.

2.2.1 Oxidized alginate and chitosan

CHI is a weak cationic linear polysaccharide, which is found naturally in the exoskeleton of some shellfish and insects[163]. Contrary to most polysaccharides, CHI is cationic, which combined with its other properties, such as non-toxicity, biocompatibility, and biodegradability makes it a very interesting structure for use in multilayers[164–167]. The CHI used was purchased commercially in a purified state, and its chemical structure is shown in Figure 2.2.

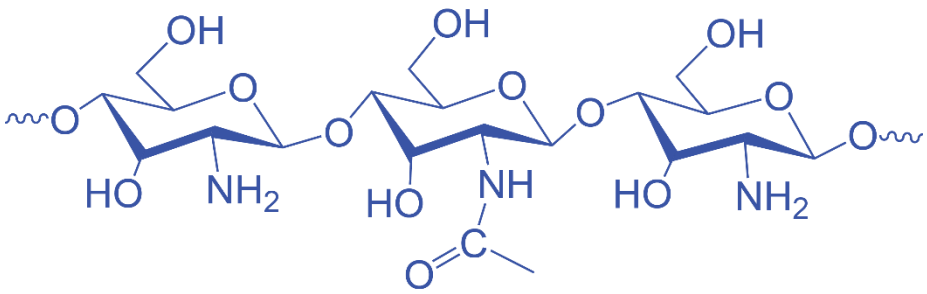

Figure 2.2: Molecular structure of Chitosan. Adapted with permission from [168].

The negative polymer is oxidized alginate or ADA which was synthesized from alginate. Alginate is a weak anionic linear polysaccharide that is found naturally (e.g., in brown seaweed). It has properties similar to that of CHI, making it an interesting material for biological applications, as it is biocompatible, biodegradable, and non-toxic[169–171]. The modification of alginate to ADA results in a ring opening that creates aldehyde groups. The synthesis was performed using a simple and established procedure[95,172,173]. First, 10 g of sodium alginate and 20 mol% sodium periodate (relative to the repeating groups of alginate) were dissolved in 1 L ultrapure water and stirred in darkness for 24 h. Then, 3.5 mL ethylene glycol was added and stirred for 30 min to quench the reaction. The ADA was then precipitated by adding 3 g of sodium chloride and 1 L of ethanol, after which it was filtered. Then, the precipitation process was repeated first by dissolving the ADA in 500 mL ultrapure water and adding 1 g sodium chloride followed by the addition of 500 mL ethanol and filtration. The process was repeated with 500 mL ultrapure water, 0.5 g sodium chloride, and 1 L acetone. Finally, ADA was washed with 500 mL ethanol and then freeze-dried. The chemical structure before and after oxidation is shown in Figure 2.3.

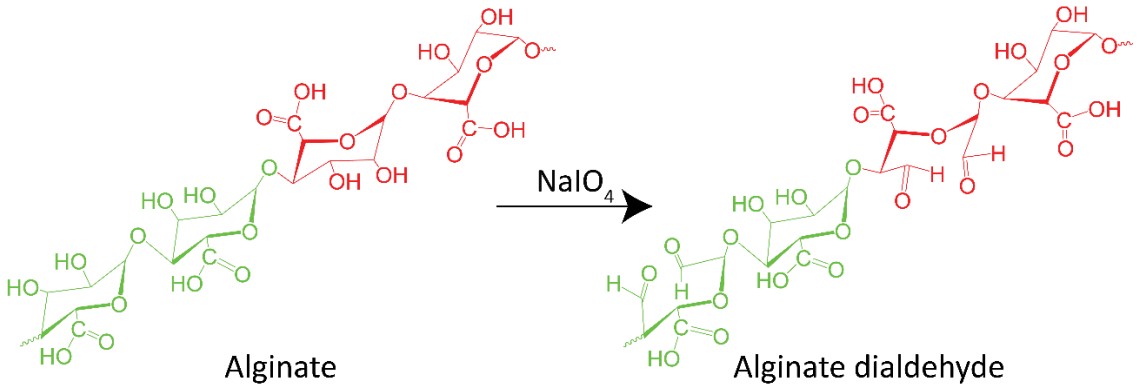

Figure 2.3: Molecular structure of alginate and alginate dialdehyde (ADA). Adapted with permission from [168].

The 20 mol% of sodium periodate used in the oxidation of alginate determines the oxidation degree, which indicates the ratio of aldehyde groups created. These aldehyde groups form imine bonds with the amine groups of CHI through Schiff base reactions, which causes a chemical crosslinking between the layers formed in the multilayered film. The main effect of the crosslinking is to keep the film stable and reversible even if all electrostatic bonds are fully screened[10,102,128]. Figure 2.4 illustrates how these bonds can allow a multilayer film to swell and still maintain its structure without the physical crosslinks.

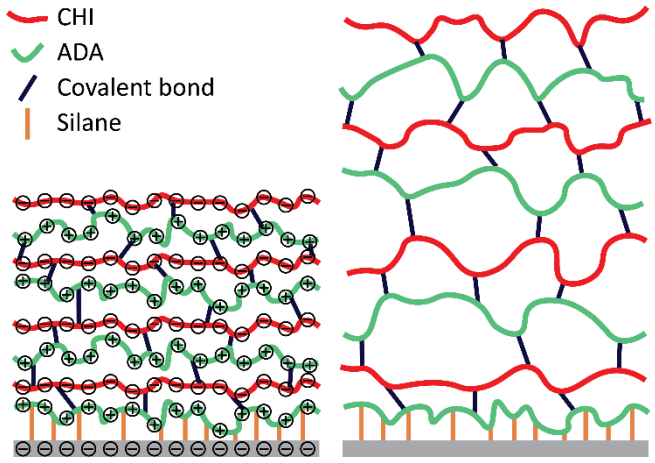

Figure 2.4: Swelling of a multilayer film with electrostatic and covalent bonds (left) and the same film with only the covalent bonds to illustrate the maintained stability.

To prepare the multilayer film a CHI and an ADA solution were used. The target concentrations of these solutions were either 100 mg/L for CHI or 200 mg/L for ADA in 15 mM NaCl solution at a pH value of either 3 or 6 in ultrapure water. At pH 3, the solutions can be prepared by simply mixing the components; however, at pH 6, CHI cannot be dissolved directly. Instead, a concentrated CHI solution was prepared using HCl, in which CHI can be dissolved, and then used as a stock solution to obtain the desired

concentration of 100 mg/L in ultrapure water; subsequently, the pH was adjusted using NaOH, and the total ionic strength was adjusted to 15 mM NaCl.

2.2.2 Preparation of substrate

The substrates used for the multilayers contain SiO_2 at the interface with the multilayer film, which becomes negatively charged when hydrated in water. Although CHI can bind electrostatically to the substrate, it results in the film detaching in solutions with large screening. To avoid this, the substrates were modified using 3-glycidoxypropyltrimethoxysilane (GPS), which binds to the substrate and allows CHI to be grafted covalently[128,174].

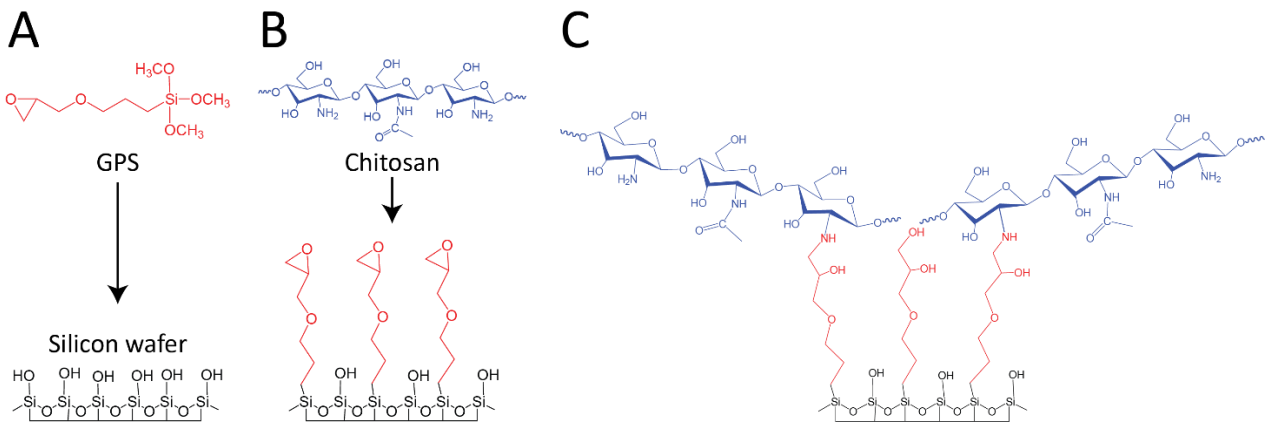

Figure 2.5: Procedure for preparing the substrate for multilayer film. A) Uncoated silicon substrate and GPS. B) Silanized silicon substrate and CHI. C) Silanized silicon substrate with initial grafted chitosan layer. Adapted with permission from [168].

The substrates were prepared by first rinsing with acetone, ethanol, and ultrapure water, and then plasma cleaning for 5 min (using a Harrick Plasma PDC-32G plasma cleaner at medium power). Then the substrate was submerged in a solution of 18 vol.% acetone for 24 h, followed by rinsing with acetone. The substrate was then submerged in a 1000 mg/L CHI solution with 15 mM NaCl and the desired pH for the multilayer build. After 1 h and rinsing in ultrapure water with 15 mM NaCl and the pH adjusted to match that of the CHI and ADA solutions, the substrate was placed in the flow cell and the process of depositing the layers was started. The change in the chemical structure of the substrate is illustrated in Figure 2.5.

2.2.3 Flow cell

The multilayer film was prepared in two different ways following the same procedure. For QCM-D measurements, the film was deposited in the flow cell of QCM-D on a QCM-D sensor. For ellipsometry measurements, the film was deposited on a silicon wafer in a custom-made flow cell that was similar to the QCM-D flow cell with respect to the internal volume, placement of the inlet and outlet, and coated

area. The custom flow cell was used to replicate the layer formed in the QCM-D under the same conditions, while using a silicon wafer substrate, which is better for ellipsometry measurements. This allowed the substrate to be bigger than the QCM-D sensor, which is necessary for using the liquid cells of the ellipsometer and AFM (although the coated area was the same to have comparable conditions for the deposition process).

The setup shown in Figure 2.6 was used to prepare the layers. In this setup, a hydrostatic pump was placed after the flow cell and a constant flow rate of 250 µL/min was maintained. The build process was then started with 30 min of rinsing, followed by 40 min of ADA deposition, 30 min of rinsing, and finally 40 min of CHI deposition. This process was repeated until the desired number of layers were deposited.

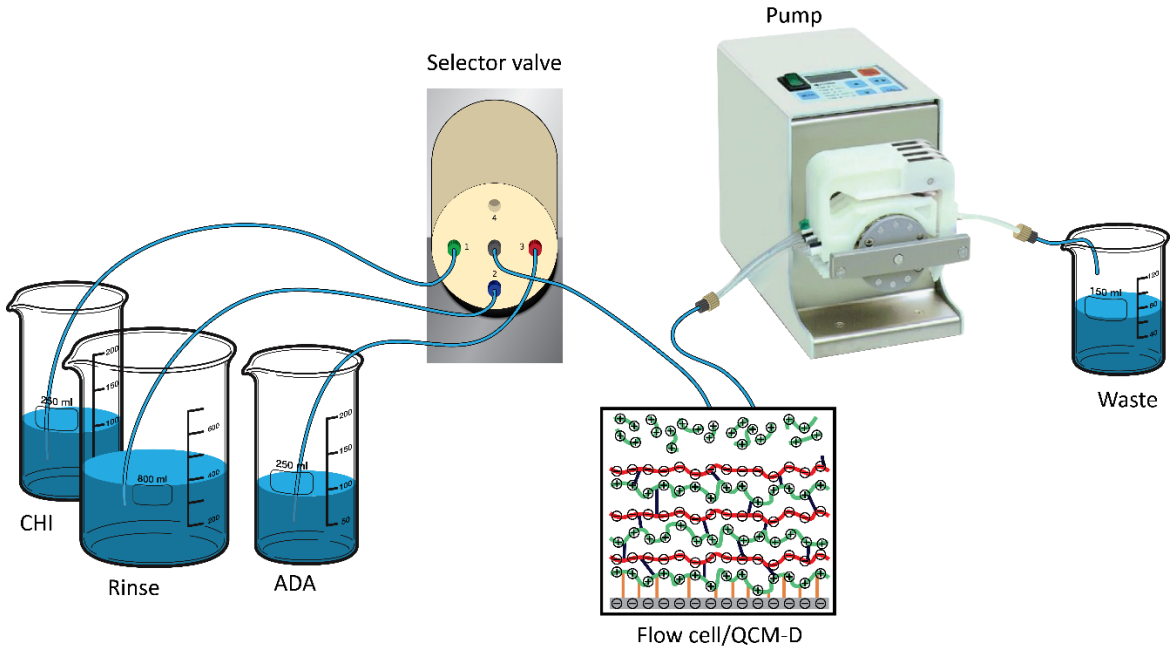

Figure 2.6: Schematic of an experimental setup for preparing multilayer films with the layer-by-layer technique.

Solutions of different pH values were used for the ellipsometry and QCM-D measurements. To maintain an identical and simple ion type across different pH values, they were not prepared in a buffer solution; however, this posed challenges when dealing with high pH. The solutions at pH values of 3 and 6 were stable enough during the time when the layers were deposited and measurements were performed; however, the solution at pH 9 changed during the full length of the measurements and needed to be adjusted right before each measurement with that pH to maintain it at the correct pH value. This was especially a challenge during the QCM-D measurements because the flow rate was very low, resulting in

slow stabilizing when the pH was changed. During ellipsometry, the liquid was exchanged with a flowrate of approximately 100 mL/min.

2.2.4 Automated selector Valve

The solution at the inlet tube can be changed manually by turning the pump off and moving the tube to a new beaker. However, especially during QCM-D measurements, this caused perturbations that can be seen in the data and introduced inaccuracy in the timing. To avoid these concerns, an automated selector valve (ASV, Vici Valco - C25-3184EUHA) was utilized for building the layers. This ASV is programmable and can be timed to switch between the different solutions at the inlet without moving the tubes or turning the pump off. The internal schematic of ASV is illustrated in Figure 2.7, where it is seen that the selector valve has eight different inlets and one outlet. By rotating the red tube, the active inlet that is connected to the outlet can be changed. The movement of this tube is possible to program so that it changes according to a specific pattern with a specific timing.

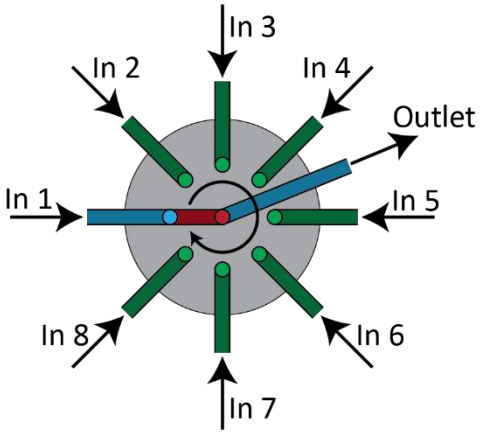

Figure 2.7: Internal schematic of the automated selector valve.

I have written the software and interface for the ASV in LabVIEW (National Instruments). This ASV had a huge impact on the number of samples practically possible to create because previously it was a very tedious process, and required many hours to obtain a single multilayer film. The instrument and its software have benefited several other group members, both for preparing multilayered films and to perform other tasks where timed alternation was required in the solutions. The interface of the program used to prepare the multilayer films is shown in Figure 2.14.

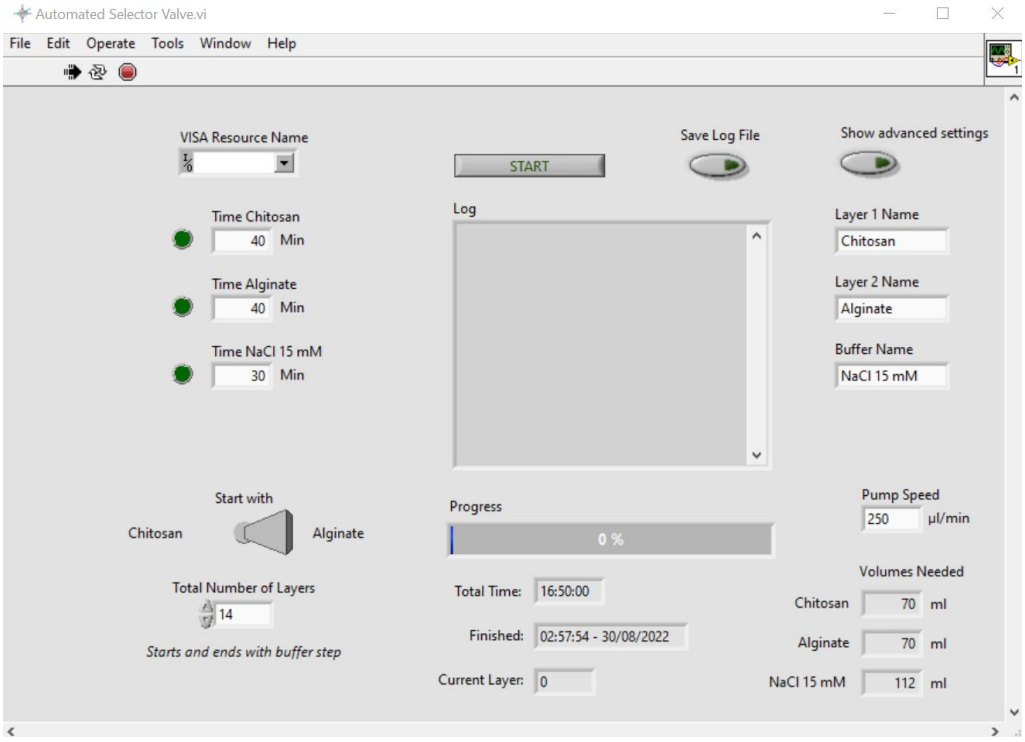

Figure 2.8: Graphical user interface of the program for controlling the automated selector valve written in LabVIEW.

2.3 Quartz crystal microbalance with dissipation monitoring

The QCM-D is commonly used for measuring the buildup of multilayered films and the response of the films to changes. The QCM-D is extremely sensitive to changes in the mass of a film and to some conformational changes, making it the favored technique in a majority of studies on multilayered films[114,121,122,128,175–180]. A Q-Sense E1 QCM-D equipped with a standard Q-Sense flow module (Biolin Scientific, Gothenburg, Sweden) was used, as shown in Figure 2.9.

Figure 2.9: Quartz crystal microbalance with dissipation monitoring. The Q-Sense E1 QCM-D is equipped with a standard Q-Sense flow module.

The QCM-D performs the measurements using a sensor chip consisting of a thin quartz disc at the core with an electrode on either side, as shown in Figure 2.10. A voltage applied over the electrodes leads to a deformation of the core, and an alternating voltage oscillates the core. When the alternating voltage is tuned to match the resonance frequency of the core, a standing wave is created inside it. The principle behind this is known as the inverted piezoelectric effect[181,182].

The resonance frequency, f_n, of an acoustic wave in the quartz core of the sensor chip can be calculated from the speed of the wave, v, and its wavelength, λ. For a standing wave, the product of the half-wavelength of the wave and an integer, n, should match the thickness of the quartz core, h; this is given by the relation:

$$\frac{\lambda}{2} = \frac{h}{n} \qquad and \qquad f_n = \frac{v}{\lambda} = \frac{vn}{2h} \tag{2.1}$$

Therefore, the resonance frequency depends on some constants determined by the properties and thickness of the quartz core. When a thin film is added to the surface of the sensor chip, the total thickness changes, leading to a shift in the frequency, Δf. This frequency shift is one of the parameters measured in QCM-D, and for the simple case of a thin rigid film, the following relation is obtained:

$$\Delta f = -\frac{nf_0}{\rho_0 h} = -C\Delta m \tag{2.2}$$

Here ρ_0 is the density of the quartz crystal and Δm is the mass change, and this equation corresponds to the Sauerbrey model[183,184]. This model shows an inverse relationship between the added mass and frequency, which is illustrated in Figure 2.10.

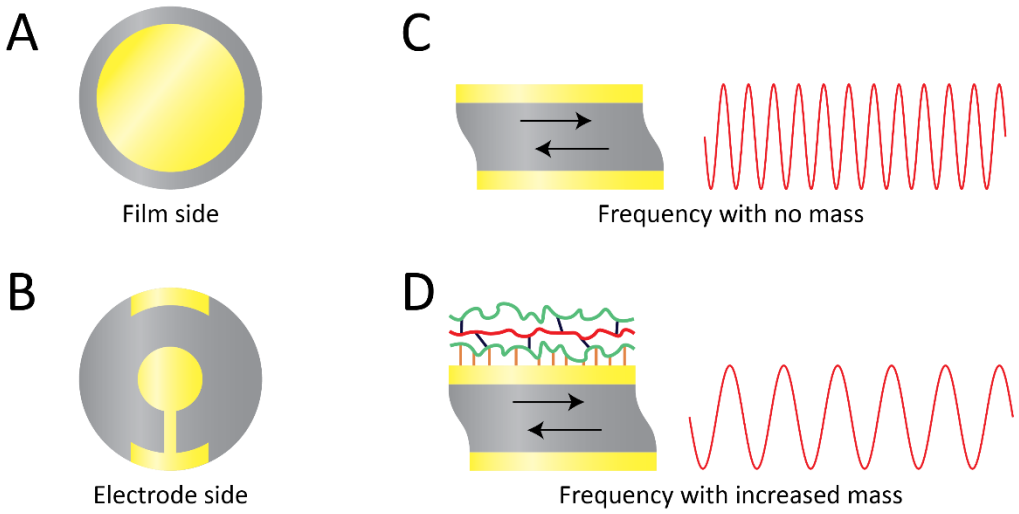

Figure 2.10: Illustration of QCM-D chip (QSX335) of the side used for film substrate (A) and the electrode side (B). Illustration of the oscillation frequency of chip without mass (C) and with increased mass causing decreased frequency (D).

By intermittently turning off the alternating voltage over the quartz core, the decay of the oscillations can be monitored. Based on this, a dissipation or dampening factor, D, is calculated as the energy lost per oscillation, E_{lost}, relative to the total stored energy, E_{stored}:

$$D = \frac{E_{lost}}{2\pi E_{stored}} \qquad 2.3$$

The dissipation for a rigid film is typically relatively small as the film follows the oscillations with little deformation. A more flexible film is deformed more, leading to a greater energy dissipation due to the dampening effects of the liquid[185]. This concept is illustrated in Figure 2.11. The dissipation of a film is dependent on, amongst other factors, the viscoelastic properties of the film. If these properties are changed, for example by adjusting the number of crosslinks or the degree of swelling of the film, a dissipation shift will be observed. Therefore, the dissipation shift will provide some information regarding the configuration of the layer.

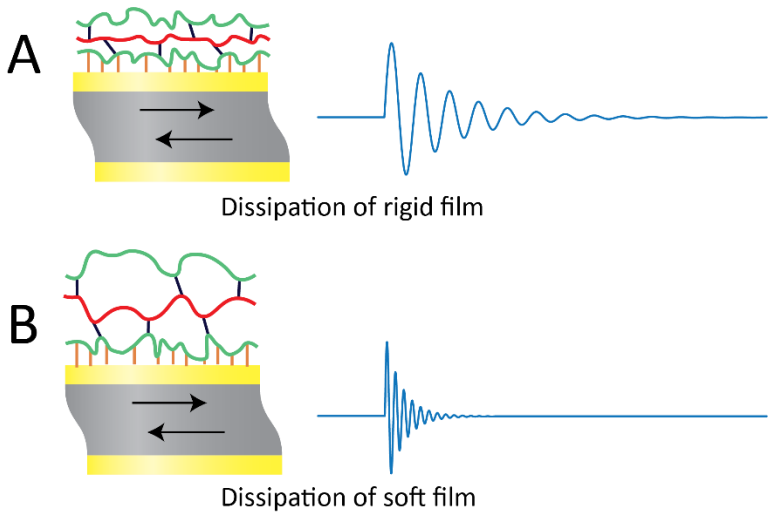

Figure 2.11: Illustration of dissipation shift with a rigid film (A) and with a more swollen film (B).

Unfortunately, when the dissipation shift becomes significant ($\Delta D > 10^{-6}$), the linear relation between added mass and frequency shift no longer holds, and instead, the Sauerbrey model underestimates the mass[186]. For the thin multilayered polymer films studied in this project, the dissipation shift is too large for using the Sauerbrey model to translate the frequency shift into mass. However, even though the model does not hold linearly, the trends still provide information regarding the changes that happen. Typically, when a polymer film swells, the frequency decreases, implying an increase in the mass due to the higher amount of water present inside the film; in addition, the dissipation increases indicating a less restrictive conformation.

The Voigt model is another popular model used with QCM-D data. This model takes the viscoelasticity of a film into account and is therefore typically more appropriate for polymer films. This model can be described using the following relations.

$$\Delta f = \mathrm{Im}\left(\frac{\beta}{2\pi\rho_0 h_0}\right) \qquad and \qquad \Delta D = -\mathrm{Re}\left(\frac{\beta}{\pi f \rho_0 h_0}\right) \tag{2.4}$$

where f, ρ_0, and h_0 are the resonant frequency, density, and thickness of the quartz core, respectively, and β is a variable that depends on the shear elasticity and shear viscosity of the film[187–189]. By fitting this model to multiple overtones of the Δf and ΔD data, the thickness and shear elasticity of the polymer films can be determined, along with either the films density or shear viscosity, if the other is known. Typically, the density of the polymer film is either determined using another technique or by approximation. Although this model is much more complex than the Sauerbrey model and has the drawback that the density of the film should be known, it is more accurate for some types of films.

Both models assume that the film is homogeneous, which is not the case for the multilayered polymer films used in this study. Most of the charges within the film match with an opposite charge from the other polymer, causing attraction and resulting in a dense layer. The last layer at the top of the film contains unmatched charges, that depending on the counterion concentration, will have some degree of entropic repulsion. This yields a significantly less dense layer, where the polymer chains stretch into the bulk solution. Thus, a density gradient of the polymer is created, which affects the frequency shift and especially the dissipation shift. The conformation of the top layer can therefore have a significant influence in comparison to the fraction of the film it constitutes mass-wise[136].

The QCM-D measurements were performed on the multilayers to understand their responses to different stimuli, and therefore the frequency and dissipation shifts were not translated into physical thickness, instead, the shifts were investigated relative to each other. This increased the transparency of the comparisons, as they were not dependent on underlying assumptions from a fitted model.

2.4 Ellipsometry

Ellipsometry is an optical technique that measures the changes in polarization of thin transparent films. The thickness of a film can be determined by fitting the measurement to a specific model for the film. The advantage of this technique is that it is non-invasive, making it optimal for repeated measurements at the same location on a sample under different conditions. Typically, the optical properties of a film depend significantly on its thickness, and therefore, ellipsometry is sensitive to very small thickness changes. As this is an indirect technique to determine the thickness, the quality of the thickness measurement depends significantly on the model the film is fitted to; therefore, if the model represents the film poorly, the measurement will not be accurate. Ellipsometry is commonly used on polymer films that can be represented well with the available models[190,191].

Light can be seen as an electromagnetic wave with an electrical field, described by an E vector perpendicular to the direction of the light. If this vector moves in a chaotic pattern, the light is called unpolarized, which is the case for most light sources in our daily life, such as, sunrays, typical light bulbs, and candle lights. However, if the E vector moves in a well-defined pattern, the light is called polarized. The E vector of polarized light can be described by two harmonic oscillators, perpendicular to each other along the direction of the light (illustrated as the red and blue plane in Figure 2.12). Although these have the same frequency, they can have different amplitude and phase. If the E vector is observed along the direction of propagation of the light, it moves in an elliptical pattern, which will be either left or right polarized depending on whether it moves anticlockwise or clockwise, respectively. The phase and the

amplitude determine the shape of this ellipse, which turns into a line if the two oscillators have the same phase or the amplitude of one of them is zero; furthermore, it turns into a circle if the amplitudes are equal and the phases are offset by $\pi/2$. These are known as linear and circularly polarized lights, respectively, and the manipulations that can be performed with these types of polarized light are the foundation for ellipsometry.

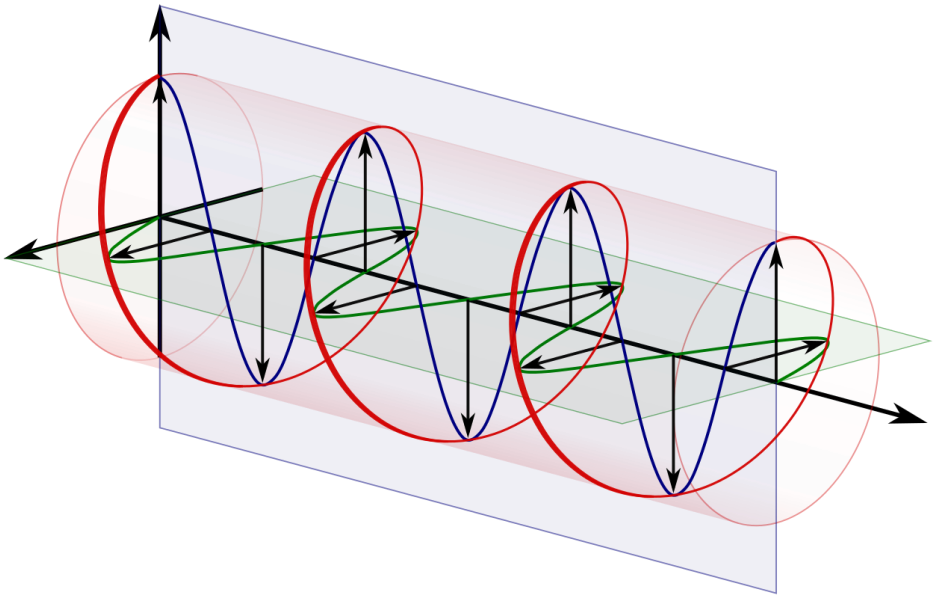

Figure 2.12: Illustration of components of polarized light. Reprinted with permission from [192].

In ellipsometry, light is manipulated using two different types of filters. With a linear polarizer, which polarizes the E vector linearly in one direction, and with a retarder which allows one component of the E vector to pass through freely and slows the other component passing through, causing a phase shift of the light. The effects of both these filters depend on their rotation. When the light hits the sample, it is partly transmitted and partly reflected. The light that is transmitted will continue further, at a different angle determined by Snell's law, to the bottom of the layer where some of it will be reflected up again. This creates interference and the outgoing light is phase shifted to a degree that depends on the optical properties and the thickness of the film. This phase shift, β, is calculated as:

$$\beta = \frac{2\,\pi\,d\,n\,cos\theta_t}{\lambda} \qquad 2.5$$

where *d* is the thickness of the film, *n* is the real part of the refractive index, θ_t is the angle of the light from the normal of the surface, and λ is the wavelength of the light.[193]

Figure 2.13 shows the main components of the ellipsometer. First, there is a light source that sends out light at a specific wavelength. Next, is a linear polarizer which has an angle that determines the direction in which the light is polarized. Subsequently, the compensator is present which is a retarder fixed at a specific angle ($\pi/4$). Next, the sample is placed followed by the analyzer, which is another linear polarizer. Finally, the light hits the detector, which measures the intensity.

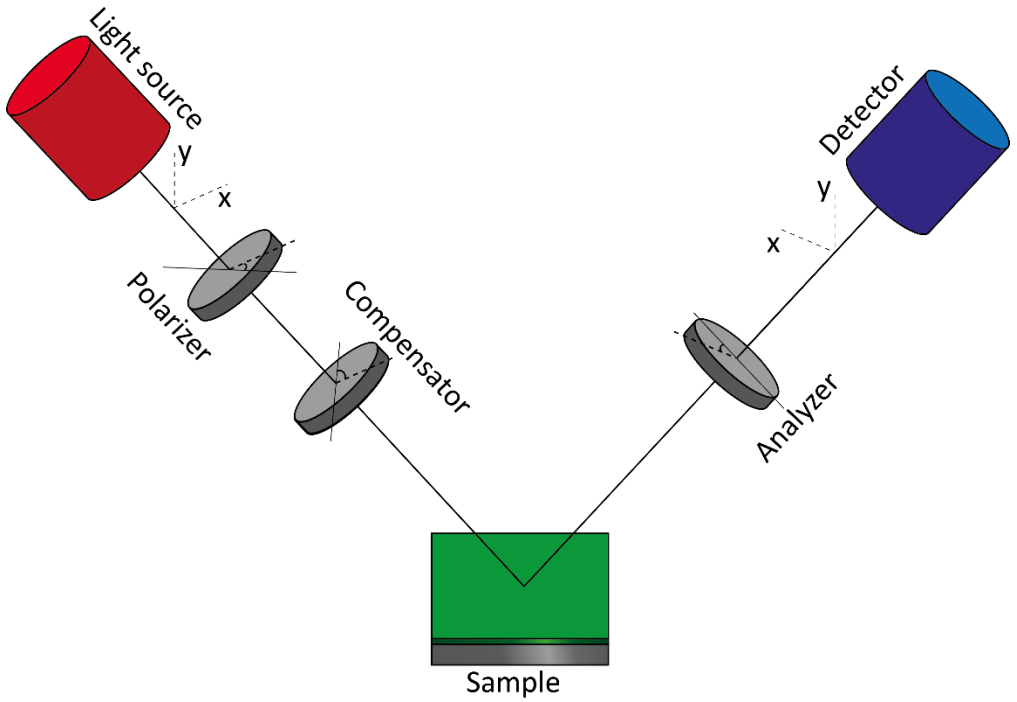

Figure 2.13: Illustration of the components present in an ellipsometer

When polarized light interacts with a thin film at an angle, the properties of the film typically result in a different polarization of the outgoing light. When linearly polarized light interacts with the film, it typically gets some sort of elliptical polarization. However, if the incoming light has a specific elliptical polarization in the opposite direction, the outgoing light is linearly polarized. If a linear polarizer is placed after the sample and rotated $\pi/2$ to the polarized light, the outgoing beam would be completely canceled. This is how the ellipsometer works; the polarizer and analyzer are rotated iteratively to determine when the minimum intensity is obtained at the detector. Then, these angles are used to determine the properties of the film.

The effect of the different components can be described using Jones calculus where the light is represented with a vector. In addition, the influence of the components can be described using a matrix

that describes the effect and the rotation matrix. The Jones matrices, including the linear polarizer, T_L, the retarder, T_R, and the sample, T_S, are described by

$$T_L = \begin{bmatrix} 1 & 0 \\ 0 & 0 \end{bmatrix} \qquad T_R = \begin{bmatrix} 1 & 0 \\ 0 & \rho_C \end{bmatrix} \qquad T_S = \begin{bmatrix} r_p & 0 \\ 0 & r_s \end{bmatrix} \tag{2.6}$$

where $\rho_C = \exp(i\delta_C)$ causes a phase shift of δ_C while r_p and r_s are the reflection coefficients given by Fresnel's equations. The complete effect on the light is described by:

$$E_f = T_A R(A) T_S R(-C) T_C R(C - P) T_P E_i \tag{2.7}$$

where R(x) corresponds to the rotational matrix and x refers to the angle of the component. Based on the matrix calculations, and setting the light at the detector to zero, the following relation is obtained:

$$\rho_s = \frac{r_p}{r_s} = \tan \Psi \, e^{i\Delta} \tag{2.8}$$

where $\Psi = -A$ and $\Delta = 2(P - \pi/4)$. The properties of the film can be estimated by measuring Ψ and Δ for a range of wavelengths of light and using them along with equation 2.5. During dry measurements, this is typically repeated for a range of angles, θ_t, to collect more data for a better fit. However, if the sample is hydrated, the measurement can be performed at only one angle with most types of ellipsometers, including the one used in this study.

To determine the thickness of the polymer films, the refractive index of the film is required during ellipsometry. As the refractive index of the film is not known and changes depending on the degree of swelling and ion concentration inside the film, the index is fitted along with the thickness. To specify the physical significance of the fitting of the refractive index of the polymer film, it is described using the Cauchy relation:

$$n(\lambda) = A + \frac{B}{\lambda^2} + \frac{C}{\lambda^4} \tag{2.9}$$

where λ is the wavelength, and A, B, and C are constants. Typically, C has a small influence and is set to zero to limit the number of fitting parameters; A and B are fitted, which is necessary to obtain a meaningful fit for the thickness.[194]

The polymer films studied in this project were prepared on a silicon wafer having an approximately 100-nm-thick SiO_2 layer on top and hydrated in ultrapure water containing a salt of a specific type and concentration. A model for these layers was built in the software of the ellipsometer using the thickness

and refractive properties of each layer; an intermediate layer of 1 nm thickness was added between these two layers. In contrast to the polymer layer, the refractive properties of the layers below were known and fixed throughout the measurements. The ambient conditions include the solution in which the refractive index is also needed, which depends on the type of salt and its concentration. The process for characterizing the ambient solution is described later in this section and the model is shown in Figure 2.14.

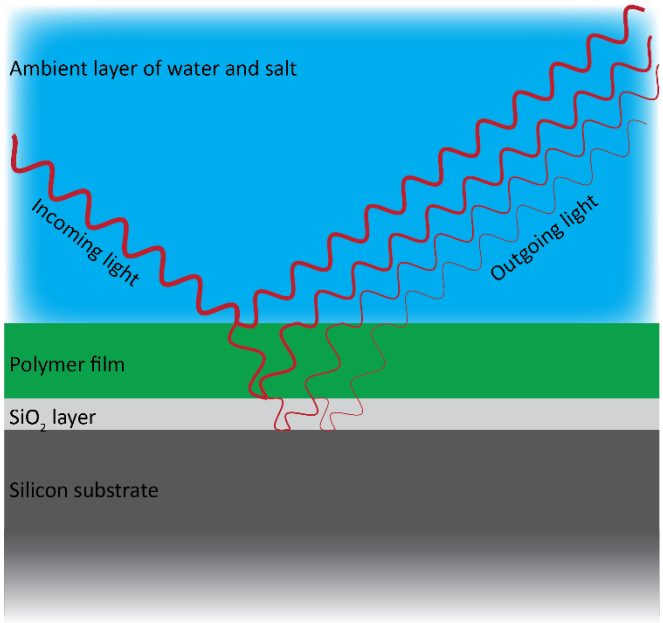

Figure 2.14: Illustration of the layers in the ellipsometry model.

This model is quite simple compared to the possible additions to it. Three different variables were fitted, including the A and B values for the Cauchy relation of the polymer film and the thickness of the polymer film. Several other additions, such as angle offset of the sample, roughness of the polymer film surface, and different models describing a gradient of density through the polymer film, can increase the physical accuracy of the model. However, this will increase the number of fitting parameters and can destabilize the fit of the thickness[193]. Therefore, it was preferred to keep the layer as simple as possible while maintaining a good fit for the data obtained. To judge the quality of the fit, the mean squared error (MSE) of the fit was calculated. Although it is beneficial to have the lowest possible MSE while keeping the fitting parameters down, in this study, the fit for the films was considered good when the MSE was below 20.

To obtain the refractive index of the salt solutions used to hydrate the polymer films, a blank wafer was first measured in the air to determine the exact thickness of the SiO_2 layer. The wafer was then hydrated in ultrapure water, where the ambient conditions were described with a Cauchy model; A and B were fitted as the only fitting parameters with a model of the silicon substrate, 1-nm-thick silicone–SiO_2

intermediate layer, and the SiO_2 layer with a fixed thickness. Subsequently, the concentration of salt in the solution was increased and the A and B values of the solution were fitted again. This was repeated for each concentration of all the salts used for the strong polyelectrolyte films and those used on the weak multilayered films; the results obtained are shown in Figure 2.15. Although the ambient conditions were described using the Cauchy model during the measurements of the polymer films, the A and B values of the ambient conditions were fixed according to the determined values. This method is reported in the literature and yields values of refractive index that fit well with the known values obtained using methods for determining refractive indices[58,61]. As can be seen from the values of A and B in the figure, the salt concentration and ion types changed very little till approximately 100 mM. At higher salt concentrations this refractive index becomes very important, and completely different thickness values will be obtained is the refractive index of water is used instead of correcting for the salt. The exact values of A and B are provided in tables in the supporting information in Appendix A and B.

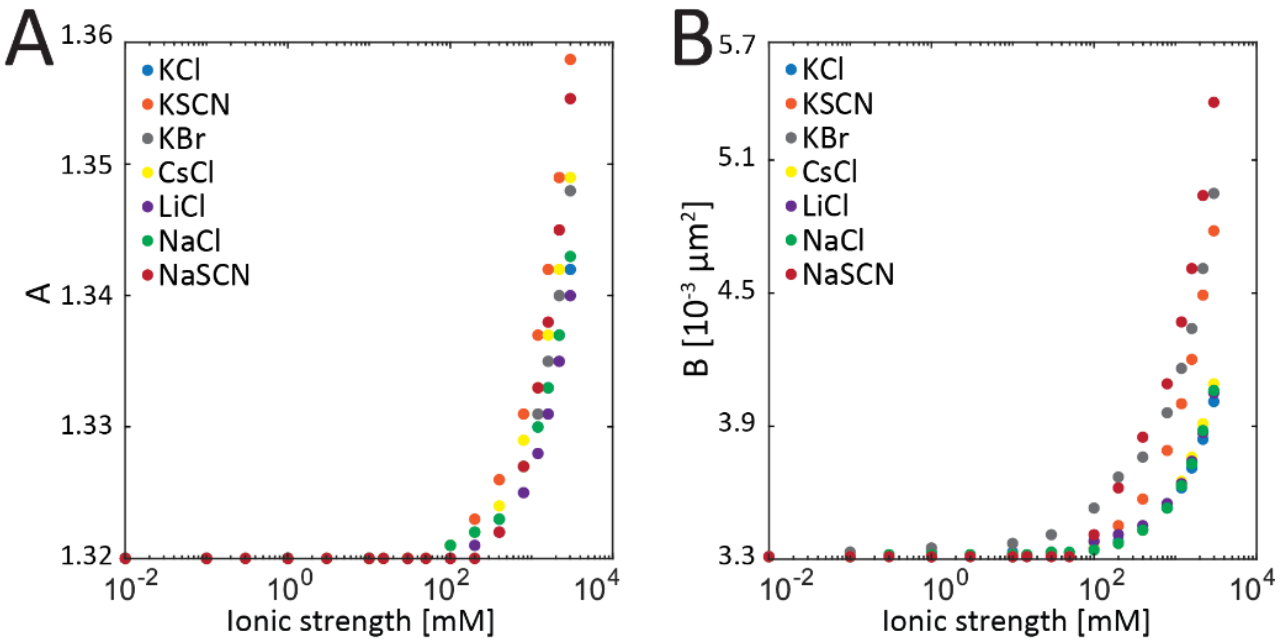

Figure 2.15: Experimentally determined A and B values for the Cauchy model describing the change in refractive index with ionic strength and ion types of the ambient layer.

In this study, a variable angle spectroscopic ellipsometer (M-2000, J. A. Woollam Co., Inc.) was used, and the polymer films were analyzed at 25 °C with a wavelength in the range of 250–1000 nm for all salts, except for KSCN which was measured in the range of 400–1000 nm because SCN^- absorbs light at lower wavelengths. The sample was inserted into the liquid cell of the ellipsometer and hydrated in a 0.01 mM solution of the chosen salt for 1 h. Subsequently, the solution was changed to a 3000 mM solution of the

same salt and back again to reconfigure the film to a stable configuration. Then, the ellipsometry measurement was started at 0.01 mM concentration and set to measure every 10 sec. After the thickness stabilized (less than 0.5 nm drift in 2 min) the solution was changed by flowing 25 mL of the next salt solution through the liquid cell (internal volume of 5 mL) and letting it stabilize again with changed ambient conditions in the model. When the highest salt concentration was reached, it was hydrated in a 100 mM solution of the next salt for 1 h to exchange the ions, and the process was then repeated with the new salt type.

2.5 Atomic force microscope

The samples were investigated using AFM (NanoWizard 3, JPK Instruments AG, Berlin, Germany) either with imaging for characterizing the roughness or with force measurements measuring the repulsion and friction forces. AFM is a scanning probe instrument that can provide three dimensional images of a surface at a sub-nanometer resolution but cannot be used to measure the thickness of the layer directly. It works by measuring the interaction between the probe and the sample and indirectly translating that into either height or force[195,196].

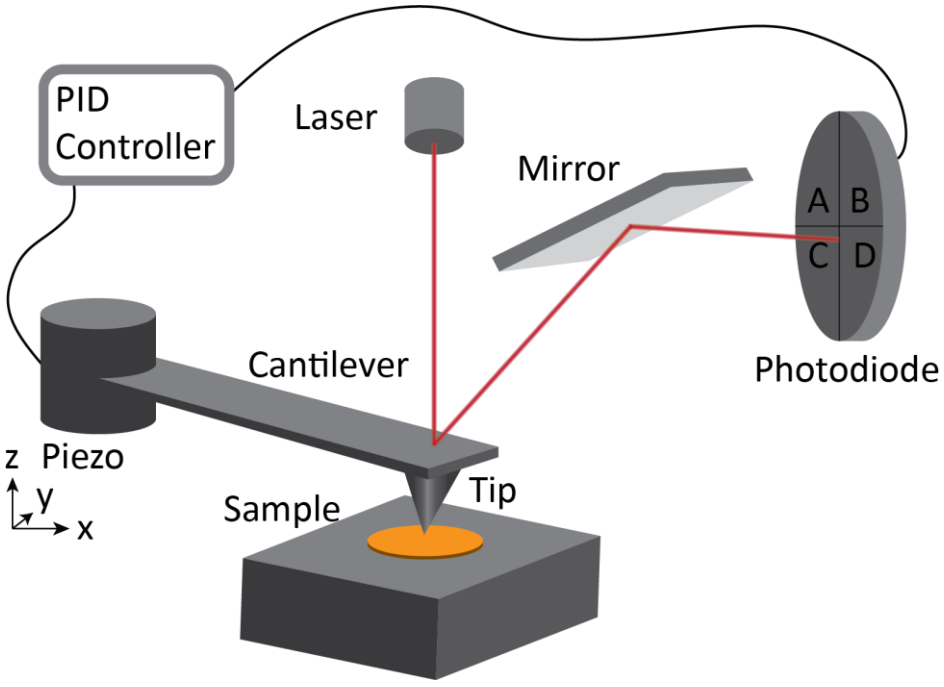

Figure 2.16: Schematic illustration of the components in an atomic force microscope.

An AFM consists of six main components (probe, cantilever, piezo stage, laser, photodiode, and proportional-integral-derivative (PID) controller) in a setup illustrated in Figure 2.16. The AFM interacts with the sample via a probe, which for imaging is typically as sharp as possible to minimize the interaction

area and thereby improve the resolution. This probe is attached to the end of a cantilever with a reflective back. The cantilevers can have different geometries, but those used in this study were rectangular except for the outermost part where the width gradually decreased. The cantilever bends depending on the force between the probe and the sample. Opposite to the probe, the cantilever is mounted to a piezoelectric motor stage that can move it along the sample (x and y) and normal to the sample (z) very accurately. On the top of the cantilever, a laser is reflected onto a photodiode via a mirror. The mirror is used to make rough adjustments to the laser spot when changing between air and liquid mode; therefore, its effect is not significant. The photodiode consists of four quadrants in which the light intensity is measured individually. When the cantilever bends, the laser spot's placement on the photodiode change, and the signal deflected from the photodiode, D_{PH}, can be measured as:

$$D_{PH} = \frac{(I_A + I_B) - (I_C + I_D)}{(I_A + I_B) + (I_C + I_D)}$$

where I_A, I_B, I_C, *and* I_D correspond to the intensity of the light measured in the respective quadrants of the photodiode. Effectively, this means that the photodiode measures the light intensity in the two top quadrants compared to those in the two bottom quadrants relative to the total intensity. This is known as the optical lever principle and allows small changes in the bend of the cantilever to be magnified onto the photodiode. Finally, this deflection signal is passed to the PID controller which then moves the cantilever in the z direction to adjust the deflection signal to the target value.[197]

2.5.1 Imaging

There are different techniques for scanning a sample with AFM, but in this study, only the contact mode was used. In this mode, the probe is lowered until the repulsion between the probe and the sample bends the cantilever up to a certain amount controlled by a chosen set point. This corresponds to pressing the probe into the sample with a specific force. When an image is scanned, the cantilever is moved along the line perpendicular to its long axis and then moved to the next line beside the first one until the entire area is scanned. When the probe moves to a new pixel, the deflection signal is measured and the PID corrects the height back to the target set point. Therefore, the value obtained from the photodiode is not used directly for measuring the height in the pixel, instead, the movement of the piezo is used to extract the height difference. The information from each pixel is then used to create an image of the surface of the sample[197].

2.5.2 Preparation of colloidal probe

For imaging, it is beneficial to keep the end of the probe as small as possible, as this controls the detail in which the probe can interact with the asperities on the surface. However, when measuring forces, it is convenient to have a consistent area of interaction that is easier to define[198]. This was obtained using a cantilever with a colloidal probe instead of a sharp tip, which was prepared in situ. To prepare the cantilevers with colloidal probes, tipless cantilevers with the desired properties were bought. Two pieces of tungsten wire were electrochemically etched in a 1 M KOH solution by dipping one end into the solution multiple times for short durations at a constant speed. This gradually reduced the thickness and finally, sharp tips were obtained. A tiny drop of epoxy was added to the cantilever using a micromanipulator and an optical microscope, and then the colloidal probe was picked up using the other wire via capillary forces and placed onto the glue. A slow curing epoxy was used with a working time of 1.5 h and a curing time of one week, to provide sufficient time for the process. The colloidal probes used consisted of SiO_2 spheres with a diameter of 7 µm. The process of attaching the glue and the colloidal probe is illustrated in Figure 2.17

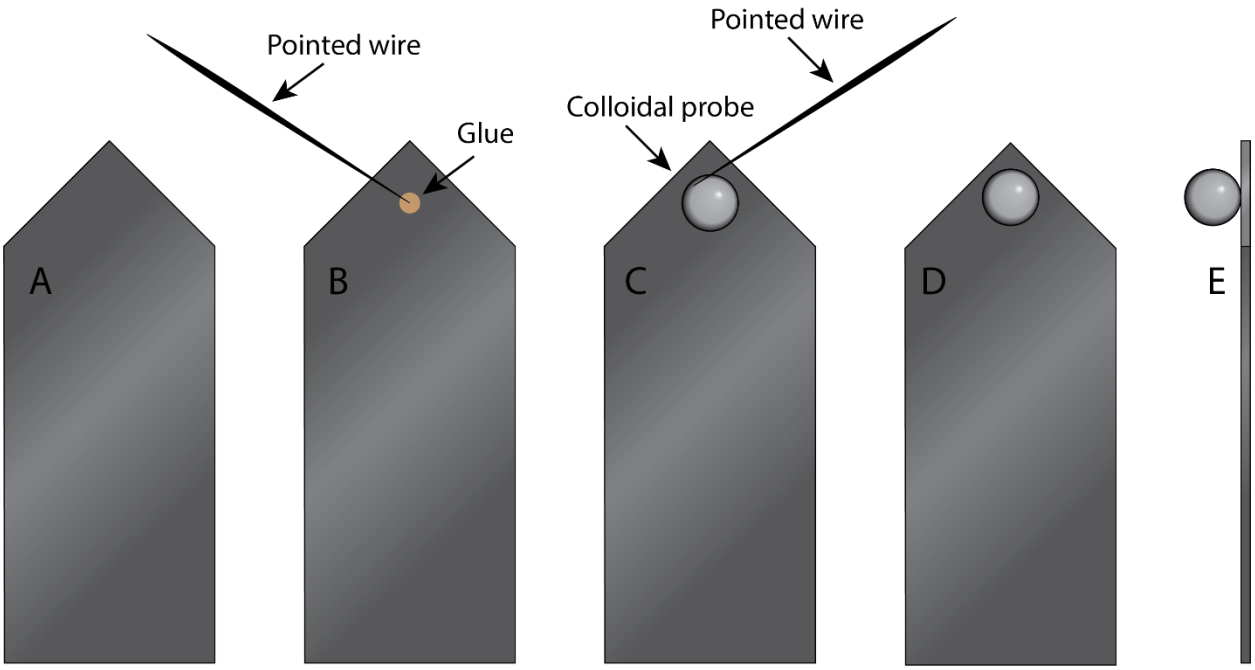

Figure 2.17: Illustration of the process used to prepare the cantilevers with a colloidal probe: A) Tipless cantilever, B) glue droplet attached with etched tungsten wire, C) colloidal probe attached to the glue with different etched tungsten wire, D) bottom view, and E) side view of final colloidal probe cantilever.

2.5.3 Force curve measurements

A more recent application of AFM than imaging is force measurement, where the probe is approached onto the surface of the sample with increasing force and then retracted again. This method is used to determine how the probe and the surface interact with regard to attraction and repulsion, and to some degree the softness of the sample also. An example of such a force curve is shown in Figure 2.18A where the deflection in voltage (which is proportional to the force) caused by the bending of the cantilever is plotted as a function of the height along the z direction of the piezo stage. Here, the measurement was started at the right side of the red line and approached the surface until a specific deflection from the cantilever was reached. Then it was moved away from the sample following the blue line. The lines almost perfectly overlap, indicating that the probe and sample are electrostatically repulsive; if they were attractive, a sudden jump would have been observed, where the deflection would decrease as the probe jumped to contact with the sample. Three different zones are shown. In zone 3 the separation between the probe and the sample is so large that there are no interactions, in zone 2 the repulsion between the cantilever and surface increases when the sample is pressed to a collapsed state, and in zone 1 the cantilever can no longer compress the surface with an increase in force, which is known as hard-wall contact. Although this provides a good overview of the interactions between the probe and the sample, the deflection in voltage vs position of the piezo is not an optimal parameter for understanding the interactions or comparing them with other systems.

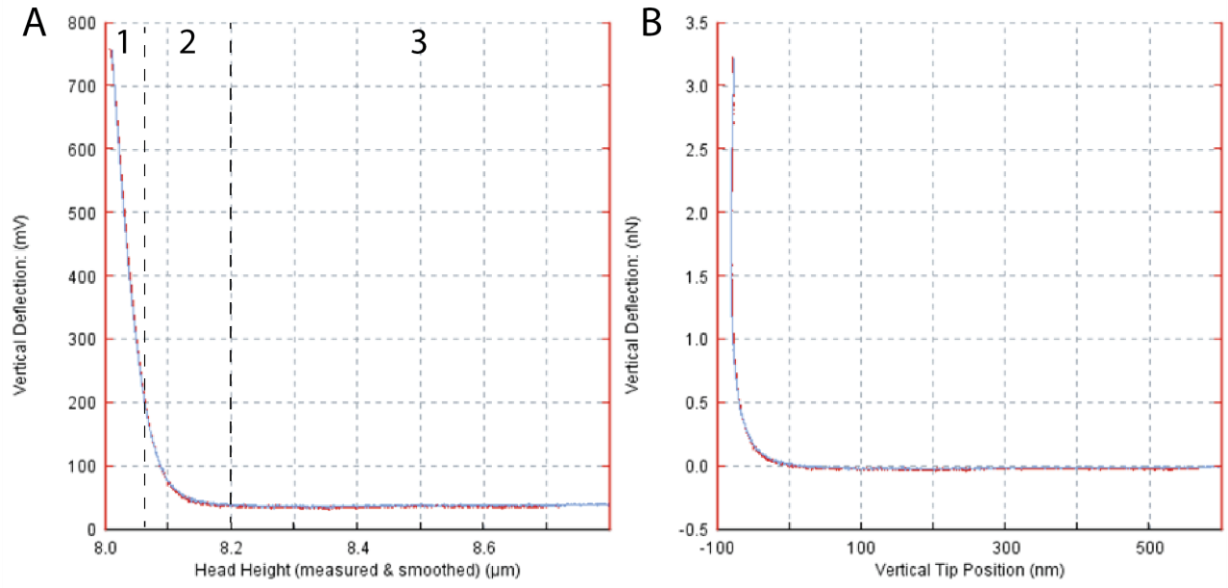

Figure 2.18: Example of a force curve measured with AFM. Graph A) displays an un-calibrated force curve showing the relation between the relative height of the cantilever base and the resulting voltage deflection divided into three regions. Graph B) displays

the calibrated version of the same curve showing the relation between the relative position of the probe and the applied vertical force.

The relationship between the probe height and the actual force applied to it is an easier way to understand and compare the force curves. The photodiode and cantilever require some calibration before this conversion. By assuming a hard wall contact in zone 1 of Figure 2.18A (meaning that the probe is not moving in the z-direction), the slope in this zone relates the voltage deflection in the photodiode with the physical change in the angle of the cantilever and is known as the vertical sensitivity. To relate this to a force, it is necessary to know the vertical spring constant of the cantilever as well. An estimated spring constant was provided with the purchased cantilever used in this study; however, the values were provided with an uncertainty of a factor of 10 in either direction, making it extremely imprecise for force measurements. Several methods are present for obtaining a more accurate value of the spring constant. Depending on the geometry of the cantilever and the medium, they have different drawbacks[199]. A thermal noise-based method was chosen for this, and it is described in detail in section 3. When these values are obtained, the force plot can be converted into a plot describing more relevant physical values, such as the one shown in Figure 2.18B.

2.5.4 Friction

In addition to measuring the forces when the probe is pressed into the sample, the friction force between the probe and the sample can also be measured. This measurement is performed by sliding the cantilever perpendicular to its long axis along the surface of the sample at a constant downward force (normal force), similar to that during imaging[200–203]. Instead of measuring the change in the position of the piezo, the lateral deflection in the detector is measured, which is caused by the torsional twisting of the cantilever. This twisting scales with the friction between the probe and the sample, and by measuring the deflection in both directions on a line, a so-called friction loop is obtained[204–206]. Although the difference between the twisting is related to the amount of friction, the deflection is again provided in terms of voltage and needs to be converted into a force before it can be compared with the measurement results obtained using different techniques.

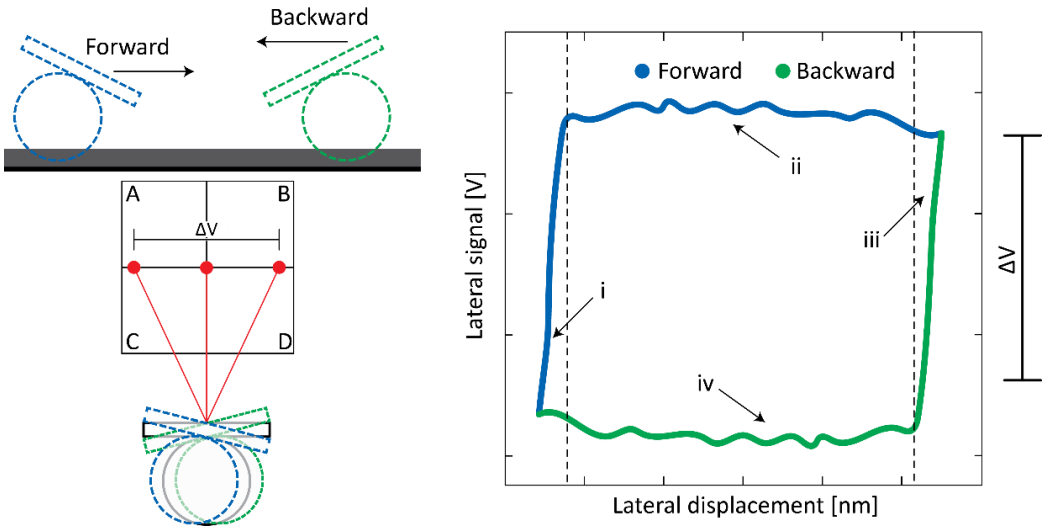

Figure 2.19: Schematic illustration of friction measurements using an atomic force microscope. Left: torsional twisting of the cantilever with colloidal probe and the consequent lateral deflection. Right: friction loop obtained by moving the cantilever forth and back on a line.

Figure 2.19 illustrates this concept, where the left image shows the twisting mechanism of the cantilever when moved across a surface and its relationship to a change in lateral deflection in the photodetector; the right image shows a friction loop. The friction loop has four regions. i) The cantilever is in an untwisted state and starts moving in the forward direction, increasing the torsional twist. ii) When the force required to increase the torsional twist becomes more than the friction between the colloidal probe and the surface, the probe starts sliding across the surface. iii) At the end of the line, the cantilever moves in the opposite direction causing a buildup of the twist in the opposite direction. iv) The final region is similar to region ii, but with the twist in the opposite direction. The mean difference between regions ii and iv, ΔV, is proportional to the friction and was used to calculate the actual friction force. For each normal force measured, at least one friction loop should be measured.

To relate the lateral deflection voltage to a force, it is necessary to determine the torsional spring constant and sensitivity. In this direction, contrary to the vertical direction, no straightforward procedure is present for obtaining the sensitivity[207,208]. A thermal noise-based method, described in section 3, was used for both sensitivity and spring constant.

The friction loops were measured at specific normal forces which influence the magnitude of the friction. Depending on the system, friction can increase proportionally to the normal force, according to Amontons law, but it can also exhibit a more complex relationship. However, for measuring the friction, the normal force should be in the range of zone 2 shown in Figure 2.18A. If the force is lower, the probe does not interact with the sample, and for a higher force, the friction is measured for a completely compressed

film. Therefore, it is important that the friction measurements are performed using the force curves, where the interactions between the specific probe and surface are measured. A challenge in measuring forces with an AFM to improve the understanding of a sample is that friction is not just dependent on the sample, but also on the probe's interactions with the sample. Therefore, the complete system has to be considered, as any change, such as changes in the probe from a sharp tip to a colloidal probe or the coating on the probe, could significantly influence the quantity being measured.

2.5.5 Analysis script for friction data

To measure the friction on a sample, typically, it is necessary to measure multiple friction loops at each normal force, and then measure the friction loops at a range of normal forces. This yields large amounts of data that need to be analyzed, and the data needs to be translated from the measured voltage into an actual force. For obtaining the data presented in this thesis, friction loops were measured at five different locations with 60 different normal forces under 15 different conditions, yielding 9000 files. Therefore, it was necessary to automate this analysis process. To do this I have written a Matlab script and a graphical user interface (GUI), which is shown in Figure 2.20.

Figure 2.20: Graphical user interface for Matlab program created to automate the analysis of raw friction data.

In this program, the properties of the cantilever and tip were the input parameters along with the raw friction files from AFM, and the results were obtained by calculating the friction force vs the normal force. Automating this tedious process saved time and allowed for more accurate measurements, as significantly more data could be collected and analyzed.

3 Theory of sensitivity and spring constant calibration

The discussion in this section includes the procedure for determining the spring constant and sensitivity of the cantilever in both vertical and torsional directions, which is done with a procedure that has previously been reported to be a convenient method. Besides this proven method, an alternative method is also presented for relating the vertical and torsional sensitivities in air with each other and with the sensitivities in liquids. These relationships were obtained by calculating the light path geometrically. The steps between the equations in this section are further elaborated in Appendix C. In the last part of this section, the accuracies of this method are compared with the proven method as a reference.

3.1 Vertical spring constant

The spring constant of the cantilever in the vertical direction can be calculated purely from the material properties and the dimensions of the cantilever. This relationship is described by:

$$k_v = \frac{Et^3w}{4L^3} \qquad 3.1$$

where *E* is Young's modulus and *L*, *w*, and *t* are the length, width, and thickness of the cantilever, respectively[209], or by:

$$k_v = M_e \rho_c L w t \omega_{vac,v}^2 \qquad 3.2$$

where $\omega_{vac,v}$ is the angular resonance frequency in the vertical direction in a vacuum, ρ_c is the density of the cantilever, and M_e is the normalized effective mass; approximately $M_e = 0.2427$ for cantilevers where $L/b > 5$[208].

Two main drawbacks are present for these material-oriented methods. First, although the length and width of the cantilever can be determined easily and relatively accurately using an optical microscope, it is difficult to determine the thickness. This would typically require a scanning electron microscope or something similar. Because the thickness of the cantilever is very small compared to the two other dimensions, an error that is insignificant in the length and width dimensions could be a much larger error in the thickness dimension. This especially creates a problem in Equation 3.1, where the thickness is cubed. Second, it is extremely difficult to determine the material properties of the cantilever because the main substrate is often coated with different materials, including a chromium and gold layer. The chromium layer increases the adhesion between the substrate and the gold layer, and the gold layer

increases the reflectivity. The layers are typically not prepared in a way that allows their thickness to be known, which makes it difficult to accurately determine the material properties of the cantilever[210].

Therefore, a different and more convenient method is required. In this study, a method based on the thermal noise of the cantilever was used as it is a practical method that can be used to determine both spring constant and sensitivity. If the fluctuations of a cantilever due to thermal noise are measured as deflection voltages and Fourier transformed, they depend on the frequency, f, as:

$$S(f) = \frac{P_{DC,v} f_{0,v}^4}{\left(f^2 - f_{0,v}^2\right)^2 + \frac{f^2 f_{0,v}^2}{Q_{f,v}^2}} \qquad 3.3$$

where $Q_{f,v}$ is the quality factor in the vertical direction which describes the relationship between the resonance peak energy of the cantilevers and the energy lost per angular movement; thus, for a highly dampened cantilever $Q_{f,v}$ will be low[211]. The values of $f_{0,v}$, $Q_{f,v}$, and $P_{DC,v}$ can be determined using these as fitting parameters[212]. All these values can be determined by the non-contact thermal noise measurements, and used in an expression for the vertical spring constant derived as:

$$k_v = 0.1906 \rho_f L w^2 Q_{f,v} \omega_{f,v}^2 Im\left(\Gamma_{rect}^v\left(\omega_{f,v}\right)\right) \qquad 3.4$$

This equation can be used to determine the vertical spring constant from the width and length of the cantilever, the density, and the viscosity of the surrounding fluid, thermal noise deflection measurement, and the hydrodynamic function for a rectangular beam. Therefore, the unknown material properties of the cantilever and the calculation of the thickness of the cantilever are avoided.

3.2 Vertical sensitivity

The AFM measures the deflection of the cantilever based on the voltage change in the photodiode. However, typically, the voltage change need not be related to a deflection distance when imaging using the AFM. However, when the force is measured, it is necessary to determine the amount of deflection of the cantilever from the voltage change. The sensitivity of the AFM, γ, is typically given in a unit of voltage change per distance of probe movement (δ_L in Figure 3.1), which means that the sensitivity of the system is changed if the length of the cantilever is changed. In the following sections, the sensitivity is redefined as the relationship between the deflection voltage and the change in the angle of the endpoint of the cantilever (θ_L in Figure 3.1). This provides a constant sensitivity for a specific AFM, independent of the cantilever (for a specific medium). This relation, in the vertical direction, can be determined using the

cantilever dimensions and the fitting parameters of the fluctuation spectrum, as given by the following equation:

$$\gamma_v = 0.7830 \sqrt{\frac{6k_B T}{\pi L^2 k_v f_{0,v} P_{DC,v} Q_{f,v}}} \quad 3.5$$

where 0.7830 is an analytically determined correction factor from the literature, k_B is Boltzmann's constant, *T* is the temperature, *L* is the length of the cantilever, k_v is the vertical spring constant, and $f_{0,v}$, $P_{DC,v}$, and $Q_{f,v}$ are the fitting parameters determined from the fluctuation spectrum[213].

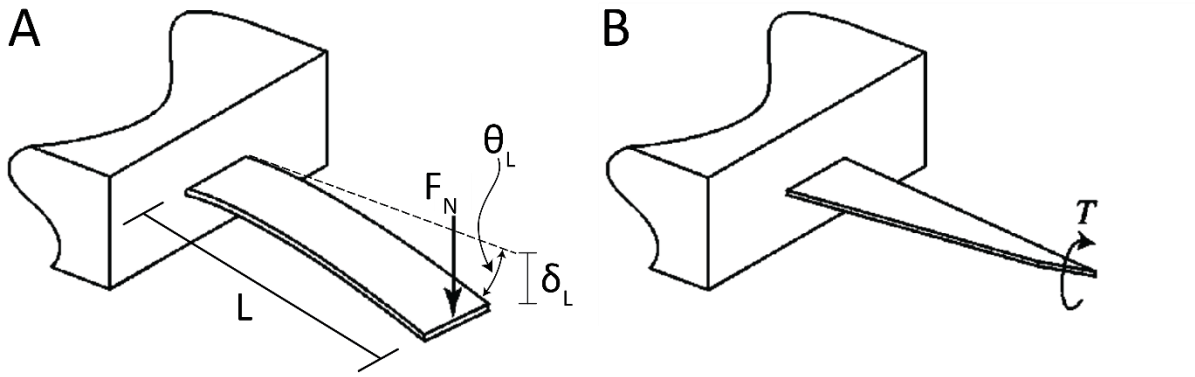

Figure 3.1: Schematic illustration of vertical bending of a cantilever due to an applied normal force (A) and torsional twisting of a cantilever due to applied torque (B). Adapted with permission from Green et al., Review of Scientific Instruments 75, 1988 (2004), 114, 677–71141 Copyright 2004 American Institute of Physics.[214]

To change the sensitivity into a parameter independent of the cantilevers length a relation describing the deflection height of an end-loaded uniform cantilever which is fixed at one end is used:

$$\frac{\delta_L}{\theta_L} = \frac{2L}{3} \quad 3.6$$

Where θ_L is the angle from the rest position, δ_L is the tip's distance from the rest position[215].

3.3 Torsional spring constant and sensitivity

Similar to the vertical spring constant, the torsional spring constant can be described as:

$$k_t = \frac{1}{2\pi} \rho_f w^4 L Q_{f,t} \omega_{f,t}^2 \Gamma_i^t(\omega_{f,t}) \quad 3.7$$

and the torsional sensitivity can be described as:

$$\gamma_t = \sqrt{\frac{2k_B T}{\pi k_t f_{0,t} P_{DC,t} Q_{f,t}}} \quad 3.8$$

where $Q_{f,t}$, $\omega_{f,t}$, and $f_{0,t}$ are the fitting parameters for the power spectrum in the torsional direction, and $\Gamma_{f,t}$ is the hydrodynamic function for a rectangular beam in the torsional direction[216].

For calculating the spring constants and sensitivities in both torsional and vertical directions using this thermal noise method, the quality factor should be much greater than 1.[214] This is can be done in air and because the spring constants do not change in different mediums, the same value can be applied in different mediums. However, determining the sensitivity is more complicated, as it varies depending on whether it is in air or water. In water, the quality factor was found to be approximately 4–8, which has been shown to result in an overestimation of the sensitivity[217]. In an effort to find a different and more convenient way to determine the sensitivity, the sensitivity in air was described geometrically, and then it was predicted in water based on this description. The results of this are described in the following section and the calculations are presented more fully in Appendix C.

3.4 Geometrical sensitivities

The sensitivity depends on the internal components of the AFM and is significantly dependent on the distance traveled by the light. Figure 3.2A shows a simplified version of the vertical light path in an AFM when the cantilever is at its rest position, as well as the parameters affecting the path of the light. The light comes down through the air over the cantilever holder, after which it passes through the cantilever holder of quartz glass, through the air over the cantilever, and is then reflected. The distances traveled in these regimes through the top, the glass, and the bottom are given by h_t, h_g, and h_b, respectively, and these are considered constant. The angle of the unbend cantilever, α (10° for this AFM), reflects the light at an angle after which the light passes through the air/glass and glass/air interfaces again. This affects its path according to the refractive indices before reaching the photodiode, having moved $S_1 + S_2 + S_3$ in the horizontal direction from its starting point (defined in Figure 3.2A). The same behavior is observed in Figure 3.2B, except that the cantilever is now bent at an angle, θ, which alters the path of the light after it crosses the cantilever and shifts its position at the photodiode by δS from the position at rest. In Figure 3.2C, the system is instead viewed from the torsional direction, where the cantilever is twisted at an angle, φ, compared to its horizontal rest position. Similar to (B), this moves the laser spot a distance away from its position at rest. These geometrical descriptions of the system were used to determine the relationship between the vertical and torsional sensitivities.

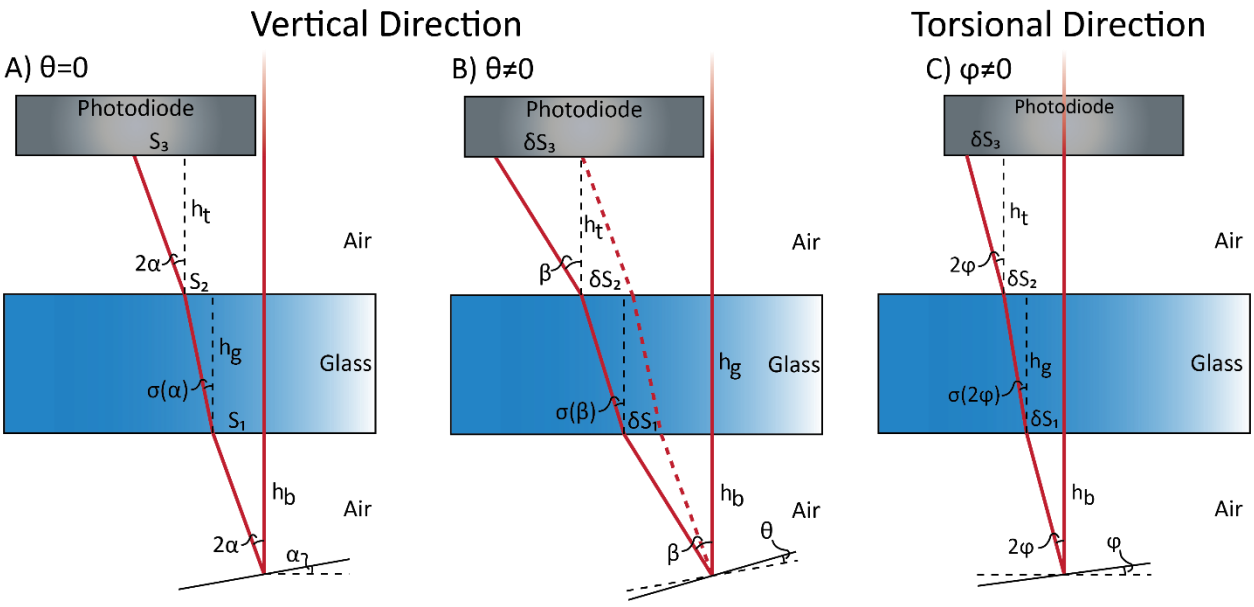

Figure 3.2: Deflection path of laser interacting with an unbend cantilever (A) and for a cantilever bent at an angle θ (B) in the vertical direction and for a cantilever twisted at an angle φ in the torsional direction (C).

In the vertical direction, the angle between the incoming and reflected light at the cantilever can be described by $\beta = 2\alpha + 2\theta$ and the position of the laser spot on the photodiode can be expressed by the lateral movement of the laser spot which at $\theta = 0$ is given by:

$$S(\theta = 0) = h_b \tan(2\alpha) + h_g \tan\big(\sigma(2\alpha)\big) + h_t \tan(2\alpha) \qquad 3.9$$

and the distance when $\theta \neq 0$ is given by:

$$S(\theta) = h_b \tan(\beta) + h_g \tan\big(\sigma(\beta)\big) + h_t \tan(\beta) \qquad 3.10$$

After determining the difference, $\delta S(\theta) = S(\theta) - S(\theta = 0)$, and using Snell's law along with some trigonometric approximations to simplify the expression, $\delta S(\theta)$ can be expressed as

$$\delta S(\theta) = 2\theta \frac{h_b + h_t + h_g n_a / n_g}{\cos^{-2}(2\alpha)} \qquad 3.11$$

where n_a and n_g are the refractive indices of the medium (air in this case) and the cantilever holder from quartz glass, respectively. The change in the dependency of the vertical deflection voltage on the angle can is described by:

$$\gamma_{v,a} = \frac{dD_v(\theta)}{d\theta} = \frac{dk\delta S(\theta)}{d\theta} = 2k \frac{h_b + h_t + h_g n_a / n_g}{\cos^{-2}(2\alpha)} \qquad 3.12$$

where *k* is a proportionality constant relating the change in position of the light spot on the photodiode with the change in voltage, which is independent of the medium of the cantilever and assumed to be the same in the vertical and torsional direction. This proportionality constant is determined by the photodiode and is one of the factors for the varying sensitivities of different AFMs. This is also one of the factors relating the voltage change to a physical change of the cantilever, indicating that this method alone cannot be used to determine the sensitivity; it can be used only to relate the sensitivities in different directions or mediums to each other, because *k* is not known.

3.5 Torsional sensitivity

The dependency of the torsional sensitivity on the deflection angle can be calculated using an approach similar to that used for the vertical sensitivity.

As illustrated in Figure 3.2C the torsional deflection can be described by:

$$\delta S(\varphi) = \delta S_1(\varphi) + \delta S_2(\varphi) + \delta S_3(\varphi) = (h_b + h_t)\tan(2\varphi) + h_g \tan\big(\sigma(2\varphi)\big) \qquad 3.13$$

where σ can be approximated as:

$$\sigma(2\varphi) = 2\varphi \frac{n_a}{n_g} \qquad 3.14$$

due to the angle, φ, being close to zero. This means that the deflection simplifies to:

$$\delta S(\varphi) = 2\varphi\big(h_b + h_t + h_g n_a / n_g\big) \qquad 3.15$$

and the deflection from an angular change is given by:

$$\gamma_{t,a} = \frac{dD_t(\varphi)}{d\varphi} = \frac{dk\delta S(\varphi)}{d\varphi} = 2k\left(h_b + h_t + h_g \frac{n_a}{n_g}\right) \qquad 3.16$$

which has the same form as that of the vertical deflection, but is differently scaled. The deflections in the vertical and torsional directions are therefore related as:

$$\gamma_{t,a} = \gamma_{v,a} \cos^{-2}(2\alpha) \qquad 3.17$$

which can be used to calculate the torsional sensitivity from the vertical and vice versa, as they are related by a factor of $\cos^{-2}(2\alpha) \approx 1.13$.

3.5.1 Sensitivity with the cantilever immersed in a liquid

If the cantilever is immersed in a liquid instead of in air, the liquid is present below the cantilever holder, and the sensitivity changes based on the refractive index of the liquid. This sensitivity can be calculated similarly to that for the cantilever in air, but with a glass/air interface at the top of the glass and a glass/liquid interface at its bottom. The torsional sensitivity with the liquid interface is with a similar approach found to be described by the following equation:

$$\delta S = 2\varphi\left(h_b + h_g\frac{n_w}{n_g} + h_t\frac{n_w}{n_a}\right) \Rightarrow \gamma_{t,l} = 2k\left(h_b + h_g\frac{n_w}{n_g} + h_t\frac{n_w}{n_a}\right) \quad 3.18$$

where n_w, n_g, and n_a are the refractive indices for water, glass, and air, respectively. Therefore, as both h_t and h_g are significantly larger than h_b, the relationship between the torsional sensitivity in air and in water is given by:

$$\frac{\gamma_{t,l}}{\gamma_{t,a}} = \frac{2k\left(h_b + h_g\frac{n_w}{n_g} + h_t\frac{n_w}{n_a}\right)}{2k\left(h_b + h_g\frac{n_a}{n_g} + h_t\right)} \approx \frac{h_g\frac{n_w}{n_g} + h_t n_w}{h_g\frac{1}{n_g} + h_t} = n_w \quad 3.19$$

Accordingly, for the type of AFM used in this study, the torsional sensitivity in water was determined to be 1.35 times higher than the torsional sensitivity in the air according to this geometrical approach.

3.6 Verification of spring constant and sensitivity determination technique

The thermal noise technique to determine the spring constant is considered to be fairly accurate. To test this technique, eight different cantilevers were analyzed (two csc37 Cr-Au tipless (A and B), three csc38 Cr-Au with tip (A, B, and C), and three csc38 Cr-Au without tip (A, B, and C) where A, B, and C corresponds to the lengths of 250, 300, and 350 µm, respectively). The spring constants and sensitivities of these were measured in air using a normal cantilever holder for air measurements and in air and water using a cantilever holder for liquid mode measurements (the holders used in the air and liquid modes have heights of 1.4 and 1.2 cm, respectively). The spring constants measured are shown in Figure 3.3; large differences are observed in the spring constants of different cantilevers. Considering individual cantilevers, the spring constants measured in air are very similar and the one measured in water is higher, which is consistent with the expected trend as the quality factor measured in water is low. The spring constant should not change from air to liquid; therefore, the spring constant can reliable be determined in air and used in water.

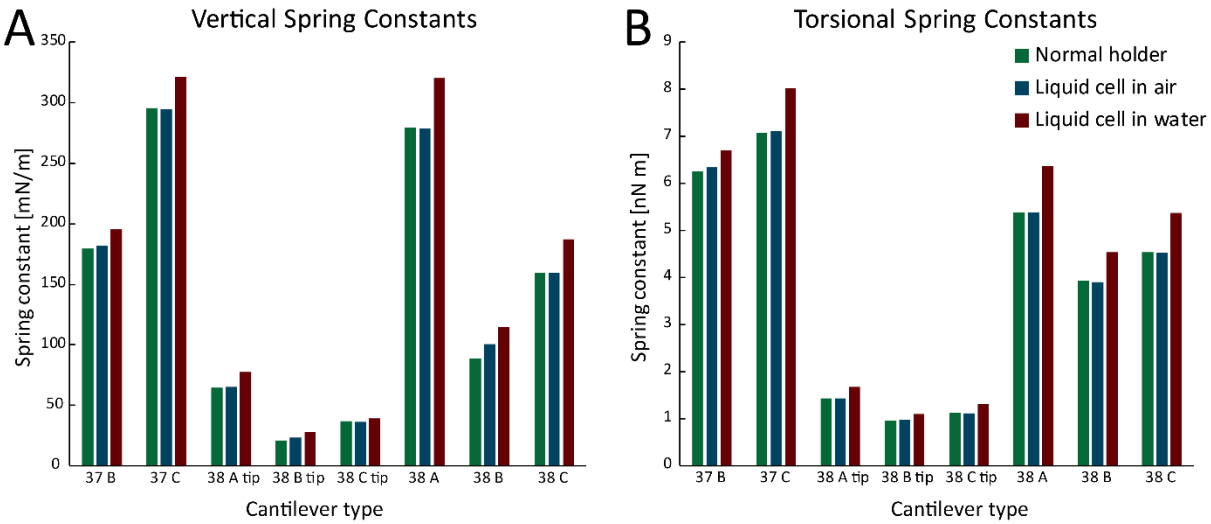

Figure 3.3: Vertical (A) and torsional (B) spring constants measured for a range of cantilever types using thermal noise technique with either a regular cantilever holder in air, a liquid mode cantilever holder in air, or a liquid mode cantilever holder in water.

Based on this, the spring constant was measured for a specific cantilever in air before attaching the colloidal probe, and this value was used for subsequent experiments in liquid.

It is difficult to accurately measure the sensitivities as they change depending on the medium, and therefore both vertical and torsional sensitivities were measured using different techniques to compare their consistency. First, the vertical sensitivity was measured by obtaining a force curve on a hard substrate in both air and water. Although this is an easy and reliable method to determine the vertical sensitivity, it can be performed in the vertical direction only. Second, the sensitivities in both directions were measured with the thermal noise method. The spring constants were determined using the cantilever holder for air measurements in air and the cantilever holder for liquid mode in both air and in water. In contrast to the spring constants, the sensitivities are expected to change depending on the holder and the medium, while being independent of the cantilever type. The results for eight different cantilevers obtained using the thermal noise method are shown in Figure 3.4. Although some variations are observed in the values in the figure, the standard deviation is below 200 V/rad when measured in air and approximately 350 V/rad when measured in water. The average value of vertical sensitivity measured with the force curves is within the standard deviation of the thermal noise measurements (approximately 100 V/rad lower in air and 200 V/rad lower in water).

A third method to determine both vertical and torsional sensitivities in air was also tested. In this method, the AFM was set up and approached a sample, which in this case was a reflective silicon wafer. The cantilever was then removed, and thus the silicon wafer simulated the cantilever as the laser was reflected

from the silicon wafer. This was done because it allowed moving the AFM head (which is the unit containing the cantilever holder, the laser, and the photodiode) independent of the simulated cantilever (silicon wafer), which corresponds to moving the cantilever. The sensitivities were determined by tilting the AFM head in the vertical and torsional directions and relating the voltage changes to the angles of tilt. These measurements yielded vertical sensitivities, which on average, were less than 100 V/rad lower than the ones found with force curves, and torsional sensitivities, which on average, were approximately 200 V/rad lower than those found with the thermal noise method.

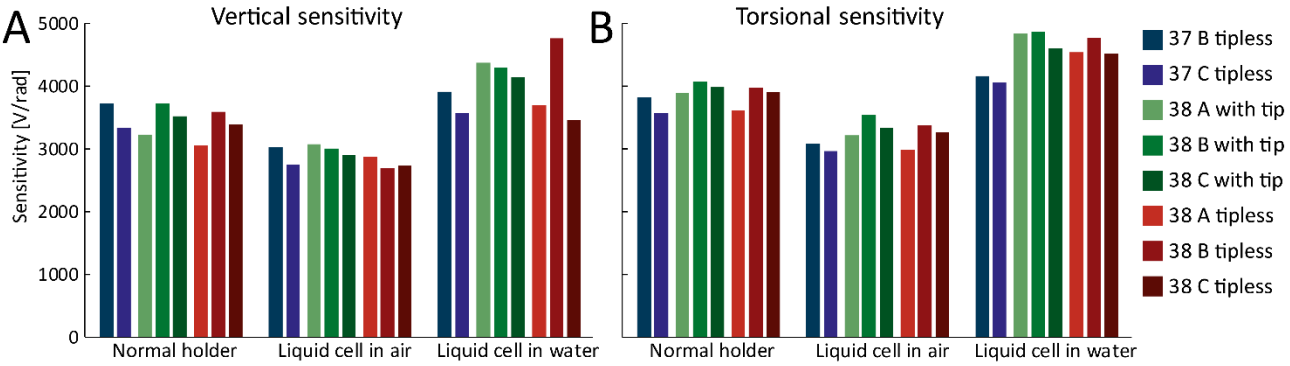

Figure 3.4: Vertical (A) and torsional (B) sensitivities measured for different cantilever types using thermal noise technique with either a regular cantilever holder in air, a liquid mode cantilever holder in air, or a liquid mode cantilever holder in water.

Based on the geometrical description, the torsional sensitivity was expected to be $\cos^{-2}(20\text{deg}) = 1.13$ times larger than the vertical. The result obtained using the thermal noise method showed the torsional sensitivities to be 1.12 times higher than the vertical, which is surprisingly consistent with the geometrical approach. Similarly, the difference between the torsional sensitivity in air and water was expected to be approximately 1.35, and the corresponding determined value from the thermal noise method is 1.43. Especially, as the latter relation is approximated, the low difference of the experimentally determined constant is surprising, especially as the thermal noise data in water is expected to overestimate the sensitivity.

Two conclusions can be drawn based on these results. First, the thermal noise technique for determining the sensitivity seems to be fairly reliable and the average values were used as the sensitivities of the instrument for subsequent experiments. This method is extremely practical to use, compared to the method which uses the reflective surface; it can be used to determine the sensitivities in both torsional and vertical directions, contrary to the force curve technique that only yields the sensitivity in the vertical direction. Second, at least for this instrument, the approach used to geometrically determine the relation between the sensitivities is in fair agreement with those determined using other methods. Therefore,

using this method, it is possible to measure the vertical sensitivity in air with the force curves, and then use the geometrical relations to calculate the torsional sensitivity in air and the vertical and torsional sensitivities in a liquid.

4 Theoretical model

Section 5.1 describes the experimental investigation of the ion-specific swelling of monocomponent polyelectrolyte films with different ion types to decouple the effects causing the swelling, and subsequently understand the individual mechanisms better. Similarly, it is interesting to simulate the mechanisms in a polyelectrolyte film theoretically, as this could provide an easier way to investigate the importance of individual contributions. This would afford a better understanding of all types of polyelectrolyte films, and would especially be beneficial for more complicated films, such as zwitterionic or multilayer polyelectrolyte films, which are still not as well understood as cationic and anionic polymer films. A theoretical description of the films could potentially make it easier to decouple the different effects that change the swelling of the film.

In this section, the theoretical description of the polyelectrolyte film is discussed which was developed during the external stay with associate professor Drew Parsons at the University of Cagliari, Sardinia. It was expected that the model developed herein will be able to describe the main contributions to the swelling of the film and the ion dependency, and thereby predict the experimentally observed trends. However, the model demonstrated some unexpected challenges. Therefore, a model was developed with some restrictions for the swelling and collapse of the film, and the swelling mechanisms and specific ion dependency were implemented without considering the main contributions. Thus, the model provides a platform that can be used to elucidate the polyelectrolyte films at a later stage, and where the film can potentially be changed between cationic, anionic, and zwitterionic polymer films, or even as a multilayered polymer film. An already existing model was used as the starting point, and it described the ion distribution that was implemented to determine the distribution of ions inside and outside a polymer film.

4.1 Elastic swelling restrain

If the polyelectrolyte film is simplified to an uncharged polymer film bound to a substrate in a solution without ions, the film will reach some equilibrium thickness. Therefore, something must be present that prevents it from collapsing at some point and also from stretching infinitely.

The limiting factor preventing the stretching of the film at some thickness is typically described with an elastic term for a polymer brush:

$$E_{el,Brush} = \sigma r a^2 \frac{3 - r^2}{1 - r^2} \qquad 4.1$$

where σ is the grafting density, a is the length between the repeating units and r is a relative thickness calculated as $r = H/(aN)$ with H being the actual thickness and N the number of repeating units[218,219]. The polymer brush can be described geometrically in a simpler manner as it has a maximum thickness of aN, compared to that of a polymer film consisting of a crosslinked network. To fit the expression to a network, σ and N are redefined as the polymers per area and number of monomers per polymer, respectively. The maximum thickness still depends on the number of monomers and the distance between them, and it also depends on how tightly the network is cross-linked. Therefore, the maximum thickness of the network can be described as $aN(1-k)$, where k is zero for a brush and increases as the crosslinking increases. Combining this, the elastic energy of a polymer network is described as

$$E_{el} = \frac{\sigma H a}{N(1-k)} \frac{3 - \left(\frac{H}{aN(1-k)}\right)^2}{1 - \left(\frac{H}{aN(1-k)}\right)^2} = \sigma r a^2 \frac{3 - r^2}{1 - r^2} \qquad 4.2$$

where $r = H/(aN(1-k))$. This energy contribution is shown in Figure 4.1 as a function of film thickness where it is observed to be relatively low until it reaches a specific thickness, after which it increases rapidly.

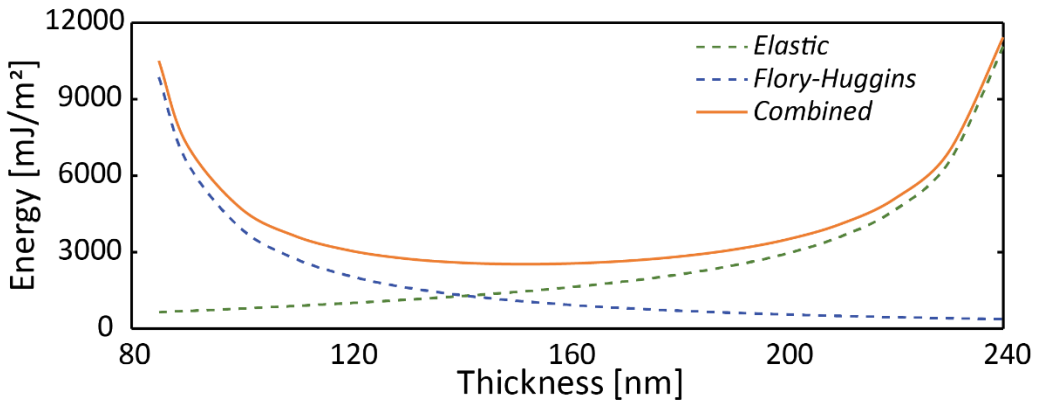

Figure 4.1: Swelling and collapse preventing the energy contributions on an uncharged polymer film. The shape of the elastic energy preventing swelling (green), a Flory–Huggins-based energy preventing collapse (blue), and the two energies combined (orange) and their dependency on the thickness of the film.

4.2 Flory–Huggins collapsing restrain

A thermodynamic term arising from Gibbs free energy of mixing and Flory–Huggins theory of semi-diluted polymer solutions provides a restraint that prevents the film from collapsing at a specific thickness; this is given by the following equation:

$$\frac{\Delta G_M}{RT} = ln(1-\phi_2) + \left(1-\frac{1}{N}\right)\phi_2 + \chi\phi_2^2 \qquad 4.3$$

where N is the number of monomers per polymer, ϕ_2 is the volume fraction of polymer, and χ is a parameter describing the interaction between the solvent and polymer compared to their self-interactions[220,221]. The interaction parameter, χ, is maintained constant and independent of the salt concentration and ion type. This Flory–Huggins based energy contribution's variation with thickness is shown in Figure 4.1. This figure also shows the combined energy from these contributions, which creates a potential well with a relatively flat middle section. Consequently, the thickness of the film settles at the minimum energy; however, additional energy contributions can skewer the minimum to a different thickness. However, this is possible only on the flat part as the energy required to counteract the two peaks at low or high thicknesses is unphysically large.

Both of these outer restrains are independent of the ion concentration and type owing to the way they are formulated in this model, which is an approximation that is a rough simplification for some ion types. The next step is to determine the charges in the film and describe their effects.

4.3 Ion specific contribution

The specific ion effects typically arise from an ion osmotic pressure difference between the polymer film and the bulk solution, and although this might be the dominating driving force, it is not the only one. Other ion-specific contributions to the swelling and collapse are also present, which are typically neglected. The effects of the ions depend on their distribution, which in this model is determined by treating the ions as point charges and formulating their distribution using nonlinear Poisson–Boltzmann theory with their length scales described based on their Debye length. This provides a distribution profile of the ions where a specific ion density is present inside and outside the film, along with a narrow transition at the interface of the film. Based on this density difference, an ion entropic energy can be determined which depends significantly on the ion concentration in the bulk solution[222].

The Born self-energy is an ion-specific contribution that is often not considered when discussing the effects that cause changes in the thickness of a polyelectrolyte film. The Born self-energy describes the

enthalpy of ion solvation. This includes the cost of the ion being in a certain environment, which in this study, is the polymer layer or the solvent, compared to that in a vacuum. In the simplified version used in this study, it is described as the work required to discharge the ion in a vacuum, insert it into the environment, and finally recharge it again. Therefore, the Born self-energy is highly dependent on the dielectric constant of the surroundings[223]. The difference in these self-energies inside the polymer layer and the solution is described by:

$$\Delta G_{Born} = -\frac{N_A z^2 e^2}{8\,\pi \varepsilon_0 r_0}\left(\frac{1}{\varepsilon_w} - \frac{1}{\varepsilon_{pol}}\right) \qquad 4.4$$

where N_A, z, e, and ε_0 are the Avogadro's number, ion charge, elementary charge, and vacuum permittivity, respectively. The remaining terms, ε_w, ε_{pol}, and r_0 correspond to the dielectric constants for the solvent and polymer phases, and the ion radius, respectively[224]. The dielectric constant of the hydrated polymer layer depends on the fraction of polymer and solvent. It is calculated with the Clausius–Mossotti relation using the dielectric constant of the solvent and the polarizability of the monomers determined using a quantum chemistry model[225]. The ionic radius in the Born energy creates a part of the ion-specific effects in this term. The radii of the ions used on this film are: K^+ = 0.96 Å^3, Cs^+ = 1.47 Å^3, and Li^+ = 0.38 Å^3 for the cations and Cl^- = 1.69 Å^3, Br^- = 1.97 Å^3, and SCN^- = 2.18 Å^3 for the anions[226].

When the Born energy is included, the model struggles in determining the ion distribution with the charge concentration of the polyelectrolyte film set to a physical level in the model. Therefore, the charge concentration was lowered by a factor of five in the model compared to that of the sample film used as a reference. When the charge concentration is increased further, or more energy contributions are added, the model cannot determine the numerical description of the ion distribution. This problem should be solved before adding more contributions, as it hinders the addition of more complex factors to the model.

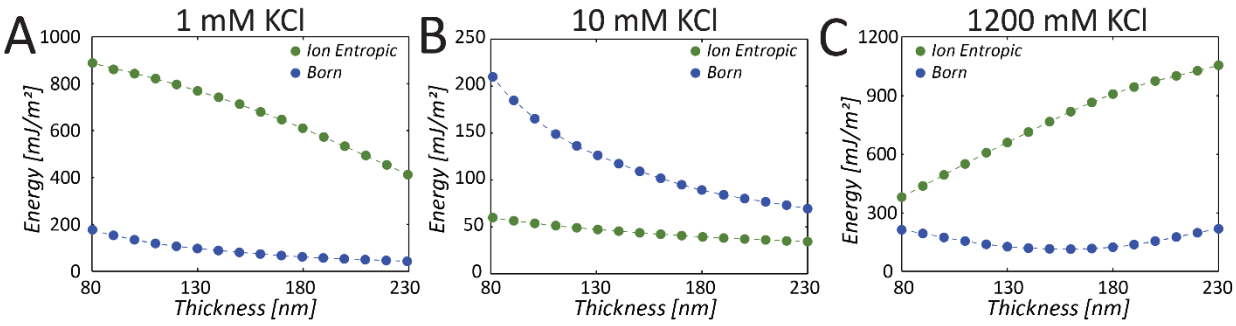

Figure 4.2: Dependence of ion concentration-dependent energy contributions on the thickness of a polyelectrolyte film. The ion entropic and Born energy were calculated for KCl at either 1 mM (A), 10 mM (B), or 1200 mM (C) bulk ion strength.

Figure 4.2 shows an example of the profiles of these ion concentration-dependent terms and the changes that occur in them. The figure also shows the ion entropic energy and the Born energy, and their dependency on the thickness of a polyelectrolyte film with the bulk salt concentration of 1, 10, or 1200 mM KCl. Based on the different profiles for the ion entropic contribution, it is found that at low salt concentration this energy contribution favors a high thickness; however, with an increase in the salt concentration, the ion entropic energy first decreases and then increases, but this time a collapsed state is favored at high salt concentration. Therefore, the ion entropic contribution increases the thickness at low salt concentration and decreases it at high concentrations. The profiles of the Born energy show that at low salt concentrations, the Born energy contribution favors an increase in the thickness of the film whereas at high salt concentrations, it favors an intermediate thickness. The relative magnitude of the contributions indicates that at low and high salt concentrations, the contribution of the Born energy is small compared to the ion entropic contribution. At 10 mM, the ion entropic contribution is sufficiently low, such that the magnitude of the Born energy will be higher. However, compared to the magnitude of the energies in Figure 4.1, both the Born and ion entropic energies are very small. The ion entropic energy included here does not have any ion-specific dependency; therefore, the Born energy can still affect the total energy minimum, even though its magnitude is relatively low.

4.4 Simulated polyelectrolyte film swelling

The swelling of a polycationic film with 5% crosslinking monomer was measured experimentally (see Figure 2.1 for the chemical structure of the film) in varied salt concentrations of either KCl, KBr, KSCN, CsCl, or LiCl, and these results are used as references in this section for the modeled data. The total energy minimum was determined using the model of the film at the same salt concentration with different types of ions and the physical properties of the film used in the model. The experimentally determined thickness at the lowest KCl concentration was used to fit the model to the same starting thickness. The data in Figure 4.3 was determined using the model.

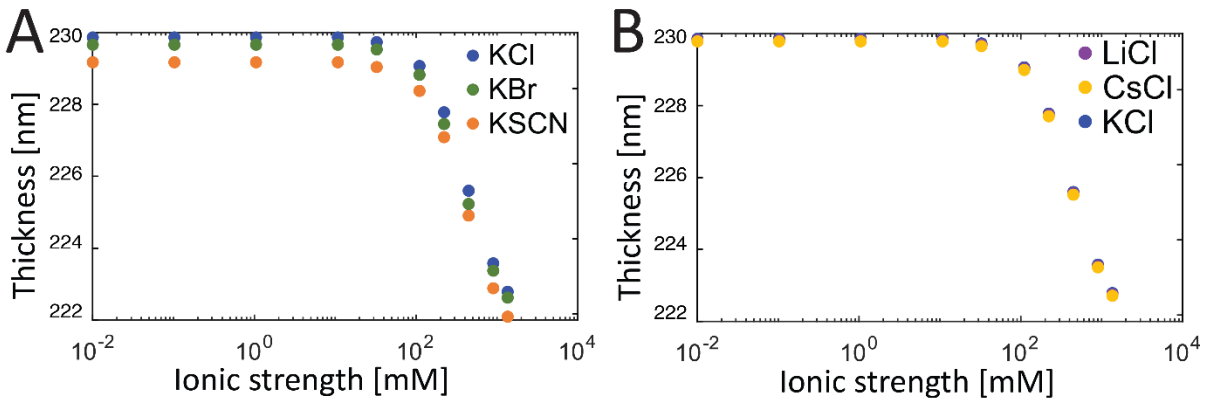

Figure 4.3: Modeled data of polycationic film thickness as a function of salt concentrations with either a constant potassium coion and varied counterions (A) or constant chloride counterion and varied coions (B).

In Figure 4.3A the modeled thicknesses change with the salt concentration of the polyelectrolyte film when a constant coion of potassium and varied counterions are present. Figure 4.3B also shows the same results but with a constant counterion of chloride and varied coions. Although a detailed discussion of the observed behavior is included in the results section, the goal here is to see how well the model describes the system. For this, three factors were considered. First, it is seen in plot A, where the counterions are varied, that the type of ions is significant, contrary to plot B, where the three different coions lead to almost identical outcomes. The order of the counterions demonstrates that the Br^- ions cause a more compressed state than the Cl^-, and the SCN^- causes a higher compression than the Br^- ions, indicating that they affect the film in the order of $SCN^->Br^->Cl^-$. Second, a transition is observed between 10 and 100 mM from a constant thickness to a constantly declining thickness for all ion types. Third, the variation in overall thickness is within 10 nm.

Figure 4.4 shows the experimental thicknesses of the film on which the modeled data was based. A comparison of the three parameters obtained from the modeled data provides the following conclusions. First, the coion variations yield very small changes compared to the counterion variations. The variations with the counterions are in the same order for the modeled thicknesses, $SCN^->Br^->Cl^-$, but with significantly larger differences in the experimental data. Second, although the change from constant thickness at low salt concentration to a different trend is between 10 and 100 mM, in this case, the second regime does not yield a constant decrease in thickness. Third, the overall change in thickness is much higher for the experimental data than for the modeled data.

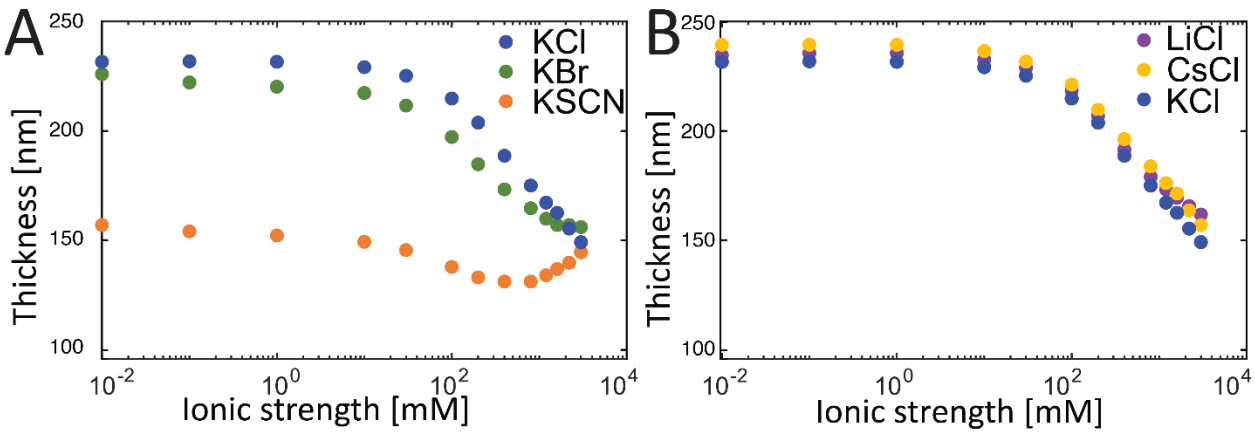

Figure 4.4: Ellipsometry-based experimental thickness of a polycationic film as a function of salt concentration in the presence of either potassium salts with various anionic counterions (A) or chloride salts with various cationic coions (B).

Based on this comparison, the modeled results are used to provide a physical meaning and to capture some of the experimentally observed behavior. The biggest difference is that the modeled thicknesses show very small differences for the specific ion effects and the overall change in thickness is very small. This can be attributed to the lower charge concentration in the model compared to the sample. In addition, this can be partly explained by the weak Born energy which is unable to cause bigger changes; this is not surprising as these changes are typically ascribed to ion pairing or chemisorption effects which are not included in the model. These effects would cause the swelling decrease to be more significant. Based on the modeled data, although the effect of Born energy is confirmed, it is very small and can be reasonably ignored. The second difference is observed in the behavior with Br^- and especially SCN^- at high salt concentrations where the trends change from a constant decrease. This effect can be captured by including nonelectrostatic effects that are ion concentration dependent. Accordingly, it is reasonable to use the model as a foundation to describe the film swelling and collapse under different ion environments. However, the model should be adjusted and expanded before it can capture the swelling of cationic and anionic polyelectrolyte films.

5 Experimental results

In this section, selected results obtained during the course of the PhD are discussed; these are divided into three different projects.

The first project focuses on thin strong polyzwitterionic films, and their swelling responses to hydration in solutions containing different ion types at varying concentrations. As these films are complex and not completely understood, polycationic and polyanionic films with the same charged groups have been studied in the same way so that these could be used to decouple the polyzwitterionic effects and through this improve the understanding.

The second project focuses on multilayered films of CHI and ADA, and their responses to salt and pH. The environments in which the layers are formed are investigated to determine the effect of pH on the adsorption and to obtain different variations of the films for further studies. The formed films are investigated, with varied ions, salt concentrations, and pH, to highlight how the behavior of these films can change completely depending on the environment. In addition, QCM-D and ellipsometry results were compared to emphasize the need for careful analysis and interpretation of the film's responses.

Furthermore, although the third project also focused on the multilayered film of CHI and ADA, the friction between the films and a CHI coated colloidal probe was studied using AFM, instead of focusing on the swelling of the film. It was assumed that based on the results of the second project, the understanding of the films could be further improved by investigating the friction under the same ion and pH environments. However, the results obtained from these measurements showed that understanding the friction behavior was more complicated than initially anticipated.

5.1 Ion-specific swelling behavior of strong polyzwitterionic film

The project aimed at understanding the swelling mechanisms of polyzwitterionic films is described in the submitted paper that is attached in Appendix A. In the following sections, the primary contents and findings reported in the paper are discussed, which means that there will be an overlap between the figures presented and the information conveyed in this section and in Appendix A.

This project is believed to have improved the current understanding of swelling in a hydrated polyzwitterionic film. The influence of the mutual interactions between the charged groups of the films (sulfonate and quaternary ammonium) and those with mobile ions in the bulk solution on a polyzwitterionic film of PMABS was elucidated. This was done by systematically measuring the swelling

response of polycationic films of METAC and polyanionic films of SPMAK by varying the type and concentration of the counterion or coion. Because the polycationic METAC and the polyanionic SPMAK contain the same charge groups as that in the polyzwitterionic PMABS, the understanding of the interactions between the polycationic and polyanionic films and the ions can be used to elucidate the effects seen in the polyzwitterionic film.

The central part of Figure 5.1 shows the chemical structure of the zwitterionic polymer along with an illustration of its interactions with itself and with cations and anions. The charges of the polymer can associate with its opposite charges and form intra/interchain bonds, or it can interact with the oppositely charged ions. The bottom left and right images respectively show the film at low salt concentration, where the intra/interchain bonds neutralize the charges, and at high salt concentration, where some of these intra/interchain bonds are broken, allowing the film to swell.

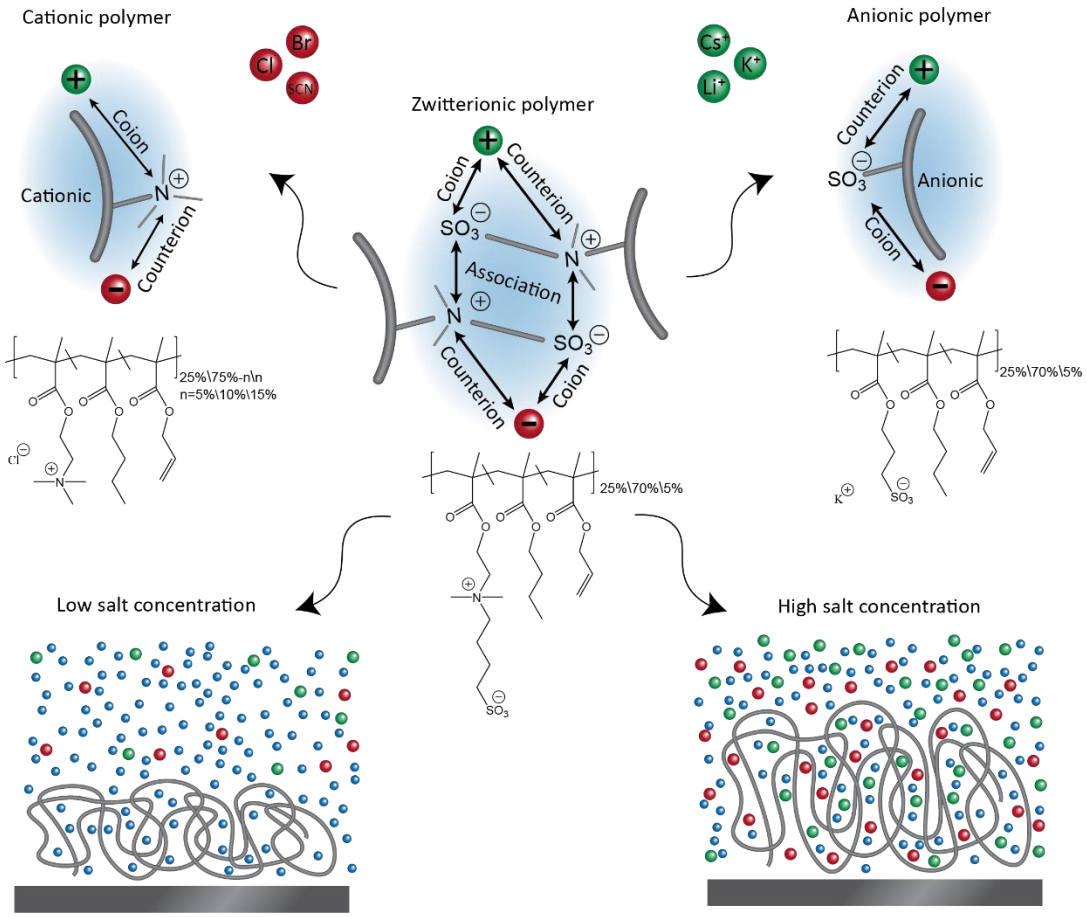

Figure 5.1: Illustration of how the polyzwitterionic swelling is investigated. The central image shows an illustration of polyzwitterionic polymer–polymer and polymer–ion interactions and the chemical structure of the polyzwitterionic film. The bottom left and right images show the swelling of a polyzwitterionic film at low and high salt concentrations, respectively. The

top left and right images show the polycationic and polyanionic polymers, respectively, along with the roles of the co- and counterions, and the chemical structures of the polymers. Reprinted from submitted paper with permission from American Chemical Society.

The chemical structures of the cationic and anionic polymers are shown in Figure 5.1 (top left and right images, respectively). The role of the cationic coions and anionic counterions of the cationic polymer along with the role of the cationic counterions and anionic coions of the anionic polymer are also shown. Random terpolymers were used which consisted of 25% charged monomer (METAC, SPMAK, or PMABS), 70% noncharged monomers (butyl methacrylate), and 5% crosslinking monomers (allyl methacrylate), except for the experiments where the crosslinking degree of the polycationic films was varied; in these experiments, the concentration of the crosslinking monomer was increased to 10 or 15% by decreasing the noncharged monomer correspondingly.

Consequently, five different films were obtained with three different charge types and two extra polycationic films with varied crosslinking. The dry thickness of these films was measured by ellipsometry, and the results are shown in Table 5.1; although the thickness of the polyanionic film is significantly large, they are all in the same order of magnitude. The swelling of the films is later referred to as the swelling ratio, which is their relative swelling from their individual dry thicknesses.

Film Type	***Cationic CL 5%***	***Cationic CL 10%***	***Cationic CL 15%***	***Anionic CL 5%***	***Zwitterionic CL 5%***
Dry Thickness	*96 nm*	*82 nm*	*98 nm*	*130 nm*	*80 nm*

Table 5.1: Ellipsometry data for the dry thickness of the five different film compositions where either the charged monomer or the amount of cross-linkable (CL) monomer is varied.

The dry surfaces of the three different types of charged films were characterized with AFM, and the films were found to be reasonably uniform. As the AFM only scans a very small area, images of the surface can be misleading or result in wrong assumptions as the surface can change significantly depending on the position of the scan. To avoid this, the scans were performed at multiple positions on the samples so that the uniformity could also be compared globally. Consequently, a similar roughness was observed at the different positions, and representative images of the surfaces are shown in Figure 5.2. Although the roughness of different types of films varies, the roughness was low in all three cases compared to the total thickness of the film.

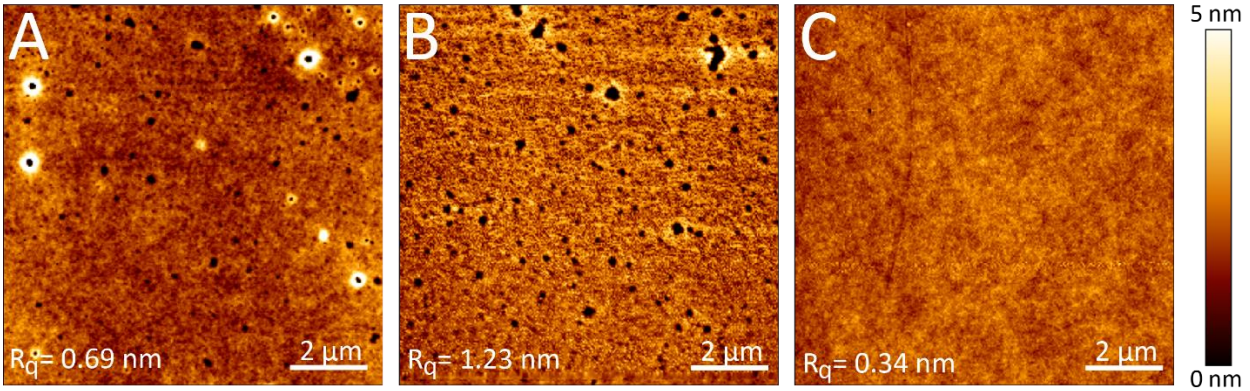

Figure 5.2: Typical AFM images of dry films of either A) polycationic, B) polyanionic, or C) polyzwitterionic with 5% crosslinking monomers. The roughness was calculated as the root mean square roughness (R_q) after a fitted plane was subtracted from the height images. Reprinted from submitted paper with permission from American Chemical Society.

5.1.1 Swelling of polycationic films with ion-specific effects

First, the swelling response of a polycationic film to changes in the salt concentration and ion types was measured. The salt concentrations were varies from 0.01 to 3000 mM in 13 increments spaced out logarithmically. As a reference salt, KCl was used from which either the cationic coion varied among K^+, Li^+, or Cs^+, or the anionic counterion varied among Cl^-, Br^-, or SCN^-. Therefore, the used salts include KCl, KBr, KSCN, LiCl, and CsCl. Figure 5.3 illustrates the presence of anionic counterion inside the film to counter the polymer charges and the typical swelling in the film at a low salt concentration (A) and a more collapsed state at a high salt concentration (B).

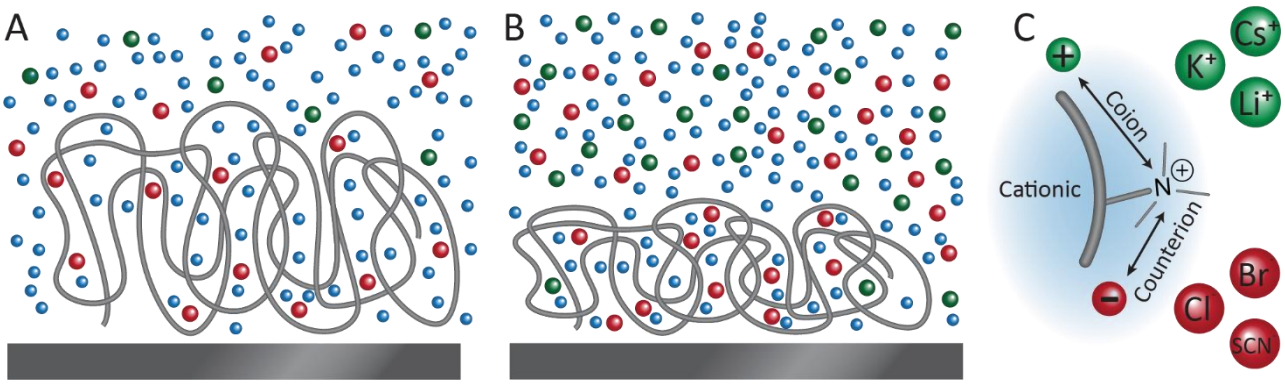

Figure 5.3: Illustration of a hydrated polycationic film at low salt concentration (A) and less hydrated at high salt concentration (B). The roles of the cationic coions and the anionic counterions when interacting with the charged quaternary ammonium group of the polymer and the different types of ions used (C). Reprinted from submitted paper with permission from American Chemical Society.

The data shown in Figure 5.4 was collected by measuring the swelling at the range of salt concentrations for different salts with ellipsometry on a polycationic film with 5% crosslinking. Figure 5.4A shows the swelling for three different anionic counterions with constant cationic coions, whereas Figure 5.4B shows

the swelling with constant anionic counterions but with three different coions. The left axes show the swelling ratio compared to the dry state while the right axes show the actual thickness of the film.

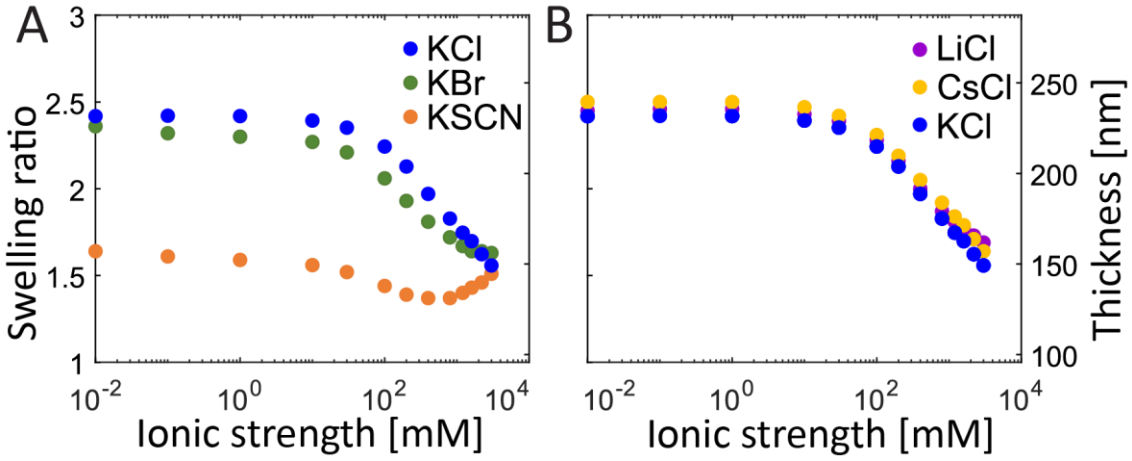

Figure 5.4: Thickness measurements using ellipsometry as a function of salt concentration on a polycationic film with 5% crosslinking monomer; either with potassium as coion with varied anionic counterion (A) or chloride with varied cationic coion (B). Reprinted from submitted paper with permission from American Chemical Society.

In the KCl curve shown in Figure 5.4A, a constant thickness region is observed at low salt concentrations, corresponding to the osmotic regime, whereas at high salt concentrations a constant decline with a logarithmic increase in salt concentrations is obtained, corresponding to the salted regime. The transition between these two regimes occurs between 10 and 100 mM KCl concentration. These scaling regimes are commonly observed for polyelectrolyte systems. The curve for KBr shows a similar trend but with a decreased thickness in the osmotic regime and most of the salted regime. At the highest salt concentration, the thickness stabilizes to a constant value. Finally, the curve for KSCN shows a significantly decreased thickness in the osmotic regime, a transition similar to that in a salted regime; subsequently, a reswelling is observed at salt concentrations above 800 mM. Therefore, a strong anionic counterion dependency is observed for the film, where the thickness in the osmotic regime follows the trend of Cl^- > Br^- > SCN^-. The different thicknesses in the osmotic regime were linked to the ability of the counterions to form ion pairs with the quaternary ammonium groups, for which the observed order of the counterion effects was consistent with those in previous reports[227,228]. At high salt concentrations, the osmotic pressure effects decline, and the stabilization with KBr and reswelling with KSCN is attributed to nonelectrostatic polymer–solvent interactions, which are commonly observed for noncharged polymers with SCN^- ions, also known as the "salting-in" effect[229–233].

Contrary to the distinct anionic counterion effect, Figure 5.4B shows the effect of change in the cationic coion, and this is found to be very small. The three curves with either K^+, Cs^+, or Li^+ coions show that they

cause a negligible variation in the thicknesses at different salt concentrations. The rate of decrease of thickness is slightly lower with Li^+ than those with Cs^+ and K^+ at the highest salt concentration. The counterions have a much larger effect on the swelling of the film in the osmotic regime, as the counterions are found inside the film at a much higher concentration.

These measurements demonstrated the mechanism for the interaction of the anions with the quaternary ammonium groups in the polycationic film. As the same quaternary ammonium groups are present in the polyzwitterionic film, the anions are expected to compete with the sulfonate groups to bind to the quaternary ammonium groups.

5.1.2 Effect of varied crosslinking on polycationic film swelling

The polycationic film studied in the previous section consisted of 5% crosslinking monomer, which was chosen because it was stable at high salt concentrations, while also showing significant changes in the thickness corresponding to the changes in the salt concentration and some of the ion types. The effect of change in the degree of crosslinking is interesting, partly because it confirms that the specific ion and salt concentration trends observed are independent of the crosslinking, but mainly because the crosslinking of the polycationic film by the crosslinking monomer is related to the crosslinking of the polyzwitterionic film caused by intra-/interchain bonds. In Figure 5.5, the top image illustrates three different degrees of crosslinking in a film representing 5, 10, and 15% crosslinking monomers for A, B, and C respectively. Consequently, with an increase in crosslinking, the film is expected to be more restricted, and therefore the swelling caused by the osmotic pressure is expected to be lower.

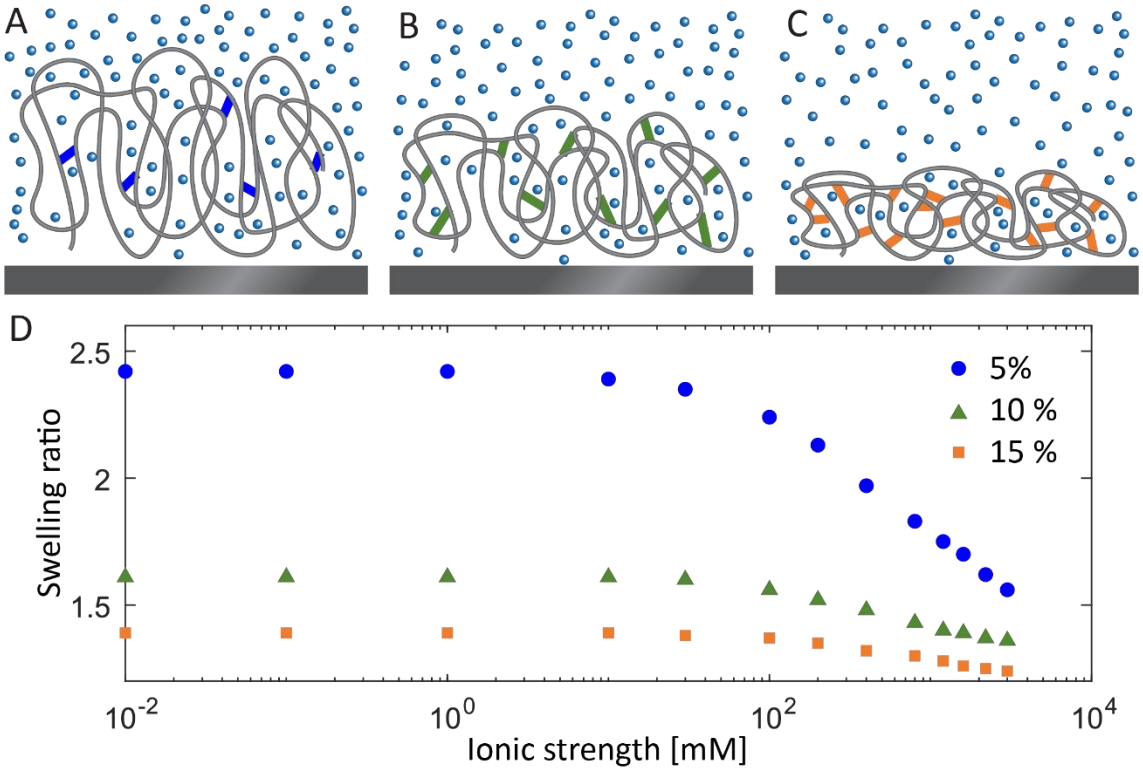

Figure 5.5: Illustration of the effects of crosslinking degree on film swelling for low (A), medium (B), and high (C) crosslinking degrees. Swelling ratios of polycationic films with either 5, 10, or 15% crosslinking monomers as a function of KCl concentration, showing the effects of change in the crosslinking degree. Reprinted from submitted paper with permission from American Chemical Society.

Figure 5.5D presents the swelling of polycationic films at varying concentrations of KCl for a film containing 5, 10, or 15% crosslinking monomers. As the dry thickness varies for the films, the swelling is presented as the swelling ratio with respect to dry thickness. For all three cases, the same trend is observed with an increasing salt concentration; first, an osmotic regime is observed followed by a transition between 10 and 100 mM to a salted regime. This confirms that as the crosslinking degree is increased, the overall thickness of the films decreased. To confirm that the specific ion effects observed previously are maintained at these different crosslinking degrees, they are measured for all the salts, and the results are presented in Figure 5.6.

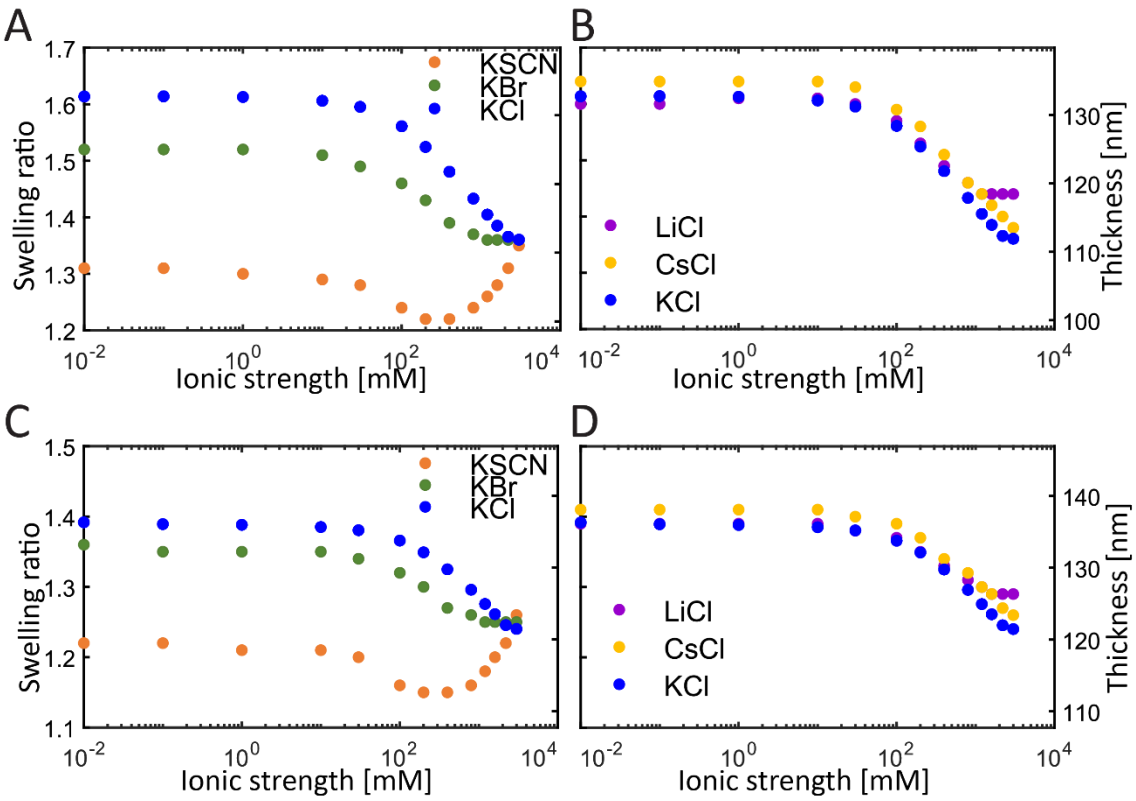

Figure 5.6: Thickness measurements with ellipsometry as a function of salt concentration on a polycationic film with 10% crosslinking monomer (A and B) or with 15% crosslinking monomer (C and D). The measurements are performed with either potassium as coion with varied anionic counterion (left) or chloride with varied cationic coion (right). Reprinted from submitted paper with permission from American Chemical Society.

Figure 5.6A and B show the polycationic film with 10% crosslinking monomer and the effect of changing the anionic counterion and the cationic coion, respectively. Similarly, Figure 5.6C and D show the same trends but with a polycationic film containing 15% crosslinking monomers. Broadly, the overall observation of these measurements indicates that the trends of each curve in increasing salt concentrations and the trends of thickness changes resulting from the change in the ions match the trends observed for the film with 5% crosslinking monomers. Although some differences are observed in the nonelectrostatic effects at the highest salt concentrations, perhaps caused by the changed chemical composition of the film, these effects are not considered significant to the purpose of this study.

The observations clearly indicated that the increased crosslinking yielded a less swollen film. The intra/interchain bonds caused by the association of the immobile charged groups in the polyzwitterionic film are expected to have a similar effect on its ability to swell, despite the variation in the type of interactions.

5.1.3 Swelling of polyanionic film with ion-specific effects

Similar to that for the polycationic film, the swelling under varying concentrations of the salts was measured on a polyanionic film with 5% crosslinking monomer. As illustrated in Figure 5.7, for this film type, the cations act as counterions inside the film, even at low salt concentrations, whereas the anions act as coions, and are primarily present outside the film.

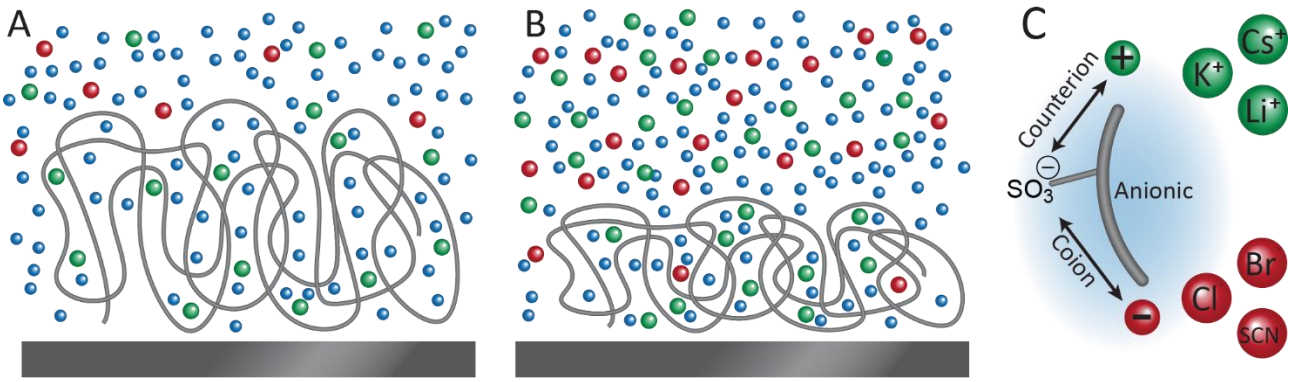

Figure 5.7: Illustration of a hydrated polycationic film at low salt concentration (A) and less hydrated at high salt concentration (B). The roles of the cationic counterions and the anionic coions when interacting with the charged sulfonate group of the polymer and the different types of ions used (C). Reprinted from submitted paper with permission from American Chemical Society.

Figure 5.8 shows the effect of the salts on the swelling of the polyanionic film. The left graph shows the effect of changing the cationic counterions with constant coions of chloride. Based on this, the specific cationic counterions are found to affect the swelling of the film very little in the osmotic regime. In the salted regime, only slight differences are observed, compared to the effect seen from variation in the anionic counterions with the polycationic film. This indicates that the counterion-induced osmotic pressure of the polyanionic film is not affected significantly by the cationic counterions used in this study.

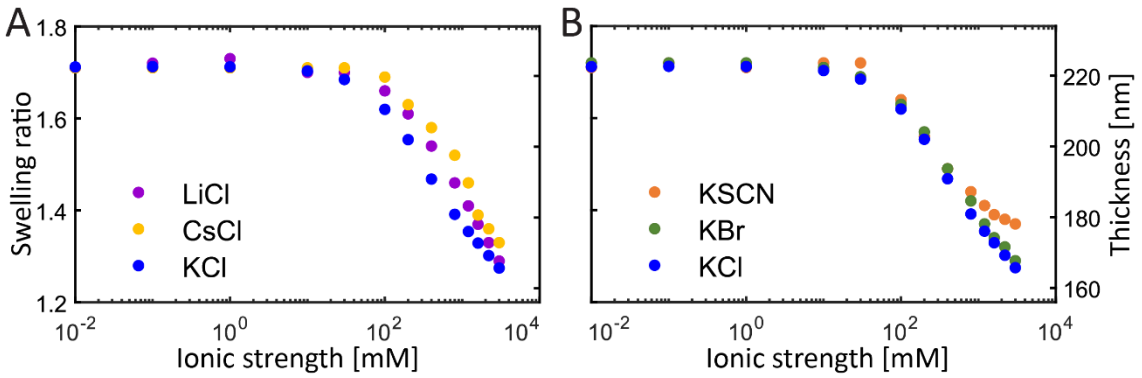

Figure 5.8: Thickness measurements with ellipsometry as a function of salt concentration on a polyanionic film with 5% crosslinking monomer; either with chloride as coion with varied cationic counterion (A) or potassium with varied anionic coion (B). Reprinted from submitted paper with permission from American Chemical Society.

Figure 5.8 shows the effect of changing the anionic coion, which has no effect in the osmotic regime and in the first half of the salted regime. At approximately 400 mM, the curve with SCN^- ions starts to collapse slower. The upturn observed with SCN^- for the polycationic film can be attributed to the nonelectrostatic effects, which is consistent with it being observed for the polyanionic case also, as it is not a counterion effect. For the polyanionic film, an upturn is however not observed, which could be explained by the significantly lower concentration of SCN^- inside the polyanionic film than in the polycationic film due to its role as coion and counterion, respectively.

Contrary to the observation for the polycationic film, the polyanionic film with different cationic counterions showed no significant effect of the specific ion type. Therefore, the interactions of the cations with the sulfonate groups did not change with the cations used here, the reason for which is discussed in the following section.

5.1.4 Ion binding affinity with polyelectrolyte charge groups

The lack of effect of the specific cationic counterions on the osmotic regime of the polyanionic film suggests, to the same degree or lack thereof, of ion pairing with the sulfonate groups with the three different ion types. To confirm this, the formation of ion pairs was investigated, which is correlated with the polarizability of the ions. Ions with high polarizability are found to form more ion pairs than ions with lower polarizability[61,71,234].

In Figure 5.9, the swelling ratios at 10 mM of the polyanionic and the three differently crosslinked polycationic films are plotted against the polarizability of the counterions. Accordingly, the polarizability of the anions was lower compared to that of the cations.

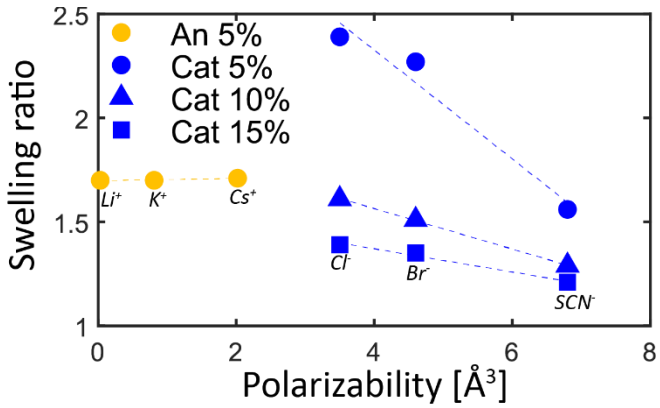

Figure 5.9: Swelling ratios for each counterion at 10 mM salt concentration of either the polyanionic film with 5% crosslinking monomer and chloride as coion or polycationic film with 5, 10, and 15% crosslinking monomer with potassium as coion, plotted against the polarizability of the counterions. The polarizabilities were obtained from[72]*. Reprinted from submitted paper with permission from American Chemical Society.*

In the case of the anions with the polycationic film, when the polarizability of the anionic counterion is increased, more ion pairs are formed, which lowers the ion osmotic activity resulting in a less swollen film. The specific cationic counterions did not affect the polyanionic film even though it was observed that their polarizability is different from each other. Accordingly, it is suggested that although the polarizability is different for the cations, it is so low that ion pairs are not formed in either case and therefore the differences become insignificant.

Based on this, the specific cations used in this study will not form ion pair interactions with the sulfonate groups in the polyzwitterionic film but instead stay osmotically active.

5.1.5 Swelling of polyzwitterionic film with ion-specific effects

Based on the interactions of the charged groups with the ions in different roles, the polyzwitterionic film can be investigated in the same way as that for the polycationic and polyanionic films. Figure 5.10 shows the behavior of the polyzwitterionic film, where it is compressed at a low salt concentration (A) due to its intra-/interchain bonds and swollen at high salt concentrations (B). The polymer–polymer and polymer–ion interactions are shown in (C), where both the cationic and anionic ions can act in coionic or counterionic roles depending on which of the polymer's charges they interact with. Consequently, the ions compete with the polymer groups of the same charge to interact with the oppositely charged polymer groups.

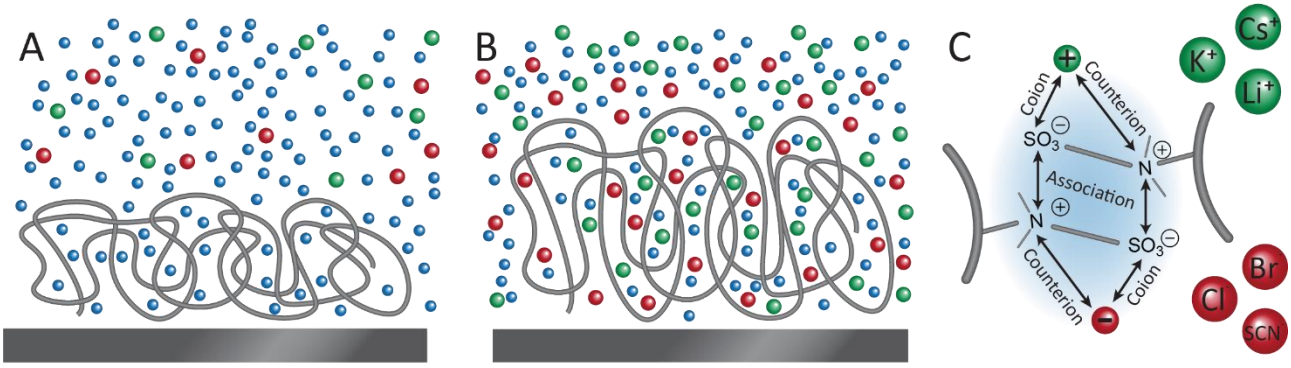

Figure 5.10: Illustration of hydrated polyzwitterionic film at low salt concentration (A) and more swollen at high salt concentration (B). Schematic of the roles of the cations, anions, and oppositely charged moieties of the polymer when interacting with each other and the different types of ions used (C). Reprinted from submitted paper with permission from American Chemical Society.

Figure 5.11 shows the polyzwitterionic film with swelling behavior of the 5% crosslinking monomer under different salt environments. In part A, the cation was fixed as potassium with varying anions, and in part B, the cation was varied with chloride fixed as the anion.

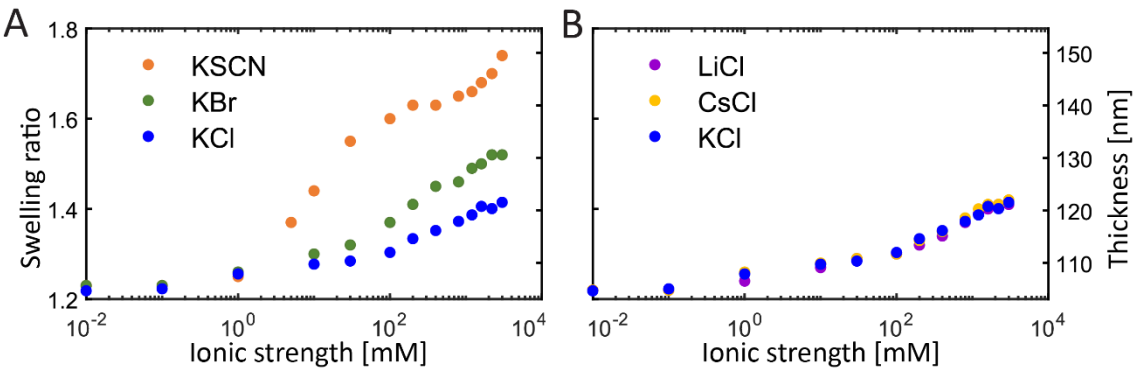

Figure 5.11: Thickness measurements with ellipsometry as a function of salt concentration on a polyzwitterionic film with 5% crosslinking monomer, either for potassium with varied anions (A) or chloride with varied cations (B). Reprinted from submitted paper with permission from American Chemical Society.

In Figure 5.11A, the KCl yields a small plateau at very low salt concentrations before the initiation of an increase in thickness. Therefore, in contrast to the polycationic and polyanionic films, the polyzwitterionic film seems to be in a collapsed state, with a low swelling ratio at low salt concentration, and the thickness increases with an increase in the salt concentration. When the salt is changed to KBr, a similar trend is observed but with a more rapid increase in thickness as the salt concentration is increased. Finally, the swelling rate of the KSCN series becomes higher, followed by a small plateau at approximately 100 mM, before increasing further. The effect of change in the cation is measured and shown in Figure 5.11B, where it is found to cause no significant changes in swelling.

The behavior of the film in salt shows an expected “anti-polyelectrolyte” effect. This effect is commonly explained by the film being in a collapsed state at low salt concentrations due to intra/interchain bonds. With an increase in the salt concentration, the electrostatic attraction of these bonds is screened, and consequently, the thickness of the film increases, similar to when the number of crosslinks was low for the polycationic film. However, as the effect of changing the anion is clearly observed, this screening effect alone cannot explain the swelling behavior. This is supported by the literature as well, and the suggested explanation is that it is caused by the different binding affinities of the ion; however, it has not been established convincingly. In this study, the results of the cationic and anionic films were used to explain the specific ion behavior of the polyzwitterionic film. In the case of the polycationic film, the ion pairing between the anions and the quaternary ammonium groups depends strongly on the ion types, with the interactions following the order of SCN^- > Br^- > Cl^-; this ordering is the same as that observed for the polyzwitterionic film. From the polyanionic film, an insignificant effect was observed for the change in the cations with the sulfonate groups; this can be attributed to the low polarizability of the cations, which prevents them from forming ion pairs.

Accordingly, the proposed mechanism suggests that the polyelectrolyte film is in a collapsed state at low salt concentration due to the intra/interchain bonds causing physical crosslinks. When the salt concentration is increased, the ions enter the film and the screening effect lowers the interaction between the charged polymer groups. This causes the ions inside the film to compete with the bonds between the charged polymer groups, which will favor the ions when the salt concentration is increased. The ions with strong interactions with the oppositely charged moieties, herein the anions, can break the intra/interchain bonds first, indicating that the anions will follow the order of their interaction strength SCN^- > Br^- > Cl^-, as observed in Figure 5.11A. The cations then compensate the sulfonate groups to maintain electroneutrality, inducing an osmotic pressure. Both the induced osmotic pressure and the lowering of the crosslinking allow the film to swell.

Thus, the interactions of the ions with the polyzwitterionic film and the resulting swelling behavior indicate a complicated mechanism that depends not only on the salt concentration but also on the interactions of the ions interactions with the charged moieties of the film.

5.2 Swelling of weak polyelectrolyte multilayer films

The second study in this project is related to multilayer films and their swelling responses under varied conditions. The films studied were prepared using alternating layers of CHI and ADA in solutions with two different pH conditions. The swelling responses of the films to changes in pH, salt concentration, and ion types were measured with QCM-D and ellipsometry. There were two overall goals of this study. First and most important was to enhance the fundamental understanding of the mechanisms of interactions of the weak polyelectrolytes in the film with each other and with the ions in the solution to improve the ability to predict the response and design films for specific applications. Second, as the pH-dependent response of the films depends significantly on the salt conditions, this study establishes the importance of considering the environment when designing films for specific applications. This is an important point to emphasize, as it is shown that if the testing conditions vary from the application conditions, completely wrong conclusions can be drawn about the pH responsiveness.

In the following sections, I will present a condensed version of the paper attached in Appendix B, leaving the fully detailed discussions in the paper. There will therefore be an overlap between the figures presented and the information conveyed in this section and in Appendix B.

The films used were prepared using the technique described in section 2.2 and consisted of 15 layers, starting with a CHI layer on a silanized substrate, resulting in the top layer being a CHI layer (odd-numbered layers are CHI and even-numbered layers are ADA). Depending on the use, the substrate can either be a QCM-D chip or a silicon wafer for the QCM-D or ellipsometry studies, respectively.

5.2.1 Layer build-up under different pH conditions

First, the build-up of the film was investigated with QCM-D at different pH values. These measurements can be used to investigate the effect of pH on the added amount of each type of layer as well as the layer configurations.

The films were prepared in ultrapure water in which 15 mM NaCl was added and the pH was adjusted to either 3 or 6 using HCl. Although a buffer solution was not used as it would introduce different types of ions, the pH of the solution was stable within the time required for preparing the layers in this simple version. Each layer was obtained by flowing the solution with the polyelectrolytes over the surfaces and then rinsing before the solution containing the oppositely charged polyelectrolyte was flown over the surface. The values of the frequency and dissipation shift from the QCM-D data were determined after they stabilized during the rinsing.

Figure 5.12A shows the QCM-D frequency and dissipation shift for a film prepared at pH 3. The first layer measured is layer 2 as layer 1 is the CHI layer created by dip coating outside the liquid cell. The frequency decreases gradually, in almost identical steps for the two different polyelectrolytes. Although a higher rate of decrease is observed with the addition of more layers, the increase is not significant. The dissipation is significantly higher with CHI in the top layer than with ADA. The dissipation is not constant for the initial layers, but after five layers the dissipation becomes almost constant for CHI and ADA individually.

The dissipation of the layers is quite different for the two polymer types; the CHI layers are significantly more dissipative than the ADA layers. This shows that polymers in the CHI layer have a more stretched confirmation when present in the outer layer which can be attributed to the different charge densities of the polymer due to their degree of dissociation; it can also be attributed to different hydrophobicity. The frequency shift shows that the mass added to the film with each layer type is similar. However, as seen from the dissipation, the outer layer of CHI is more outstretched and therefore contains more water than the outer ADA layer. Therefore, it can be concluded that the ADA layers contain more mass than the CHI layers, which fits well with the assumption that CHI has a higher charge density than ADA at low. The small change in the frequency shifts is likely due to the formation of small aggregates, which although unavoidable, is insignificant for the QCM-D and ellipsometry measurements of the final film at this level.

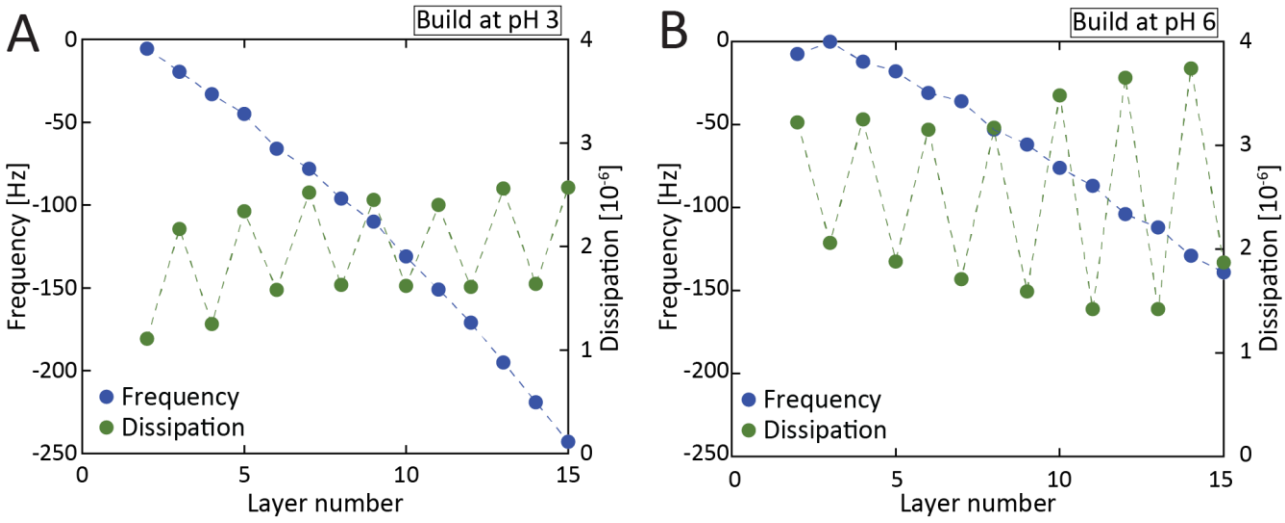

Figure 5.12: Frequency and dissipation shift of layer building in QCM-D for multilayers of CHI and ADA built at pH 3 (A) and pH 6 (B) with 15 mM NaCl. CHI is present in odd-numbered layers and ADA in even-numbered layers.

Figure 5.12B shows the QCM-D results of a film obtained at pH 6 and otherwise under the same conditions as the film prepared at pH 3. A small increase is observed in the frequency shifts of this film from layer 2

to layer 3. The total frequency shift is approximately 150 Hz only, whereas at pH 3 it is close to 250 Hz, showing that the film consists of less mass than the one created at pH 3. At pH 6, a larger dissipation shift is caused by the ADA layer. This indicates that the CHI/ADA ratio at pH 6 is higher than it was at pH 3.

The film prepared at pH 6 is significantly thinner than that prepared at pH 3, and the ratio of the two polymers is also changed. At pH 3, more ADA than CHI is needed to counter the charges of the previous layer as their charge density is different, whereas, at pH 6, the polyelectrolytes are closer to being attached in an equal ratio. The unmatched charge densities at pH 3 necessitate a need for thicker ADA layers to compensate, and this leads to the increased thickness of this film. Since the layer-by-layer process is electrostatically driven, it is expected that the films are close to electrostatically neutral at the pH at which they are created.

5.2.2 Swelling response to variation of NaCl and pH

After studying the prepared films, their swelling response was analyzed. First, the swelling effect of NaCl concentration was studied at different pH values using ellipsometry. To measure the film with ellipsometry, the film was prepared on a silicon wafer instead of a QCM-D chip, while the rest of the procedure remained unchanged.

Figure 5.13A shows the swelling against the NaCl concentration at pH 3, 6, and 9 for a film created at pH 3, where the points are the measured values and the lines are to guide the eyes of the reader. At pH 3, the thickness of the film is almost constant from low salt concentration up to approximately 1000 mM. Further increasing the salt concentration causes a complete change in the behavior of the film as the film starts to swell significantly with the salt concentration. At pH 6 for the same film a similar behavior is found, but with an overall lower thickness and a small peak in the thickness at 30-50 mM. The last graph at pH 9 shows a behavior that is different from those at pH 3 and 6. At low salt concentrations, it is significantly more swollen than it was at pH 3. As the salt concentration is increased, a constant thickness regime is observed similar to that in the two other cases, but at an approximate salt concentration of 10–50 mM, the thickness of the film increases rapidly. Further increases in the salt concentration result in a constant decrease, but at the highest salt concentration measured, the film is still significantly thicker than at the same salt concentration at pH 3 and 6.

The charged amine groups of CHI and carboxylic acid groups of ADA can form ionic bonds which will increase the effective crosslinking of the film and decrease the swelling. If oppositely charged groups are not matched equally, due to a change in pH, the film can have an overall negative or positive charge, which

results in counterions entering the film and increases the osmotic pressure. The weak nature of CHI and ADA means that they can also adjust the excess charge by protonation and deprotonation of the amine and carboxylic acid groups, which is a process strongly affected by ionic strength. These processes are used when the swelling behaviors are interpreted.

Because the film is created at pH 3, the polyelectrolytes at the interfaces between each layer are expected to have a matching number of charges at this pH. When the salt concentration is increased, the swelling of the film can be explained by the increased salt concentration breaking the physical interchain bonds between the layers. This results in a higher osmotic pressure inside the film and an effectively lower crosslinking of the film and consequently causes swelling. This behavior, and the assumptions made about it, is very similar to the “anti-polyelectrolyte” effect that was seen for the zwitterionic film discussed in section 5.1.

When the film is hydrated in pH 9 at a low salt concentration, the charges of ADA and CHI are unmatched because CHI becomes less charged and ADA becomes more charged at this pH. This causes both fewer interchain bonds and an overall negative charged film. If the charges creating interchain bonds are ignored, the film can in this case be viewed as a weak monocomponent polyelectrolyte film. As described, the swelling behavior of a weak polyelectrolyte film as a function of salt concentration is typically divided into three different regimes. A neutral regime at low ionic strength where the swelling is constant due to self-regulation of the charges, an osmotic regime where the film swells as the ionic strength is increased, and then a salted regime where the swelling decreases with an increase in the ionic strength. The multilayer film shows similar regimes with first a salt-independent regime, an osmotic regime, and finally a salted regime. The salted regime shows a slower decrease than what is typically expected for weak polyelectrolyte films, which is expected to be due to the increased salt concentration breaking the interchain bonds which is a process counteracting the film's thickness decrease. This behavior is therefore considered a mixture of those seen for weak monocomponent polyelectrolyte films and polyzwitterionic films but dominated by the weak polyelectrolyte trends.

At pH 6 the polyzwitterion-like behavior is again primarily seen with the small peak at 30-50 mM indicating a very small weak polyelectrolyte effect with an osmotic and salted regime. The top layer of CHI, which is expected to be positively charged at pH 3, is assumed to be less charged at pH 6 which could explain why the overall thickness of the film is lower at pH 6.

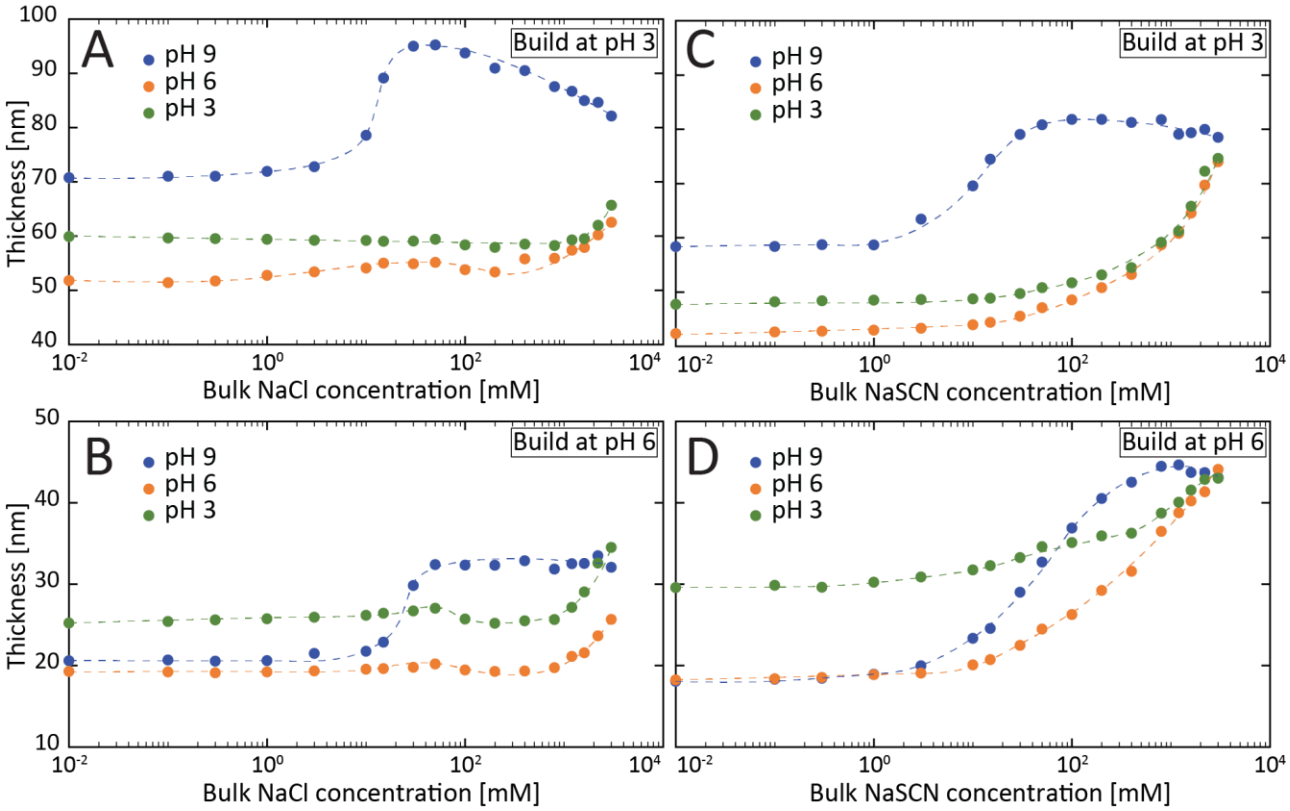

Figure 5.13: Swelling of multilayer films of 15 alternating layers of CHI and ADA at a range of salt concentrations at pH 3, 6, or 9; either with NaCl as the salt for films created at pH 3 (A) and pH 6 (B) or with NaSCN as the salt for films created at pH 3 (C) and pH 6 (D).

Figure 5.13B shows the results for the measurement of swelling behavior at the same pH and salt variations, but this time for a film prepared at pH 6 instead of pH 3. Previously, this film is shown to be significantly thinner owing to the more similar charge densities, which is confirmed by the ellipsometry measurements. Furthermore, in this film, the charges at pH 6 are expected to match up and are neutralized by the formation of interchain bonds. The salt response at the three different pH values has a similar shape to that observed for the film prepared at pH 3, but with some differences. At pH 6 the film is in its most collapsed state, which is expected as the charges should match and form interchain bonds, which will restrict its swelling. A small peak between 30 and 50 mM is however still found indicating a small charge imbalance causing a weak polyelectrolyte effect. At pH 3, the thickness at low salt concentration is significantly higher than at pH 6, which corresponds with the expectation of fewer crosslinks. The swelling behavior resembles that at pH 6, including the small peak. Finally, at pH 9 the film is again showing a drastically different swelling behavior compared to at pH 3 and 6. The swelling is similar to that seen for the film created at pH 3, except that in this case, the swelling at the “salted” regime is

now constant. As this film contains more crosslinks, the effect of breaking these by increasing the salt concentration could counteract the salted weak polyelectrolyte effects resulting in a constant thickness.

Based on the behavior of the film in Figure 5.13A and B, it is found that the swelling behavior can be described by a mixture of a zwitterionic film, similar to the one in the previous project, and a weak polyelectrolyte film, which has been the focus of previous studies in our group.

5.2.3 Swelling response to variation of NaSCN and pH

To better elucidate the factors driving the swelling, the same measurements were performed on the same films (still prepared in 15 mM NaCl), but with the salt changed from NaCl to NaSCN in the response measurements. Thus, the specific ion effects on swelling can be studied and the learnings from the zwitterionic film in the previous project can be applied. The SCN^- ion is often used when studying counterion effects because it has a relatively high binding affinity compared to simpler ions, such as Cl^-, which indicates that a bigger difference will be observed for ion-specific effects.

Figure 5.13C shows the change in swelling behavior of the film prepared at pH 3 when the salt is changed from NaCl to NaSCN. At pH 6 and pH 3 the films start to swell at a significantly lower salt concentration and the swelling is much larger than that with NaCl. This accentuates that the swelling is caused by the same dynamics that are seen for a polyzwitterionic film as this effect aligns well with what was observed for the polyzwitterionic film in the previous project: The higher binding affinity of the SCN^- ions can break the interchain bonds of the film at a lower salt concentration than that with Cl^-, which causes swelling by lowering the number of crosslinks and introducing counterions. At pH 9 the film is expected to be overall negatively charged, which means that the SCN^- ions will not act as counterions when the film is viewed as a weak monocomponent polyelectrolyte film. The swelling of the film at this pH is similar to what was seen with NaCl, but this time with a more gradual osmotic regime and a constant thickness at high ionic strength. This corresponds well with a stronger polyzwitterionic effect that is expected to influence the film more at increasing ionic strength.

Figure 5.13D shows the film prepared at pH 6 with NaSCN. At pH 3 and 6 trends similar to the film created at pH 3 are found. This is in agreement with the comparative trends found for the films with NaCl. At pH 9 the effect of NaSCN seems to be that the film's combination of weak polyelectrolyte and polyzwitterion

behavior is shifted more towards the polyzwitterionic behavior. This is again in line with what was seen with NaCl for the two films at pH 9.

5.2.4 Response to pH measured with QCM-D

As the QCM-D technique is sensitive enough to study the build-up of the individual layers of a multilayer film, this technique is often also used to study the responsiveness of the films to changes in the environment and the stability of the film. In this study, the effect of varying the pH between 3 to 6 and 6 to 9 at three different salt concentrations (1, 50, and 3000 mM) was investigated. This was performed for the film prepared at pH 3 and 6 with both NaCl and NaSCN. The salt concentrations were chosen to target the different regimes of the swelling according to the ellipsometry data. The frequency shifts occurring from the films' pH responses under the different salt conditions are compared to the ellipsometry data. It should be noted that ellipsometry and QCM are two different methods that measure different properties of the film, refractive and viscoelastic responses, respectively. Each technique is dependent on the method of interpretation to provide the swelling of the film. The main purpose of the QCM-D measurements is to show how an application requiring a specific response from the film needs to be tested in similar conditions, as conclusions of the response could otherwise be completely different from the actual response.

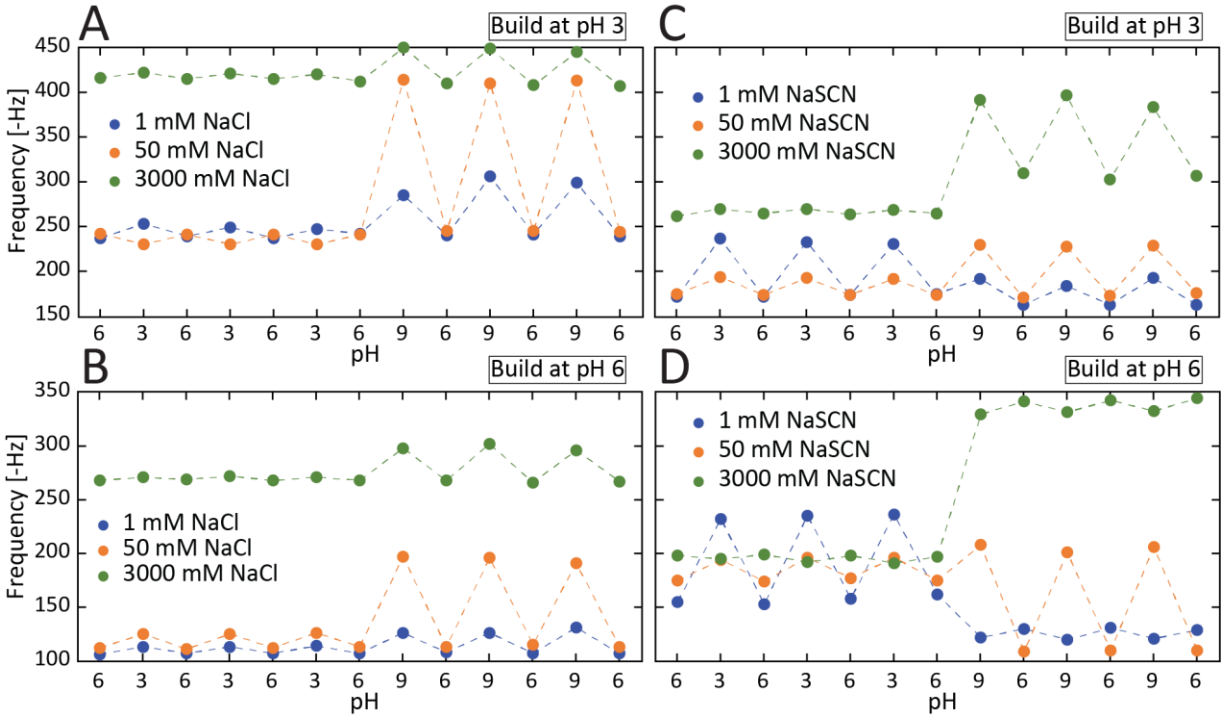

Figure 5.14: pH cycles of films with CHI as the top layer for the layer prepared at pH 3 (left) and pH 6 (right) at different concentrations of NaCl measured with QCM-D.

In Figure 5.14A and B, the swelling response with NaCl between pH 3 and 6 is shown to be very small, while between pH 6 and 9 the response is significantly larger. Especially the response between pH 6 and 9 at 50 mM is much larger than the rest. These responses are in good agreement with the ellipsometry swelling data, where similar responses are seen.

In Figure 5.14C and D, the same film's swelling responses are shown with NaSCN instead of NaCl. These responses are showing fewer agreements with the ellipsometry responses. A larger response is again found when going between pH 6 and 9 at 50 mM, however, at 1 mM the largest response is now between pH 3 and 6 instead of between pH 6 and 9. A new effect of NaSCN that is found is also that the return to pH 6 is now dependent on the previous pH, which was not the case with NaCl. This could be due to the stronger ion pairing affinity of SCN^- and the amine groups of CHI.

The learnings emphasized by these QCM-D measurements are overall that the responses of the film are very dependent on pH, but also on ionic strength, ion types, and the composition of the film. The complexity of the films means that a measurement of the pH responsiveness at a single salt concentration gives very limited insights into the films' behavior.

5.3 Multilayer friction

In this section, the friction measurements performed on a CHI/ADA multilayer sample are presented, along with the variation in friction depending on the conditions of the medium. These results were to be used to enhance the fundamental understanding of multilayer films as a continuation of the previous discussion. However, these results were more complicated to interpret than first anticipated. The purpose of this section is therefore mainly to show that the process of setting the AFM microscope up for friction measurements and performing the measurements was successful and secondary to providing a short description of the trends observed.

5.3.1 Sample for friction measurements

The friction measurements were performed on a sample with seven layers of CHI and ADA, instead of the 15 layers in the previous section; the layers were prepared at pH 3 with 15 mM NaCl. The number of layers was reduced because this gives a smoother layer which is beneficial for these measurements. In contrast, the 15 layers are rougher at the top layer, but also have a larger total thickness and more attached mass, which is an advantage for ellipsometry and QCM-D studies. The layer was analyzed with a Cr/Au HQ:CSC37B tipless cantilever having length and width of 350 and 35 µm, along with a glass bead of 7-µm-diameter attached as a colloidal probe. This probe was silanized and a layer of CHI was grafted to it through the same procedure as that used for the first layer of the multilayer film.

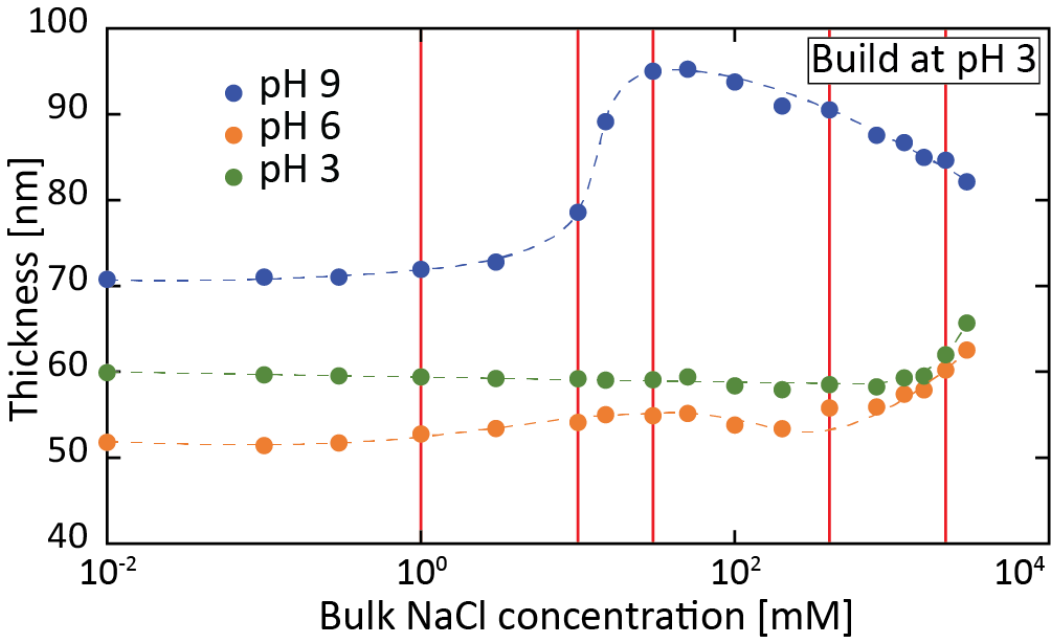

Figure 5.15: Swelling of multilayer films of CHI and ADA at a range of NaCl concentrations at pH 3, 6, or 9 and red lines indicating the salt concentrations where the friction was measured.

The friction was measured at pH values of 3, 6, and 9 and with NaCl concentrations of 1, 10, 30, 400, and 2200 mM at each pH, which was chosen based on the ellipsometry swelling data determined for the film prepared under the same conditions but with 15 layers. Figure 5.15 shows this swelling data with indicators of the conditions at which the friction was measured. At the lowest salt concentration, 1 mM, the film is at a stable thickness at all three pH values. Then, at 10 mM the film at pH 9 starts to swell and it swells completely at 30 mM. The two highest concentrations are 400 mM, which is before the film starts to swell at pH 3 and 6, and 2200 mM which is after their swelling has begun.

5.3.2 Determination of the normal force range

To determine the force range at which it was relevant to measure the friction, vertical force curves were obtained at the different pH and salt conditions. At each of the conditions, a grid of 50 by 50 points force curves at a 100 by 100 µm area was measured. The curves generally showed that the force between the sample and the colloidal probe was repulsive and that the range of this force was lowered with an increase in the salt concentration. This was as expected as the top layer of the film and the coating of the colloidal probe contain CHI, and the salt causes screening of the charges. However, force curves showing adhesion between the sample and the probe when retracting the probe from the sample were also observed. This was quite unsystematic and was therefore not chosen to draw any conclusion on.

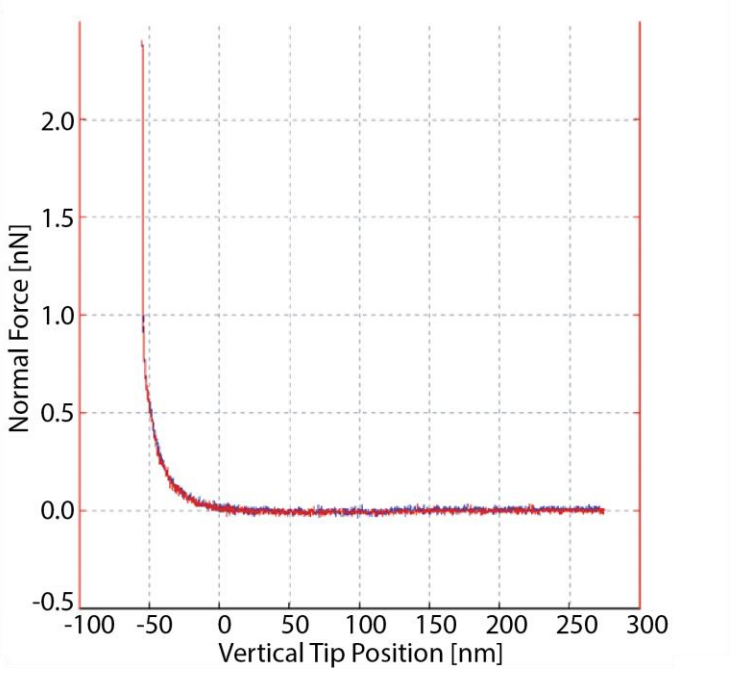

Figure 5.16: Representative force curve on 7 layers CHI/ADA sample with CHI coated colloidal probe taken at pH 3 and 1 mM NaCl.

The repulsive force curves indicated that at force above 1 nN, hard wall contact was reached and therefore, normal forces below this are interesting for friction measurements. Figure 5.16 shows an example of such a force curve for the sample at pH 3 and 1 mM NaCl. To confirm that no unexpected friction trends were present at higher normal forces, the friction was measured up to approximately 4 nN.

5.3.3 Friction and normal force relation

The friction was measured at 60 different normal forces ranging from 0.05 to 3.75 nN. The friction was measured in a 10-µm-line with 512 points, first at the lowest normal force, then again at the second lowest normal force, and this was continued until the highest normal force was reached. This was performed for five different lines each spaced 20 µm away from the previous. After completion, the pH or salt concentration was changed and the friction measurements were repeated. For each normal force of each line, the average torsional twist in each direction was measured and used to calculate the friction. Figure 5.17 shows an example of a friction measurement at pH 3 with 2200 mM NaCl. Here, the points correspond to the average friction plotted against the entire range of normal forces. The error bars indicate the variations between the five lines. This plot shows that the friction measured is almost not dependent on changes in the measured position, at least not within the positions investigated. It also shows a clear increase in friction with the normal force, which is almost linear in this case. There seems to be a small difference in the slope above and below the normal forces of 1 nN, which was observed only in some of the conditions.

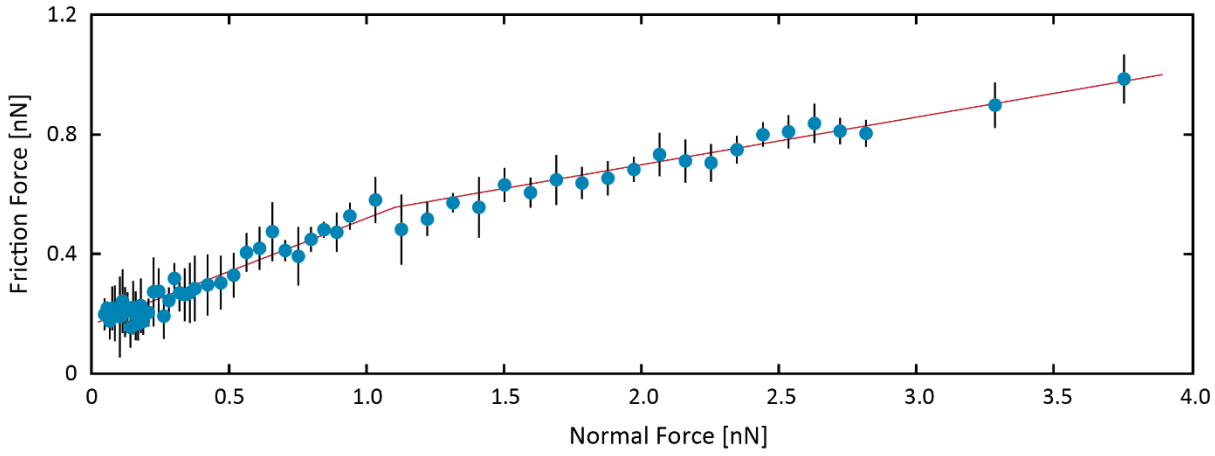

Figure 5.17: Friction measurements on 7 layer CHI/ADA sample at pH 3 and 2200 mM at a range of normal forces.

Figure 5.18 shows the friction against the normal force in the range below hard wall contact for the five salt concentrations at the three different pH values. Notably, the friction force axes are different to ease the comparison of the data in the individual plots. The relation between the friction force and the normal force in this normal force range is close to linear. In Figure 5.18A, at pH 3, a small increase in friction is observed across the range of normal forces as the salt concentration is increased. However, all curves except the one measured with 2200 mM NaCl are very similar and the friction is overall low. Figure 5.18B shows that at pH 6, the friction has changed significantly. Most noticeable are the curves at 1 and 10 mM NaCl, where higher friction is observed compared to the other curves. With a further increase in the salt concentration, the friction decreases significantly, but stays at higher values than those at the same salt concentrations at pH 3, and increases slightly when the salt concentration is increased. Finally, at pH 9, as shown in Figure 5.18C, the friction becomes very low, which causes the noise in the measurements to make the data appear messier than the data curves at the other pH values. At pH 9, especially the highest salt concentration shows increased friction, while the other curves are similar and difficult to distinguish. In addition to the actual value of the friction force, the slope and intersections of the lines with the friction force axes can also be used to understand the friction dynamics. Although the slope can be complex to interpret, the meaning of the friction force at zero normal force is simpler to understand, as this indicates an attractive force between the film and the probe. At pH 6, a clear indication of an attractive force is observed, where all curves intersect the friction force axis somewhere above zero; however, especially the curves for 1 and 30 mM are significantly higher than all other curves.

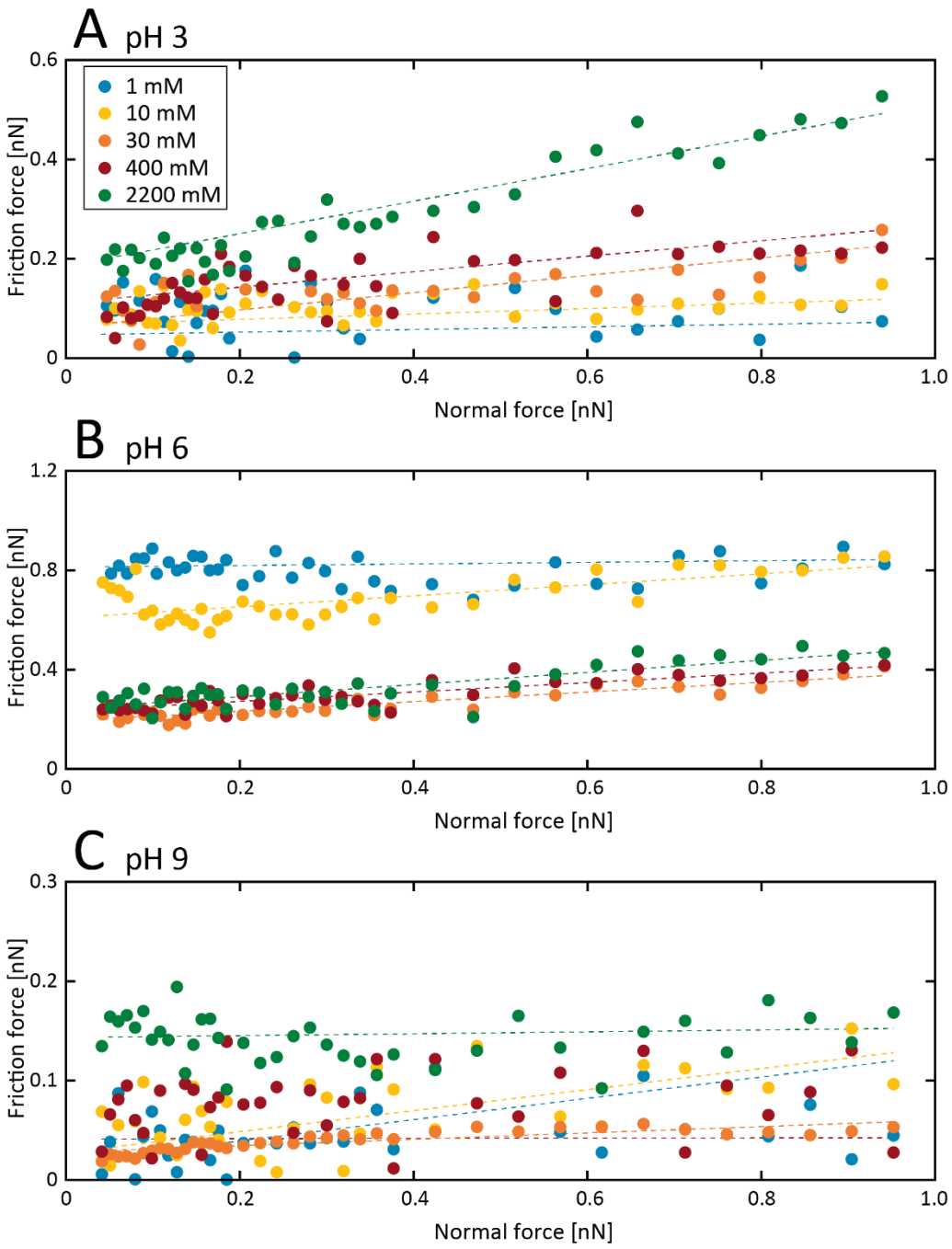

Figure 5.18: Friction as a function of the normal force under varying NaCl concentrations for 7 layers CHI/ADA samples at pH 3 (A), pH 6 (B), and pH 9 (C).

5.3.4 Friction affected by pH and salt concentration

To better quantify the magnitude of the friction force under the variations in the environment, the friction at 0.3 nN normal force was considered and the variations in it corresponding to the changes in the environment were analyzed. Although this normal force was chosen based on the relevant part of the force curves, fair arguments can also be made for choosing a higher or lower normal force. Based on the results obtained, the specific normal force chosen does not result in significant changes in the relative friction values compared to most of the other normal forces in this range. To calculate the friction at this normal force, the median of the five measurements (around 0.3 nN) was considered as the friction, and the corresponding results are shown in Figure 5.19.

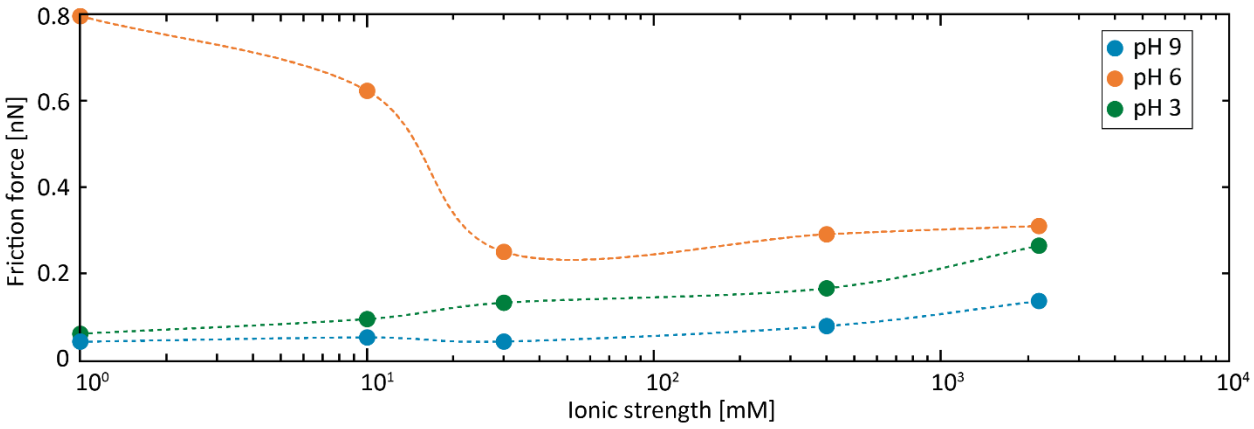

Figure 5.19: Friction force at 0.3 nN (median of five data points around 0.3 nN) normal force as a function of salt concentration at different pH values.

The trends shown at pH 3 and pH 9 in Figure 5.19 indicates that the friction is approximately increasing as the salt concentration is increased. This is also the trend for the three highest salt concentrations at pH 6 while at the two lowest the friction is significantly larger than all other points. At pH 6 the ADA has started to become more charged than at pH 3, while CHI is still staying more charged than at pH 9. Based on this it seems reasonable that the friction at pH 6 should be higher than at pH 3 and pH 9, due to the film having more physical crosslinks to break causing energy dissipation. However, it is also expected that when the salt concentration is increased, there are fewer crosslinks which then should lead to lower friction, which is generally not seen. This might be due to the repulsion between the probe and the film, which decreased with the increased salt concentration, making the interpretation more complex.

The main point of this section is to show that it was possible to measure the friction and to show that these measurements give some interesting results that are too complex to understand from the current knowledge of the multilayer systems. I do, however, believe that if an understanding of how these results

should be interpreted, e.g. by measuring simpler variations of the system, this technique could provide some new contributions to the understanding of the multilayer films' fundamental behavior.

Conclusions

The main goal of this project was to improve the current understanding of the fundamental dynamics in polyelectrolyte films and through this knowledge increase the possibilities of predicting and tuning their swelling responses.

Ion-specific swelling behavior of polyzwitterionic films was the focus of the first study. The current understanding and experimental measurements were used to describe the specific ion interactions in coion and counterion roles with polycationic and polyanionic film. It was shown how the high polarizability of the anions compared to the cations allowed different types of anionic counterions to significantly affect the swelling of the polycationic film through ion-pairing. Meanwhile, the cationic counterions showed that these had no specific ion-dependent effects on the polyanionic film. This knowledge was used with measurements of the polyzwitterionic film, where increased swelling with a rise in ionic strength was observed in accordance with the “anti-polyelectrolyte” effect. The magnitude of the swelling was found to be strongly affected by the anion types, while it did not depend on the type of cations. Based on the results it is proposed that the antipolyelectrolyte effect is a complicated swelling mechanism related to the electrostatic and nonelectrostatic ion-specific interactions. Dissociation of the intrachain and interchain bonds was derived via electrostatic screening and enhanced by specific ion-pair interactions, in cases where ions from the salt could strongly bind to one of the polyzwitterion’s charged groups. When an ion bind to one of the polyzwitterionic charges, the effect is that the intra-/interchain bond is broken and the oppositely charged group introduces a counterion to neutralize it, which both leads to increased swelling.

Multilayer films were the focus of the second study, where a selection of parameters affecting the multilayer films’ responsiveness was systematically investigated. In this study, it was shown how the pH-dependent swelling response of the film is very dependent on the salt concentration, the ion types, and the composition of the layers. The swelling response of the film was found to be affected significantly different by the pH at increasing salt concentrations. By using the understanding of polyzwitterionic films from the previous study and the literature description of weak polyelectrolyte films salt dependent swelling response, it was shown how the films' behavior could be described by a mixture of these. When the film's two component’s charges balance each other, the film’s swelling behavior was found to be similar to the antipolyelectrolyte effect observed from the polyzwitterionic film. If one of the components of the multilayer film was charged significantly more than the other, a swelling behavior with regimes similar to those of a weak polyelectrolyte film was found. By comparing ellipsometry and QCM-D data for

swelling responses it was shown how typical QCM-D measurements can lead to misinterpretations of the pH responsiveness if the ionic strength and ion composition are not carefully considered.

In an attempt to improve the understanding of the multilayer films with a new method, the friction between the film and a colloidal probe coated identically to the film's top layer was measured under different salt and pH conditions with an AFM. These results were too complicated to interpret meaningfully, but they did show that it was possible to measure the friction with the instrument. The calibration of the instruments and the cantilever, together with the analysis program created, meant that it was possible to elevate these friction measurements from relative comparisons of the friction into measurements of the actual size of the friction force.

Perspectives

As a part of this project, there have been directions and experiments which I have tested that turned out to be dead ends. I believe that a part of a PhD project is to test things out and reach the conclusion that this is a track that should no longer be continued. So even though it has been frustrating in the situation and time-consuming compared to if I had just done all the "correct" steps throughout the project, I think they are an essential part. However, if I have had more time to spare, or a longer project, I think that there are parts of the work I have done that would be both interesting and rewarding to pursue further.

The first part is the theoretical model describing the polyelectrolyte films' swelling responses to specific ion types at specific concentrations. As is the case with the studies I have performed, most fundamental studies for these films are based on experimental measurements with varied parameters. These measurements can typically not show the internal dynamics in the film, but only the resulting effects. Therefore, the parameters are varied, and based on the effects, an explanation for the found behavior is suggested. This is a perfectly valid method that has worked well in many scenarios, but the interpretations of the results could benefit hugely from an independent theoretical method. Ideally, the theoretical model in my project should be developed further, so that it could be given the properties of the polyelectrolyte film and the solution and from that show the same magnitude and trends of the swelling behavior as observed experimentally. The benefit of a theoretical model is that the different contributions leading to the swelling behavior can be decoupled, giving a much stronger foundation for explaining the dynamics in the film.

The second part that could be further pursued is the friction measurements as a tool to improve the fundamental understanding of the polyelectrolyte films. As the friction measurements with the AFM allow the friction to be measured at extremely small scales, which could provide results that would be a great supplement to ellipsometry and QCM-D results. I have in this project tried to use it on the quite complex multilayer films, which lead to results that were difficult to get a meaningful understanding from. To use this method on the complex multilayer films, it would be necessary to develop an understanding of how these friction measurements should be interpreted. This could be done similarly to how the zwitterionic films were understood, where simpler polycationic and polyanionic films were first studied, before the knowledge from these films was applied to more complex films. This could lead to a method that could provide important and unique insides into the multilayer film's dynamics.

References

1. Zhang, Z., Chao, T., Chen, S. & Jiang, S. Superlow fouling sulfobetaine and carboxybetaine polymers on glass slides. *Langmuir* **22**, 10072–10077 (2006).
2. Chang, Y. *et al.* A highly stable nonbiofouling surface with well-packed grafted zwitterionic polysulfobetaine for plasma protein repulsion. *Langmuir* **24**, 5453–5458 (2008).
3. Zhang, Z. *et al.* Nonfouling behavior of polycarboxybetaine-grafted surfaces: Structural and environmental effects. *Biomacromolecules* **9**, 2686–2692 (2008).
4. Saigal, T., Dong, H., Matyjaszewski, K. & Tilton, R. D. Pickering emulsions stabilized by nanoparticles with thermally responsive grafted polymer brushes. *Langmuir* **26**, 15200–15209 (2010).
5. Willott, J. D., Humphreys, B. A., Webber, G. B., Wanless, E. J. & De Vos, W. M. Combined Experimental and Theoretical Study of Weak Polyelectrolyte Brushes in Salt Mixtures. *Langmuir* **35**, 2709–2718 (2019).
6. Kobayashi, M. *et al.* Friction behavior of high-density poly(2-methacryloyloxyethyl phosphorylcholine) brush in aqueous media. *Soft Matter* **3**, 740–746 (2007).
7. Tadmor, R., Janik, J., Klein, J. & Fetters, L. J. Sliding friction with polymer brushes. *Phys. Rev. Lett.* **91**, (2003).
8. Tairy, O., Kampf, N., Driver, M. J., Armes, S. P. & Klein, J. Dense, highly hydrated polymer brushes via modified atom-transfer-radical-polymerization: Structure, surface interactions, and frictional dissipation. *Macromolecules* **48**, 140–151 (2015).
9. Mu, B., Lu, C. & Liu, P. Disintegration-controllable stimuli-responsive polyelectrolyte multilayer microcapsules via covalent layer-by-layer assembly. *Colloids Surfaces B Biointerfaces* **82**, 385–390 (2011).
10. Jia, Y. *et al.* pH-responsive polysaccharide microcapsules through covalent bonding assembly. *Chem. Commun.* **47**, 1175–1177 (2011).
11. Wang, Z. *et al.* Self-assembled Biodegradable Nanoparticles and Polysaccharides as Biomimetic ECM Nanostructures for the Synergistic effect of RGD and BMP-2 on Bone Formation. *Sci. Rep.* **6**, 1–12 (2016).
12. Zhao, X., Chen, S., Lin, Z. & Du, C. Reactive electrospinning of composite nanofibers of carboxymethyl chitosan cross-linked by alginate dialdehyde with the aid of polyethylene oxide. *Carbohydr. Polym.* **148**, 98–106 (2016).
13. Chen, H. *et al.* Covalently antibacterial alginate-chitosan hydrogel dressing integrated gelatin microspheres containing tetracycline hydrochloride for wound healing. *Mater. Sci. Eng. C* **70**, 287–295 (2017).
14. Vieira, E. F. S., Cestari, A. R., Airoldi, C. & Loh, W. Polysaccharide-based hydrogels: Preparation, characterization, and drug interaction behaviour. *Biomacromolecules* **9**, 1195–1199 (2008).
15. Chen, F. *et al.* Preparation and characterization of oxidized alginate covalently cross-linked galactosylated chitosan scaffold for liver tissue engineering. *Mater. Sci. Eng. C* **32**, 310–320 (2012).
16. Liang, Y. *et al.* An in situ formed biodegradable hydrogel for reconstruction of the corneal endothelium. *Colloids Surfaces B Biointerfaces* **82**, 1–7 (2011).
17. Feng, W. *et al.* Effect of pH-responsive alginate/chitosan multilayers coating on delivery efficiency, cellular uptake and biodistribution of mesoporous silica nanoparticles based nanocarriers. *ACS Appl. Mater. Interfaces* **6**, 8447–8460 (2014).
18. Yang, H. *et al.* Chemo-photodynamic combined gene therapy and dual-modal cancer imaging achieved by pH-responsive alginate/chitosan multilayer-modified magnetic mesoporous silica nanocomposites. *Biomater. Sci.* **5**, 1001–1013 (2017).
19. Orr, W. J. C. Statistical treatment of polymer solutions at infinite dilution. *Trans. Faraday Soc.* **43**, 12–27 (1947).
20. de Gennes, P. G. & Witten, T. A. Scaling Concepts in Polymer Physics. *Phys. Today* **33**, 51–54 (1980).
21. Fixman, M. Radius of gyration of polymer chains. *J. Chem. Phys.* **36**, 306–310 (1962).
22. Rubinstein, M. & Colby, R. H. *Polymer Physics*. (Oxford University Press, 2003).
23. Flory, P. J. The configuration of real polymer chains. *J. Chem. Phys.* **17**, 303–310 (1949).
24. Huggins, M. L. Some properties of solutions of long-chain compounds. *J. Phys. Chem.* **46**, 151–158 (1942).
25. Fleer, G. J., Stuart, M. A. C., Scheutjens, J. M. H. M., Cosgrove, T. & Vincent, B. *Polymers at Interfaces*. *Polymers at Interfaces* (Springer Netherlands, 1998). doi:10.1007/978-94-011-2130-9.
26. de Gennes, P. G. Polymers at an interface; a simplified view. *Advances in Colloid and Interface Science* vol. 27 189–209 (1987).

27. Thakur, G., Rodrigues, F. C. & Singh, K. Crosslinking Biopolymers for Advanced Drug Delivery and Tissue Engineering Applications. in *Advances in Experimental Medicine and Biology* vol. 1078 213–231 (Springer New York LLC, 2018).
28. Hess, M. *et al.* Terminology of polymers containing ionizable or ionic groups and of polymers containing ions (IUPAC Recommendations 2006). *Pure Appl. Chem.* **78**, 2067–2074 (2006).
29. Mc Naught, a. D. & Wilkinson, A. *The IUPAC Compendium of Chemical Terminology*. *The IUPAC Compendium of Chemical Terminology* (International Union of Pure and Applied Chemistry (IUPAC), 2019). doi:10.1351/goldbook.
30. Toomey, R. & Tirrell, M. Functional polymer brushes in aqueous media from self-assembled and surface-initiated polymers. *Annual Review of Physical Chemistry* vol. 59 493–517 (2008).
31. Dobrynin, A. V., Deshkovski, A. & Rubinstein, M. Adsorption of polyelectrolytes at an oppositely charged surface. *Phys. Rev. Lett.* **84**, 3101–3104 (2000).
32. Currie, E. P. K., Norde, W. & Cohen Stuart, M. A. C. Tethered polymer chains: Surface chemistry and their impact on colloidal and surface properties. *Adv. Colloid Interface Sci.* **100**–**102**, 205–265 (2003).
33. Chakraborty, G., Bhattarai, A. & De, R. Polyelectrolyte–Dye Interactions: An Overview. *Polymers (Basel).* **14**, (2022).
34. Kumar, R. & Fredrickson, G. H. Theory of polyzwitterion conformations. *J. Chem. Phys.* **131**, 1543 (2009).
35. Kudaibergenov, S., Jaeger, W. & Laschewsky, A. Polymeric betaines: Synthesis, characterization, and application. *Advances in Polymer Science* vol. 201 157–224 (2006).
36. Wang, F., Yang, J. & Zhao, J. Understanding anti-polyelectrolyte behavior of a well-defined polyzwitterion at the single-chain level. *Polym. Int.* **64**, 999–1005 (2015).
37. Israëls, R., Leermakers, F. A. M., Fleer, G. J. & Zhulina, E. B. Charged Polymeric Brushes: Structure and Scaling Relations. *Macromolecules* **27**, 3249–3261 (1994).
38. Willott, J. D., Murdoch, T. J., Webber, G. B. & Wanless, E. J. Physicochemical behaviour of cationic polyelectrolyte brushes. *Progress in Polymer Science* vol. 64 52–75 (2017).
39. Israëls, R., Leermakers, F. A. M. & Fleer, G. J. On the Theory of Grafted Weak Polyacids. *Macromolecules* **27**, 3087–3093 (1994).
40. Lyatskaya, Y. V., Leermakers, F. A. M., Fleer, G. J., Zhulina, E. B. & Birshtein, T. M. Analytical Self-Consistent-Field Model of Weak Polyacid Brushes. *Macromolecules* **28**, 3562–3569 (1995).
41. Lindhoud, S. *Polyelectrolyte complex micelles as wrapping for enzymes*. (Wageningen University, 2009).
42. Kagawa, I. & Gregor, H. P. Theory of the effect of counterion size upon titration behavior of polycarboxylic acids. *J. Polym. Sci.* **23**, 477–484 (1957).
43. Samanta, T. & Mukherjee, M. Swelling dynamics of ultrathin films of strong polyelectrolytes. *Macromolecules* **44**, 3935–3941 (2011).
44. Chen, W. L., Cordero, R., Tran, H. & Ober, C. K. 50th Anniversary Perspective: Polymer Brushes: Novel Surfaces for Future Materials. *Macromolecules* vol. 50 4089–4113 (2017).
45. Azzaroni, O. Polymer brushes here, there, and everywhere: Recent advances in their practical applications and emerging opportunities in multiple research fields. *J. Polym. Sci. Part A Polym. Chem.* **50**, 3225–3258 (2012).
46. Zoppe, J. O. *et al.* Surface-Initiated Controlled Radical Polymerization: State-of-the-Art, Opportunities, and Challenges in Surface and Interface Engineering with Polymer Brushes. *Chem. Rev.* **117**, 1105–1318 (2017).
47. Wei, Q., Cai, M., Zhou, F. & Liu, W. Dramatically Tuning Friction Using Responsive Polyelectrolyte Brushes. **46**, 30 (2013).
48. Feng, W., Zhu, S., Ishihara, K. & Brash, J. L. Adsorption of fibrinogen and lysozyme on silicon grafted with poly(2-methacryloyloxyethyl phosphorylcholine) via surface-initiated atom transfer radical polymerization. *Langmuir* **21**, 5980–5987 (2005).
49. Baggerman, J., Smulders, M. M. J. & Zuilhof, H. Romantic Surfaces: A Systematic Overview of Stable, Biospecific, and Antifouling Zwitterionic Surfaces. *Langmuir* vol. 35 1072–1084 (2019).
50. Sin, M. C., Chen, S. H. & Chang, Y. Hemocompatibility of zwitterionic interfaces and membranes. *Polymer Journal* vol. 46 436–443 (2014).
51. Lowe, A. B. & McCormick, C. L. Synthesis and solution properties of zwitterionic polymers. *Chem. Rev.* **102**, 4177–4189 (2002).
52. Ishihara, K. *et al.* Why do phospholipid polymers reduce protein adsorption? *J. Biomed. Mater. Res.* **39**, 323–

330 (1998).
53. West, S. L. *et al.* The biocompatibility of crosslinkable copolymer coatings containing sulfobetaines and phosphobetaines. *Biomaterials* **25**, 1195–1204 (2004).
54. Javan Nikkhah, S. & Vandichel, M. Modeling Polyzwitterion-Based Drug Delivery Platforms: A Perspective of the Current State-of-the-Art and Beyond. *ACS Eng. Au* **2**, 274–294 (2022).
55. Salloum, D. S. & Schlenoff, J. B. Protein adsorption modalities of polyelectrolyte multilayers. *Biomacromolecules* **5**, 1089–1096 (2004).
56. Zhulina, E. B., Birshtein, T. M. & Borisov, O. V. Theory of Ionizable Polymer Brushes. *Macromolecules* **28**, 1491–1499 (1995).
57. Pincus, P. Colloid Stabilization with Grafted Polyelectrolytes. *Macromolecules* **24**, 2912–2919 (1991).
58. Ehtiati, K., Z. Moghaddam, S., Daugaard, A. E. & Thormann, E. Crucial Nonelectrostatic Effects on Polyelectrolyte Brush Behavior. *Macromolecules* **54**, 3388–3394 (2021).
59. Xu, X., Billing, M., Ruths, M., Klok, H. A. & Yu, J. Structure and Functionality of Polyelectrolyte Brushes: A Surface Force Perspective. *Chemistry - An Asian Journal* vol. 13 3411–3436 (2018).
60. Kou, R., Zhang, J., Chen, Z. & Liu, G. Counterion Specificity of Polyelectrolyte Brushes: Role of Specific Ion-Pairing Interactions. *ChemPhysChem* **19**, 1404–1413 (2018).
61. Ehtiati, K., Moghaddam, S. Z., Klok, H.-A., Daugaard, A. E. & Thormann, E. Specific Counterion Effects on the Swelling Behavior of Strong Polyelectrolyte Brushes. *Macromolecules* **55**, 5130 (2022).
62. Ehtiati, K. Fundamental Studies of Polyelectrolyte Brushes. (Technical University of Denmark, 2020).
63. Zimmermann, R. *et al.* Evidence of Ion-Pairing in Cationic Brushes from Evaluation of Brush Charging and Structure by Electrokinetic and Surface Conductivity Analysis. *J. Phys. Chem. C* **121**, 2915–2922 (2017).
64. Higaki, Y. *et al.* Counteranion-Specific Hydration States of Cationic Polyelectrolyte Brushes. *Ind. Eng. Chem. Res.* **57**, 5268–5275 (2018).
65. Hofmeister, F. Zur Lehre von der Wirkung der Salze - Dritte Mittheilung. *Arch. für Exp. Pathol. und Pharmakologie* **25**, 1–30 (1888).
66. Kunz, W., Henle, J. & Ninham, B. W. 'Zur Lehre von der Wirkung der Salze' (about the science of the effect of salts): Franz Hofmeister's historical papers. in *Current Opinion in Colloid and Interface Science* vol. 9 19–37 (Elsevier, 2004).
67. Okur, H. I. *et al.* Beyond the Hofmeister Series: Ion-Specific Effects on Proteins and Their Biological Functions. *Journal of Physical Chemistry B* vol. 121 1997–2014 (2017).
68. Kang, B., Tang, H., Zhao, Z. & Song, S. Hofmeister Series: Insights of Ion Specificity from Amphiphilic Assembly and Interface Property. *ACS Omega* vol. 5 6229–6239 (2020).
69. Mazzini, V. & Craig, V. S. J. What is the fundamental ion-specific series for anions and cations? Ion specificity in standard partial molar volumes of electrolytes and electrostriction in water and non-aqueous solvents. *Chem. Sci.* **8**, 7052–7065 (2017).
70. Matsuno, R. *et al.* Molecular Design and Characterization of Ionic Monomers with Varying Ion Pair Interaction Energies. *Macromolecules* **53**, 1629–1637 (2020).
71. Kunz, W., Belloni, L., Bernard, O. & Ninham, B. W. Osmotic coefficients and surface tensions of aqueous electrolyte solutions: Role of dispersion forces. *J. Phys. Chem. B* **108**, 2398–2404 (2004).
72. Marcus, Y. Ion Properties, Marcus Dekker. *Inc, New York* 1–33 (1997).
73. Zhang, Z. *et al.* Effect of Salt on Phosphorylcholine-based Zwitterionic Polymer Brushes. *Langmuir* **32**, 5048–5057 (2016).
74. Matsuda, Y., Kobayashi, M., Annaka, M., Ishihara, K. & Takahara, A. Dimensions of a free linear polymer and polymer immobilized on silica nanoparticles of a zwitterionic polymer in aqueous solutions with various ionic strengths. *Langmuir* **24**, 8772–8778 (2008).
75. Zhang, Z. J. *et al.* Influence of salt on the solution dynamics of a phosphorylcholine-based polyzwitterion. *Eur. Polym. J.* **87**, 449–457 (2017).
76. Wang, T. *et al.* Anion Specificity of Polyzwitterionic Brushes with Different Carbon Spacer Lengths and Its Application for Controlling Protein Adsorption. *Langmuir* **32**, 2698–2707 (2016).
77. Wang, T., Wang, X., Long, Y., Liu, G. & Zhang, G. Ion-specific conformational behavior of polyzwitterionic brushes: Exploiting it for protein adsorption/desorption control. *Langmuir* **29**, 6588–6596 (2013).
78. Higaki, Y. *et al.* Effect of Charged Group Spacer Length on Hydration State in Zwitterionic Poly(sulfobetaine) Brushes. *Langmuir* **33**, 8404–8412 (2017).

79. Kobayashi, M., Ishihara, K. & Takahara, A. Neutron reflectivity study of the swollen structure of polyzwitterion and polyeletrolyte brushes in aqueous solution. *J. Biomater. Sci. Polym. Ed.* **25**, 1673–1686 (2014).
80. Higaki, Y., Kobayashi, M. & Takahara, A. Hydration State Variation of Polyzwitterion Brushes through Interplay with Ions. *Langmuir* **36**, 9015–9024 (2020).
81. Georgiev, G. S. *et al.* Self-assembly, antipolyelectrolyte effect, nonbiofouling properties of polyzwitterions. *Biomacromolecules* **7**, 1329–1334 (2006).
82. Sakamaki, T. *et al.* Ion-Specific Hydration States of Zwitterionic Poly(sulfobetaine methacrylate) Brushes in Aqueous Solutions. *Langmuir* **35**, 1583–1589 (2019).
83. Shao, Q. *et al.* Differences in cationic and anionic charge densities dictate zwitterionic associations and stimuli responses. *J. Phys. Chem. B* **118**, 6956–6962 (2014).
84. Schulz, D. N. *et al.* Phase behaviour and solution properties of sulphobetaine polymers. *Polymer (Guildf).* **27**, 1734–1742 (1986).
85. Kikuchi, M. *et al.* Chain dimension of polyampholytes in solution and immobilized brush states. *Polym. J.* **44**, 121–130 (2012).
86. Yang, J. *et al.* Salt-Responsive Zwitterionic Polymer Brushes with Tunable Friction and Antifouling Properties. (2015) doi:10.1021/acs.langmuir.5b02119.
87. Delgado, J. D. & Schlenoff, J. B. Static and Dynamic Solution Behavior of a Polyzwitterion Using a Hofmeister Salt Series. *Macromolecules* **50**, 4454–4464 (2017).
88. Schlenoff, J. B. Zwitteration: Coating surfaces with zwitterionic functionality to reduce nonspecific adsorption. *Langmuir* vol. 30 9625–9636 (2014).
89. Zhao, Y. H., Wee, K. H. & Bai, R. A novel electrolyte-responsive membrane with tunable permeation selectivity for protein purification. *ACS Appl. Mater. Interfaces* **2**, 203–211 (2010).
90. Mary, P., Bendejacq, D. D., Labeau, M. P. & Dupuis, P. Reconciling low- and high-salt solution behavior of sulfobetaine polyzwitterions. *J. Phys. Chem. B* **111**, 7767–7777 (2007).
91. Shao, Q. & Jiang, S. Influence of charged groups on the properties of zwitterionic moieties: A molecular simulation study. *J. Phys. Chem. B* **118**, 7630–7637 (2014).
92. Shao, Q., He, Y., White, A. D. & Jiang, S. Difference in hydration between carboxybetaine and sulfobetaine. *J. Phys. Chem. B* **114**, 16625–16631 (2010).
93. Leng, C. *et al.* In situ probing of the surface hydration of zwitterionic polymer brushes: Structural and environmental effects. *J. Phys. Chem. C* **118**, 15840–15845 (2014).
94. Shao, Q., He, Y. & Jiang, S. Molecular dynamics simulation study of ion interactions with zwitterions. *J. Phys. Chem. B* **115**, 8358–8363 (2011).
95. Pawar, S. N. & Edgar, K. J. Alginate derivatization: A review of chemistry, properties and applications. *Biomaterials* vol. 33 3279–3305 (2012).
96. Dragan, E. S. & Dinu, M. V. Polysaccharides constructed hydrogels as vehicles for proteins and peptides. A review. *Carbohydrate Polymers* vol. 225 115210 (2019).
97. Schneider, A. *et al.* Layer-by-layer films from hyaluronan and amine-modified hyaluronan. *Langmuir* **23**, 2655–2662 (2007).
98. Rinaudo, M. New way to crosslink chitosan in aqueous solution. *Eur. Polym. J.* **46**, 1537–1544 (2010).
99. Sahariah, P. & Másson, M. Antimicrobial Chitosan and Chitosan Derivatives: A Review of the Structure-Activity Relationship. *Biomacromolecules* vol. 18 3846–3868 (2017).
100. Szczęsna, W. *et al.* Insight into multilayered alginate/chitosan microparticles for oral administration of large cranberry fruit extract. *Eur. Polym. J.* **160**, 110776 (2021).
101. Taketa, T. B. & Beppu, M. M. Layer-by-layer thin films of alginate/chitosan and hyaluronic acid/chitosan with tunable thickness and surface roughness. in *Materials Science Forum* vols 783–786 1226–1231 (Trans Tech Publications Ltd, 2014).
102. Aston, R., Wimalaratne, M., Brock, A., Lawrie, G. & Grøndahl, L. Interactions between chitosan and alginate dialdehyde biopolymers and their layer-by-layer assemblies. *Biomacromolecules* **16**, 1807–1817 (2015).
103. Tan, H., Chu, C. R., Payne, K. A. & Marra, K. G. Injectable in situ forming biodegradable chitosan-hyaluronic acid based hydrogels for cartilage tissue engineering. *Biomaterials* **30**, 2499–2506 (2009).
104. Jia, Y. & Li, J. Molecular assembly of Schiff base interactions: Construction and application. *Chemical Reviews* vol. 115 1597–1621 (2015).

105. Steitz, R., Jaeger, W. & Klitzing, R. V. Influence of charge density and ionic strength on the multilayer formation of strong polyelectrolytes. *Langmuir* **17**, 4471–4474 (2001).
106. Koetse, M., Laschewsky, A., Jonas, A. M. & Wagenknecht, W. Influence of charge density and distribution on the internal structure of electrostatically self-assembled polyelectrolyte films. *Langmuir* **18**, 1655–1660 (2002).
107. Volodkin, D. & Von Klitzing, R. Competing mechanisms in polyelectrolyte multilayer formation and swelling: Polycation-polyanion pairing vs. polyelectrolyte-ion pairing. *Current Opinion in Colloid and Interface Science* vol. 19 25–31 (2014).
108. Mermut, O. & Barrett, C. J. Effects of charge density and counterions on the assembly of polyelectrolyte multilayers. *J. Phys. Chem. B* **107**, 2525–2530 (2003).
109. Schlenoff, J. B., Ly, H. & Li, M. Charge and mass balance in polyelectrolyte multilayers. *J. Am. Chem. Soc.* **120**, 7626–7634 (1998).
110. Bucur, C. B., Sui, Z. & Schlenoff, J. B. Ideal mixing in polyelectrolyte complexes and multilayers: Entropy driven assembly. *J. Am. Chem. Soc.* **128**, 13690–13691 (2006).
111. Liu, C., Thormann, E., Claesson, P. M. & Tyrode, E. Surface grafted chitosan gels. Part II. Gel formation and characterization. *Langmuir* **30**, 8878–8888 (2014).
112. Hillberg, A. L., Holmes, C. A. & Tabrizian, M. Effect of genipin cross-linking on the cellular adhesion properties of layer-by-layer assembled polyelectrolyte films. *Biomaterials* **30**, 4463–4470 (2009).
113. Yuan, W. *et al.* pH-controlled construction of chitosan/alginate multilayer film: Characterization and application for antibody immobilization. *Langmuir* **23**, 13046–13052 (2007).
114. Martins, G. V., Mano, J. F. & Alves, N. M. Nanostructured self-assembled films containing chitosan fabricated at neutral pH. *Carbohydr. Polym.* **80**, 570–573 (2010).
115. Xie, H. G. *et al.* Effect of surface wettability and charge on protein adsorption onto implantable alginate-chitosan-alginate microcapsule surfaces. *J. Biomed. Mater. Res. - Part A* **92**, 1357–1365 (2010).
116. Costa, N. L., Sher, P. & Mano, J. F. Liquefied capsules coated with multilayered polyelectrolyte films for cell immobilization. *Adv. Eng. Mater.* **13**, (2011).
117. Silva, J. M. *et al.* PH Responsiveness of Multilayered Films and Membranes Made of Polysaccharides. *Langmuir* **31**, 11318–11328 (2015).
118. Zhou, J. *et al.* Layer by layer chitosan/alginate coatings on poly(lactide-co-glycolide) nanoparticles for antifouling protection and Folic acid binding to achieve selective cell targeting. *J. Colloid Interface Sci.* **345**, 241–247 (2010).
119. Hatami, J. *et al.* Multilayered films produced by layer-by-layer assembly of chitosan and alginate as a potential platform for the formation of human adipose-derived stem cell aggregates. *Polymers (Basel).* **9**, 440 (2017).
120. Choi, I. *et al.* PH-controlled exponential and linear growing modes of layer-by-layer assemblies of star polyelectrolytes. *J. Am. Chem. Soc.* **133**, 9592–9606 (2011).
121. Schönhoff, M. & Bieker, P. Linear and exponential growth regimes of multilayers of weak polyelectrolytes in dependence on pH. *Macromolecules* **43**, 5052–5059 (2010).
122. Lundin, M., Solaqa, F., Thormann, E., MacAkova, L. & Blomberg, E. Layer-by-layer assemblies of chitosan and heparin: Effect of solution ionic strength and pH. *Langmuir* **27**, 7537–7548 (2011).
123. Burke, S. E. & Barrett, C. J. pH-responsive properties of multilayered poly(L-lysine)/hyaluronic acid surfaces. *Biomacromolecules* **4**, 1773–1783 (2003).
124. Itano, K., Choi, J. & Rubner, M. F. Mechanism of the pH-induced discontinuous swelling/deswelling transitions of poly(allylamine hydrochloride)-Containing polyelectrolyte multilayer films. *Macromolecules* **38**, 3450–3460 (2005).
125. Delcea, M., Möhwald, H. & Skirtach, A. G. Stimuli-responsive LbL capsules and nanoshells for drug delivery. *Advanced Drug Delivery Reviews* vol. 63 730–747 (2011).
126. Kim, B. S. & Vinogradova, O. I. pH-controlled swelling of polyelectrolyte multilayer microcapsules. *J. Phys. Chem. B* **108**, 8161–8165 (2004).
127. Huang, J., Moghaddam, S. Z. & Thormann, E. Chitosan/Alginate Dialdehyde Multilayer Films with Modulated pH-Responsiveness and Swelling. *Macromol. Chem. Phys.* **221**, (2020).
128. Huang, J., Zajforoushan Moghaddam, S. & Thormann, E. Structural Investigation of a Self-Cross-Linked Chitosan/Alginate Dialdehyde Multilayered Film with in Situ QCM-D and Spectroscopic Ellipsometry. *ACS*

Omega **4**, 2019–2029 (2019).
129. Erel-Unal, I. & Sukhishvili, S. A. Hydrogen-bonded hybrid multilayers: Film architecture controls release of macromolecules. *Macromolecules* **41**, 8737–8744 (2008).
130. Glinel, K. *et al.* Responsive polyelectrolyte multilayers. *Colloids Surfaces A Physicochem. Eng. Asp.* **303**, 3–13 (2007).
131. Sui, Z. & Schlenoff, J. B. Phase separations in pH-responsive polyelectrolyte multilayers: Charge extrusion versus charge expulsion. *Langmuir* **20**, 6026–6031 (2004).
132. Hiller, J. & Rubner, M. F. Reversible molecular memory and pH-switchable swelling transitions in polyelectrolyte multilayers. *Macromolecules* **36**, 4078–4083 (2003).
133. Gero Decher and Joseph B. Schlenof. *Multilayer Thin Films. second edition*. *Angewandte Chemie International Edition* vol. 42 (Wiley-VCH Verlag GmbH & Co. KGaA, 2012).
134. Korecz, L., Csákvári, É. & Tüdos, F. Physical chemistry of polyelectrolytes - 1. Viscometry of a polyacid in salt-free aqueous solution. *Polym. Bull.* **19**, 493–500 (1988).
135. Huang, J., Zajforoushan Moghaddam, S., Maroni, P. & Thormann, E. Swelling Behavior, Interaction, and Electrostatic Properties of Chitosan/Alginate Dialdehyde Multilayer Films with Different Outermost Layer. *Langmuir* **36**, 3782–3791 (2020).
136. Ehtiati, K., Moghaddam, S. Z., Daugaard, A. E. & Thormann, E. How Dissociation of Carboxylic Acid Groups in a Weak Polyelectrolyte Brush Depend on Their Distance from the Substrate. *Langmuir* **36**, 2339–2348 (2020).
137. Hollingsworth, N. R., Wilkanowicz, S. I. & Larson, R. G. Salt- And pH-induced swelling of a poly(acrylic acid) brush: Via quartz crystal microbalance w/dissipation (QCM-D). *Soft Matter* **15**, 7838–7851 (2019).
138. Willott, J. D. *et al.* Critical salt effects in the swelling behavior of a weak polybasic brush. *Langmuir* **30**, 1827–1836 (2014).
139. Dubas, S. T. & Schlenoff, J. B. Polyelectrolyte multilayers containing a weak polyacid: Construction and deconstruction. *Macromolecules* **34**, 3736–3740 (2001).
140. Tang, K. & Besseling, N. A. M. Formation of polyelectrolyte multilayers: Ionic strengths and growth regimes. *Soft Matter* **12**, 1032–1040 (2016).
141. Svoboda, K. & Block, S. M. Biological applications of optical forces. *Annual Review of Biophysics and Biomolecular Structure* vol. 23 247–285 (1994).
142. Sader, J. E., Chon, J. W. M. & Mulvaney, P. Calibration of rectangular atomic force microscope cantilevers. *Rev. Sci. Instrum.* **70**, 3967–3969 (1999).
143. Neumeister, J. M. & Ducker, W. A. Lateral, normal, and longitudinal spring constants of atomic force microscopy cantilevers. *Rev. Sci. Instrum.* **65**, 2527–2531 (1994).
144. Hutter, J. L. & Bechhoefer, J. Calibration of atomic-force microscope tips. *Rev. Sci. Instrum.* **64**, 1868–1873 (1993).
145. Gibson, C. T., Watson, G. S. & Myhra, S. Determination of the spring constants of probes for force microscopy/spectroscopy. *Nanotechnology* **7**, 259–262 (1996).
146. BUTT, H. -J *et al.* Scan speed limit in atomic force microscopy. *J. Microsc.* **169**, 75–84 (1993).
147. Liu, X. *et al.* Low friction and high load bearing capacity layers formed by cationic-block-non-ionic bottle-brush copolymers in aqueous media. *Soft Matter* **9**, 5361–5371 (2013).
148. Wu, Y., Wei, Q., Cai, M. & Zhou, F. Interfacial Friction Control. *Adv. Mater. Interfaces* **2**, 1400392 (2015).
149. Chen, H. *et al.* Mechanically strong hybrid double network hydrogels with antifouling properties. *J. Mater. Chem. B* **3**, 5426–5435 (2015).
150. Chen, M., Briscoe, W. H., Armes, S. P. & Klein, J. Lubrication at physiological pressures by polyzwitterionic brushes. *Science (80-.).* **323**, 1698–1701 (2009).
151. Chen, Q., Chen, H., Zhu, L. & Zheng, J. Fundamentals of double network hydrogels. *Journal of Materials Chemistry B* vol. 3 3654–3676 (2015).
152. Hutchings, I. M. Leonardo da Vinci's studies of friction. *Wear* **360**–**361**, 51–66 (2016).
153. Hölscher, H., Schirmeisen, A. & Schwarz, U. D. Principles of atomic friction: From sticking atoms to superlubric sliding. *Philos. Trans. R. Soc. A Math. Phys. Eng. Sci.* **366**, 1383–1404 (2008).
154. Gao, J. *et al.* Frictional forces and Amontons' law: From the molecular to the macroscopic scale. *J. Phys. Chem. B* **108**, 3410–3425 (2004).
155. Yoshizawa, H., Chen, Y. L. & Israelachvili, J. Fundamental mechanisms of interfacial friction. 1. Relation between adhesion and friction. *J. Phys. Chem.* **97**, 4128–4140 (1993).

156. Bowden, F. P. & Young, L. Influence of interfacial potential on friction and surface damage. *Research* **3**, 235–237 (1950).
157. Park, J. Y. & Salmeron, M. Fundamental aspects of energy dissipation in friction. *Chem. Rev.* **114**, 677–711 (2014).
158. Liamas, E., Connell, S. D., Ramakrishna, S. N. & Sarkar, A. Probing the frictional properties of soft materials at the nanoscale. *Nanoscale* **12**, 2292–2308 (2020).
159. Bowden, F. P., Tabor, D. & Palmer, F. The Friction and Lubrication of Solids. *Am. J. Phys.* **19**, 428 (2005).
160. Ramakrishna, S. N., Nalam, P. C., Clasohm, L. Y. & Spencer, N. D. Study of adhesion and friction properties on a nanoparticle gradient surface: Transition from JKR to DMT contact mechanics. *Langmuir* **29**, 175–182 (2013).
161. Zhan, S. *et al.* Molecular dynamics simulation of microscopic friction mechanisms of amorphous polyethylene. *Soft Matter* **15**, 8827–8839 (2019).
162. Li, Q. *et al.* Friction between a viscoelastic body and a rigid surface with random self-affine roughness. *Phys. Rev. Lett.* **111**, (2013).
163. Chandy, T. & Sharma', C. P. Chitosan - as a Biomaterial. *Biomater. Artif. Cells Artif. Organs* **18**, 1–24 (1990).
164. Jelkmann, M. *et al.* Chitosan: The One and Only? Aminated Cellulose as an Innovative Option for Primary Amino Groups Containing Polymers. *Biomacromolecules* **19**, 4059–4067 (2018).
165. Tanaka, Y. *et al.* Effects of chitin and chitosan particles on BALB/c mice by oral and parenteral administration. *Biomaterials* **18**, 591–595 (1997).
166. Berscht, P. C., Nies, B., Liebendörfer, A. & Kreuter, J. In vitro evaluation of biocompatibility of different wound dressing materials. *J. Mater. Sci. Mater. Med.* **6**, 201–205 (1995).
167. Muzzarelli, R. Depolymerization of methyl pyrrolidinone chitosan by lysozyme. *Carbohydr. Polym.* **19**, 29–34 (1992).
168. Huang, J. Formation, Structure, and Properties of Stimuli-Responsive Polyelectrolyte Films. (Technical University of Denmark, 2020).
169. Blaine, G. Experimental Observations on Absorbable Alginate Products in Surgery : Gel, Film, Gauze and Foam. *Ann. Surg.* **125**, 102–114 (1947).
170. Gombotz, W. R. & Wee, S. F. Protein release from alginate matrices. *Advanced Drug Delivery Reviews* vol. 31 267–285 (1998).
171. Solandt, O. M. SOME OBSERVATIONS UPON SODIUM ALGINATE. *Q. J. Exp. Physiol. Cogn. Med. Sci.* **31**, 25–30 (1941).
172. Tian, M. *et al.* Long-term and oxidative-responsive alginate-deferoxamine conjugates with a low toxicity for iron overload. *RSC Adv.* **6**, 32471–32479 (2016).
173. Gomez, C. G., Rinaudo, M. & Villar, M. A. Oxidation of sodium alginate and characterization of the oxidized derivatives. *Carbohydr. Polym.* **67**, 296–304 (2007).
174. Wong, A. K. Y. & Krull, U. J. Surface characterization of 3-glycidoxypropyltrimethoxysilane films on silicon-based substrates. *Anal. Bioanal. Chem.* **383**, 187–200 (2005).
175. Ramasamy, T. G. & Haidar, Z. S. Alginate-chitosan versus chitosan-alginate multi-layered assembled systems: In situ comparative QCM-D study. *J. Biomater. Tissue Eng.* **2**, 83–88 (2012).
176. Alves, N. M., Picart, C. & Mano, J. F. Self assembling and crosslinking of polyelectrolyte multilayer films of chitosan and alginate studies by OCM and IR spectroscopy. *Macromol. Biosci.* **9**, 776–785 (2009).
177. Easley, A. D. *et al.* A practical guide to quartz crystal microbalance with dissipation monitoring of thin polymer films. *Journal of Polymer Science* vol. 60 1090–1107 (2022).
178. Silva, J. M. *et al.* Nanostructured 3D Constructs Based on Chitosan and Chondroitin Sulphate Multilayers for Cartilage Tissue Engineering. *PLoS One* **8**, 55451 (2013).
179. Pinheiro, A. C. *et al.* Chitosan/fucoidan multilayer nanocapsules as a vehicle for controlled release of bioactive compounds. *Carbohydr. Polym.* **115**, 1–9 (2015).
180. Findenig, G., Kargl, R., Stana-Kleinschek, K. & Ribitsch, V. Interaction and structure in polyelectrolyte/clay multilayers: A QCM-D study. *Langmuir* **29**, 8544–8553 (2013).
181. Reviakine, I., Johannsmann, D. & Richter, R. P. Hearing what you cannot see and visualizing what you hear: Interpreting quartz crystal microbalance data from solvated interfaces. *Anal. Chem.* **83**, 8838–8848 (2011).
182. Ward, M. D. & Buttry, D. A. In situ interfacial mass detection with piezoelectric transducers. *Science* vol. 249 1000–1007 (1990).

183. Dunér, G., Thormann, E. & Dedinaite, A. Quartz Crystal Microbalance with Dissipation (QCM-D) studies of the viscoelastic response from a continuously growing grafted polyelectrolyte layer. *J. Colloid Interface Sci.* **408**, 229–234 (2013).
184. Sauerbrey, G. Verwendung von Schwingquarzen zur Wägung dünner Schichten und zur Mikrowägung. *Zeitschrift für Phys.* **155**, 206–222 (1959).
185. Dixon, M. C. Quartz crystal microbalance with dissipation monitoring: Enabling real-time characterization of biological materials and their interactions. *Journal of Biomolecular Techniques* vol. 19 151–158 (2008).
186. Larsson, C., Rodahl, M. & Höök, F. Characterization of DNA immobilization and subsequent hybridization on a 2D arrangement of streptavidin on a biotin-modified lipid bilayer supported on SiO2. *Anal. Chem.* **75**, 5080–5087 (2003).
187. Rodahl, M. *et al.* Simultaneous frequency and dissipation factor QCM measurements of biomolecular adsorption and cell adhesion. *Faraday Discuss.* **107**, 229–246 (1997).
188. Voinova, M. V, Rodahl, M., Jonson, M. & Kasemo, B. Viscoelastic Acoustic Response of Layered Polymer Films at Fluid-Solid Interfaces: Continuum Mechanics Approach. *Phys. Scr.* **59**, 391–396 (1999).
189. McNamara, T. P. & Blanford, C. F. A sensitivity metric and software to guide the analysis of soft films measured by a quartz crystal microbalance. *Analyst* **141**, 2911–2919 (2016).
190. Woollam, J. A., Snyder, P. G. & Rost, M. C. Variable angle spectroscopic ellipsometry: A non-destructive characterization technique for ultrathin and multilayer materials. *Thin Solid Films* **166**, 317–323 (1988).
191. Ogieglo, W., Wormeester, H., Eichhorn, K. J., Wessling, M. & Benes, N. E. In situ ellipsometry studies on swelling of thin polymer films: A review. *Progress in Polymer Science* vol. 42 42–78 (2015).
192. Circular polarization - Wikipedia. https://en.wikipedia.org/wiki/Circular_polarization.
193. Fujiwara, H. *Spectroscopic Ellipsometry: Principles and Applications*. *Spectroscopic Ellipsometry: Principles and Applications* (John Wiley and Sons, 2007). doi:10.1002/9780470060193.
194. Woollam, J. A. *et al.* Overview of variable-angle spectroscopic ellipsometry (VASE): I. Basic theory and typical applications. in *Optical Metrology: A Critical Review* vol. 10294 1029402 (SPIE, 1999).
195. Binnig, G., Quate, C. F. & Gerber, C. Atomic force microscope. *Phys. Rev. Lett.* **56**, 930–933 (1986).
196. Sugimoto, Y. *et al.* Chemical identification of individual surface atoms by atomic force microscopy. *Nature* **446**, 64–67 (2007).
197. Jalili, N. & Laxminarayana, K. A review of atomic force microscopy imaging systems: application to molecular metrology and biological sciences. *Mechatronics* **14**, 907–945 (2004).
198. Ducker, W. A., Senden, T. J. & Pashley, R. M. Direct measurement of colloidal forces using an atomic force microscope. *Nature* **353**, 239–241 (1991).
199. Burnham, N. A. *et al.* Comparison of calibration methods for atomic-force microscopy cantilevers. *Nanotechnology* **14**, 1–6 (2003).
200. Dong, Y., Vadakkepatt, A. & Martini, A. Analytical models for atomic friction. *Tribol. Lett.* **44**, 367–386 (2011).
201. Achanta, S., Drees, D. & Celis, J. P. Friction from nano to macroforce scales analyzed by single and multiple-asperity contact approaches. *Surf. Coatings Technol.* **202**, 6127–6135 (2008).
202. Bhushan, B., Israelachvili, J. N. & Landman, U. Nanotribology: Friction, wear and lubrication at the atomic scale. *Nature* vol. 374 607–616 (1995).
203. Samyn, P., Schoukens, G. & De Baets, P. Micro- to nanoscale surface morphology and friction response of tribological polyimide surfaces. *Appl. Surf. Sci.* **256**, 3394–3408 (2010).
204. Perry, S. S. Scanning probe microscopy measurements of friction. *MRS Bulletin* vol. 29 478–483 (2004).
205. Liamas, E., Connell, S. D., Ramakrishna, S. N. & Sarkar, A. Probing the frictional properties of soft materials at the nanoscale. *Nanoscale* vol. 12 2292–2308 (2020).
206. Wang, Y. & Wang, J. Friction determination by atomic force microscopy in field of biochemical science. *Micromachines* vol. 9 (2018).
207. Pettersson, T., Nordgren, N., Rutland, M. W. & Feiler, A. Comparison of different methods to calibrate torsional spring constant and photodetector for atomic force microscopy friction measurements in air and liquid. *Rev. Sci. Instrum.* **78**, (2007).
208. Sader, J. E., Larson, I., Mulvaney, P. & White, L. R. Method for the calibration of atomic force microscope cantilevers. *Rev. Sci. Instrum.* **66**, 3789–3798 (1995).
209. Cannara, R. J., Eglin, M. & Carpick, R. W. Lateral force calibration in atomic force microscopy: A new lateral force calibration method and general guidelines for optimization. *Rev. Sci. Instrum.* **77**, (2006).

210. Sader, J. E., Chon, J. W. M. & Mulvaney, P. Calibration of rectangular atomic force microscope cantilevers. *Rev. Sci. Instrum.* **70**, 3967–3969 (1999).
211. Harlow, J. H. *Electric Power Transformer Engineering*. *Electric Power Transformer Engineering* (CRC Press, 2004). doi:10.5860/choice.41-4065.
212. Walters, D. A. *et al.* Short cantilevers for atomic force microscopy. *Rev. Sci. Instrum.* **67**, 3583–3590 (1996).
213. Attard, P., Pettersson, T. & Rutland, M. W. Thermal calibration of photodiode sensitivity for atomic force microscopy. *Rev. Sci. Instrum.* **77**, (2006).
214. Green, C. P. *et al.* Normal and torsional spring constants of atomic force microscope cantilevers. *Rev. Sci. Instrum.* **75**, 1988–1996 (2004).
215. Gere, J. M. & Goodno, B. J. *Mechanics of Materials (8th ed)*. *Brooks Cole* (2012).
216. Green, C. P. *et al.* Normal and torsional spring constants of atomic force microscope cantilevers. *Rev. Sci. Instrum.* **75**, 1988–1996 (2004).
217. Mullin, N. & Hobbs, J. K. A non-contact, thermal noise based method for the calibration of lateral deflection sensitivity in atomic force microscopy. *Rev. Sci. Instrum.* **85**, (2014).
218. Chen, L., Merlitz, H., He, S. Z., Wu, C. X. & Sommer, J. U. Polyelectrolyte brushes: Debye approximation and mean-field theory. *Macromolecules* **44**, 3109–3116 (2011).
219. Cohen, A. A Padé approximant to the inverse Langevin function. *Rheol. Acta* **30**, 270–273 (1991).
220. Ross, R. S. & Pincus, P. The Polyelectrolyte Brush: Poor Solvent. *Macromolecules* **25**, 2177–2183 (1992).
221. Flory, P. J. Themodynamics of high polymer solutions. *J. Chem. Phys.* **10**, 51–61 (1942).
222. Parsons, D. F. & Salis, A. The impact of the competitive adsorption of ions at surface sites on surface free energies and surface forces. *J. Chem. Phys.* **142**, 134707 (2015).
223. Atkins, P. W. & MacDermott, A. J. The born equation and ionic solvation. *J. Chem. Educ.* **59**, 359–360 (1982).
224. Bazhin, N. The Born Formula Describes Enthalpy of Ions Solvation. *ISRN Thermodyn.* **2012**, 1–3 (2012).
225. Van Rysselberghe, P. Remarks concerning the clausius-mossotti law. *J. Phys. Chem.* **36**, 1152–1155 (1932).
226. Parsons, D. F. & Ninham, B. W. Ab initio molar volumes and gaussian radii. *J. Phys. Chem. A* **113**, 1141–1150 (2009).
227. Kunz, W. Specific ion effects in colloidal and biological systems. *Current Opinion in Colloid and Interface Science* vol. 15 34–39 (2010).
228. Kunz, W. Specific Ion Effects, Evidences. in *Encyclopedia of Applied Electrochemistry* 2045–2050 (Springer, New York, NY, 2014). doi:10.1007/978-1-4419-6996-5_26.
229. Moghaddam, S. Z. & Thormann, E. The Hofmeister series: Specific ion effects in aqueous polymer solutions. *Journal of Colloid and Interface Science* vol. 555 615–635 (2019).
230. Thormann, E. On understanding of the Hofmeister effect: How addition of salt alters the stability of temperature responsive polymers in aqueous solutions. *RSC Adv.* **2**, 8297–8305 (2012).
231. Cacace, M. G., Landau, E. M. & Ramsden, J. J. The Hofmeister series: Salt and solvent effects on interfacial phenomena. *Quarterly Reviews of Biophysics* vol. 30 241–277 (1997).
232. Zajforoushan Moghaddam, S. & Thormann, E. Hofmeister effect of salt mixtures on thermo-responsive poly(propylene oxide). *Phys. Chem. Chem. Phys.* **17**, 6359–6366 (2015).
233. Zhang, Y., Furyk, S., Bergbreiter, D. E. & Cremer, P. S. Specific ion effects on the water solubility of macromolecules: PNIPAM and the Hofmeister series. *J. Am. Chem. Soc.* **127**, 14505–14510 (2005).
234. Salis, A. & Ninham, B. W. Models and mechanisms of Hofmeister effects in electrolyte solutions, and colloid and protein systems revisited. *Chemical Society Reviews* vol. 43 7358–7377 (2014).
235. Eysden, C. A. Van & Sader, J. E. Frequency response of cantilever beams immersed in viscous fluids with applications to the atomic force microscope : Arbitrary mode order Frequency response of cantilever beams immersed in viscous fluids with applications to the atomic force microscope : *J. Appl. Phys.* **101**, 044908-0,044908-11 (1998).

Appendix A

Ion-specific antipolyelectrolyte effect on the swelling behavior of polyzwitterionic layers.

Frederik Hegaard, Robert Biro, Koosha Ehtiati and Esben Thormann

(Submitted)

Ion-specific antipolyelectrolyte effect on the swelling behavior of polyzwitterionic layers

Journal:	*Langmuir*
Manuscript ID	la-2022-027982
Manuscript Type:	Article
Date Submitted by the Author:	13-Oct-2022
Complete List of Authors:	Hegaard, Frederik; Technical University of Denmark, Department of Chemistry Biro, Robert; Danmarks Tekniske Universitet, Department of Chemistry Ehtiati, Koosha; Technical University of Denmark, Department of Chemistry Thormann, Esben; Danmarks Tekniske Universitet, Department of Chemistry

Ion-specific antipolyelectrolyte effect on the swelling behavior of polyzwitterionic layers

*Frederik Hegaard, Robert Biro, Koosha Ehtiati and Esben Thormann**

Department of Chemistry, Technical University of Denmark, 2800 Kgs. Lyngby, Denmark.

ABSTRACT

In this study, we systematically investigate the interactions between mobile ions generated from added salts and immobile charges within a sulfobetaine-based polyzwitterionic film in the presence of five salts (KCl, KBr, KSCN, LiCl, and CsCl). The sulfobetaine groups contain quaternary alkyl ammonium and sulfonate groups, giving the positive and negative charges. The swelling of the zwitterionic film in the presence of different salts is compared with the swelling behavior of a polycationic or polyanionic film containing the same charged groups. For such a comparative study, we design crosslinked terpolymer films with similar thicknesses, crosslink densities, and

charge fractions, but with varying charged moieties. While the addition of salt in general leads to a collapse of both cationic and anionic films, the presence of specific types of mobile anions (Cl^-, Br^-, and SCN^-) considerably influences the swelling behavior of polycationic films. We attribute this observation to a different degree of ion-pair formations between the different types of anionic counterions and the immobile cationic quaternary alkyl ammonium groups in the films where highly polarizable counterions such as SCN^- lead to a high degree of ion pairing and less polarizable counterions, such as Cl^-, cause a low degree of ion pairing. Conversely, we do not observe any substantial effect of varying the type of cationic counterions (K^+, Li^+, and Cs^+), which we assign to the lack of ion pairing between the weakly polarizable cations and the immobile anionic sulfonate groups in the films. Further, we observe that the zwitterionic films swell with increasing ionic strength and the degree of swelling is anion dependent, which is in agreement with previous reports on the "antipolyelectrolyte" effect. Herein, we explain this ion-specific swelling behavior with the different cation and anion abilities to form ion pairs with quaternary alkyl ammonium and sulfonate in the sulfobetaine groups.

Introduction

Polyzwitterions are polymers containing functional groups, which carry both positive and negative charges. In their simplest form, as seen for polymers containing, e.g., phosphorylcholine or sulfobetaine groups, each chain carries an equal number of positive and negative charges and is therefore overall electrically neutral. This overall electrically neutrality will provide such polymers with unique hydration and swelling properties compared with uncharged polymers or polyelectrolytes that carry an overall positive or negative charge. Polyzwitterions also provide several interesting properties that make them interesting when used in films and coatings, e.g., antifouling applications and in aqueous lubricating systems.[1–6] One of the unique properties of some polyzwitterionic films is the so-called "antipolyelectrolyte effect," which refers to the aqueous swelling behavior of polyzwitterionic films in response to changes in the ionic strength. As implied by the term, the antipolyelectrolyte effect means that the swelling response is opposite to the response of the polyanionic or polycationic films. More specifically, polyzwitterionic films often swell with increasing ionic strength, whereas polyanionic or polycationic films collapse with increasing ionic strength.[7–10]

At low ionic strength, owing to the strong dipole–dipole pairing of zwitterionic groups on either the same polymer chain or on neighboring chains, the polyzwitterionic films are normally found

in a collapsed state. Therefore, a zwitterionic film comprises a tight bond network with a high number of interchain and intrachain physical crosslinks, resulting in a low ability of the film to swell even if the polymers are hydrophilic. However, the dipole–dipole interactions are disrupted and the film is able to swell when the ionic strength is increased. As discussed by Wang et al., this disruption can occur either in a symmetric manner, where both internal ions in the zwitterionic ion pair are similarly affected by the increasing ionic strength (e.g., by electrostatic screening), or in an asymmetric manner, where the positive and the negative charges in the zwitterionic group are differently affected by the external salt (e.g., through the chemisorption of mobile ions).[11–13]

To further explain the molecular mechanisms of the "antipolyelectrolyte effect," it is interesting to mention that the swelling induced by increasing ionic strength has been found to be strongly dependent on the type of the added salt.[14,15] Most experimental studies have focused on varying the anions of the added salt, [7,8,16–18] for which parallels have been drawn to the Hofmeister series, where varying the type of anions has been shown to have a crucial effect on the solution behavior of both charged and uncharged macromolecules.[19–23] This is, for example, the case for several studies of polymer films containing sulfobetaine groups, where the exact degree of swelling with increasing ionic strength has been shown to be strongly dependent on the specific type of anions.

However, the fact that the swelling behavior is ion type-dependent shows that the electrostatic screening of the dipole–dipole interactions cannot be the only reason for swelling. Yet, a full molecular understanding of the "antipolyelectrolyte effect" is still lacking, especially, when it comes to how specific types of ions affect the swelling behavior. To this end, we believe that comparing this swelling behavior with the swelling behavior of structurally simpler cationic and anionic analogs is the key to understanding the complex swelling behavior of polyzwitterionic films.

For polycationic and polyanionic films, the swelling behavior is caused by a balance between counterion-induced osmotic pressure, polymer–polymer and polymer–solvent nonelectrostatic interactions, and chain entropic elasticity.[24–27] The response of the polycationic and polyanionic films to changes in ionic strength is derived from the variation in the counterion-induced osmotic pressure. This arises from the excess counterion concentration within the film compared with the concentration in the bulk solution, which is required to compensate the charges on the polyelectrolyte chains and causes swelling of the film at low salt concentrations. This swelling regime is known as the osmotic regime. With increasing ionic strength of the medium, the difference between the ion concentration inside and outside the film decreases; thus, the osmotic

pressure decreases and the film collapses accordingly in the so-called salted regime. Finally, when the salt concentration reaches a high level, the osmotic pressure is supposedly no longer effective for the swelling of the film and the film enters a regime with a low, ionic strength-independent thickness, known as the quasineutral regime.[24,28–30]

The specific ion type can affect the counterion-induced osmotic pressure and polymer–solvent nonelectrostatic interactions. However, these effects are different depending on whether the ion is a counterion or a coion. Even when the salt concentration in bulk is low, the counterions inside the polymer film are always present in a high amount, and are therefore always affecting the film. According to the Boltzmann distribution caused by the chemical potential difference, the coion concentration inside the film is considerably lower than that in the bulk.[31]

In the present study, we aim to decouple the interactions between mobile ions generated from the added salt and two immobile charges in the zwitterionic group. This was achieved first by studying the specific ion and ionic strength–dependent swelling behavior of polycationic films containing positively charged quaternary alkyl ammonium groups and polyanionic films containing negatively charged sulfonate groups. These films' swelling behavior was directly compared with the swelling behavior of polyzwitterionic films containing sulfobetaine groups that are zwitterionic

owing to a combination of quaternary alkyl ammonium and sulfonate groups. Thus, we were able to study the effects of different counterions and coions on the quaternary alkyl ammonium and the sulfonate groups, separately, and use this knowledge to predict how different mobile cations and anions would interact with the positive and negative charges in the zwitterionic groups.

Experimental Section

Chemicals

[2-(methacryloyloxy)ethyl]trimethylammonium chloride (METAC, 75 wt.% in H_2O), 3-sulfopropyl methacrylate potassium (SPMAK, 98%), 2-(dimethylamino)ethyl methacrylate (98%), 1,4-butane sultone (BS, ≥99%), 4-cyano-4-[(dodecylsulfanylthiocarbonyl)sulfanyl] pentanoic acid (CDPA, 97%), allyl methacrylate (AMA, 98%), *n*-butyl methacrylate (*n*-BMA, 99%), 3-mercaptopropyl trimethoxysilane (MPTMS, 95%), 2,2,2-trifluoroethanol (TFE, ≥99%), pentaerythritol tetrakis(3-mercaptopropionate) (PETMP, ≥95%), 4,4′-azobis(4-cyanovaleric acid) (ACVA, ≥98%), potassium chloride (KCl, 99.5%), potassium thiocyanate (KSCN, 99%), potassium bromide (KBr, 99%), lithium chloride (LiCl, 99%), and cesium chloride (CsCl, 98%) were purchased from Sigma-Aldrich Denmark. *N*,*N*-Dimethylformamide (≥99.9%), diethyl ether

(≥99.9), toluene (≥99.8), and acetonitrile (≥99.9) were received from VWR Chemicals BDH and passed through activated basic aluminum oxide (Brockman I, Sigma-Aldrich) before use to remove any inhibitors. Zwitterionic monomer *N*-(2-methacryloylxyethyl)-*N*,*N*-diemthylammonium butanesulfonate (MABS) was prepared beforehand using the procedure reported in a previous study.[32] Ultrapure water (Sartorius Arium Pro; 18.2 MΩ·cm) was used for preparing aqueous salt solutions.

Polymer films

Polymer films were produced through a stepwise process: reversible addition–fragmentation chain-transfer (RAFT) polymerization, surface functionalization of the substrate, and then spin coating and curing.

First, charged terpolymers were synthesized using RAFT polymerization by incorporating 25 mol.% of charged monomer (METAC, SPMAK, or MABS) and varying amounts of AMA and *n*-BMA (corresponding to the targeted AMA composition and eventual film crosslink density). CDPA and ACVA were added in a 200:1:0.1 molar ratio (monomer:CDPA:ACVA). Cationic and anionic polyelectrolytes were synthesized using METAC and SPMAK, as the charged monomers,

in a 2.5-M monomer solution in 4:1 *N*,*N*-dimethylformamide/H_2O. Accordingly, zwitterionic polymers were synthesized using MABS and polymerized in TFE (2.5 M with respect to the monomers). AMA contents were selected as 5, 10, or 15 mol.%, equating to *n*-BMA contents of 70, 65, or 60 mol.%, respectively, which corresponded to the eventual crosslink density of the polymer films. Ultimately, the total monomer concentration was 2.5 M, and the solution was degassed by sparging with N_2 for 30 min after which the temperature was raised to 70 ˚C, initiating polymerization. The polymerization was conducted under N_2 atmosphere and monitored via ^{1}H-NMR until completion. Then, the reaction was precipitated in cold-stirred diethyl ether. Once collected via vacuum filtration, the product was dried overnight at 30 ˚C in a vacuum oven and characterized using ^{1}H-NMR, which confirmed the approximate composition of the polymer.

Silicon wafers were used as the substrate for the films, which needed to be functionalized before grafting the film. The wafers were rinsed with water, ethanol, and acetone, then dried under a N_2 stream, and cleaned using plasma for 180 s under a 500-mTorr water-vapor atmosphere. Then the wafers were submerged in a 15-vol.% MPTMS toluene solution and stirred at room temperature (~23-˚C). After 3 h, the functionalized wafers were removed from the solution, dried under an N_2 stream, and placed in a 130-˚C vacuum oven to induce silanization.

The polymer solution was spin coated onto the functionalized wafer and anchored via thermally initiated crosslinking. First, an ~1 wt.% polymer in TFE solution was prepared, and tetrafunctional thiol PETMP and a radical initiator ACVA was added. PETMP (though tetrafunctional) was loaded at a 1:1 molar ratio to that of the -ene- functionality of the polymer. After stirring for 30 min, the solution was spin coated onto the previously prepared thiol-functionalized silicon wafer (2000 rpm for 40 s) before being placed in a 90-˚C oven for 2 h to induce a thermally initiated thiol–ene crosslinking reaction. The wafers were then removed from the oven and cooled to room temperature. Then they were washed twice with an excess of water to remove any unattached materials and then dried under N_2 atmosphere.

Ellipsometry

The thicknesses of the films were measured using an ellipsometer (J. A. Woollam, M-2000) equipped with a liquid cell. The measurements were conducted with a fixed angle of incidence of 75˚ and at wavelengths of 250–1000 nm. The measurements were analyzed using the instrument's software, CompleteEase, where the sample was described with a model containing multiple layers. The model was created with Si as the substrate, a 1 nm–thick Si–SiO_2 transition layer, a 100 nm–thick SiO_2 layer, a uniform polymer film without absorption of light, and finally ambient

conditions matching the refractive index of the solvent. The properties of the polymer film were described using a Cauchy model with the form $n(\lambda) = A + B/\lambda^2$ where n and λ are the refractive index and the wavelength, respectively, and A and B are fitting parameters. The fitting parameters for the film were A and B from the Cauchy model and the thickness of the polymer film. The refractive index of the salt solution changed with the concentration and type of the salt, which was adjusted accordingly in the model. See supporting information Section S1 for details on the procedure of performing the measurements and the optical model.

Results and Discussion

In this study, we have used random terpolymers comprising three repeating units: a noncharged unit (*n*-butyl methacrylate), a crosslinkable unit (allyl methacrylate), and a charged unit (Figure 1). While the fraction of the charged units was kept constant (25 mol.%) for all polymer films, the fraction of crosslinkable units was systematically varied between 5, 10, and 15 mol.% to obtain polymer films with various crosslink densities. Three types of charged units were chosen: either a positively charged unit (METAC), a negatively charged unit (SPMAK), or a zwitterionic unit (MABS) (Figure 1). With such molecular designs, we were able to first systematically vary the crosslink density for the polyelectrolyte systems while keeping the charge fraction constant.

Second, we were able to compare the swelling behavior of the polycationic, polyanionic, and polyzwitterionic films, which have the same fraction of charged units, similar crosslink density (controlled via the fraction of crosslinkable units), and controlled nonelectrostatic interactions arising from the fraction of noncharged units. Dry-film thicknesses determined using the ellipsometry and topographical information from AFM images of the prepared polymer films are provided in Supporting Information Section S2.

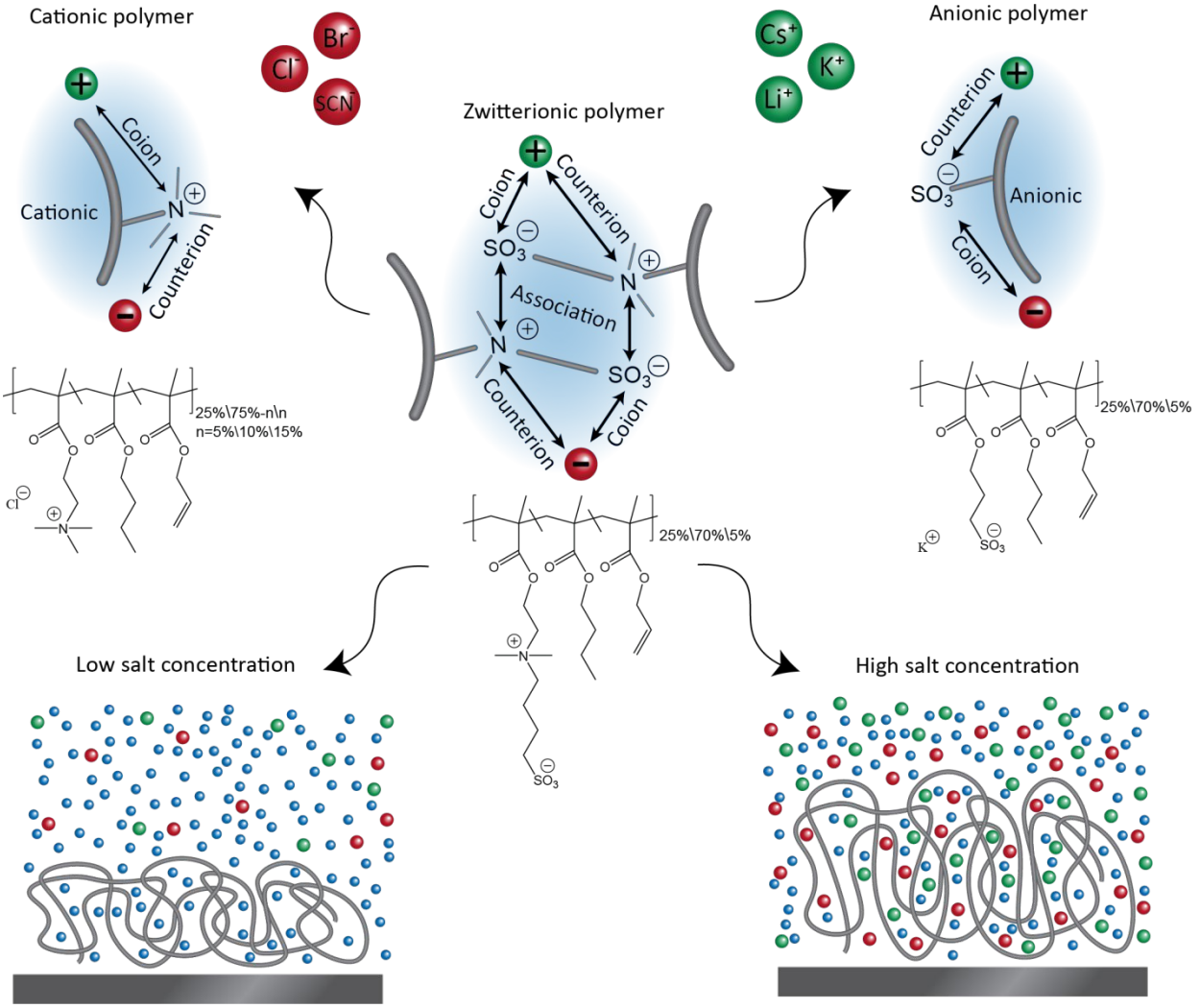

Figure 1. Schematic of the investigated systems and relevant ionic interactions. Three random terpolymers with cationic, anionic, and zwitterionic groups were used to prepare surface grafted, crosslinked polymer films. Swelling behavior was investigated as a function of the concentration of added salts (KCl, KBr, KSCN, LiCl, and CsCl), corresponding to three different anions and three different cations. Then, the different cations and anions worked as counterions, coions, or both, depending on the ionic nature of the polymers.

Next, we investigated the swelling behavior of the systems: polycationic, polyanionic, and polyzwitterionic films. For this, we first considered the effect of the ionic strength on the swelling behavior of the polymer films in the presence of KCl and then determined how this response is affected by the type of counterions and coions. To later provide a detailed discussion of the polyzwitterionic films based on these understandings, we studied the polycationic and polyanionic films to investigate the interactions between the mobile ions and the immobile charged groups in the films

Effects of ionic strength and crosslink density on polycationic films

For the polycationic films with different crosslink densities, the absolute thicknesses of the hydrated films and the swelling ratios (relative to the dry-film thickness) are plotted in Figure 2 as a function of KCl concentration. The overall swelling behavior of the polycationic film follows the typical behavior of strong polyelectrolyte films with respect to ionic strength.[10,25,33] We observed that this film exhibited a high and constant thickness at low salt concentrations, from 0.01 to 10 mM, which corresponds to the osmotic regime, where the counterion-induced osmotic pressure caused considerable swelling of the film.[29,30,34] From ~10–30 mM, the salted regime started, where a decline in swelling was observed because the osmotic pressure difference

decreased due to the addition of external salts. In addition to the osmotic and salted regimes, a quasineutral regime is sometimes observed for polyelectrolyte films at very-high salt concentrations, depending on the films properties.[25,35,36] In the current case, this regime is, however, not manifested below 3 M KCl.

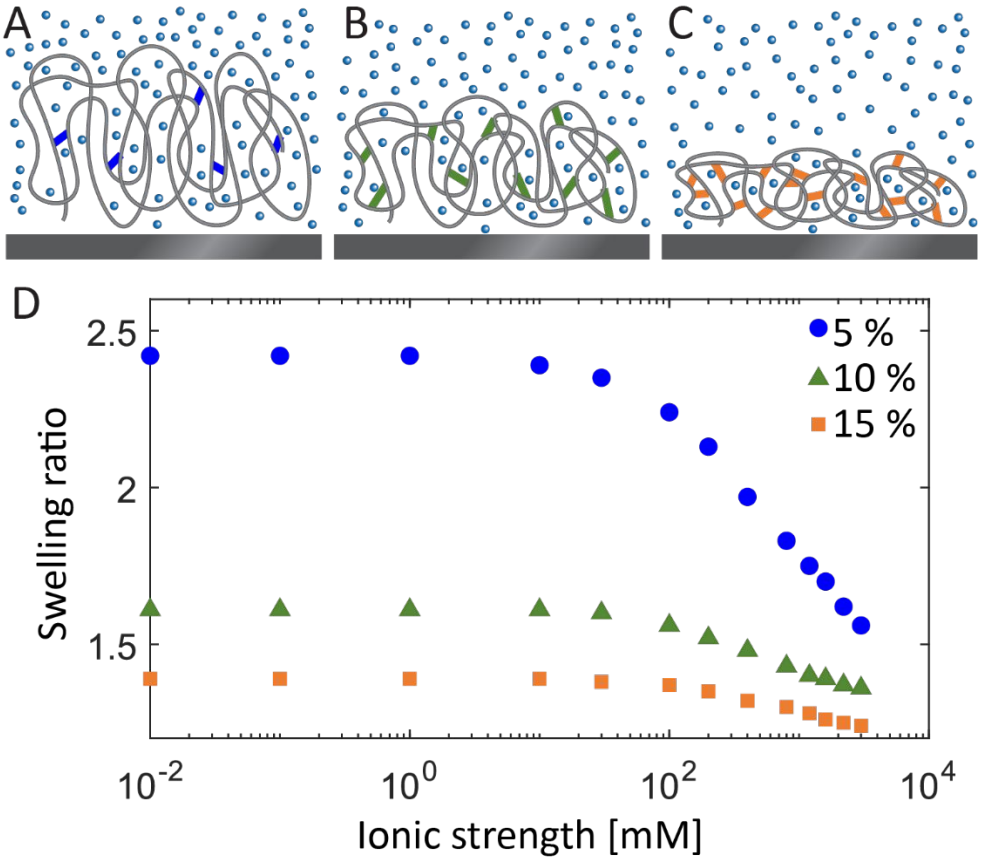

Figure 2. Illustration of the crosslinking effect for (A) low, (B) intermediate, and (C) high crosslinking degrees. (D) Swelling ratios of hydrated polycationic films (hydrated-film thickness compared with dry-film thickness, see Supporting Information S2 for dry-film thicknesses) as a function of KCl concentration for films with either 5, 10, or 15 mol.% of the crosslinked monomer.

Films of different degrees of crosslinking but with the same charge density were investigated to show how the degree of crosslinking can influence the swelling behavior. As shown in Figure 2, all the three films qualitatively followed the same trends with an osmotic regime in the first part (constant thickness) and a salted regime in the last part (declining thickness). However, with increased crosslink density, chain stretching became restricted; thus, the swelling decreased in the osmotic regime. This observation is not surprising; however, it is important for the interpretation of the zwitterionic films' swelling, where it is expected that dipole–dipole intrachain and interchain bonds will also limit the swelling due to a similar effect (although the effect is caused by a different type of crosslinking).

Specific ion effects on polycationic films

Five monovalent salts KCl, KBr, KSCN, LiCl, and CsCl were chosen to demonstrate how swelling of the polycationic film depends on the specific types of ions. Here, it is possible to systematically vary either the coions or the counterions.

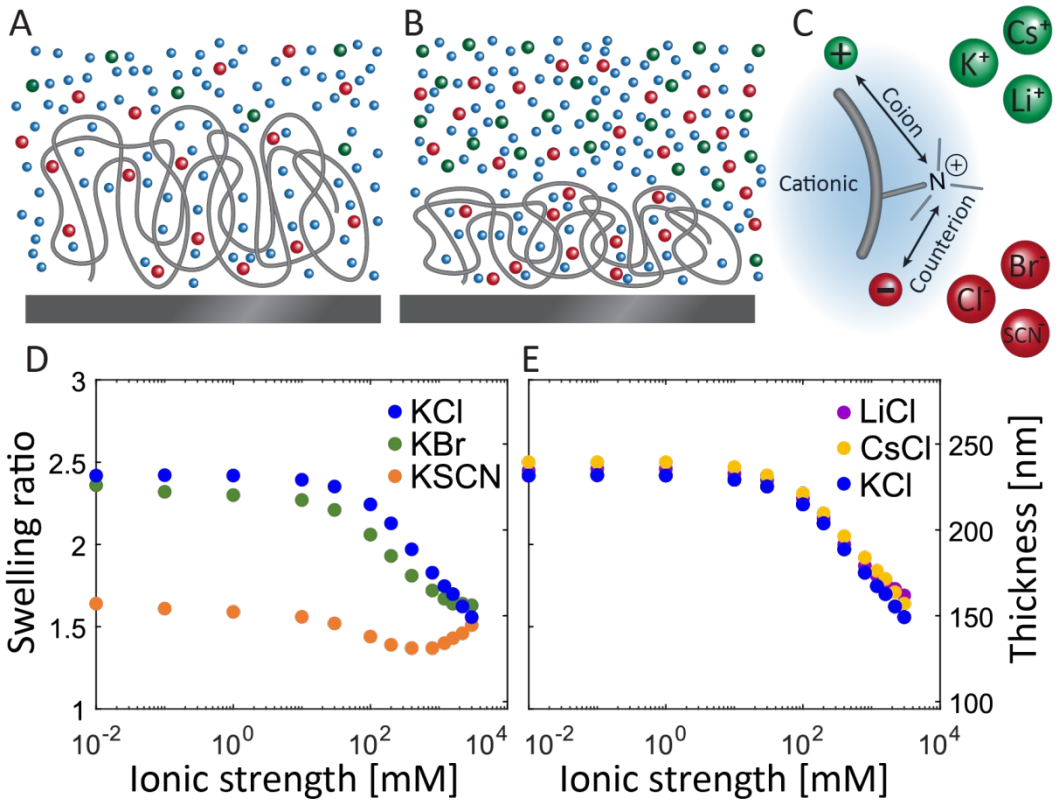

Figure 3. Illustration of polycationic film swelling when hydrated in (A) low and (B) high salt concentrations. (C) Role of ions when interacting with the charged quaternary alkyl ammonium groups (of polymers) as either cationic coions or anionic counterions. Ellipsometry-based thickness of the polycationic film as a function of salt concentration in the presence of (D) either potassium salts with various anionic counterions or (E) chloride salts with various cationic coions.

Figure 3D shows the effect of different anions (counterions) on the swelling behavior of the polycationic film with a low crosslink density (5 mol.% of the crosslinker monomer) while keeping the cation (coion) unchanged as K^+. Here, where the thickness of the films follows the trend Cl^- >

$Br^- > SCN^-$ at low salt concentrations, in the osmotic regime, the anionic counterions considerably affect the swelling of the film. However, the thicknesses converge to an approximately similar level at high salt concentrations. This difference in the osmotic regime indicates a lower counterion-induced osmotic pressure in the case of SCN^- compared to other ions. Counterion-specific behavior has previously been observed in other cationic films, and here, it has been explained by the effect of specific types of counterions on the counterion-induced osmotic pressure and the polymer–polymer and polymer–solvent nonelectrostatic interactions.[10,25,37–39] Thus, we have linked the trend of thickness at low ionic strength to the ability of anionic counterions to form ion pairs with the quaternary alkyl ammonium groups on the polyelectrolyte chains, and thus, become osmotically passive. To this end, based on our results, it is expected that the degree of ion-pair formation follows the trend $SCN^- > Br^- > Cl^-$, which agrees with previous reports.[40,41] Beside this overall behavior, the film with SCN^- as counterions started to swell with increasing salt concentration, from approximately 800 mM. At such high ionic strength, the counterion-induced osmotic pressure declined and the swelling was thus attributed to the effect of SCN^- on the nonelectrostatic polymer–solvent interactions. This effect could thus be similar to the "salting-in" effect of SCN^- observed for many noncharged polymers at high salt concentrations.[19,42–45]

Figure 3E shows the effect of the cations (coions) on the swelling behavior of polycationic films, while the anion (counterion) was kept as Cl^-. In contrast to the drastic variations observed with varying anionic counterions, different cationic coions afforded an almost identical swelling behavior, both with respect to the overall trend (first an osmotic regime and then a salted regime) and the absolute thicknesses. However, at the highest salt concentrations (>1 M) a weak specific cationic coion effect was observed, and we assigned this weak effect to the influence of ions on the polymer–solvent nonelectrostatic interactions (Hofmeister effects).

To investigate the effect of crosslink density on the ion-specific response of the polycationic films, measurements on polycationic films with 10 and 15 mol.% crosslinking monomers have been conducted using the same salts specified in Figure 3 (see Supporting Information Section S3). The thickness of the hydrated films showed a similar trend with the variation of anionic counterions, as observed for the low-crosslink polycationic film ($Cl^- > Br^- > SCN^-$). Similarly, the variation of cationic coions afforded almost identical swelling behavior for each film with fixed crosslink density. However, with increasing crosslink density, the overall swelling of the films and their response to specific anionic counterion effects became less pronounced.

Most relevantly, while the cationic coions only begin to show small variations at very-high salt concentrations, these variations in coions and counterions show how the anionic counterions considerably affect the swelling at very-low salt concentrations. This agrees well with the idea that the anionic counterions are present inside the film in high concentrations at all times and affect the ion osmotic pressure. However, the concentration of cationic coions inside the film is lower than the concentration in bulk; thus, their effect on the film is negligible in this concentration range.

As demonstrated here, anions can interact and form ion pairs with the quaternary alkyl ammonium groups on the polycationic chain. Therefore, it is expected that in a polyzwitterionic system with the same cationic groups, these anions (Cl^-, Br^- and SCN^-) will compete with the sulfonate groups to bind with the quaternary alkyl ammonium groups. Such a competition in ion-pair formation and the resulting anion-specific behavior of polyzwitterionic systems are discussed later.

Specific ion effects on polyanionic films

Next, we investigated the swelling behavior of polyanionic films that were designed with similar physical properties (charge density and crosslink density) but with a sulfonate side group to develop negative charges on the chain. This makes it possible to investigate the effect of the same

five salts used on the polycationic film, but this time, with the reversed roles of coions and counterions (Figure 4).

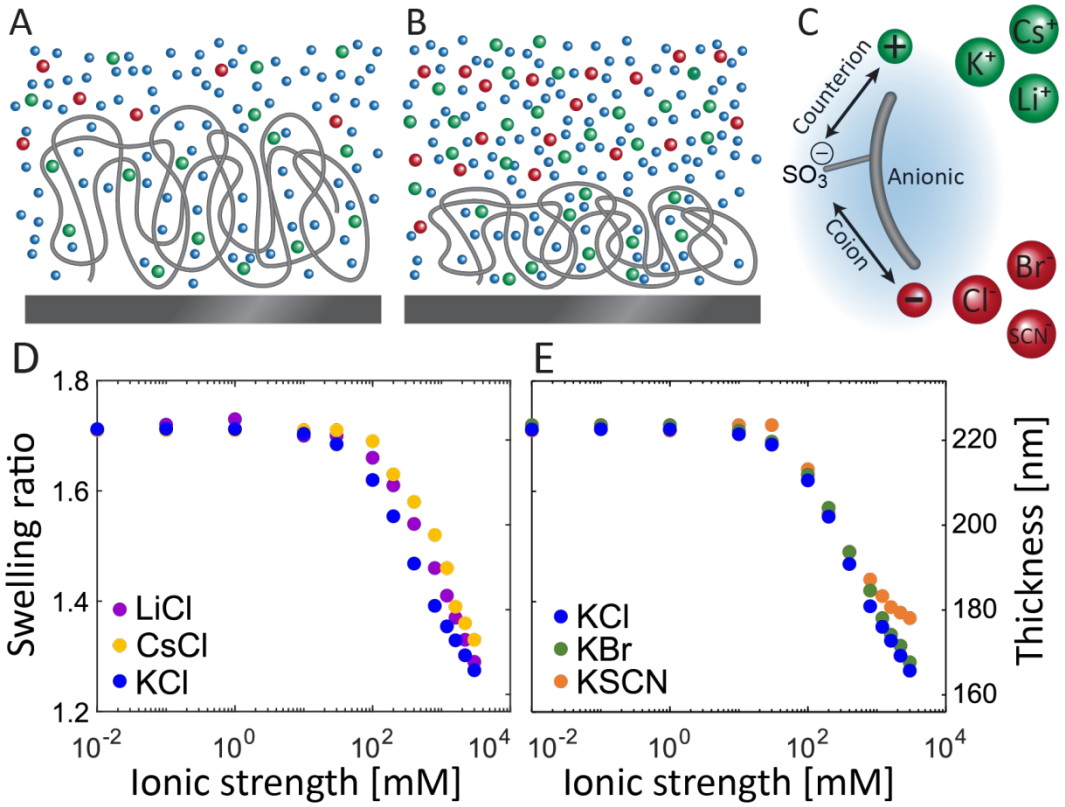

Figure 4. Illustration of polyanionic film swelling when hydrated in (A) low and (B) high salt concentrations. (C) Role of ions when interacting with the charged sulfonated groups (of polymers) as either anionic coions or cationic counterions (C). Ellipsometry-based thickness of the polyanionic film as a function of salt concentration in the presence of (D) either chloride salts with various cationic counterions or (E) potassium salts with various anionic coions.

By comparing Cs^+, K^+, and Li^+, the effect of cations (counterions) on the swelling behavior of the polyanionic film was investigated (Figure 4D). A typical swelling behavior was observed for all the cases with an osmotic regime at low salt concentration, up to ~10–30 mM, followed by a salted regime with a further increase in the salt concentration. However, the variation of the type of cationic counterions showed an insignificant influence on the swelling behavior of the polyanionic film in the osmotic regime because the thickness of the films with various cationic counterions exhibited similar thicknesses at low ionic strength. This indicates that the counterion-induced osmotic pressure is not affected by the type of cationic counterions. This can be explained by a similar degree of ion-pair formation (or no ion pairing) between the sulfonate groups in the film and these mobile cationic counterions. This is in contrast to the observed effect of the anionic counterions on the polycationic film where we observed various degrees of ion pairs with the quaternary alkyl ammonium groups in the films. To understand and explain this difference, focus should be placed on the mechanism through which ion pairs are formed. Ion-pair formation has been suggested to be correlated with the polarizability of the ions in the pair in such a manner that highly polarizable ions tend to interact stronger with the (also highly polarizable) quaternary ammonium groups and thus form a larger number of ion pairs compared to weakly polarizable

ions with sulfonate groups.[10,46,47] In our current study, the polarizability of the mobile anions ranged between 3.5 and 7.0 Å^3, while the polarizability of the mobile cations was much lower (0–2 Å^3).[48] To this end, we suggest that although the cations used here have different polarizabilities, they are all so low that the ion-pair formation in those cases is negligible (i.e., no ion pairing). Thus, the anion-specific swelling on the polycationic film is associated with higher polarizabilities of some anions, which leads to different degrees of ion-pair formation with the quaternary alkyl ammonium groups. It is worth mentioning that formation of ion pairs is of course dependent on the polarizability of both charged moieties. Thus, while in our system containing sulfonate groups we observed similar counterion-induced osmotic pressure for Cs^+, K^+, and Li^+ as the counterion, the same counterions might result in different counterion-induced osmotic pressure in a polyanionic film with differently charged moieties (see Supporting Information Section S4 for a more detailed discussion).

In Figure 4E, the effect of changing the type of anion (coion) is shown to have an insignificant effect on the swelling of the films at low to medium ionic strength (up to around 400 mM). However, it is observed that the film with SCN^- as the counterion collapses less than those with Cl^- and Br^- as counterions, at higher concentrations of salts. Although the local salt concentrations

in the films are not identical in the two situations, this observation is in line with the previously discussed behavior of SCN^- in the polycationic film at high ionic strength.

Here it was demonstrated that various cations have an insignificant ion-pair interaction with the sulfonate groups, in contrast to the various interactions of anions with quaternary alkyl ammonium groups. For the sulfobetaine, we can expect an asymmetric ion association for some types of added salts where mobile anions can form ion pairs with the positively charged quaternary alkyl ammoniums, while mobile and osmotically active cations balance the negatively charged sulfonates.

Specific ion effects on polyzwitterionic films

We next turned the focus to the swelling behavior of the sulfobetaine-based polyzwitterionic film, which contains a quaternary alkyl ammonium and a sulfonate group in each zwitterionic unit. The thickness of the polyzwitterionic film as a function of the ionic strength of the salts with systematic variations of cations and anions is shown in Figure 5.

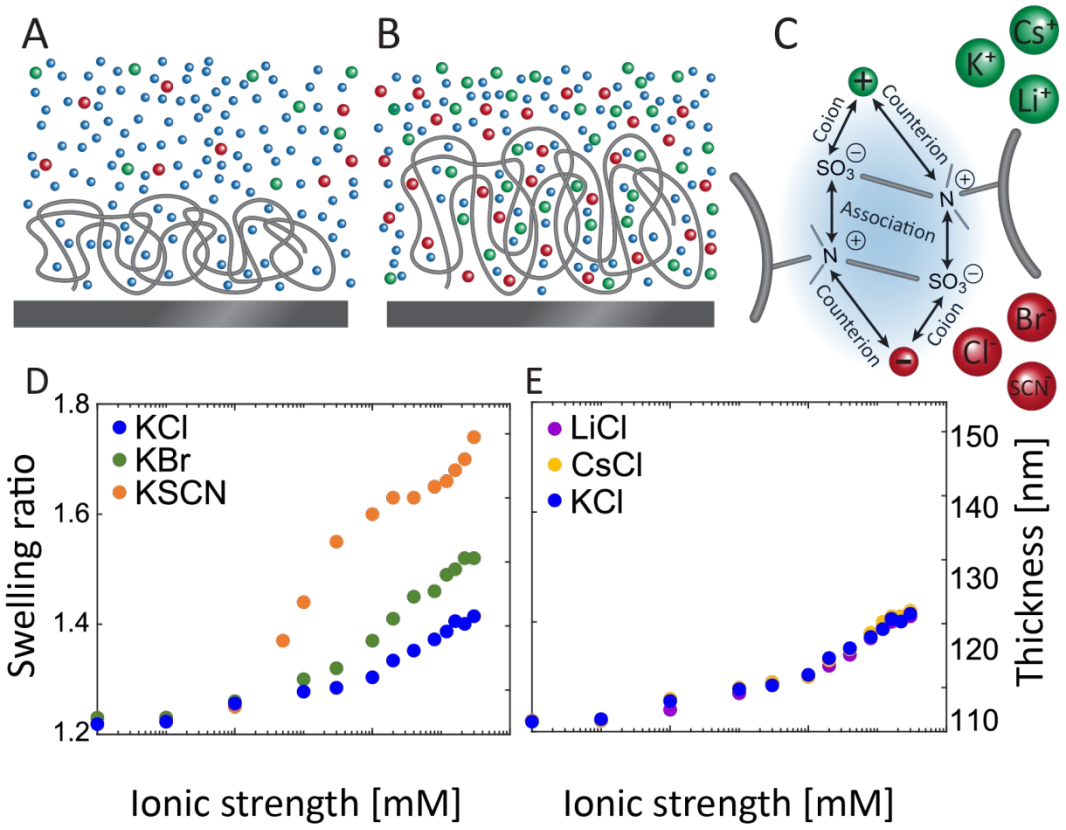

Figure 5. Illustration of polyzwitterionic film swelling when hydrated in (A) low and (B) high salt concentrations. (C) Role of ions when interacting with the charged groups (of polymers) as either coions or counterions (C). Ellipsometry-based thickness of the polyzwitterionic film as a function of salt concentration in the presence of (D) either potassium salts with various anions or (E) chloride salts with various cations.

Starting with the effect of varying the anions, Figure 5D shows the swelling behavior of the polyzwitterionic film in the presence of KCl, KBr, and KSCN. For all three cases, the film was found in a collapsed state at a low salt concentration up to around 1 mM followed by an increase

in thickness with a further increase in salt concentration. Secondly, it was observed that the swelling behavior of the polyzwitterionic film is strongly anion dependent. The film undergoes the most pronounced swelling in the presence of SCN^-, while in the presence of Br^- swelling occurs to a lower extent, and the least pronounced swelling is found in the case of Cl^-. Contrary to this observed effect of different anions, the swelling behavior of the polyzwitterionic film is shown, in Figure 5B, to be independent of the type of cation.

The swelling of polyzwitterionic films with the addition of salt is commonly referred to as the "antipolyelectrolyte" effect and is attributed to the dissociation of intrachain and interchain dipole–dipole bonds between the zwitterionic groups. The electrostatic interactions between the two groups are screened upon increasing medium ionic strength, whereby these groups can undergo dissociation. However, the fact that this behavior depends on the ion type demonstrates that an electrostatic effect cannot solely explain the behavior. In particular, the specific interactions between the salt ions and the immobile ions should be considered. We can implement the learnings from the cationic and anionic systems, to explain this behavior.

In the case of interactions between the mobile anions and the sulfonate group in the anionic film, we observed no significant influence of anionic coions on the swelling behavior of films except

for very-high concentrations of SCN^-, where a change in nonelectrostatic interactions was observed (the coion effect in the polyanionic film, Figure 4E). On the other hand, we concluded that the interactions between the anions and the quaternary alkyl ammonium groups in the cationic film could be ranked based on their tendency to form ion pairs with the trend $SCN^- > Br^- > Cl^-$ (the counterion effect in the polycationic film, Figure 3D). This was also the trend of swelling observed in the polyzwitterionic film, indicating that the stronger the interaction of the anions with the quaternary alkyl ammonium groups, the higher degree of dissociation of the intrachain and interchain bonds, and thus the higher swelling of the film.

Regarding the effect of cations (Figure 5E), we observed, on the other hand, no significant interaction between the cations and the immobile groups, neither in the case of the polycationic film where the cations are coions nor in the case of polyanionic films where the cations are counterions. The cations did not form strong ion pairs with the sulfonate groups, in contrast to the case of anions in a polycationic film. We, therefore, suggest that this also can explain why the type of cations does not influence the swelling behavior of the polyzwitterionic systems.

By systematically comparing specific cation and anion effects on quaternary alkyl ammonium groups and sulfonate groups, we have now demonstrated that the swelling of the polyzwitterionic

films is enhanced by ions that can strongly interact with one of the charges in the zwitterionic groups (in our case, anions pairing with the quaternary alkyl ammonium groups). We can also speculate about how this dissociation induced swelling of the polyzwitterionic film. At low ionic strength, the polyzwitterionic film was found in a collapsed state due to the formation of intrachain and interchain dipole–dipole bonds. These bonds between the chains act as physical crosslinks that limited swelling of the film, similar to the case observed with varying chemical crosslinks (Figure 2 and Supporting Information Section S3). With increasing ionic strength in the medium, more ions enter the polyzwitterionic film. This phenomenon first screens the electrostatic interactions between the quaternary alkyl ammonium groups and the sulfonate groups. Second, ions with strong interactions with one of the charged moieties (e.g., SCN^- and quaternary alkyl ammonium groups) break the bond between the sulfonate and quaternary alkyl ammonium groups to bind to the favored site. Because of this dissociation, the film swells due to a combination of two effects. First, breaking the interchain bonds yields a lower degree of ionic crosslinking, which allows increased swelling. Second, when SCN^- binds to a quaternary alkyl ammonium group, it is required by electroneutrality that an oppositely charged ion (for example K^+) enters the film to compensate the charge on the sulfonate group. Because K^+ is mobile and osmotically active (as demonstrated in

the case of polyanionic film), it can induce an osmotic pressure, which further increases the swelling of the film (similar to the case of the polyanionic film).

Conclusions

We have systematically studied the effect of interactions between mobile ions and immobile charges in polycationic and polyanionic films to understand the swelling behavior of polyzwitterionic films with similar charged moieties. We observed that the change in the type of cation did not considerably influence the swelling of the films, neither when acting as coions in the polycationic film nor when acting as counterions in the polyanionic film. Changing the type of anion had an insignificant effect on the swelling of the films when the anions acted as coions in the polyanionic film but exhibited a considerable effect when they acted as counterions in the polycationic film. The counterion-specific effect in the polycationic films is explained by different abilities of anions to form ion pairs with the quaternary alkyl ammonium groups.

For the polyzwitterionic film, we observed increased swelling with increasing ionic strength in accordance with the so-called "antipolyelectrolyte effect," and the magnitude of the swelling was found to be to be strongly affected by the anion types following the order $SCN^- > Br^- > Cl^-$, while

it did not depend on the type of cations. By studying all the possible interactions between the mobile ions and immobile charges on the polyzwitterionic chain, we proposed that the antipolyelectrolyte effect is a complicated swelling mechanism related to the electrostatic and nonelectrostatic ion-specific interactions. Dissociation of the intrachain and interchain bonds was derived via electrostatic screening and enhanced by specific ion-pair interactions, in cases where ions from the salt could strongly bind to one of the immobile charged groups. In addition, as another result of dissociation, the osmotic pressure of mobile counterions (which are present to compensate the charge of the immobile charged groups) increased the swelling of films.

ASSOCIATED CONTENT

Supporting Information. Expanded description of ellipsometry technique and film characterization. Expanded discussion of polarisability of ions and additional data for crosslinking dependent film swelling. (PDF)

AUTHOR INFORMATION

Corresponding Author

*esth@kemi.dtu.dk

Department of Chemistry, Technical University of Denmark, 2800 Kgs. Lyngby, Denmark

Author Contributions

The manuscript was written through contributions of all authors. All authors have given approval to the final version of the manuscript.

Funding Sources

Independent Research Fund Denmark (8022-00040B)

Notes

The authors declear no conflicts of interests.

ACKNOWLEDGMENT

Frederik Hegaard gratefully acknowledges a grant from the Technical University of Denmark. Esben Thormann and Robert A. Biro gratefully acknowledges the financial support from the Independent Research Fund Denmark (8022-00040B).

REFERENCES

(1) Zhang, Z.; Chao, T.; Chen, S.; Jiang, S. Superlow Fouling Sulfobetaine and Carboxybetaine Polymers on Glass Slides. *Langmuir* **2006**, *22* (24), 10072–10077. https://doi.org/10.1021/la062175d.

(2) Chang, Y.; Liao, S. C.; Higuchi, A.; Ruaan, R. C.; Chu, C. W.; Chen, W. Y. A Highly Stable Nonbiofouling Surface with Well-Packed Grafted Zwitterionic Polysulfobetaine for Plasma Protein Repulsion. *Langmuir* **2008**, *24* (10), 5453–5458. https://doi.org/10.1021/la800228c.

(3) Zhang, Z.; Vaisocherová, H.; Cheng, G.; Yang, W.; Xue, H.; Jiang, S. Nonfouling Behavior of Polycarboxybetaine-Grafted Surfaces: Structural and Environmental Effects. *Biomacromolecules* **2008**, *9* (10), 2686–2692. https://doi.org/10.1021/bm800407r.

(4) Kobayashi, M.; Terayama, Y.; Hosaka, N.; Kaido, M.; Suzuki, A.; Yamada, N.; Torikai, N.; Ishihara, K.; Takahara, A. Friction Behavior of High-Density Poly(2-Methacryloyloxyethyl Phosphorylcholine) Brush in Aqueous Media. *Soft Matter* **2007**, *3* (6), 740–746. https://doi.org/10.1039/b615780g.

(5) Tadmor, R.; Janik, J.; Klein, J.; Fetters, L. J. Sliding Friction with Polymer Brushes. *Phys. Rev. Lett.* **2003**, *91* (11). https://doi.org/10.1103/PhysRevLett.91.115503.

(6) Tairy, O.; Kampf, N.; Driver, M. J.; Armes, S. P.; Klein, J. Dense, Highly Hydrated Polymer Brushes via Modified Atom-Transfer-Radical-Polymerization: Structure, Surface Interactions, and Frictional Dissipation. *Macromolecules* **2015**, *48* (1), 140–151. https://doi.org/10.1021/ma5019439.

(7) Wang, T.; Kou, R.; Liu, H.; Liu, L.; Zhang, G.; Liu, G. Anion Specificity of Polyzwitterionic Brushes with Different Carbon Spacer Lengths and Its Application for Controlling Protein Adsorption. *Langmuir* **2016**, *32* (11), 2698–2707. https://doi.org/10.1021/acs.langmuir.6b00293.

(8) Wang, T.; Wang, X.; Long, Y.; Liu, G.; Zhang, G. Ion-Specific Conformational Behavior of Polyzwitterionic Brushes: Exploiting It for Protein Adsorption/Desorption Control. *Langmuir* **2013**, *29* (22), 6588–6596. https://doi.org/10.1021/la401069y.

(9) Cheng, N.; Brown, A. A.; Azzaroni, O.; Huck, W. T. S. Thickness-Dependent Properties of Polyzwitterionic Brushes. *Macromolecules* **2008**, *41* (17), 6317–6321. https://doi.org/10.1021/ma800625y.

(10) Ehtiati, K.; Moghaddam, S. Z.; Klok, H.-A.; Daugaard, A. E.; Thormann, E. Specific Counterion Effects on the Swelling Behavior of Strong Polyelectrolyte Brushes. *Macromolecules* **2022**, *55*, 5130. https://doi.org/10.1021/acs.macromol.2c00411.

(11) Wang, F.; Yang, J.; Zhao, J. Understanding Anti-Polyelectrolyte Behavior of a Well-Defined Polyzwitterion at the Single-Chain Level. *Polym. Int.* **2015**, *64* (8), 999–1005. https://doi.org/10.1002/pi.4907.

(12) Mary, P.; Bendejacq, D. D.; Labeau, M. P.; Dupuis, P. Reconciling Low- and High-Salt Solution Behavior of Sulfobetaine Polyzwitterions. *J. Phys. Chem. B* **2007**, *111* (27), 7767–7777. https://doi.org/10.1021/jp071995b.

(13) Huglin, M. B.; Radwan, M. A. Selective Adsorption of Potassium Thiocyanate to a Zwitterionic Polymethacrylate. *Macromolecules* **1992**, *25* (2), 999–1002. https://doi.org/10.1021/ma00028a077.

(14) Higaki, Y.; Kobayashi, M.; Takahara, A. Hydration State Variation of Polyzwitterion Brushes through Interplay with Ions. *Langmuir* **2020**, *36* (31), 9015–9024. https://doi.org/10.1021/acs.langmuir.0c01672.

(15) Berlinova, I. V.; Dimitrov, I. V.; Kalinova, R. G.; Vladimirov, N. G. Synthesis and Aqueous Solution Behaviour of Copolymers Containing Sulfobetaine Moieties in Side Chains. *Polymer (Guildf)*. **2000**, *41* (3), 831–837. https://doi.org/10.1016/S0032-3861(99)00264-5.

(16) Sakamaki, T.; Inutsuka, Y.; Igata, K.; Higaki, K.; Yamada, N. L.; Higaki, Y.; Takahara, A. Ion-Specific Hydration States of Zwitterionic Poly(Sulfobetaine Methacrylate) Brushes in Aqueous Solutions. *Langmuir* **2019**, *35* (5), 1583–1589. https://doi.org/10.1021/acs.langmuir.8b03104.

(17) Delgado, J. D.; Schlenoff, J. B. Static and Dynamic Solution Behavior of a Polyzwitterion Using a Hofmeister Salt Series. *Macromolecules* **2017**, *50* (11), 4454–4464. https://doi.org/10.1021/acs.macromol.7b00525.

(18) Yang, J.; Chen, H.; Xiao, S.; Shen, M.; Chen, F.; Fan, P.; Zhong, M.; Zheng, J. Salt-Responsive Zwitterionic Polymer Brushes with Tunable Friction and Antifouling Properties. **2015**. https://doi.org/10.1021/acs.langmuir.5b02119.

(19) Zajforoushan Moghaddam, S.; Thormann, E. Hofmeister Effect of Salt Mixtures on Thermo-Responsive Poly(Propylene Oxide). *Phys. Chem. Chem. Phys.* **2015**, *17* (9), 6359–6366. https://doi.org/10.1039/c4cp05677a.

(20) Jungwirth, P.; Tobias, D. J. Molecular Structure of Salt Solutions: A New View of the Interface with Implications for Heterogeneous Atmospheric Chemistry. *J. Phys. Chem. B* **2001**, *105* (43), 10468–10472. https://doi.org/10.1021/JP012750G/ASSET/IMAGES/LARGE/JP012750GF00002.JPEG.

(21) Jungwirth, P.; Tobias, D. J. Specific Ion Effects at the Air/Water Interface. *Chemical Reviews*. American Chemical Society April 2006, pp 1259–1281. https://doi.org/10.1021/cr0403741.

(22) Yang, L.; Fan, Y.; Gao, Y. Q. Differences of Cations and Anions: Their Hydration, Surface Adsorption, and Impact on Water Dynamics. *J. Phys. Chem. B* **2011**, *115* (43), 12456–12465. https://doi.org/10.1021/jp207652h.

(23) Morita, T.; Westh, P.; Nishikawa, K.; Koga, Y. How Much Weaker Are the Effects of Cations than Those of Anions? The Effects of K+ and Cs+ on the Molecular Organization of Liquid H2O. *J. Phys. Chem. B* **2014**, *118* (29), 8744–8749. https://doi.org/10.1021/jp504245c.

(24) Pincus, P. Colloid Stabilization with Grafted Polyelectrolytes. *Macromolecules* **1991**, *24* (10), 2912–2919. https://doi.org/10.1021/ma00010a043.

(25) Ehtiati, K.; Z. Moghaddam, S.; Daugaard, A. E.; Thormann, E. Crucial Nonelectrostatic Effects on Polyelectrolyte Brush Behavior. *Macromolecules* **2021**, *54* (7), 3388–3394. https://doi.org/10.1021/acs.macromol.0c02526.

(26) de Gennes, P. G. Conformations of Polymers Attached to an Interface. *Macromolecules* **1980**, *13* (5), 1069–1075. https://doi.org/10.1021/ma60077a009.

(27) Moh, L. C. H.; Losego, M. D.; Braun, P. V. Solvent Quality Effects on Scaling Behavior of Poly(Methyl Methacrylate) Brushes in the Moderate- and High-Density Regimes. *Langmuir* **2011**, *27* (7), 3698–3702. https://doi.org/10.1021/la2002139.

(28) Zhulina, E. B.; Birshtein, T. M.; Borisov, O. V. Theory of Ionizable Polymer Brushes. *Macromolecules* **1995**, *28* (5), 1491–1499. https://doi.org/10.1021/ma00109a021.

(29) Borisov, O. V; Zhulina, E. B.; Birshtein, T. M. Diagram of the States of a Grafted Polyelectrolyte Layer. *Macromolecules* **1994**, *27* (17), 4795–4803. https://doi.org/10.1021/ma00095a021.

(30) Lyatskaya, Y. V.; Leermakers, F. A. M.; Fleer, G. J.; Zhulina, E. B.; Birshtein, T. M. Analytical Self-Consistent-Field Model of Weak Polyacid Brushes. *Macromolecules* **1995**, *28* (10), 3562–3569. https://doi.org/10.1021/ma00114a009.

(31) Ubbink, J.; Khokhlov, A. R. Poisson-Boltzmann Theory of the Charge-Induced Adsorption of Semi-Flexible Polyelectrolytes. *J. Chem. Phys.* **2004**, *120* (11), 5353–5365. https://doi.org/10.1063/1.1647048.

(32) Gauthier, M.; Carrozzella, T.; Penlidis, A. Sulfobetaine Zwitterionomers Based on N-Butyl Acrylate and 2-Ethoxyethyl Acrylate: Monomer Synthesis and Copolymerization Behavior. *J. Polym. Sci. Part A Polym. Chem.* **2002**, *40* (4), 511–523. https://doi.org/10.1002/pola.10138.

(33) Xu, X.; Billing, M.; Ruths, M.; Klok, H. A.; Yu, J. Structure and Functionality of Polyelectrolyte Brushes: A Surface Force Perspective. *Chemistry - An Asian Journal*. John Wiley and Sons Ltd November 16, 2018, pp 3411–3436. https://doi.org/10.1002/asia.201800920.

(34) Pincus, P. Colloid Stabilization with Grafted Polyelectrolytes. *Macromolecules* **1991**, *24* (10), 2912–2919. https://doi.org/10.1021/ma00010a043.

(35) Israëls, R.; Leermakers, F. A. M.; Fleer, G. J.; Zhulina, E. B. Charged Polymeric Brushes: Structure and Scaling Relations. *Macromolecules* **1994**, *27* (12), 3249–3261. https://doi.org/10.1021/ma00090a018.

(36) Dobrynin, A. V.; Rubinstein, M. Theory of Polyelectrolytes in Solutions and at Surfaces. *Progress in Polymer Science (Oxford)*. 2005, pp 1049–1118. https://doi.org/10.1016/j.progpolymsci.2005.07.006.

(37) Stuart, M. A. C.; Huck, W. T. S.; Genzer, J.; Müller, M.; Ober, C.; Stamm, M.; Sukhorukov, G. B.; Szleifer, I.; Tsukruk, V. V; Urban, M.; Winnik, F.; Zauscher, S.; Luzinov, I.; Minko, S. Emerging Applications of Stimuli-Responsive Polymer Materials. *Nature Materials*. 2010, pp 101–113. https://doi.org/10.1038/nmat2614.

(38) Willott, J. D.; Murdoch, T. J.; Webber, G. B.; Wanless, E. J. Physicochemical Behaviour of Cationic Polyelectrolyte Brushes. *Progress in Polymer Science*. Elsevier Ltd January 1,

2017, pp 52–75. https://doi.org/10.1016/j.progpolymsci.2016.09.010.

(39) Toomey, R.; Tirrell, M. Functional Polymer Brushes in Aqueous Media from Self-Assembled and Surface-Initiated Polymers. *Annual Review of Physical Chemistry*. Annu Rev Phys Chem 2008, pp 493–517. https://doi.org/10.1146/annurev.physchem.59.032607.093623.

(40) Kunz, W. Specific Ion Effects, Evidences. In *Encyclopedia of Applied Electrochemistry*; Springer, New York, NY, 2014; pp 2045–2050. https://doi.org/10.1007/978-1-4419-6996-5_26.

(41) Kunz, W. Specific Ion Effects in Colloidal and Biological Systems. *Current Opinion in Colloid and Interface Science*. Elsevier April 1, 2010, pp 34–39. https://doi.org/10.1016/j.cocis.2009.11.008.

(42) Moghaddam, S. Z.; Thormann, E. The Hofmeister Series: Specific Ion Effects in Aqueous Polymer Solutions. *Journal of Colloid and Interface Science*. Academic Press November 1, 2019, pp 615–635. https://doi.org/10.1016/j.jcis.2019.07.067.

(43) Thormann, E. On Understanding of the Hofmeister Effect: How Addition of Salt Alters the Stability of Temperature Responsive Polymers in Aqueous Solutions. *RSC Adv.* **2012**, *2* (22), 8297–8305. https://doi.org/10.1039/c2ra20164j.

(44) Cacace, M. G.; Landau, E. M.; Ramsden, J. J. The Hofmeister Series: Salt and Solvent Effects on Interfacial Phenomena. *Quarterly Reviews of Biophysics*. Cambridge University Press 1997, pp 241–277. https://doi.org/10.1017/S0033583597003363.

(45) Zhang, Y.; Furyk, S.; Bergbreiter, D. E.; Cremer, P. S. Specific Ion Effects on the Water Solubility of Macromolecules: PNIPAM and the Hofmeister Series. *J. Am. Chem. Soc.* **2005**, *127* (41), 14505–14510. https://doi.org/10.1021/ja0546424.

(46) Kunz, W.; Belloni, L.; Bernard, O.; Ninham, B. W. Osmotic Coefficients and Surface Tensions of Aqueous Electrolyte Solutions: Role of Dispersion Forces. *J. Phys. Chem. B* **2004**, *108* (7), 2398–2404. https://doi.org/10.1021/jp036113x.

(47) Salis, A.; Ninham, B. W. Models and Mechanisms of Hofmeister Effects in Electrolyte Solutions, and Colloid and Protein Systems Revisited. *Chemical Society Reviews*. Royal Society of Chemistry October 6, 2014, pp 7358–7377. https://doi.org/10.1039/c4cs00144c.

(48) Marcus, Y. Ion Properties, Marcus Dekker. *Inc, New York* **1997**, 1–33.

Supporting Information

Ion-specific antipolyelectrolyte effect on the swelling behavior of polyzwitterionic layers

*Frederik Hegaard, Robert Biro, Koosha Ehtiati and Esben Thormann**

Department of Chemistry, Technical University of Denmark, 2800 Kgs. Lyngby, Denmark.

*Corresponding Author: esth@kemi.dtu.dk

S1: Ellipsometry technique

To measure the thickness of the polymer films, a spectroscopic ellipsometer from J. A. Woollam (M-2000) was used. This instrument has a 5 ml liquid cell in which the solvent can be exchanged without changing the placement of the sample and the alignment of the light. The ability to

exchange the solvent easily and the non-invasive nature of ellipsometry mean that this technique works well for repeated comparable measurements of the same film in different environments.

The refractive index of the solvent must be known for each measuring point, as it is changing with the ionic strength and the type of ions. To find the refractive index of a specific solution, a wafer with a SiO_2 layer of known thickness is measured with the solution as the medium. Here Si as the substrate, a 1 nm Si-SiO_2 transition layer, an approximately 100 nm SiO_2 layer, and the solution are described by a Cauchy model. This model is fitted to the data with the A and B values of the solution as the only fitting parameters. The values found with this method are shown in Table S1. This method is found to give values of the refractive indices that are in good agreement with values reported in literature.[1,2]

Table S1: A and B values obtained with the Cauchy model of salt solution for each of the five salts used at varying concentrations.

	KCl		KSCN		KBr		CsCl		LiCl	
c [mM]	A	B [µm^2]	A	B [µm^2]	A	B [µm^2]	A	B [µm^2]	A	B [µm^2]
0,01	1.320	0.00331	1.320	0.00331	1.320	0.00331	1.320	0.00331	1.320	0.00331
0.1	1.320	0.00333	1.320	0.00331	1.320	0.00333	1.320	0.00331	1.320	0.00331
1	1.320	0.00333	1.320	0.00331	1.320	0.00335	1.320	0.00331	1.320	0.00331
10	1.320	0.00333	1.320	0.00332	1.320	0.00337	1.320	0.00331	1.320	0.00331

30	1.320	0.00333	1.320	0.00333	1.320	0.00341	1.320	0.00332	1.320	0.00332
100	1.321	0.00335	1.321	0.00338	1.320	0.00353	1.321	0.00335	1.320	0.00338
200	1.322	0.00338	1.323	0.00345	1.320	0.00367	1.322	0.00337	1.321	0.00341
400	1.323	0.00343	1.326	0.00357	1.322	0.00376	1.324	0.00343	1.322	0.00345
800	1.327	0.00353	1.331	0.00379	1.327	0.00396	1.329	0.00354	1.325	0.00355
1200	1.330	0.00362	1.337	0.00400	1.331	0.00416	1.333	0.00365	1.328	0.00364
1600	1.333	0.00371	1.342	0.00420	1.335	0.00434	1.337	0.00376	1.331	0.00374
2200	1.337	0.00384	1.349	0.00449	1.340	0.00461	1.342	0.00391	1.335	0.00387
3000	1.342	0.00401	1.358	0.00478	1.348	0.00495	1.349	0.00409	1.340	0.00405

The measurements were performed at 25 °C with a wavelength range from 250 nm to 1000 nm for all salts except for KSCN which is measured from 400 nm to 1000 nm because SCN^- is absorbing light at the lower wavelengths.

The ellipsometry measurement is done by hydrating the sample in a 0.01 mM salt solution inside the liquid cell for about 1 hour. Hereafter the solution is exchange between a 3 M and a 0.01 mM salt solution twice, in order to compress and re-swell the film and allow the polymers to

reconfigure into a stable configuration. After this, the sample is kept at 0.01 mM salt until the drift in thickness is less than 0.5 nm in 2 minutes. Next, the salt concentration is increased by slowly flowing the next solution into the 5 ml liquid cell until a total of 30 ml liquid has been passed through the cell. The thickness is then usually stable within a couple of minutes and after the stabilization period, the thickness is determined as an average of 8 measurements over 2 minutes. This is repeated until the highest salt concentration is reached and the cell is then rinsed slowly with 1 L of ultra-pure water. To prepare the sample for measurements with a new salt, the sample is hydrated in a 100 mM solution of the new salt for 1 hour and then rinsed with 30 mL 0.01 mM solution of the new salt. This causes an exchange of the ions inside the polymer and the previous steps can then be repeated.

S2: Film characterizations

To ensure that the surface of the films was uniform in height, they were characterized by AFM. Figure S1 shows 10x10 μm^2 AFM images of the dry polycationic, polyanionic, and polyzwitterionic films (with 5 % crosslinks), which confirms that the produced surfaces are flat and only contain minor defects.

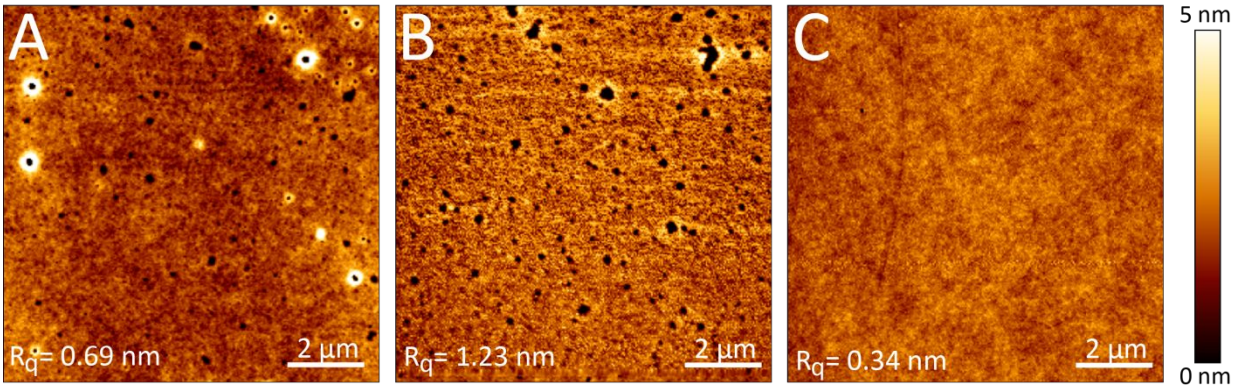

Figure S1: Representative AFM images of dry polycationic film (A), polyanionic film (B), and polyzwitterionic film (5) all with 5 % crosslinks. Root mean square roughness (R_q) is reported in the figures for each case.

To compare the swelling of the different films shown in this study, the thickness is converted to a swelling ratio which is defined by the thickness of the hydrated film divided by its dry thickness. The dry thicknesses obtained with ellipsometry are shown in Table S2.

Table S2: Dry thickness measured with ellipsometry of the polycationic films with varying degrees of crosslinks and for the polyanionic and polyzwitterionic films with 5 % crosslinks.

Film Type	Cat - 5 %	Cat - 10 %	Cat - 15 %	An - 5 %	Zwitter - 5 %
Dry Thickness	96 nm	82 nm	98 nm	130 nm	80 nm

S3: Specific ion effects on polycationic films with 10 % and 15 % crosslinks

The ion-specific swelling behavior of polycationic films with 10 % and 15 % crosslinks have also been measured as a function of the ionic strength. These are relevant control experiments in order to see if the observed ion-specific effects are depending on the crosslink density or if the trends reported in the main manuscript are more universal. However, the effect of the crosslink density on the swelling behavior is also of interest because it can improve the understanding of the ion-induced swelling of the polyzwitterionic film where intrachain and interchain crosslinking occur as well.

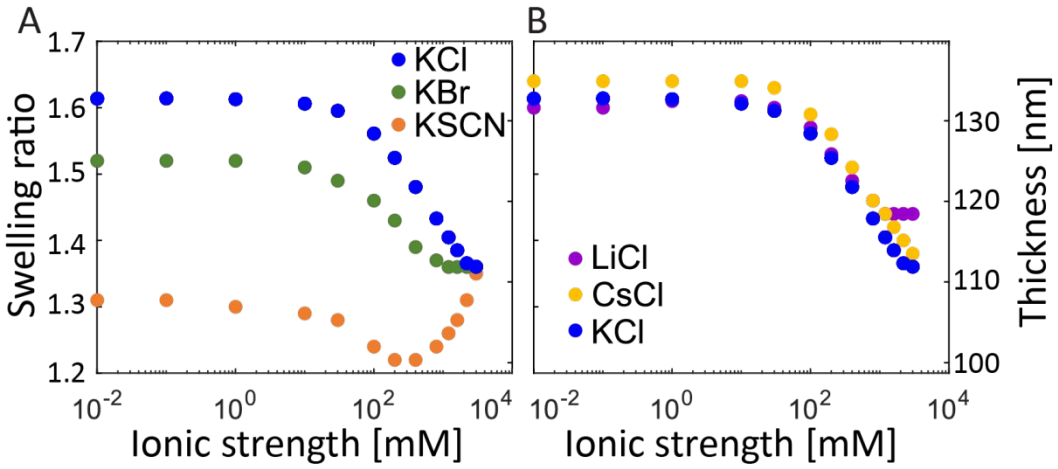

Figure S2: Ellipsometry-based thickness swelling data for a polycationic film with 10 % crosslinks as a function of salt concentration in the presence of either potassium salts with various anionic counterions (A) or chloride salts with various cationic coions (B).

Figure S2A shows the swelling behavior of a polycation film with 10 % crosslinks with K^+ as the coion but with varying counterions and Figure S2B shows the swelling behavior of the same film with Cl^- as the counterion and varying coions. Comparing this to the results from the polycationic film with 5 % crosslinks in Figure 3 in the main manuscript, it is seen that the degree of swelling decreases with increasing crosslink density at all ionic strengths. However, the trends for the different salts are almost identical.

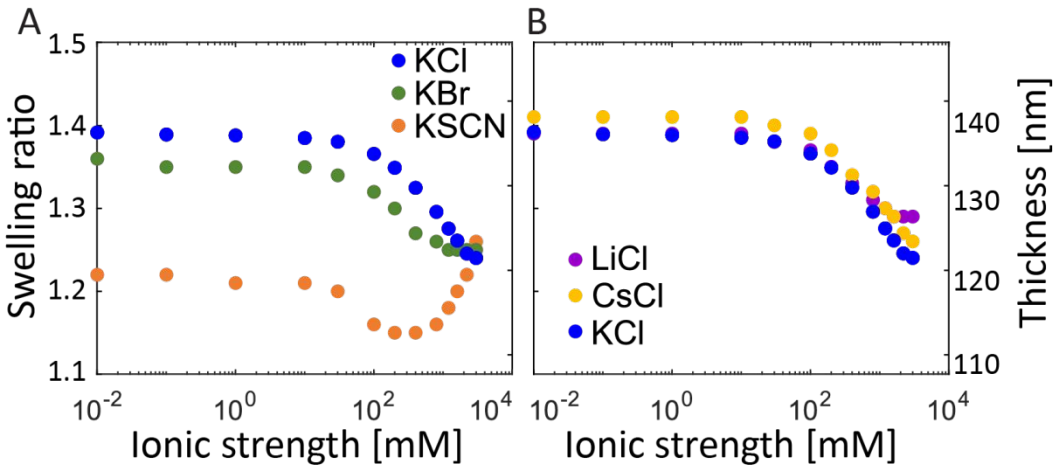

Figure S3: Ellipsometry-based thickness swelling data for a polycationic film with 15 % crosslinks as a function of salt concentration in the presence of either potassium salts with various anionic counterions (A) or chloride salts with various cationic coions (B).

Similar Figure S3A shows the swelling behavior of a polycation film with 15 % crosslinks with K^+ as the coion but with varying counterions and Figure S3B shows the swelling behavior of the same film with Cl^- as the counterion but with varying coions. Again, it is seen that increasing the

crosslink density is leading to less swelling and that the trends for the specific ion effects do not change significantly.

S4: Specific Ion Properties

For the films in our study, the ion osmotic effect is dominating at low ionic strength while nonelectrostatic hydration effects start to play a role at the highest salt concentrations. In the osmotic regime the concept of ion pairing between mobile counterions and immobile charges in the film is extremely important for the swelling behavior of the films. Here, an ion's ability to form ion pairs with the polyelectrolyte chains has previously been reported to depend on the ion polarizability.[2–4]

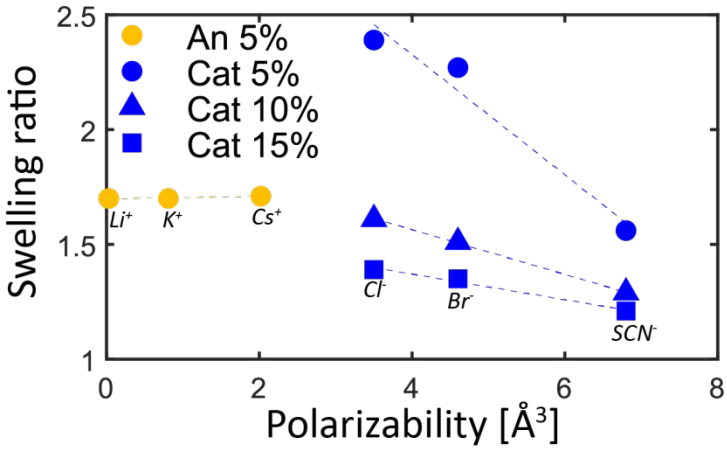

Figure S4: Swelling ratio at 10 mM salt concentration vs polarizability with either K+ or CL- as coion of polycationic/polyanionic films with either 5, 10, or 15 % crosslinks. Polarizability data are obtained from Marcus.[5]

In Figure S4, the swelling ratio for the three polycationic films with different degrees of crosslinks and the polyanionic film with 5 % crosslinks at an ionic strength of 10 mM (osmotic regime), are

plotted against the polarizabilities of the counterions. The coions are either Cl^- or K^+ for all the films. For the polycationic films, this shows that the swelling ratio scales with the polarizability of counterion but with a different dependency for the different crosslink densities. This observation is interpreted as if a higher polarizability of the counterion leads to a higher degree of ion pairing and thus a lower degree of ion osmotically driven swelling. This means that the polarizability of the ions can be used to predict the relative swelling in the osmotic regime. Since increased crosslinking restricts the ability of a film to swell, it is rational that the relative effect of influencing the ion osmotic pressure becomes smaller when the degree of crosslinking is increased. For the polyanionic film, it was oppositely found that the swelling in the osmotic regime is independent of the type of the cationic counterions despite a significant variations in the polarizabilities of the different counterions. Relative to the anions, the cations used as counterions for the polyanionic film have significantly lower polarizabilities. As this is linked to its ion paring ability, we suggest that the lower polarizabilities does not results in any significant ion pair formation why the osmotically driven swelling will be large and independent of the type of counterion.

At higher salt concentrations the relative thicknesses across counterions cannot be explained solely from the polarizabilities. The competing effects become more complicated to describe, but they

can possibly be partially captured by the partition coefficient for the polymer systems as shown in different studies.[6,7]

Bibliography

(1) Ehtiati, K.; Z. Moghaddam, S.; Daugaard, A. E.; Thormann, E. Crucial Nonelectrostatic Effects on Polyelectrolyte Brush Behavior. *Macromolecules* **2021**, *54* (7), 3388–3394. https://doi.org/10.1021/acs.macromol.0c02526.

(2) Ehtiati, K.; Moghaddam, S. Z.; Klok, H.-A.; Daugaard, A. E.; Thormann, E. Specific Counterion Effects on the Swelling Behavior of Strong Polyelectrolyte Brushes. *Macromolecules* **2022**, *55*, 5130. https://doi.org/10.1021/acs.macromol.2c00411.

(3) Kunz, W.; Belloni, L.; Bernard, O.; Ninham, B. W. Osmotic Coefficients and Surface Tensions of Aqueous Electrolyte Solutions: Role of Dispersion Forces. *J. Phys. Chem. B* **2004**, *108* (7), 2398–2404. https://doi.org/10.1021/jp036113x.

(4) Salis, A.; Ninham, B. W. Models and Mechanisms of Hofmeister Effects in Electrolyte Solutions, and Colloid and Protein Systems Revisited. *Chemical Society Reviews*. Royal Society of Chemistry October 6, 2014, pp 7358–7377. https://doi.org/10.1039/c4cs00144c.

(5) Marcus, Y. Ion Properties, Marcus Dekker. *Inc, New York* **1997**, 1–33.

(6) Pegram, L. M.; Record, M. T. Hofmeister Salt Effects on Surface Tension Arise from

Partitioning of Anions and Cations between Bulk Water and the Air-Water Interface. *J. Phys. Chem. B* 2007, *111* (19), 5411–5417. https://doi.org/10.1021/jp070245z.

(7) Moghaddam, S. Z.; Thormann, E. The Hofmeister Series: Specific Ion Effects in Aqueous Polymer Solutions. *Journal of Colloid and Interface Science*. Academic Press November 1, 2019, pp 615–635. https://doi.org/10.1016/j.jcis.2019.07.067.

Appendix B

Influence of ionic strength and specific ion effects on the pH responsiveness of weak polyelectrolyte multilayer films.

Frederik Hegaard and Esben Thormann

(To be submitted)

Influence of ionic strength and specific ion effects on the pH responsiveness of weak polyelectrolyte multilayer films

*Frederik Hegaard and Esben Thormann**

Department of Chemistry, Technical University of Denmark, 2800 Kgs. Lyngby, Denmark.

ABSTRACT

Layer-by-layer assembled multilayer films have shown great potential for applications due to their responsive behavior. In this study, we are systematically investigating how pH responses of covalently crosslinked chitosan and alginate dialdehyde multilayer films are affected by their composition, the salt concentration, and ion specificity. With ellipsometry, the changes in film swelling are measured from low (0.01mM) to high salt concentrations (3 M) of either NaCl or NaSCN at three different pH values. The trends in the swelling responses to increased ionic strength are, to different degree depending on multilayer composition, pH, and ion specificity, found to match the swelling responses seen for polyzwitterionic and weak monocomponent polyelectrolyte films. Finally, we have used the knowledge obtained from ellipsometry measurements to demonstrate how the pH responsiveness of such multilayer films measured by quartz crystal microbalance with dissipation monitoring (QCM-D) strongly depends on the ionic condition in which the responses are measured. This work thus shows that wrong conclusions about the pH responsiveness of polyelectrolyte multilayer films easily can be obtained if the ionic environment of the application area does not closely resemble the ionic condition under which the pH responsiveness is tested.

1. **Introduction**

Layer-by-layer (LbL) assembly of polyelectrolyte multilayer films is a versatile and widespread method for creating coatings with tunable and responsive properties.[1–3] Most often, the LbL process is driven by electrostatic interaction, and multilayer films are constructed by alternate adsorption of two oppositely charged polyelectrolytes to a substrate. [4–7] In this study, we focus on films consisting of two oppositely charged weak polyelectrolytes, alginate dialdehyde (ADA) and chitosan (CHI), with covalent crosslinks formed between the layers. Multilayer films of chitosan and alginate have attracted much interest due to their physiochemical properties, the abundance of the two biopolymers, and their biocompatibility, which have made such films attractive for diverse applications, ranging from antifouling of proteins[8–10] and stimuli-responsive emulsification[11,12] to lubrication[13–15] and targeted drug delivery[16–22]. By using the ADA instead of untreated alginate, we can without further effort obtain pH-responsive and crosslinked CHI-ADA multilayer films that allow for systematic studies of pH and ion-induced multilayer swelling without having irreversible disintegration of the films.[23–26]

The composition of a multilayer film and thus its responsiveness to specific parameters can be tuned by the conditions under which the films are prepared.[27,28] As the assembly method is driven by stepwise partly electrostatic neutralization it is typically assumed that the films are approximately charge-neutral at the conditions (pH and salt) of the assembly process.[29] Subsequent changes in pH or ionic environment will however shift the dissociation degree of the polyelectrolytes and introduce excess charges which will require counterions to enter the film to restore the overall charge balance.[30–32] These counterions will lead to increased osmotic pressure

and swelling of the film.[33–35] However, the composition of a multilayer film makes the response to external stimuli significantly more complicated to describe than for e.g. monocomponent polyelectrolyte film. Despite the huge amount of fundamental research on multilayer films and the widespread interest in their application the complex interplay between different mechanisms responsible for their responsiveness is still not fully understood.[36–38]

It is well-recognized that the swelling of multilayer films can be affected by changes in pH after completion of the LBL process. [39–42] It was e.g. shown by Itano et al. how multilayer films containing poly(allylamine hydrochloride) showed dramatic pH responsiveness when prepared at high pH while showing almost no pH responsiveness when prepared at lower pH. This is important because a high degree of pH responsiveness of LbL-assembled films is advantageous in some applications. This has been exploited by creating microcapsules containing different drug molecules , which was stable at high pH and then released the drug once the pH was decreased sufficiently.[43–47] Studies of the ADA-CHI films have shown the effect of salt concentration on the swelling to be complex and dependent on both the top layer, the preparation conditions, and the ion types.[23,28,48–51] Joana et al. have studied the very similar chitosan-alginate multilayers and the pH effect on their swelling. It was found that a film created at pH 5.5 was collapsing when at pH 3-4 and swelling again at pH 2.[52] This was partly explained as being due to a complex dissociation of the polyelectrolytes affected by both the solution pH and the simultaneous presence of opposite charges. The salt concentration during the layers buildup is likewise found to be significant, e.g. by Guzmán et al. which has shown how an increased salt concentration can increase the adsorbed mass and can shift the buildup from being linear to exponential with the number of layers. [53]

Our group has previously shown how the salt response of CHI-ADA films can be insignificant at low salt concentrations (<100 mM) for pH 3 and 6 while causing significant swelling in the same salt range at pH 9 due to a shifted charge balance.[50] Likewise we studied the pH responsiveness of the formed multilayer ADA-CHI film and found it to be strongly influenceable by the ionic strength and the composition of the top layer. [50]

However, despite the many good and well conducted studies, we see still three challenges with respect to the pH responsiveness of multilayer films composed of weak polyelectrolytes: (1) There exists a complex interplay between different mechanisms driving the pH responsiveness of multilayer films; (2) a full understanding of how the pH responsiveness is affected by ionic strength is lacking, and (3) specific ion effect can interfere with the fundamental swelling mechanisms of multilayer films. Thus, in this study, we want to improve the current understanding of the swelling behavior of multilayer films in response to pH, ionic strength, and ion specificity. To do this we have prepared CHI-ADA multilayer films with two different CHI/ADA ratios by changing the pH at which they are assembled. Subsequently, we have then used ellipsometry to systematically measure their swelling responses to changes in the above-mentioned parameters. Finally, QCM-D has been used to study the pH responsiveness of the CHI-ADA multilayer films in presence of NaCl and NaSCN at three specific concentrations which, based on ellipsometry measurements, were predicted to provide different responses.

2. Experimental method

2.1 Materials

Sodium alginate (NaALG, viscosity ≥20 Pa for 2% solution in water at 25 °C), hydrochloric acid (HCl, 37%), sodium hydroxide (NaOH, ≥97%), sodium chloride (NaCl, ≥99%), sodium thiocyanate (NaSCN, ≥98%), sodium periodate ($NaIO_4$, ≥99.5%), ethylene glycol (99.8%), 3-glycidoxypropyltrimethoxysilane (GPS, ≥98%) all from Sigma-Aldrich. Chitosan (CHI, deacetylation degree of 80%, viscosity 100 mPa for 1% solution in acetic acid at 20 °C) from HMC. Ethanol (≥96%), and acetone (≥99.8%) from VWR. Aquarius solutions were made with ultrapure water (Milli-Q plus 185 system with a 0.2 µm Millipak filter) with a resistivity of 18.2 MΩ cm.

2.2 ADA preparation

Alginate dialdehyde (ADA) is prepared from sodium alginate (NaALG) following a previously described procedure.[54–56] Briefly, 10 g NaALG and 20 molar % $NaIO_4$ (relative to the repeating groups of alginate) are dissolved in 1 l ultrapure water and stirred in darkness for 24 hr. Then 3.5 ml ethylene glycol was added and stirred for 30 min. to quench the reaction. The ADA was then precipitated by adding 3 g of sodium chloride and 1 l of ethanol after which it was filtered. The precipitation process was then repeated first by dissolving the ADA in 500 ml ultrapure water and adding 1 m sodium chloride followed by 500 ml ethanol and filtration and then repeating a final time with 500 ml ultrapure water, 0.5 g sodium chloride, and 1 l acetone. Finally, ADA was washed in 500 ml ethanol and then freeze-dried.

2.3 QCM-D based multilayer film build-up and pH response

For the multilayer film build-up, solutions of CHI (100 mg/l) and ADA (200 mg/l) containing 15 mM NaCl in ultrapure water with the pH adjusted to either 3 or 6 were used. Here, the preparation of the solutions at pH 3 was straightforward while at pH 6, the CHI cannot be directly dissolved. In this case, CHI was first dissolved in pure water at low pH, whereafter the pH and ionic strength were adjusted using NaOH and NaCl.

The multilayer film is built in two different ways that follow the same procedure. For QCM-D (quartz crystal microbalance with dissipation monitoring) measurements the film is built in the QCM-D's flow cell on a QCM-D silicone sensor. The sensor is prepared by first rinsing it in acetone, ethanol, and ultrapure water and then plasma cleaning for 5 minutes (in a Harrick Plasma PDC-32G plasma cleaner at medium power). After this, the substrate is submerged in a solution of 18 vol. % GPS in acetone for 24 hours and hereafter rinsed with acetone and submerged, in a 1000 mg/l CHI solution with 15 mM NaCl and the pH desired for the multilayer film built up. After 1 hour and a rinse in ultrapure water with 15 mM NaCl and pH adjusted to match that of the CHI and ADA solutions, the substrate is inserted into the flow cell and the process of building the layers is started.

The QCM-d measurements were performed with a Q-Sense E1 from Biolin using their WSX 335 silica sputtered sensors. The rinse step of the multilayer film build was started together with the QCM-d and once a stable frequency and dissipation were obtained the built-up was started. As the first layer is grafted to the sensor before the sensor is entered into the flow cell, this layer is not measured.

To build the layers a hydrostatic pump is placed after the flow cell and kept at a constant flowrate of 250 µl/min. The build process is then started with 30 minutes of rinsing, then 40 minutes of ADA followed by 30 minutes of rinsing, and then 40 minutes of CHI. This process is repeated until the desired number of layers is reached. The solution at the inlet tube is changed automatically using an automated selector valve (Vici Valco - C25-3184EUHA). This automated selector valve is programmable and can be timed to switch between the different solutions at the inlet without moving the tubes or turning the pump off, which results in a less perturbed system and better timing compared to manually switching between the solutions.

The film's response to changes in pH and salt concentration was measured in QCM-D by changing the solution flown over the sensor. These solutions are not buffer solutions, instead, they are only containing the specific salt and either HCl or NaOH to adjust the pH, to control the ion types and keep them identical across pH. The solutions at low and intermediate pH are stable during the timescale that the built-up and measurements last, but at high pH, the solution's pH value is found to change fast enough that it is necessary to adjust the pH before each measurement to keep the correct pH value.

2.4 Multilayer film build-up on Silicon wafers

For ellipsometry measurements, multilayer films are built on silicon wafers in a custom-made flow cell that is constructed to mimic the QCM-D flow cell with respect to cell dimensions and flow conditions. The purpose of the custom flow cell is to replicate the films made on the QCM-D while having a substrate that is more suitable for use in our ellipsometry liquid cell.

2.5 Ellipsometry measurements

The ellipsometry measurements are performed with a J. A. Woollam, M-2000 ellipsometry with a liquid cell. This technique gives the thickness of the film in a non-invasive way and allows for hydration and exchange of medium without moving the sample and thereby the measured area. The ellipsometry model of the film is created with Si as the substrate, a 1 nm Si-SiO_2 transition layer, a SiO_2 layer, a uniform polymer film, and ambient conditions matching the refractive index of the solvent. The polymer film is fitted to a Cauchy model ($n = A + B/\lambda^2$), where n and λ are the refractive index and the wavelength, respectively, and A and B are fitting parameters, using the instrument's software (CompleteEase). There are 3 fitting parameters for the film which are A and B for the film's Cauchy model and then the 8thickness of the film. The refractive indices of the solutions are measured with the ellipsometer beforehand and the method for this is described in Supporting Information, section S1.

3. Results

3.1 Multilayer film build-up

In order to prepare CHI-ADA multilayer films with two different CHI/ADA rations, the layer-by-layer assembly process was conducted at pH 3 and 6, respectively and in the presence of 15 mM NaCl.

Figure 1A displays the frequency and dissipation changes for the layer assembled at pH 3. Here, an almost linear decrease in frequency is observed as a function of the layer deposition number indicating a continuous growth of the multilayer film. The dissipation does in contrast not change much during the multilayer film build-up. However, a clear oscillatory behavior with an increase in dissipation each time CHI is introduced and a decrease each time ADA is introduced is observed.

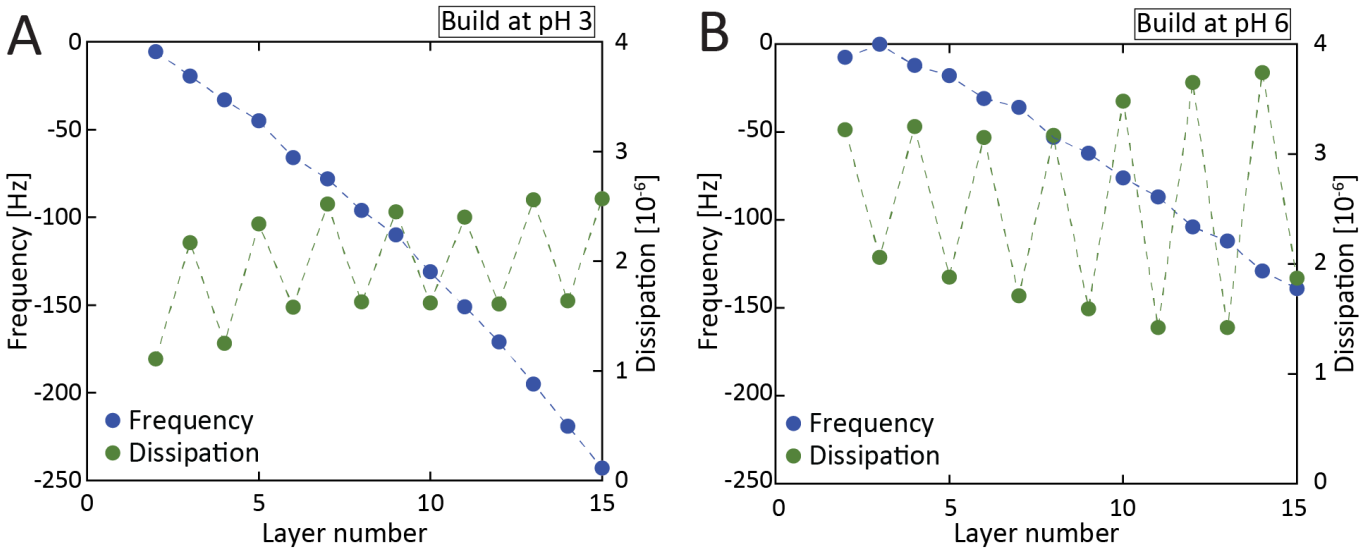

Figure 1: Frequency and dissipation shift of layer building in QCM-D for multilayer films of CHI and ADA built at pH 3 (A) and pH 6 (B) with 15 mM NaCl. CHI is odd-numbered layers and ADA is even-numbered layers. The first layer measured is layer 2, as layer 1 is the CHI layer created with dip coating outside the liquid cell.

Similarly, Figure 1B displays the frequency and dissipation changes for the layer assembled at pH 6. Here, an apparent continuous growth of the multilayer film is also observed as an approximately linear decrease in frequency with layer deposition number. However, compared to the case of the multilayer film prepared at pH 3, the overall decrease in frequency is here much lower, which indicates that the LbL process is less effective at pH 6. As for the build-up at pH 3 the dissipation data does also oscillate between deposition numbers at pH 6. However, in this case, the dissipation value oppositely increases when ADA is introduced and decreases when CHI is introduced.

Overall, the two multilayer films prepared at pH 3 and 6 are expected to possess some different characteristics and properties. At pH 3 and 6, CHI and ADA will have different charge densities so a different amount of the two polymers are required for balancing the charges of each other during the deposition of each layer.[57,58] Therefore, it is expected that the multilayer film prepared at pH 3 (where more ADA is needed to compensate for the charges on CHI) will have a relatively lower CHI/ADA ratio while the multilayer film prepared at pH 6 (where less ADA is needed to compensate the charges on CHI) will have a higher CHI/ADA ratio. Additionally, because the LbL process is driven by charge compensation we expect the multilayer film to be electrostatically neutral (or weakly positively charged, since CHI is the concluding layer) at the pH value where it is prepared. Specifically, we thus expect the multilayer film prepared at pH 3 to be close to neutral at pH 3 and the multilayer film prepared at pH 6 to be close to neutral at pH 6.

3.2 Ionic strength and pH dependent swelling with NaCl

After designing multilayer films with two different compositions, their swelling behavior in response to pH, ionic strength and specific ion effects can now be studied by ellipsometry. Here, we have first studied how the swelling is changing with increasing NaCl concentration at three different pH values.

3.2.1 Multilayer film formed at pH 3 – relatively lower CHI/ADA ratio

Figure 2A shows the swelling behavior at pH 3, 6, and 9 for the multilayer film prepared at pH 3 as functions of the NaCl concentration. Here, it is seen that the swelling behavior is both pH and ionic strength-dependent. At pH 3 the multilayer film is found in a relatively collapsed conformation from low ionic strength all the way up to approximately 1 M whereafter the swelling starts to increase by increasing ionic strength. At pH 6, a very similar behavior is observed although the multilayer film appears to be slightly less swollen and an indication of a "bump" in the swelling is seen at around 30-50 mM NaCl. The most extreme response to the change in ionic strength is however seen at pH 9. Firstly, the film is more swollen at low ionic strength compared to at pH 3 and 6. Next, the swelling at low ionic strength is seen to be independent of the ionic strength up to around 30 mM where the film is starting to swell extensively by increasing ionic strength. This continues up to approximately 50 mM NaCl where the film again starts to collapse.

The interpretation of these observations is far from straightforward due to the complexity of the system. A multilayer film consisting of CHI and ADA contains amine and carboxylic acid groups, which can be either charged or uncharged depending on pH and ionic strength. Herein positive (amine) and negative (carboxylic acid) groups will form ionic bonds, which will keep the CHI and

ADA chains together and reduce the swelling. Depending on the pH, the multilayer film can further carry a net negative charge, a net positive charge, or be overall charge neutral. In case of a net negative or positive charge of the multilayer film, this charge needs to be balanced by oppositely charged counterions, which will induce an osmotic swelling of the film. However, due to the weak nature of the charged groups, the net charge will also be self-regulated by protonation and deprotonation of the acid and basic groups – processes that are strongly dependent on ionic strength. With these concepts in mind, we will here provide some interpretations of the observations in Figure 2A.

When the pH is increased to 9, for the multilayer film formed at pH 3, the film will carry both positively and negatively charged groups but possess a net negative charge due to a full deprotonation of the carboxylic acid on ADA and partly deprotonation of the amine groups on CHI. Thus, the positive charges will be neutralized by parts of the negative charges and form ionic bonds between CHI and ADA, while the remaining negative charges will be either self-regulated or balanced by sodium counterions. To some extent, we can thus expect the multilayer film at pH 9 to behave similarly to a weak monocomponent polyelectrolyte film containing only one charged moiety (in this case a basic group). Such films have a rather well-understood and documented swelling behavior with the presence of different swelling regimes dependent on the ionic strength.[59–62] At low ionic strength a “neutral regime” with a relative collapsed film and an ionic strength independent swelling is expected. At intermediate ionic strength, an “osmotic regime” where the degree of swelling increases with increasing ionic strength is expected. Finally, at higher ionic strength a “salted regime” where the film collapses with increasing ionic strength is expected. These expectations for the swelling behavior of a weak monocomponent

polyelectrolyte film are in good qualitative agreement with the swelling behavior observed for the CHI-ADA multilayer film at pH 9 in Figure 2A. However, compared to the simpler weak monocomponent polyelectrolyte film some differences compared to the multilayer film should be highlighted. Firstly, in the "neutral regime" at low ionic strength, we do only expect the excess negative charges to be self-regulated while the charges involved in the ionic crosslinking between CHI and ADA are expected to remain. Secondly, in the "salted regime" starting at around 50 mM NaCl, we note that the decrease in swelling with increasing ionic strength is weaker than expected for a weak monocomponent polyelectrolyte film[63,64]. We, therefore, here suggest that the salt-induced collapse of the multilayer film is partly counteracted by another mechanism, which is leading to increased swelling of the multilayer film. This mechanism could be breaking of the ionic crosslinked due to increased electrostatic screening.

If the pH is instead kept at 3 for this film formed at pH 3, the film is expected to contain both negative and positive charges but to be overall charge neutral (or weakly positively charged due to the conclusive layer being CHI). Thus, again we expect the positive and negative charges to neutralize each other by forming ionic crosslinks between CHI and ADA. However, in this case, there will be no (significant) excess of either positive or negative charges and no mobile counterions need to be associated with the multilayer film. Therefore, at this pH value, the swelling behavior should not be compared to the swelling behavior of a weak monocomponent polyelectrolyte film but rather to the swelling behavior of a polyzwitterionic film. At low ionic strength, polyzwitterionic films are typically found in a rather collapsed confirmation due to strong dipole-dipole intra- and interchain crosslinks between the polyzwitterionic groups.[65–67] In the present case of the CHI-ADA multilayer film, we can likewise imagine that the ionic bonds

have a similar effect. This is the same situation as at pH 9 at low ionic strength (where the excess charge has self-regulated) but we expect a larger number of ionic crosslinks and thus a more collapsed multilayer film at pH 3 due to better charge matching at the pH conditions where the multilayer film is formed. This expectation agrees with the observations in Figure 2A. As the ionic strength is increased, polyzwitterionic films can undergo a swelling process known as the "anti-polyelectrolyte effect" due to electrostatic screening for the polyzwitterionic dipole-dipole bonds.[68,69] It is obvious to believe that the increased swelling observed at high ionic strength in our multilayer film is similarly due to the screening of the ionic crosslinks.

For the film at pH 6, the swelling behavior closely resembles the behavior at pH 3, except for the "bump" at 30-50 mM NaCl which appears as a light version of the "osmotic" and "salted" regimes observed at pH 9. We, therefore, suggest that the multilayer film at pH 6 has a behavior with elements of both a polyzwitterionic film and a weak monocomponent polyelectrolyte film. Finally, we also note that the multilayer film at pH 6 appears to be slightly less swollen than the multilayer film at pH 3 across all values of ionic strength. If the film is assumed to carry a low net negative charge at pH 6 it could be expected to be more swollen than at pH 3. This is however not the case, and an explanation could be that the outer layer of the multilayer film, which has the most unrestricted swelling, is CHI, which will be less swollen at pH 6 compared to at pH 3.[50,70]

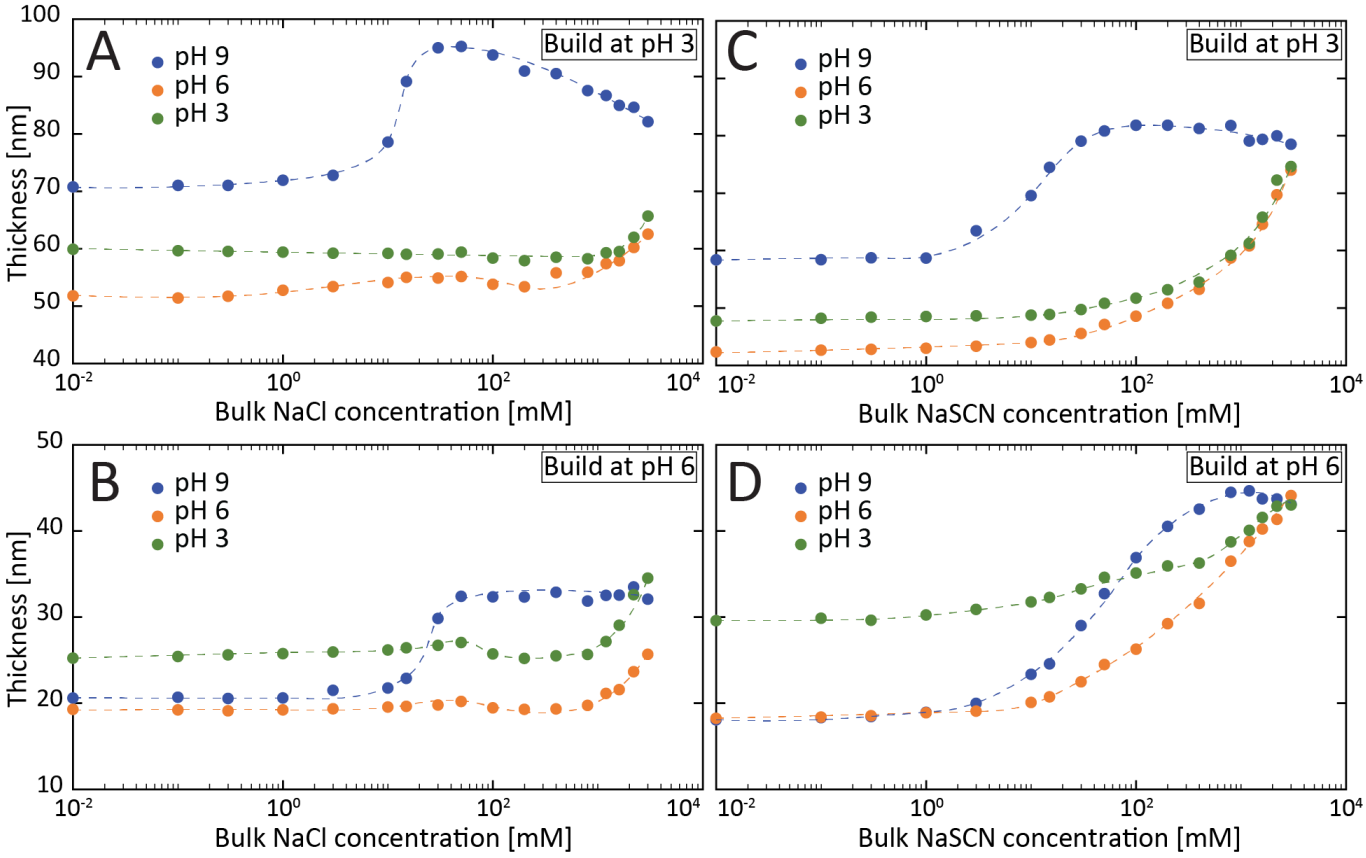

Figure 2: Swelling of multilayer films of 15 layers alternating CHI and ADA at a range of salt concentrations at pH 3, 6, or 9. Either with NaCl as the salt for films created in pH 3 (A) or pH 6 (B) or with NaSCN as the salt for films created in pH 3 (C) or pH 6 (D)

3.2.1 Multilayer film formed at pH 6 – relatively higher CHI/ADA ratio

Figure 2B shows the swelling behavior at pH 3, 6, and 9 for the multilayer film prepared at pH 6 as functions of the NaCl concentration. Here, it is firstly seen that the multilayer film is generally thinner than the multilayer film prepared at pH 3. This observation is consistent with observations from the multilayer build-up studied with QCM-D as discussed in relation to Figure 1. Secondly, it is seen that the multilayer film prepared at pH 6, like the multilayer film prepared at pH 3, shows strong pH and ionic strength-dependent swelling – and while there are some similarities in the trends, there are also some differences.

At pH 6, the multilayer film is expected to be overall charge neutral (or weakly positively charged). Therefore, we expect the swelling behavior to mainly resembles the swelling behavior of a polyzwitterionic film with a relatively collapsed conformation at low ionic strength due to a high degree of ionic crosslinks between CHI and ADA and an increased swelling at high ionic strength where these crosslinks are electrostatically screened. This is also exactly what is seen in Figure 2B, although a weak "bump" in the swelling behavior around 30-50 mM also indicates a moderate monocomponent polyelectrolyte-like element for the film.

Changing the pH to 3 for this multilayer film prepared at pH 6 leads to a decrease in negative charges (protonation of carboxylic groups on ADA) and potential an increase in positive charges (protonation of amine groups on CHI) and thus a potential net positive charge which will depend on the ionic strength. While the change in charge balance manifests itself in a higher degree of swelling, likely due to fewer ionic crosslinks, the overall swelling behavior as a function of ionic strength closely resembles the swelling behavior of a polyzwitterionic film. However again with a small "bump" around 30-50 mM as a weak sign of osmotic behavior.

At pH 9, we again observe an effect of changing the ionic strength which qualitatively differs from the swelling behaviors observed at pH 3 and 6. As for the case of the multilayer film prepared at pH 3, a sharp increase in thickness is seen around 30 mM which in this case is followed by a plateau in thickness when further increasing the ionic strength. At pH 9, we expect a net negative charge, and we thus assign the sharp increase in thickness to osmotic swelling due to an increased number of counterions needed to balance the negative charges as the ionic strength is increased. The lack of a clear "salted" regime at higher ionic strength, we, like for the multilayer film prepared at pH 3, assign to screening of ionic crosslinks which counteracts the else expected

collapse in a “salted regime”. This effect should be stronger for the film prepared at pH 6 where the CHI/ADA ratio in the multilayer film is higher and a relatively higher number of ionic crosslinks thus are expected.

3.3 Ion-specific swelling behavior – NaCl versus NaSCN

So far, we have discussed the swelling behavior of CHI-ADA multilayer films when the ionic strength is controlled by NaCl. In the following, we will compare this, to a case where the ionic strength is controlled by NaSCN. This comparison is inspired by a recent study where we have shown how the swelling behavior of polyzwitterionic films is significantly influenced by the type of salt used to control the ionic strength. Specifically, we have shown that “soft” and polarizable ions like SCN^- can form ion pairs with quaternary ammonium groups in the polyzwitterionic units of a sulfobetaine-based polyzwitterionic film. Compared to NaCl which can only rupture the polyzwitterionic dipole-dipole interaction through electrostatic screening, NaSCN can thus rupture these bonds by preferential binding to the positively charged moieties which leads to a new charge imbalance and an osmotically driven swelling of the films.

Figure 2C shows the swelling behavior, of the CHI-ADA multilayer film prepared at pH 3, in response to an increasing concentration of NaSCN. When comparing the swelling behavior at pH 3 and 6 to the situation when the ionic strength was controlled by NaCl, it is seen that the swelling with NaSCN starts at a much lower ionic strength and is significantly more pronounced. This result is well aligned with our previous observations for polyzwitterionic films and therefore further confirms that the multilayer film can be treated as a polyzwitterionic film when the pH value is not much higher than the value at which the multilayer film is formed. At pH 9, the swelling

behavior in presence of NaSCN is more similar to the case with NaCl. This makes sense since the multilayer film at pH 9 has fewer positive charges and an excess of negatively charged groups which are not involved in any ion-specific interactions with SCN^-. Anyhow, it should be noted that the increase in swelling starts at a lower ionic strength and are more gradual compared to the case with NaCl. This indicates that the zwitterionic-like behavior has started to mix more with the weak monocomponent polyelectrolyte-like behavior also in the osmotic regime. Additionally, the decrease in thickness in the "salted regime" is less pronounced in the presence of NaSCN compared to the case with NaCl. This again suggests that SCN^- more effectively ruptures the ionic crosslinks compared to Cl^-.

Finally, Figure 2D shows the swelling behavior in presence of NaSCN for the multilayer film formed at pH 6. At pH 3 and 6 qualitatively similar behaviors are observed as for the multilayer film prepared at pH 3. However, at pH 9 the swelling behavior of the multilayer film seems to have shifted even further towards a zwitterionic-like behavior compared to the weak monocomponent polyelectrolyte-like behavior seen for the other. That is in line with the observation for the NaCl case where the apparent rupture of the ionic crosslinks also appears to become more pronounced for the multilayer film prepared at pH 6 where the CHI/ADA ratio is higher.

QCM-D based pH responsiveness

As the responsiveness and in particular, the pH responsiveness of polyelectrolyte multilayer films is important for many applications such as controlled drug delivery, it is of course of high importance to demonstrate such behavior in-situ. Besides, being a popular tool for showing the multilayer film build-up process, QCM-D is also an often used tool for demonstrating the pH responsiveness.[70–75] Here, we will therefore complement our ellipsometry studies of the effect of ionic strength, ion specificity, and layer composition on the swelling behavior of multilayer films with QCM-D studies. We will do that by reporting the changes in QCM frequency for the two multilayer films prepared at pH 3 and 6 (with relatively lower and higher CHI/ADA ratios, respectively), at three selected ionic strengths (1 mM, 50 mM, and 3 M) and with the ionic strength controlled by either NaCl or NaSCN, respectively (dissipation measurements is presented in Supporting Information section S2). When comparing QCM frequencies with ellipsometry thicknesses it is however important to be aware that the two method measures fundamentally different things. While the QCM frequency often is considered as a synonym to the wet mass of the film and the ellipsometry thickness as the absolute height of the hydrated film, the methods are based on different measuring principles (viscoelastic response versus optical response) and different models are used to interpret the measured responses. A full discussion of that is beyond the scope of this paper but we will here only note that ellipsometry measurements are mostly sensitive to the densest part of the film where the difference in refractive index between the hydrated film and the solvent is largest (i.e. in the inner part of the multilayer film) while the QCM frequency also is highly responsive the regions in the film with very high water content (i.e. in the outer layer of the multilayer film where swelling is less

restricted).[70,76] Finally, it should also be noted that the multilayer films studied with ellipsometry and QCM are similar but not identical as they are built on two different substrates, i.e. oxidized silicon wafers and silica-coated QCM sensors, respectively.

Figure 3A and 3B show the swelling behavior of the two multilayer films prepared at pH 3 and 6, respectively, when the ionic strength is controlled by NaCl. Across both multilayer films and for all three ionic strengths, we only observe weak responses when changing the pH between 3 and 6 which is mostly in agreement with the observation obtained with ellipsometry (Figures 2A and B). Oppositely, strong responses are observed when changing the pH between 6 and 9. Here the significantly strongest response is obtained in presence of 50 mM NaCl compared to at low ionic strength (1 mM) and high ionic strength (3 M). This observation is also in agreement with the ellipsometry data and can be explained by the strong osmotically driven swelling found at pH 9 at around 30-50 mM NaCl. Also, in agreement with the ellipsometry data the magnitude of the response when changing the pH from 6 to 9, is largest for the multilayer film with the lower CHI/ADA ratio (Figures 2A and 3A).

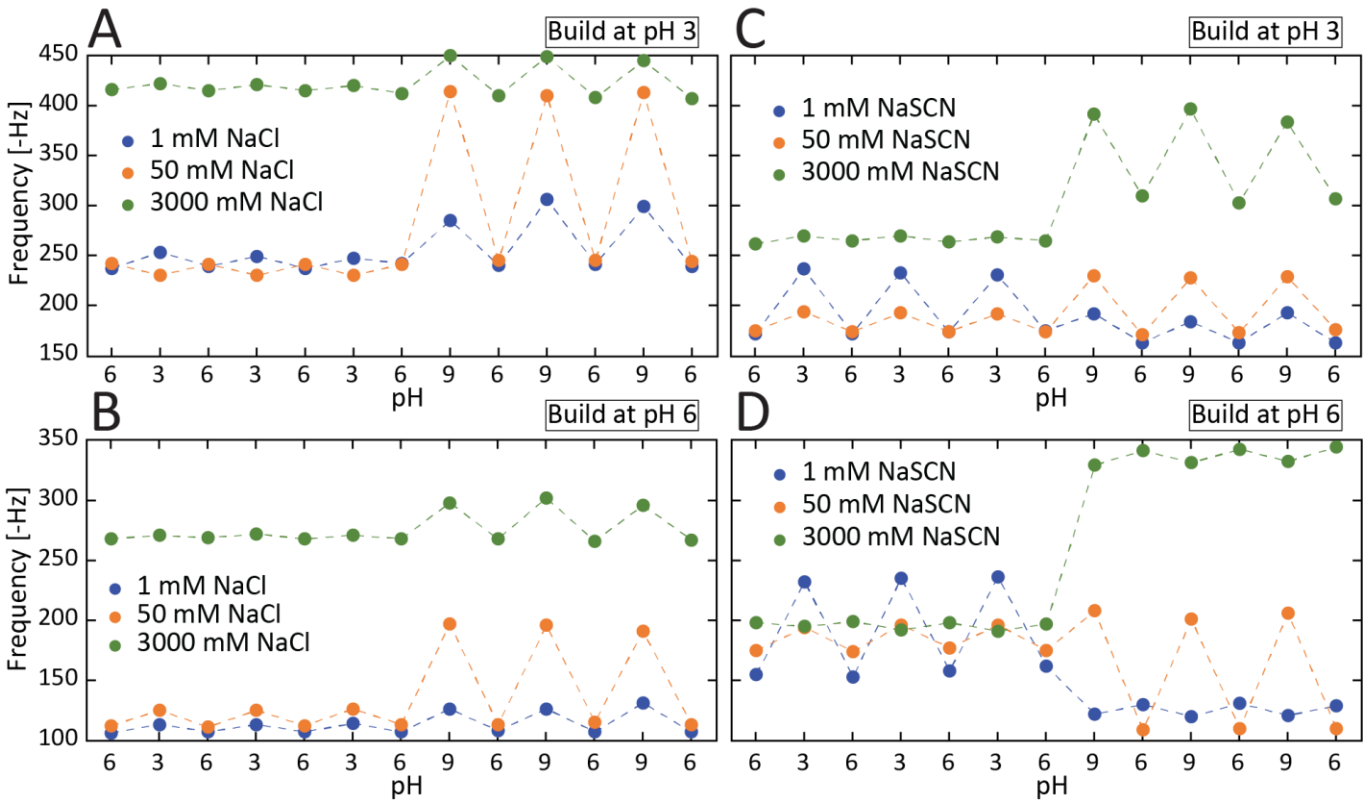

Figure 3: pH cycles showing the frequency shift of multilayer films of 15 layers alternating CHI and ADA at 1, 50, or 3000 mM salt at pH 3, 6, or 9. Either with NaCl as the salt for films created in pH 3 (A) or pH 6 (B) or with NaSCN as the salt for films created in pH 3 (C) or pH 6 (D)

Figure 3C and 3D show, in agreement with the ellipsometry data, that the pH responsiveness of the multilayer films becomes greatly different when the ionic strength is controlled by NaSCN. At 50 mM NaSCN, we again see a larger response when the pH is changed between 6 and 9 than between 3 and 6. At 1 mM NaSCN, we however see a larger response when changing the pH from 3 to 6 than when changing the pH from 6 to 9. At 3 M NaSCN the film prepared at pH 3, on the other hand, has the largest response when changing the pH from 6 to 9 while that is not the case for the film prepared at pH 6. These trends observed at 1 mM and 3 M NaSCN with QCM are not clear from the ellipsometry data. Finally, some degree of irreversible swelling appears after the

film has been exposed to pH 9 in presence of NaSCN. We believe that the rupture of more ionic crosslinks at pH 9 allows for more ion pairing between SCN^- and amine groups on CHI and that the balance is not immediately reversed when the pH is returned to 6. This observation also reminds us that a multilayer film is not an equilibrium configuration but a system that is a result of a dynamic build-up under certain environmental conditions.

Overall the results presented in Figure 3 have demonstrated that the pH response of multilayer films can be very dependent on ionic strength, specific ions, and multilayer composition. For the same film, very different conclusions about pH responsiveness can be reached depending on the conditions.

Conclusion

In this work, we have used ellipsometry to study the swelling behavior of multilayer films consisting of oppositely charged weak polyelectrolytes, i.e. CHI and ADA, at three different pH values as a function of ionic strength controlled by addition or either NaCl or NaSCN.

For these systems, we have observed that the ion strength-dependent swelling behavior shows characteristics of both the swelling behavior of weak monocomponent polyelectrolyte films (with distinct swelling regimes) and polyzwitterionic films with an “anti-polyelectrolyte”-like swelling behavior. However, whether the multilayer film behaves more like one or the other is strongly pH-dependent. Additionally, we have shown that the pH and ionic strength-dependent swelling behavior are also strongly ion-dependent. We have compared the effect of the “hard” chloride ion with the “soft” thiocyanate ion and found that the ion pairing effect, similar to what has been

previously reported for polyzwitterionic films, is of significant importance for the swelling behavior.

With the understanding obtained through analysis of our ellipsometry data, we have further demonstrated that pH responsiveness illustrated through typical QCM-D experiments can lead to distinctively different conclusions depending on the multilayer composition, ionic strength, and the types of ions that are used to control the ionic strength.

The conclusion from this work should thus both be considered as an inspiration for how to design responsive multilayer films with the desired functionality at certain environmental conditions, but the work should also stand as a warning for potential misinterpretation of the pH responsiveness of multilayer films if the testing condition does not exactly match the conditions for the application. Specifically, if one test the responsiveness at ionic conditions which do not resemble the environment of the application, wrong conclusions might be drawn.

ASSOCIATED CONTENT

Supporting Information. Description (File type)

AUTHOR INFORMATION

Corresponding Author

*esth@kemi.dtu.dk

Department of Chemistry, Technical University of Denmark, 2800 Kgs. Lyngby, Denmark

Author Contributions

The manuscript was written through contributions of all authors. All authors have approved the final version of the manuscript.

Notes

The authors declare no conflicts of interest.

ACKNOWLEDGMENT

Frederik Hegaard gratefully acknowledges a grant from the Technical University of Denmark.

References

1. Feng, W. *et al.* Effect of pH-responsive alginate/chitosan multilayers coating on delivery efficiency, cellular uptake and biodistribution of mesoporous silica nanoparticles based nanocarriers. *ACS Appl. Mater. Interfaces* **6**, 8447–8460 (2014).

2. Silva, J. M. *et al.* Tailored freestanding multilayered membranes based on chitosan and alginate. *Biomacromolecules* **15**, 3817–3826 (2014).

3. Carneiro-da-Cunha, M. G. *et al.* Physical and thermal properties of a chitosan/alginate nanolayered PET film. *Carbohydr. Polym.* **82**, 153–159 (2010).

4. Borges, J. & Mano, J. F. Molecular interactions driving the layer-by-layer assembly of multilayers. *Chemical Reviews* vol. 114 8883–8942 (2014).

5. Elizarova, I. S. & Luckham, P. F. Layer-by-layer adsorption: Factors affecting the choice of substrates and polymers. *Advances in Colloid and Interface Science* vol. 262 1–20 (2018).

6. Rydzek, G. *et al.* Electrochemical nanoarchitectonics and layer-by-layer assembly: From basics to future. *Nano Today* vol. 10 138–167 (2015).

7. Decher, G. Fuzzy nanoassemblies: Toward layered polymeric multicomposites. *Science (80-.).* **277**, 1232–1237 (1997).

8. Zhang, Z., Chao, T., Chen, S. & Jiang, S. Superlow fouling sulfobetaine and carboxybetaine polymers on glass slides. *Langmuir* **22**, 10072–10077 (2006).

9. Chang, Y. *et al.* A highly stable nonbiofouling surface with well-packed grafted zwitterionic polysulfobetaine for plasma protein repulsion. *Langmuir* **24**, 5453–5458 (2008).

10. Zhang, Z. *et al.* Nonfouling behavior of polycarboxybetaine-grafted surfaces: Structural and environmental effects. *Biomacromolecules* **9**, 2686–2692 (2008).

11. Saigal, T., Dong, H., Matyjaszewski, K. & Tilton, R. D. Pickering emulsions stabilized by nanoparticles with thermally responsive grafted polymer brushes. *Langmuir* **26**, 15200–15209 (2010).

12. Willott, J. D., Humphreys, B. A., Webber, G. B., Wanless, E. J. & De Vos, W. M. Combined Experimental and Theoretical Study of Weak Polyelectrolyte Brushes in Salt Mixtures. *Langmuir* **35**, 2709–2718 (2019).

13. Kobayashi, M. *et al.* Friction behavior of high-density poly(2-methacryloyloxyethyl phosphorylcholine) brush in aqueous media. *Soft Matter* **3**, 740–746 (2007).

14. Tadmor, R., Janik, J., Klein, J. & Fetters, L. J. Sliding friction with polymer brushes. *Phys. Rev. Lett.* **91**, (2003).

15. Tairy, O., Kampf, N., Driver, M. J., Armes, S. P. & Klein, J. Dense, highly hydrated polymer brushes via modified atom-transfer-radical-polymerization: Structure, surface

interactions, and frictional dissipation. *Macromolecules* **48**, 140–151 (2015).

16. Mu, B., Lu, C. & Liu, P. Disintegration-controllable stimuli-responsive polyelectrolyte multilayer microcapsules via covalent layer-by-layer assembly. *Colloids Surfaces B Biointerfaces* **82**, 385–390 (2011).

17. Wang, Z. *et al.* Self-assembled Biodegradable Nanoparticles and Polysaccharides as Biomimetic ECM Nanostructures for the Synergistic effect of RGD and BMP-2 on Bone Formation. *Sci. Rep.* **6**, 1–12 (2016).

18. Zhao, X., Chen, S., Lin, Z. & Du, C. Reactive electrospinning of composite nanofibers of carboxymethyl chitosan cross-linked by alginate dialdehyde with the aid of polyethylene oxide. *Carbohydr. Polym.* **148**, 98–106 (2016).

19. Chen, H. *et al.* Covalently antibacterial alginate-chitosan hydrogel dressing integrated gelatin microspheres containing tetracycline hydrochloride for wound healing. *Mater. Sci. Eng. C* **70**, 287–295 (2017).

20. Vieira, E. F. S., Cestari, A. R., Airoldi, C. & Loh, W. Polysaccharide-based hydrogels: Preparation, characterization, and drug interaction behaviour. *Biomacromolecules* **9**, 1195–1199 (2008).

21. Chen, F. *et al.* Preparation and characterization of oxidized alginate covalently cross-linked galactosylated chitosan scaffold for liver tissue engineering. *Mater. Sci. Eng. C* **32**, 310–320 (2012).

22. Liang, Y. *et al.* An in situ formed biodegradable hydrogel for reconstruction of the corneal endothelium. *Colloids Surfaces B Biointerfaces* **82**, 1–7 (2011).

23. Huang, J., Zajforoushan Moghaddam, S. & Thormann, E. Structural Investigation of a Self-Cross-Linked Chitosan/Alginate Dialdehyde Multilayered Film with in Situ QCM-D and Spectroscopic Ellipsometry. *ACS Omega* **4**, 2019–2029 (2019).

24. Aston, R., Wimalaratne, M., Brock, A., Lawrie, G. & Grøndahl, L. Interactions between chitosan and alginate dialdehyde biopolymers and their layer-by-layer assemblies. *Biomacromolecules* **16**, 1807–1817 (2015).

25. Jia, Y. *et al.* pH-responsive polysaccharide microcapsules through covalent bonding assembly. *Chem. Commun.* **47**, 1175–1177 (2011).

26. Tan, H., Chu, C. R., Payne, K. A. & Marra, K. G. Injectable in situ forming biodegradable chitosan-hyaluronic acid based hydrogels for cartilage tissue engineering. *Biomaterials* **30**, 2499–2506 (2009).

27. Richardson, J. J. *et al.* Innovation in Layer-by-Layer Assembly. *Chem. Rev.* **116**, 14828–14867 (2016).

28. Huang, J., Moghaddam, S. Z. & Thormann, E. Chitosan/Alginate Dialdehyde Multilayer Films with Modulated pH-Responsiveness and Swelling. *Macromol. Chem. Phys.* **221**, (2020).

29. Schlenoff, J. B., Ly, H. & Li, M. Charge and mass balance in polyelectrolyte multilayers. *J. Am. Chem. Soc.* **120**, 7626–7634 (1998).

30. Burke, S. E. & Barrett, C. J. pH-responsive properties of multilayered poly(L-lysine)/hyaluronic acid surfaces. *Biomacromolecules* **4**, 1773–1783 (2003).

31. Itano, K., Choi, J. & Rubner, M. F. Mechanism of the pH-induced discontinuous swelling/deswelling transitions of poly(allylamine hydrochloride)-Containing polyelectrolyte multilayer films. *Macromolecules* **38**, 3450–3460 (2005).

32. Delcea, M., Möhwald, H. & Skirtach, A. G. Stimuli-responsive LbL capsules and nanoshells for drug delivery. *Advanced Drug Delivery Reviews* vol. 63 730–747 (2011).

33. Kim, B. S. & Vinogradova, O. I. pH-controlled swelling of polyelectrolyte multilayer microcapsules. *J. Phys. Chem. B* **108**, 8161–8165 (2004).

34. Erel-Unal, I. & Sukhishvili, S. A. Hydrogen-bonded hybrid multilayers: Film architecture controls release of macromolecules. *Macromolecules* **41**, 8737–8744 (2008).

35. Glinel, K. *et al.* Responsive polyelectrolyte multilayers. *Colloids Surfaces A Physicochem. Eng. Asp.* **303**, 3–13 (2007).

36. Schneider, A. *et al.* Layer-by-layer films from hyaluronan and amine-modified hyaluronan. *Langmuir* **23**, 2655–2662 (2007).

37. Rinaudo, M. New way to crosslink chitosan in aqueous solution. *Eur. Polym. J.* **46**, 1537–1544 (2010).

38. Sahariah, P. & Másson, M. Antimicrobial Chitosan and Chitosan Derivatives: A Review of the Structure-Activity Relationship. *Biomacromolecules* vol. 18 3846–3868 (2017).

39. Glinel, K. *et al.* Responsive polyelectrolyte multilayers. *Colloids Surfaces A Physicochem. Eng. Asp.* **303**, 3–13 (2007).

40. Sui, Z. & Schlenoff, J. B. Phase separations in pH-responsive polyelectrolyte multilayers: Charge extrusion versus charge expulsion. *Langmuir* **20**, 6026–6031 (2004).

41. Hiller, J. & Rubner, M. F. Reversible molecular memory and pH-switchable swelling transitions in polyelectrolyte multilayers. *Macromolecules* **36**, 4078–4083 (2003).

42. Itano, K., Choi, J. & Rubner, M. F. Mechanism of the pH-induced discontinuous swelling/deswelling transitions of poly(allylamine hydrochloride)-Containing polyelectrolyte multilayer films. *Macromolecules* **38**, 3450–3460 (2005).

43. Chaturbedy, P., Jagadeesan, D. & Eswaramoorthy, M. PH-sensitive breathing of clay within the polyelectrolyte matrix. *ACS Nano* **4**, 5921–5929 (2010).

44. Gillies, E. R. & Fréchet, J. M. J. pH-responsive copolymer assemblies for controlled release of doxorubicin. *Bioconjug. Chem.* **16**, 361–368 (2005).

45. Choi, D. & Hong, J. Layer-by-layer assembly of multilayer films for controlled drug release.

Archives of Pharmacal Research vol. 37 79–87 (2014).

46. Wang, K. & He, Z. Alginate-konjac glucomannan-chitosan beads as controlled release matrix. *Int. J. Pharm.* **244**, 117–126 (2002).

47. Talelli, M. *et al.* Core-crosslinked polymeric micelles with controlled release of covalently entrapped doxorubicin. *Biomaterials* **31**, 7797–7804 (2010).

48. Volodkin, D. & Von Klitzing, R. Competing mechanisms in polyelectrolyte multilayer formation and swelling: Polycation-polyanion pairing vs. polyelectrolyte-ion pairing. *Current Opinion in Colloid and Interface Science* vol. 19 25–31 (2014).

49. Dubas, S. T. & Schlenoff, J. B. Swelling and smoothing of polyelectrolyte multilayers by salt. *Langmuir* **17**, 7725–7727 (2001).

50. Huang, J., Zajforoushan Moghaddam, S., Maroni, P. & Thormann, E. Swelling Behavior, Interaction, and Electrostatic Properties of Chitosan/Alginate Dialdehyde Multilayer Films with Different Outermost Layer. *Langmuir* **36**, 3782–3791 (2020).

51. Huang, J. Formation, Structure, and Properties of Stimuli-Responsive Polyelectrolyte Films. (Technical University of Denmark, 2020).

52. Silva, J. M. *et al.* PH Responsiveness of Multilayered Films and Membranes Made of Polysaccharides. *Langmuir* **31**, 11318–11328 (2015).

53. Guzmán, E., Ritacco, H., Rubio, J. E. F., Rubio, R. G. & Ortega, F. Salt-induced changes in the growth of polyelectrolyte layers of poly(diallyl-dimethylammonium chloride) and poly(4-styrene sulfonate of sodium). *Soft Matter* **5**, 2130–2142 (2009).

54. Tian, M. *et al.* Long-term and oxidative-responsive alginate-deferoxamine conjugates with a low toxicity for iron overload. *RSC Adv.* **6**, 32471–32479 (2016).

55. Pawar, S. N. & Edgar, K. J. Alginate derivatization: A review of chemistry, properties and applications. *Biomaterials* vol. 33 3279–3305 (2012).

56. Gomez, C. G., Rinaudo, M. & Villar, M. A. Oxidation of sodium alginate and characterization of the oxidized derivatives. *Carbohydr. Polym.* **67**, 296–304 (2007).

57. Martins, G. V., Mano, J. F. & Alves, N. M. Nanostructured self-assembled films containing chitosan fabricated at neutral pH. *Carbohydr. Polym.* **80**, 570–573 (2010).

58. Schlenoff, J. B., Ly, H. & Li, M. Charge and mass balance in polyelectrolyte multilayers. *J. Am. Chem. Soc.* **120**, 7626–7634 (1998).

59. Zhang, H. & Rühe, J. Swelling of poly(methacrylic acid) brushes: Influence of monovalent salts in the environment. *Macromolecules* **38**, 4855–4860 (2005).

60. Currie, E. P. K., Sieval, A. B., Fleer, G. J. & Stuart, M. A. C. Polyacrylic acid brushes: Surface pressure and salt-induced swelling. *Langmuir* **16**, 8324–8333 (2000).

61. Wu, T. *et al.* Behavior of surface-anchored poly(acrylic acid) brushes with grafting density

gradients on solid substrates: 1. Experiment. *Macromolecules* **40**, 8756–8764 (2007).

62. Ehtiati, K., Z. Moghaddam, S., Daugaard, A. E. & Thormann, E. Crucial Nonelectrostatic Effects on Polyelectrolyte Brush Behavior. *Macromolecules* **54**, 3388–3394 (2021).

63. Zhulina, E. B., Birshtein, T. M. & Borisov, O. V. Theory of Ionizable Polymer Brushes. *Macromolecules* **28**, 1491–1499 (1995).

64. Ehtiati, K., Moghaddam, S. Z., Daugaard, A. E. & Thormann, E. How Dissociation of Carboxylic Acid Groups in a Weak Polyelectrolyte Brush Depend on Their Distance from the Substrate. *Langmuir* **36**, 2339–2348 (2020).

65. Wang, F., Yang, J. & Zhao, J. Understanding anti-polyelectrolyte behavior of a well-defined polyzwitterion at the single-chain level. *Polym. Int.* **64**, 999–1005 (2015).

66. Mary, P., Bendejacq, D. D., Labeau, M. P. & Dupuis, P. Reconciling low- and high-salt solution behavior of sulfobetaine polyzwitterions. *J. Phys. Chem. B* **111**, 7767–7777 (2007).

67. Huglin, M. B. & Radwan, M. A. Selective Adsorption of Potassium Thiocyanate to a Zwitterionic Polymethacrylate. *Macromolecules* **25**, 999–1002 (1992).

68. Higaki, Y., Kobayashi, M. & Takahara, A. Hydration State Variation of Polyzwitterion Brushes through Interplay with Ions. *Langmuir* **36**, 9015–9024 (2020).

69. Berlinova, I. V., Dimitrov, I. V., Kalinova, R. G. & Vladimirov, N. G. Synthesis and aqueous solution behaviour of copolymers containing sulfobetaine moieties in side chains. *Polymer (Guildf).* **41**, 831–837 (2000).

70. Jiang, T., Moghaddam, S. Z. & Thormann, E. A pH-responsive polyelectrolyte multilayer film with tunable interfacial properties. *Polymer (Guildf).* **214**, 123367 (2021).

71. Jiang, T., Zajforoushan Moghaddam, S. & Thormann, E. PPEGMEMA-based cationic copolymers designed for layer-by-layer assembly. *RSC Adv.* **9**, 26915–26926 (2019).

72. Silva, J. M. *et al.* PH Responsiveness of Multilayered Films and Membranes Made of Polysaccharides. *Langmuir* **31**, 11318–11328 (2015).

73. Westwood, M., Gunning, A. P. & Parker, R. Temperature-dependent growth of gelatin-poly(galacturonic acid) multilayer films and their responsiveness to temperature, pH, and NaCl. *Macromolecules* **43**, 10582–10593 (2010).

74. Cheesman, B. T. *et al.* Polyelectrolyte brush pH-response at the silica-aqueous solution interface: A kinetic and equilibrium investigation. *Phys. Chem. Chem. Phys.* **15**, 14502–14510 (2013).

75. Nicolas, H., Yuan, B., Xu, J., Zhang, X. & Schönhoff, M. pH-responsive host-guest complexation in pillar[6]arene-containing polyelectrolyte multilayer films. *Polymers (Basel).* **9**, 719 (2017).

76. Rickert, J., Brecht, A. & Göpel, W. QCM Operation in Liquids: Constant Sensitivity during Formation of Extended Protein Multilayers by Affinity. *Anal. Chem.* **69**, 1441–1448 (1997).

Supporting information

Influence of ionic strength and specific ion effects on the pH responsiveness of weak polyelectrolyte multilayer films

*Frederik Hegaard and Esben Thormann**

Department of Chemistry, Technical University of Denmark, 2800 Kgs. Lyngby, Denmark.

S1: Ellipsometry Technique

The refractive index of the solvent has to be known for each measuring point, as it is changing with the ionic strength and the type of ions. To find the refractive index of a specific solution, a wafer with a SiO_2 layer of known thickness (approximately 100 nm) is measured in the ellipsometry liquid cell with the different salt solutions present. With a slab model of Si as the substrate, a 1 nm intermediate Si-SiO_2 layer, a SiO_2 layer, and salt solutions described by a Cauchy model, the model is fitted to the data with the A and B values of the solutions. The obtained values used are shown in

Table S1 and this method is found to give values of refractive index that are in good agreement with values obtained with other methods.[1,2]

The measurements were performed at 25 °C with a wavelength range from 250 nm to 1000 nm for NaCl and from 400 nm to 1000 nm for NaSCN because SCN^- is absorbing light at the lower wavelengths.

Table S1: A and B values obtained with the Cauchy model for NaCl and NaSCN solution at varying concentrations.

	NaCl		**NaSCN**	
c [mM]	A	B [µm^2]	A	B [µm^2]
0,01	1.321	0.00331	1.320	0.00331
0.1	1.321	0.00331	1.320	0.00331
0.3	1.321	0.00331	1.320	0.00331
1	1.321	0.00332	1.320	0.00331
3	1.321	0.00332	1.320	0.00331
10	1.321	0.00332	1.320	0.00331
15	1.321	0.00332	1.320	0.00331
30	1.321	0.00333	1.320	0.00331
50	1.321	0.00333	1.320	0.00331
100	1.321	0.00334	1.320	0.00341
200	1.322	0.00337	1.320	0.00362
400	1.323	0.00343	1.322	0.00385
800	1.327	0.00353	1.327	0.00409
1200	1.330	0.00363	1.333	0.00437

1600	1.333	0.00373	1.338	0.00461
2200	1.337	0.00388	1.345	0.00494
3000	1.343	0.00406	1.355	0.00536

S2: Dissipation shift from pH responsiveness measurements

In addition to the QCM-D frequencies associated with the pH responsiveness studies presented in the main manuscript, we are here presenting the corresponding dissipation values. Comparing the dissipation values in Figure S1 to the frequencies in Figure 3 in the main manuscript, very similar trends are observed. More specifically, any increase in frequency is associated with a similar increase in dissipation. The dissipation data thus support the interpretations provided in the main manuscript but does not at such add additional information.

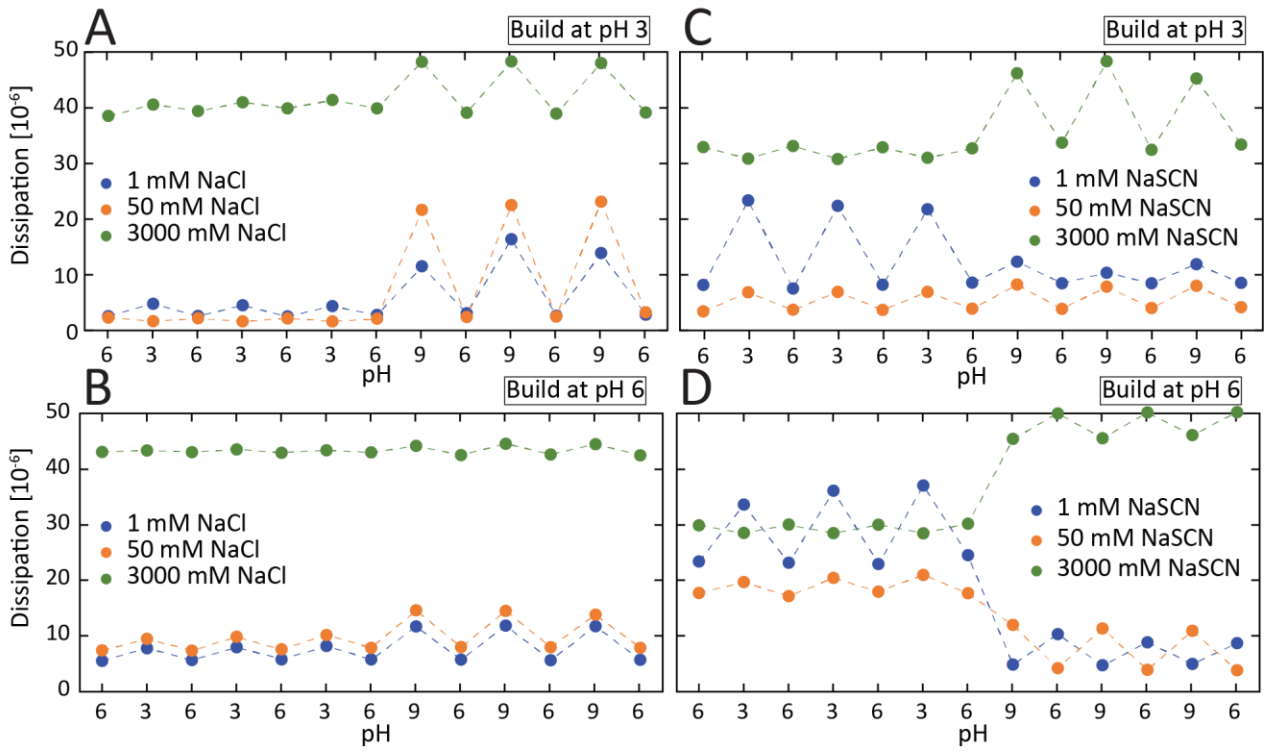

Figure S1: pH cycles showing the dissipation shift of multilayer films of 15 layers alternating CHI and ADA at 1, 50, or 3000 mM salt at pH 3, 6, or 9. Either with NaCl as the salt for films created in pH 3 (A) or pH 6 (B) or with NaSCN as the salt for films created in pH 3 (C) or pH 6 (D)

References

1. Ehtiati, K., Z. Moghaddam, S., Daugaard, A. E. & Thormann, E. Crucial Nonelectrostatic Effects on Polyelectrolyte Brush Behavior. *Macromolecules* **54**, 3388–3394 (2021).

2. Ehtiati, K., Moghaddam, S. Z., Klok, H.-A., Daugaard, A. E. & Thormann, E. Specific Counterion Effects on the Swelling Behavior of Strong Polyelectrolyte Brushes. *Macromolecules* **55**, 5130 (2022).

Appendix C: Calibration of the cantilever

This appendix will expand on parts of section 3 concerning the methods of calibrating the cantilever for friction measurements with the AFM. It will mainly focus on unfolding the considerations and intermediate calculations related to the geometrical approach of relating the sensitivities.

Calibration with thermal noise method

In this part, the implementation of the thermal noise method in the project is explained. Since this is not a method I have worked on improving, this will describe the origin of the method and my implementation of it.

In equation 3.4 it was shown that the vertical spring constant is found using the hydrodynamic function for a rectangular beam. This function is introduced because the foundation for equation 3.4 is the following equation:

$$k_v = M_e \rho_c L w t \omega_{vac,v}^2 \qquad C.1$$

where $\omega_{vac,v}$ is the angular resonance frequency in the vertical direction in a vacuum, ρ_c is the density of the cantilever and M_e is the normalized effective mass. The angular frequency in a vacuum, $\omega_{vac,v}$, can be determined very exact, but for practical reasons, it is more convenient to use the resonance frequency determined in a fluid, e.g. air. The relation between the frequency in a vacuum, $\omega_{vac,v}$, and the frequency in the fluid, $\omega_{f,v}$, can be described by:

$$\left(\frac{\omega_{vac,v}}{\omega_{f,v}}\right)^2 = 1 + \frac{\pi \rho_f w}{4 \rho_c t} Real\left(\Gamma_{rect}^v\left(\omega_{f,v}\right)\right) \qquad C.2$$

where ρ_f and ρ_c are the densities of the fluid and the cantilever respectively, t is the thickness of the cantilever and $Real\left(\Gamma_{rect}^v\left(\omega_{f,v}\right)\right)$ is the real part of the hydrodynamic function for a rectangular beam in the vertical direction[235]. There is no exact analytical expression for the hydrodynamic function of a rectangular beam, but a circular beam's hydrodynamic function is described by:

$$\Gamma_{circ}^v\left(\omega_{f,v}\right) = 1 + \frac{4iK_1\left(-i\sqrt{iRe}\right)}{\sqrt{iRe}K_0\left(-i\sqrt{iRe}\right)} \qquad C.3$$

where K_0 and $K_1$are the modified Bessel functions of the third kind and $Re = \rho_f \omega_{f,v} w^2/\left(4\eta_f\right)$ with η_f being the viscosity of the fluid and w representing the dominant length of the cross-section, which for a

circular beam is the diameter and for a rectangular beam is the width[235]. The circular hydrodynamic function can be related to the rectangular by a correction factor:

$$\Gamma_{rect}^{v}(\omega_{f,v}) = \Omega(\omega_{f,v})\Gamma_{circ}^{v}(\omega_{f,v}) \quad C.4$$

where $\Omega(\omega_{f,v})$ is a numerical approximation that has a real and an imaginary part of the form:

$$\Omega_r = \frac{0.91324 - 0.48274\tau + 0.46842\tau^2 - 0.12886\tau^3 + 0.044055\tau^4 - 0.0035117\tau^5 + 0.00069085\tau^6}{1 - 0.56964\tau + 0.48690\tau^2 - 0.13444\tau^3 + 0.045155\tau^4 - 0.0035862\tau^5 + 0.00069085\tau^6} \quad C.5$$

and

$$\Omega_i = \frac{-0.024134 - 0.029256\tau + 0.016294\tau^2 - 0.00010961\tau^3 + 0.000064577\tau^4 - 0.000044510\tau^5}{1 - 0.59702\tau + 0.55182\tau^2 - 0.18357\tau^3 + 0.079156\tau^4 - 0.014369\tau^5 + 0.0028361\tau^6} \quad C.6$$

with $\tau = \log(Re)$. This means that if the resonance frequency of the cantilever in the air is known, it is possible to calculate the real part of the hydrodynamic function for the rectangular beam, $Real\left(\Gamma_{rect}^{vert}(\omega_f)\right)$.

The term $\rho_c t$ in equation C.2 can be described by:

$$\rho_c t = \frac{\pi\rho_f w}{4}\left[Q_{f,v} Imag\left(\Gamma_{rect}^{v}(\omega_{f,v})\right) - Real\left(\Gamma_{rect}^{v}(\omega_{f,v})\right)\right] \quad C.7$$

where $Q_{f,v}$ is the quality factor in the vertical direction[211]. The fluctuations of the cantilever due to thermal noise is measured as deflection voltage, Fourier transformed and the following equation is fitted to the data:

$$S(f) = \frac{P_{DC,v} f_{0,v}^4}{\left(f^2 - f_{0,v}^2\right)^2 + \frac{f^2 f_{0,v}^2}{Q_{f,v}^2}} \quad C.8$$

where $f_{0,v}$, $Q_{f,v}$ and $P_{DC,v}$ are found by using these as fitting parameters[212] This leads to a non-contact expression for the vertical spring constant that is derived as the following:

$$k_v = M_e \rho_c L w t\left(1 + \frac{\pi\rho_f w}{4\rho_c t} Re\left(\Gamma_{rect}^{v}(\omega_{f,v})\right)\right)\omega_{f,v}^2 \quad C.9$$

$$k_v = M_e L w\left(\rho_c t + \frac{\pi\rho_f w}{4} Re\left(\Gamma_{rect}^{v}(\omega_{f,v})\right)\right)\omega_{f,v}^2 \quad C.10$$

$$k_{vert} = 0.1906\rho_f L w^2 Q_{f,v}\omega_{f,v}^2 Im\left(\Gamma_{rect}^{v}(\omega_{f,v})\right) \quad C.11$$

This equation allows the vertical spring constant to be determined from the cantilever's width and length, the density and viscosity of the surrounding fluid, and a thermal noise deflection measurement.

Geometrical sensitivities

Vertical Sensitivity in air

An illustration of how the optical lever principle works in the vertical direction is shown in Figure C.1 for a cantilever in air.

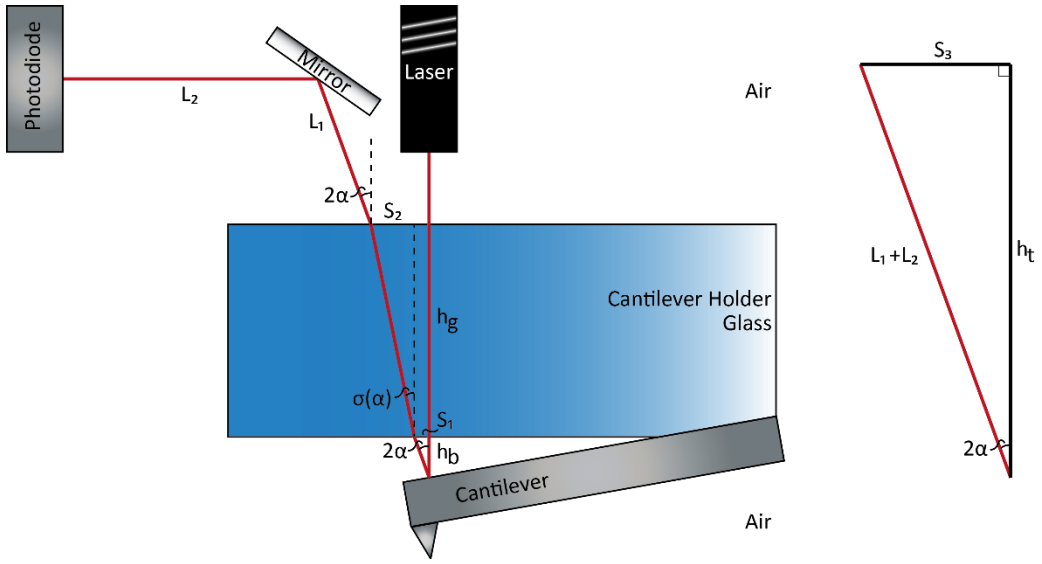

Figure C.1: Illustration of the deflection path of laser interacting with an unbend cantilever, the cantilever holder, the mirror, and the photodiode in the vertical direction.

The sensitivity is among other things dependent on the vertical distance the light travels, h_t, h_g and h_b, the angle of the unbend cantilever, α, and the relative refractive indices of the mediums the light travels between. To express the significance of these parameters analytically, the set-up is illustrated in Figure C.2A where the mirror is removed and the photodiode is moved so that the cantilever bending gives the same deflection distance.

When the distance between the cantilever holder and the cantilever, h_b, is changed, it affects only the position of the laser spot in the photodiode in the vertical direction and not in the torsional. Figure C.2B illustrates the effect of a height change δh_b in the vertical direction. When looking at the lateral displacement it is seen that the displacement occurring from the height change is conserved in all three interfaces, $\delta S_1 = \delta S_2 = \delta S_3$, which can be calculated as:

$$\delta S_3 = \delta h_b \tan(2\alpha) \qquad C.12$$

because $\delta S_3 = 0$ when $\delta h_b = 0$. If the photodiode is aligned so the deflection is zero at $\delta h_b = 0$ and it is assumed that the photodiode response is linearly depending on the laser spot placement, then the deflection can be scaled by a constant, k, which relates the deflection voltage to the deflection length. The vertical deflections dependency on the height change can then be expressed by the following:

$$\frac{dD_v(h)}{d\delta h_b} = k \tan(2\alpha) \qquad C.13$$

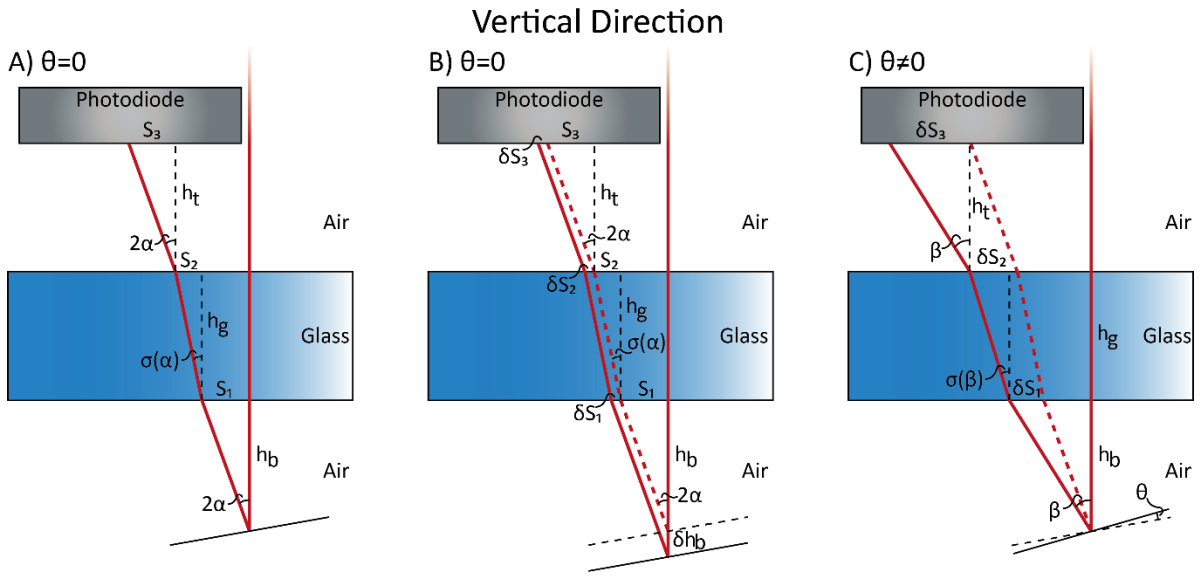

Figure C.2: Simplified illustration of deflection path of laser interacting with an unbend cantilever (A), an unbend cantilever at a shifted height (B), and a cantilever bend with an angle, θ, (C) in the vertical direction.

The vertical deflection dependency on the deflection angle is illustrated in Figure C.2C. The cantilever angle can be described by $\beta = 2\alpha + 2\theta$ and the position of the laser spot on the photodiode at $\theta = 0$ can be expressed by the lateral movement of the laser spot. The lateral movement of the laser spot at $\theta = 0$ is:

$$S(\theta = 0) = h_b \tan(2\alpha) + h_g \tan\big(\sigma(2\alpha)\big) + h_t \tan(2\alpha) \qquad C.14$$

and the distance in the case where $\theta \neq 0$ is:

$$S(\theta) = h_b \tan(\beta) + h_g \tan\big(\sigma(\beta)\big) + h_t \tan(\beta) \qquad C.15$$

This means that the deflection can be expressed as:

$$\delta S(\theta) = S(\theta) - S(\theta = 0) \qquad C.16$$

$$= (h_b + h_t)[\tan(\beta) - \tan(2\alpha)] + h_g\big[\tan\big(\sigma(\beta)\big) - \tan\big(\sigma(2\alpha)\big)\big]$$

where σ can be calculated from the refractive indices of the materials in the interface and the incoming angle by using Snell's law:

$$n_a \sin(2\alpha) = n_g \sin\big(\sigma(2\alpha)\big) \Rightarrow \sigma(2\alpha) = a\sin\left(\frac{n_a}{n_g}\sin(2\alpha)\right) \qquad C.17$$

where n_a and n_g are the refractive indices of air and glass respectively. Because the angles to the interfaces normal are fairly small, the following approximation is made:

$$\tan\big(\sigma(\beta)\big) = \tan\left[a\sin\left(\frac{n_a}{n_g}\sin(\beta)\right)\right] \sim \sin\left[a\sin\left(\frac{n_a}{n_g}\tan(\beta)\right)\right] = \frac{n_a}{n_g}\tan(\beta) \qquad C.18$$

which is a fairly rough approximation, but for typical AFM values, this gives an error of less than 2 % to the change in lateral deflection. The deflection can then be expressed as:

$$\delta S(\theta) = \left(h_b + h_t + h_g\frac{n_a}{n_g}\right)[\tan(\beta) - \tan(2\alpha)] \qquad C.19$$

which can be simplified by using trigonometric identities and small angle approximations for θ.

$$\tan(\beta) - \tan(2\alpha) = \frac{\sin(2\alpha + 2\theta)}{\cos(2\alpha + 2\theta)} - \frac{\sin(2\alpha)}{\cos(2\alpha)} \qquad C.20$$

$$= \frac{\sin(2\alpha)\cos(2\theta) + \cos(2\alpha)\sin(2\theta)}{\cos(2\alpha)\cos(2\theta) - \sin(2\alpha)\sin(2\theta)} - \frac{\sin(2\alpha)}{\cos(2\alpha)}$$

$$\tan(\beta) - \tan(2\alpha) \qquad C.21$$

$$= \frac{\cos(2\alpha)\sin(2\alpha) + 2\theta\cos^2(2\alpha)}{\cos^2(2\alpha) - 2\theta\cos(2\alpha)\sin(2\alpha)} - \frac{\cos(2\alpha)\sin(2\alpha) - 2\theta\sin^2(2\alpha)}{\cos^2(2\alpha) - 2\theta\cos(2\alpha)\sin(2\alpha)}$$

$$\tan(\beta) - \tan(2\alpha) = \frac{2\theta(\cos^2(2\alpha) + \sin^2(2\alpha))}{\cos^2(2\alpha) - \theta\sin(4\alpha)} = \frac{2\theta}{\cos^2(2\alpha) - \theta\sin(4\alpha)} \approx \frac{2\theta}{\cos^2(2\alpha)} \quad C.22$$

Where in the last step it is assumed that $\cos^2(2\alpha) \gg \theta\sin(4\alpha)$. Using this the deflection simplifies to:

$$\delta S(\theta) = 2\theta \frac{h_b + h_t + h_g n_a/n_g}{\cos^{-2}(2\alpha)} \quad C.23$$

and the change in vertical deflection voltage is described by:

$$\gamma_{v,a} = \frac{dD_v(\theta)}{d\theta} = \frac{dk\delta S(\theta)}{d\theta} = 2k\frac{h_b + h_t + h_g n_a/n_g}{\cos^{-2}(2\alpha)} \quad C.24$$

Torsional Sensitivity in air

The light path in the torsional direction is illustrated in Figure C.3. As the angle in this case only is the small angle φ, it is significantly simpler to relate the deflection distance and the torsional angle change.

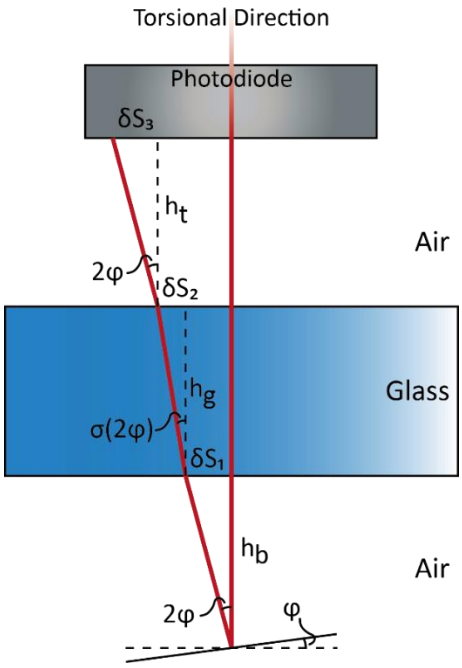

Figure C.3: Simplified illustration of the deflection path of laser interacting with a cantilever bend with an angle, φ, in the torsional direction.

The deflection is described by:

$$\delta S(\varphi) = \delta S_1(\varphi) + \delta S_2(\varphi) + \delta S_3(\varphi) = (h_b + h_t)\tan(2\varphi) + h_g\tan\big(\sigma(2\varphi)\big) \quad C.25$$

where sigma can be approximated as:

$$\sigma(2\varphi) = 2\varphi\frac{n_a}{n_g} \quad C.26$$

due to the angle, φ, being close to zero. This means that the deflection simplifies to:

$$\delta S(\varphi) = 2\varphi\left(h_b + h_t + h_g n_a/n_g\right) \quad C.27$$

and the deflection from an angular change is:

$$\gamma_{t,a} = \frac{dD_t(\varphi)}{d\varphi} = \frac{dk\delta S(\varphi)}{d\varphi} = 2k\left(h_b + h_t + h_g\frac{n_a}{n_g}\right) \quad C.28$$

which is of the same form as the vertical deflection but differently scaled. The deflection in the vertical and torsional direction is therefore related as:

$$\gamma_{t,a}(\varphi) = \gamma_{v,a}(\varphi)\cos^{-2}(2\alpha) \quad C.29$$

which can be used to compare the found sensitivities.

Torsional sensitivity in liquid

If the cantilever is immersed in a liquid instead of in air, the part below the cantilever holder is now this liquid and the torsional sensitivity is changed based on the liquid's refractive index as illustrated in Figure C.4.

This sensitivity is calculated the same way as the one where the cantilever is in air, but this time with a glass-air interface at the glass's top and a glass-liquid interface at the glass's bottom. In this system, the deflection is calculated as

$$\delta S = h_b\tan(2\varphi) + h_g\tan\left(\sigma(2\varphi)\right) + h_t\tan\left(\theta(2\varphi)\right) \quad C.30$$

which using Snell's law and small angle approximation can be simplified as

$$\delta S = 2\varphi\left(h_b + h_g\frac{n_w}{n_g} + h_t\frac{n_w}{n_a}\right) \quad C.31$$

where n_w, n_g and n_a are the refractive indices for water, glass, and air respectively.

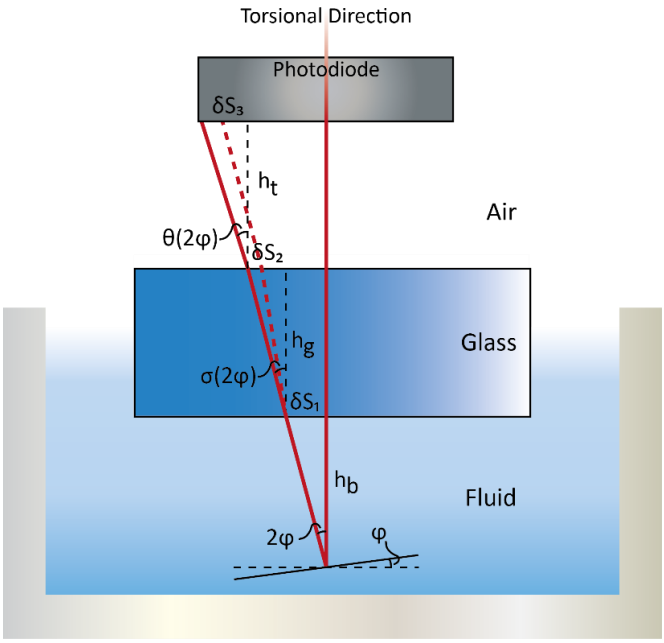

Figure C.4: Simplified illustration of the deflection path of laser interacting in a fluid with a cantilever bend with an angle, φ, in the torsional direction.